RICE UNIVERSITY

Arsenic Adsorption to Nanoparticulate Magnetite in Natural Waters: Batch versus Column-Specific Effects

By

Jesse Walter Farrell

A THESIS SUBMITTED
IN PARTIAL FULFILLMENT OF THE
REQUIREMENTS FOR THE DEGREE

Doctor of Philosophy

Approved Thesis Committee:

Mason Tomson, Professor, Chair
Civil and Environmental Engineering

Pedro Álvarez, George R. Brown Professor,
Civil and Environmental Engineering

Vicki Colvin, Pitzer-Schlumberger Professor
of Chemistry, Chemical & Biomolecular
Engineering

HOUSTON, TEXAS
APRIL 2011

ABSTRACT

Increasingly, cities in Latin America recognize the importance of drinking water quality on public health. A water assessment of Guanajuato, Mexico, and surrounding areas found arsenic in wells above the Mexican drinking water standard (25μg/l). A collaborative effort was initiated to develop and field test a new arsenic removal method using high surface area sorbents. Nanoscale magnetite, previously shown to effectively adsorb arsenic in batch systems, was packed in sand columns to create a continuous treatment process. Design and operating conditions were assessed in bench-scale columns, and subsequently, a pilot column with 456 g ($2.50 US) of commercially available, food-grade magnetite demonstrated removal of the equivalent arsenic contained in 1,360 liters of Guanajuato groundwater.

However, strong interferences were present in natural waters as breakthrough of arsenic in laboratory columns was delayed >10x with a synthetic feed solution as compared to groundwater at the same pH. Adsorption isotherms conducted with pretreated Guanajuato groundwater helped deduce the species of utmost interference: silica. By the removal or addition of silica, adsorption isotherms confirmed silica's strong effect. Low-level geothermal waters with high silica concentrations are common throughout central Mexico and other parts of the world presenting a major challenge for arsenic adsorbents. Arsenic adsorption improved through pH reduction in batch; however, pilot-scale column experiments showed no improvement with the same treatment. Silica preloading, deep-bed redox processes, and influent water impurities provided plausible explanation for the column observations. Breakthrough was monitored closely in columns sampled from 4 locations along their length. Synthetic

solution with silica, in contrast to a baseline without silica, showed decreasing arsenic adsorption with distance through the column, characteristic of preloading, and a regression in breakthrough suggested oxidation at the magnetite surface. Calcium has been shown in batch systems to improve arsenic adsorption kinetics but not equilibrium partitioning in the presence of silica. In column experiments, the addition of calcium substantially increased arsenic adsorption in the presence of silica beyond batch model predictions confirming column-specific enhancements. The column-specific effects of silica, calcium, and redox would not be observable from adsorption isotherms but have critical importance to arsenic treatment by nanomagnetite columns.

ACKNOWLEDGEMENTS

This dissertation and study was accomplished only through the immeasurable support from a treasured community of professors, colleagues, friends, and family. Foremost, I want to thank Dr. Mason Tomson for his mentorship and guidance through the process. The countless hours, days, months, and years he stood by me in the trenches of my graduate work will leave a lasting impression on me beyond any other defining moment or piece of knowledge I have gained at Rice.

I want to thank Dr. Pedro Alvarez and Dr. Vicki Colvin for the serving on my committee and their guidance through my research work in Guanajuato. I thank my co-laborers John Fortner and Carolina Avendano from the Colvin lab, Norb from C&B Plumbing, and Rafael Zárate-Araiza and the others from the Guanajuato water management team. I want to thank my group: Sarah Work, Hamad Al Saiari, Nan Zhang, Jonathon Pennington, Liu Wang, Ping Zhang, Chunfang Fan, Haiping Lu, Wei Shi, Jie Yu, Hualin Li, Lunliang Zhang, Lilin Wang, Sue Wang, and Amy Kan, your ideas, support, and company along this journey have been invaluable.

I want to thank my family and close friends Sarah, Joe, June, Jacky, Thomas, and Steven for their encouragement and prayer. Over all, I thank God for sustaining me with strength, love, and grace during this period and I trust that that will never change.

The research was supported by the National Science Foundation through the Center for Biological and Environmental Nanotechnology [EEC-0118007] and U.S. EPA ORD/NCER/STAR nanotechnology program [#83171801].

TABE OF CONTENTS

1. Introduction 1
   Objectives and Hypotheses 1
   Organization of thesis 3
   Overview of Collaboration with Guanajuato municipal water provider 3
   Background on Guanajuato 4
   Collaboration established 7
   Water quality assessment 8
   Research, development, and field testing with nanomagnetite packed-columns 10
2. Background and Literature Review 13
   Heavy metal contaminants of concern for drinking water 13
   Arsenic chemistry, occurrence, uses 20
   Arsenic health effects and regulatory limits 26
   Methods of arsenic removal 27
   Performance review of arsenic adsorbents 29
   Small scale arsenic treatment methods 32
   Conventional slow sand and rapid sand filtration 37
   CSTR versus packed column reactors 39
   Adsorption and surface complexation modeling: Chemical and electrostatic effects on K_d 41
   Adsorption Isotherms 44
   Adsorption kinetics modeling 46
   Column filtration and advection dispersion modeling 49
   Interfering species 58
   Silica in the natural environment 62
   Mechanism of silica interference 69
   Mitigating the effects of silica 74
   Silica removal 80
   Regeneration of iron-oxide adsorbents 82
   Fate and transport of spent adsorbents and adsorbed contaminants 84
3. Materials and Methods 86

Solutions and chemicals....86
Property analysis of magnetite adsorbents....88
ICP-MS elemental analysis....93
Chloride interference on ICP-MS....95
ICP-OES elemental analysis....96
Adsorption isotherms at high temperature, low oxygen wellhead conditions....101
Guanajuato groundwater adsorption isotherms at various pH conditions....102
Pilot column studies in Guanajuato, Mexico....103
Pretreatment for removal of interfering species....113
Removal of silica and arsenic with activated alumina: batch and column studies..120
Mid-column sampling used to monitor the migration of silica and arsenic....122
4. Results and Discussion....126
Magnetite product selection....126
Arsenic breakthrough in synthetic solutions versus groundwater....135
Adsorption isotherms in high temperature, low oxygen conditions....140
Single-point adsorption isotherms with pretreated groundwater....140
Adsorption isotherms with pH-adjusted Guanajuato groundwater....147
Arsenic breakthrough with raw and pH-adjusted Guanajuato groundwater....149
Influence of silica removal on adsorption....156
The impact of silica addition to synthetic solutions....158
Removal of silica by activated alumina....160
Silica and arsenic migration through the length of a column....163
Calcium effect on arsenic breakthrough in high silica feed water....169
5. Conclusions and Recommended Future Work....174
References....178
Appendices....188
Appendix A –Assessment of water samples shipped from Guanajuato to Rice University Summer of 2008....189
Appendix B – Analysis from Guanajuato water assessment trip; January 2009....191
Appendix C – Geothermometer temperatures for groundwater wells in Guanajuato and surrounding areas....194
Appendix D –Guanajuato pilot-column breakthrough curves by element....196

LIST OF FIGURES

Figure 1 - (a) The state of Guanajuato, Mexico. (b) Lake Soledad. (c) Bird's-eye view of Guanajuato. 5

Figure 2 - Photos: (a) Carrying water in historic Guanajuato prior to 1880 and (b) the La Esperanza dam after completion (1880). 6

Figure 3 - Photos of the (a) office space and (b) lab space provided by Simapag. Pictured from left to right: Jesse Farrell (Rice student), Raphael Zárate-Araiza (Simapag director), and Dr. Qilin Li (Rice professor). 7

Figure 4 – Photos of (a) CBEN researchers Jesse Farrell and Dr. Qilin Li sampling at a home in Guanajuato, and (b) a groundwater well sampling site..... 8

Figure 5 - Rice University researchers John Fortner, Isabel Raciny, and Jesse Farrell inside the Guanajuato water treatment plant lab with the first nanomagnetite pilot column..... 11

Figure 6 – A Pourbaix diagram for iron at 25°C and 1atm. The shaded region, enclosed by a dotted line, represents the conditions encountered in the present work for experiments with Guanajuato groundwater. The predominant arsenic speciation in that region is superimposed on the diagram in red (adapted from Pourbaix (1924)). 22

Figure 7 - Arsenic concentrations found in at least 25% of ground-water samples within a moving 50km radius (Ryker 2001). 23

Figure 8 – Schematic diagram of a SONO Filter (Model SF-TWIN, Patent 1003935, 2002) 34

Figure 9 - Depiction of a biosand filter (www.biosandfilter.org) 36

Figure 10 - Diagram of a slow sand filter (Huisman 1974). 38

Figure 11 - Diagram of a rapid sand filter (MECC 2009). 39

Figure 12 - Stoichiometric concentration front for ideal fixed-bed adsorpion column (Figure 15.27 from Seader 1998) 51

Figure 13 - Depiction of monodentate mononuclear and bidentate binuclear attachment of arsenate to an iron oxide surface (adapted from Weisner (2007)). 55

Figure 14 - Concentration fronts in a fixed-bed column with mass transfer effects (Figure 15.28a from Seader 1998). 58

Figure 15 – Breakthrough curve on a time basis. (Figure 15.28b from Seader 1998)..... 58

Figure 16 – Predominance diagram of silicate monomer/polymer species at various pH and silica concentrations (Stumm and Morgan 1996). 64

Figure 17 - Dissolution mechanism of silica: depolymerization by hydroxide ion (Iler 1979). 65

Figure 18 - Silicate chemically adsorbed to ferric oxide by bidentate binuclear attachment (adapted from Liao et al. (2009)) and arsenate chemically adsorbed to ferric oxide by

mononuclear monodentate and binuclear bidentate attachment (adapted from Sherman and Randall (2003)). 68

Figure 19 - Conceptualization of the stages of silica interference. Adapted from Smith and Edwards (2005). 70

Figure 20 - a. Silica adsorbed to goethite at pH 4, 6, and 8 with 0.1 and 1.0mM Si. b. Arsenic adsorbed to goethite at pH 8 in the presence of 0.1mM and 1.0mM Si pre-equilibrated for 60h in solution (Waltham and Eick 2002). 72

Figure 21 – Surface coverage depictions of silicic acid adsorbed on an iron-oxide surface: a. silicic acid monomer. b. polymerized silicic acid. c. adjacent silicic acid monomers forming a siloxane linkage (Swedlund and Webster 1999). 73

Figure 22 - Zeta potential of preformed ferric hydroxide versus pH in three solutions: Fe only, Fe and Si, and Fe, Si, and Ca. Fe = 20mg/l, SiO_2 = 40mg/l, Ca = 10mg/l (Smith and Edwards 2005). 75

Figure 23 - Fractional sorption of arsenic (arsenic adsorbed in 2 hours divided by the arsenic adsorbed after 1368 hours) versus zeta potential. Initial conditions: As = 100µg/l, Fe = 20mg/l, SiO2 = 40mg/l, and Ca = 10mg/l. Zeta potential was varied by pH adjustment (Smith and Edwards 2005). 76

Figure 24 – Comparison of kinetics of As(V) adsorption to 1.0 g/l geothite in solutions of pH 8 with 0.10 and 1.0 mM $Si(OH)_4$ and in solutions of similar zeta potential without silicate at pH 9 and 10 (Waltham and Eick 2002). 77

Figure 25 - Percent of initial arsenic removed from solution over time with amorphous $Fe(OH)_3$ at pH 8.5. Initial solution conditions: As(V) = 100µg/l, Fe = 20mg/l, SiO_2 = 40mg/l, and Ca = 10mg/l (Smith and Edwards 2005). 78

Figure 26 – Percent arsenic removal from batch experiments with 2g/l activated alumina given solutions prepared with 40mg/l SiO2, 500µg/l As, and 1mM $NaHCO_3$ (Smith and Edwards 2005). 80

Figure 27 - SEM of Rockwood Pigments, Inc. 78P food-grade magnetite. 91

Figure 28 - BET surface area analysis of 78P food-grade magnetite. 93

Figure 29 - ICP-MS calibration curve for arsenic. 94

Figure 30 - Photo of the Perkin Elmer ELAN 9000 ICP-MS during a sample run with a sample set arranged on the Perkin Elmer AS-93plus autosampler. 95

Figure 31 - Optical microscope image (3.5x magnification) showing sand and aggregated nanomagnetite individually and after shaking together vigorously for 1 minute. Upper left: sand; lower left: 78P magnetite; right: magnetite/sand blend. 98

Figure 32 - Guanajuato Municipal Well No. 8 102

Figure 33 - Schematic of pilot column setup used in Guanajuato. 104

Figure 34 – a. Jesse Farrell and John Fortner setting up piping from the water truck to the laboratory through a window on the second floor of the water treatment facility. b. John Fortner monitoring the pilot column and Jesse Farrell performing arsenic testing in the laboratory space. 105

Figure 35 – Construction of the pilot columns in Guanajuato, Mexico..... 107

Figure 36 – In this photo the Hach test indicated that the Guanajuato groundwater contained between 10 and 30µg/l of arsenic before entering the column and was essentially free of arsenic after passing through the column. 111

Figure 37 – Rice researchers and Guanajuato water staff preparing Well No. 8, testing the buffering capacity of the groundwater, and distributing groundwater and dilute acid into a water truck. 112

Figure 38 - Glassware containing an array of pretreated water solutions before 24-hour isotherms. 114

Figure 39 - Carbonate speciation in equilibrium with atmospheric CO_2 ($10^{-3.42}$ atm) at room temperature (Gustafsson 2009)..... 118

Figure 40 - Schematic for the column setup used to test granular activated alumina. ... 122

Figure 41 - Columns constructed with sampling ports along their length. A. Schematic of the system design. B. Picture of the outlet tubing with adjustable discharge height. C. From left to right: Feed tanks (with and without silica), dual-syringe pumps, columns with sample ports, and collection beaker. D. Close-up of luer sample ports with plugs. 123

Figure 42 - As(V) adsorption isotherms for commercial magnetite particles in Rice groundwater at pH 8.00..... 127

Figure 43 - Breakthrough of 100µg/l As(V)-spiked Rice GW, pH 8.5, in 1cm diameter sand columns of 5% and 20% Reade nanomagnetite by weight with varied residence times. Solid lines are fitted with CXTFIT. 131

Figure 44 - Model versus experimental C/C_0 values for As(V) breakthrough in a column of 20% magnetite with residence time of 3.2 minutes. 132

Figure 45 - Cumulative mass of As(V) adsorbed to Reade nanomagnetite calculated from experimental data in Figure 43. Solid lines are for visualization only. 134

Figure 46 – Experimental setup for 15% food-grade magnetite columns used to monitor arsenic breakthrough in synthetic and groundwater solutions. (1) Feed Tank, (2) Pharmacia P-500 Pump, (3) Nanomagnetite/sand packed column, and (4) sample port and collection beaker. 136

Figure 47 – Arsenic breakthrough for lab synthesized feed water (HPLC-grade water, pH 8.50, 30.3µg/l As(V), 6.4mM NaCl, and 2.5mM THAM) pumped with a residence time of 1.1 minutes through a 26cm packed-column bed composed of 15% magnetite, 85% sand. 137

Figure 48 – Arsenic breakthrough for spiked groundwater (Rice groundwater, pH 8.50, 29.2µg/l As(V)) pumped with a residence time of 1.2 minutes through a 30cm packed column bed of 15% magnetite, 85% sand. Solid line is fitted with CXTFIT. 138

Figure 49 - Chloride Interference to arsenic measurement on ICP-MS. 139

Figure 50 - Arsenic adsorption to 78P magnetite at Guanajuato wellhead conditions (60°C, oxygen-limited) and at room temperature in an aerated environment. Experiments

conducted in Rice groundwater, buffered with 10mM THAM and adjusted to pH 8.00. Lines are for visualization only..... 140

Figure 51 – Single point 24-hr adsorption of As(V) from various pretreated solutions to 78P magnetite. Pretreatments in legend are listed in order of their effect on subsequent arsenic adsorption to magnetite from most adsorption to least adsorption..... 142

Figure 52 - Arsenic partitioning to magnetite given initial silica concentrations in solution resulting from pretreatment with activated alumina. From left to right, the concentrations of activated alumina used in the pretreatment to reduce the silica concentration from 51 mg/l to the value shown were 10 g/l, 2.5 g/l, 1 g/l, and 0.1 g/l of activated alumina..... 145

Figure 53 - pH effect on arsenic adsorption to 78P magnetite in batch for Guanajuato groundwater compared with predictions from Visual Minteq (Gustafsson 2009). 149

Figure 54 - Guanajuato pilot column fed raw groundwater from Municipal Well No. 8; pH 7.3..... 150

Figure 55 - Arsenic breakthrough in pilot column studies in Guanajuato with raw and pH-adjusted groundwater. Solids lines are fitted by CXTFIT. 152

Figure 56 - Inlet and outlet iron concentrations for pilot column delivered Guanajuato groundwater with pH adjusted to 5.5 with acetic acid..... 153

Figure 57 - Inlet and outlet phosphate concentrations for pilot column delivered Guanajuato groundwater with pH adjusted to 5.5 with acetic acid. 153

Figure 58 - Inlet and outlet pressure gauges of a pilot column in Guanajuato, Mexico. 156

Figure 59 - Pressure loss in a Guanajuato pilot column versus flow rate..... 156

Figure 60 – Distribution of arsenic, K_d (L/g) for single point adsorption isotherms to magnetite given the initial silica concentration yielded by the indicated pretreatment.. 157

Figure 61 - 24-hour adsorption isotherms displaying the effects of silica and vanadium addition to synthetic solution containing 66µg/l As(V), 2.9mM NaCl, and 2.5mM THAM buffer adjusted to pH 7.5. 159

Figure 62 – The K_d values of single-point adsorption isotherms for arsenic to magnetite resulting from pretreated solutions with the given initial silica concentrations. 160

Figure 63 - Silica and arsenic removal through a 30.5cm packed column of activated alumina. Feed water composed of Guanajuato groundwater containing 48 mg/l SiO_2 and 8.8 µg/l As(V) at pH 7.9 was pumped with a 2.3 minute residence time. 162

Figure 64 - Arsenic and silica adsorption to Activated Alumina. Units for aqueous concentrations for arsenic and silica are µg/l and mg/l, respectively. Units for adsorbed concentrations for arsenic and silica are µg/g and mg/g, respectively. The solution was composed of Guanajuato groundwater with As(V) added to 61µg/l; pH 7.7. 163

Figure 65 - Breakthrough of silica for synthetic water feed water (50mg/l as SiO_2, 100µg/l As(V), 2.5mM THAM buffer, pH adjusted to 7.0 with HNO_3) through each quarter of a column packed 13% by-weight with 78P magnetite and 87% by-weight with plastic beads..... 164

Figure 66 - Arsenic breakthrough for synthetic feed water containing silica (see description in Figure 65) shown through each quarter of a magnetite-packed column. Solid lines are the fitted model. 164

Figure 67 - Arsenic breakthrough for synthetic water feed water not containing silica shown through each quarter of a magnetite-packed column. Solid lines are the fitted model..... 165

Figure 68 – The cumulative arsenic adsorbed per gram of magnetite in each quarter-section is shown over time for a column delivered a synthetic feed solution containing silica. 168

Figure 69 - The cumulative arsenic adsorbed per gram of magnetite in each quarter-section is shown over time for a column delivered a synthetic feed solution not containing silica. 169

Figure 70 – The total arsenic adsorbed per gram of magnetite in each quarter section of the packed column by the end of the mid-column sampling experiment for feed solutions with silica and without silica..... 169

Figure 71 – Arsenic breakthrough with synthetic feed solutions with and without calcium. Feed solutions were formulated with 100 μg/l As(V), 50 mg/l as SiO_2, 2.5mM THAM buffer, trace-metal grade HNO_3 to reduce the pH to 8.0, sufficient $NaNO_3$ to raise the conductivity to 750μS/cm, and with or without 20mg/l of Ca^{2+} from $CaCl_2$. Lines are fitted using CXTFIT. 172

Figure 72 - Cumulative arsenic adsorbed in columns with synthetic feed solutions as described in Figure 71. Lines are for visualization only..... 173

LIST OF TABLES

Table 1 - Trace heavy metals regulated by the US EPA 20

Table 2 – Comparison of As(III) and As(V) adsorbents. (Adapted from Shipley 2007) . 30

Table 3 - Freundlich isotherm constants for $qe = KFCem$ for adsorption of As(III) to various soils in West Virginia given q_e (mg/kg) and C_e (mg/l) (Bodek, Lyman et al. 1988). 45

Table 4 - Measured properties and components of aerated Guanajuato and Rice groundwater at 25°C 88

Table 5 - Summary of commercial magnetite nanoparticles screened by adsorption isotherms for use in subsequent arsenic removal batch and column studies. Values in parenthesis are estimated based on spherical geometry: $SSA(m^2/g) = 6\times10^9/(\rho\cdot D)$, where ρ is density (5×10^6 g/m^3) for magnetite and D is particle diameter (nm). †Indicates measurement by SEM or TEM at Rice. All other values and properties were provided by the manufacturer. 89

Table 6 – 24-hr adsorption isotherm parameters and cost estimates for commercial magnetite products treating As-spiked Rice groundwater from 30µg/l to 25µg/l at pH 8.0. The q_e listed corresponds to equilibrium with 30µg/l of As(V) in solution. Fraction of isotherm is 0.75 and 2 regeneration treatments are assumed. 129

Table 7 - CXTFIT model parameters with standard deviations are listed for the breakthrough curves displayed in Figure 43. 132

Table 8 - CXTFIT model parameters with standard deviations listed for the breakthrough curves displayed in Figure 55. 154

Table 9 –The impact of groundwater components on arsenic adsorption to magnetite inferred from the single-point adsorption isotherms conducted with pretreated Guanajuato groundwater. 158

Table 10 – Summary of transport parameters for the arsenic breakthrough curve displayed in Figure 66 and Figure 67, fitted simultaneously for all 4 sections of each column 166

Table 11 – Visual Minteq simulation giving the percentage of species adsorbed for the given species in solution 171

Table 12 - Fitted parameters to the column breakthrough described in Figure 71. 173

1. Introduction

This research arose out of past research activities at Rice University involving nanoparticulate magnetite: the discovery of the unique magnetic effects of magnetite nanoparticles subjected to low magnetic fields (Yavuz, Mayo et al. 2006) and the ability of magnetite to adsorb a more than proportional quantity of arsenic with increased surface area related to nanoparticle size (Yean, Cong et al. 2005; Mayo, Yavuz et al. 2007). The previous work was conducted in batch systems, while the present research also involved packed columns which take advantage of the chromatographic effect, the containment provided by fixed-bed processes, and the potential for higher volume throughput with smaller footprint. Understanding the differences in arsenic adsorption to nanomagnetite observed between batch and column studies, as well as synthetic and natural waters, was a primary focus of this work. Batch experiments and bench-scale columns were used primarily; however, a collaboration which developed between Rice University researchers from the Center for Biological and Environmental Nanotechnology (CBEN) and water management personnel from Guanajuato, Mexico, provided the opportunity for pilot-scale testing of nanomagnetite columns in a field environment.

Objectives and Hypotheses

The following objectives and hypotheses guided the course of study.

1. *Objective:* Determine whether arsenic adsorption to nanomagnetite in batch studies can be projected to column systems.

   Hypothesis: Arsenic adsorption by nanomagnetite in batch isotherms represents an upper limit to adsorption by nanomagnetite dispersed in a sand column given

the same solution conditions. Furthermore, reductions to arsenic adsorption within a column will occur due to preloading of competing species, changes to surface species over time, and potentially other column dynamics.

2. *Objective:* Determine the species present in untreated Guanajuato groundwater that interfere with arsenic adsorption to nanomagnetite. The effects of certain species will be isolated when those species are removed from groundwater by way of pretreatment or are added to synthetically composed solutions. Furthermore, at concentrations found in natural Guanajuato groundwater, the species will be ranked according to their impact on arsenic adsorption.

   Hypothesis: Due to the magnitude of arsenic adsorption interference posed by the Guanajuato groundwater in comparison to the minor interferences reported in literature for typical natural waters, an uncommon species or uncommonly high concentration of a species is the overwhelming factor limiting arsenic adsorption. Some potential interference mechanisms may include: masking of nanomagnetite surface sites by oil and grease originating from the submersible well pump or other dissolved organic compounds, preloading of high silica concentrations associated with the low-level geothermal groundwater, or competitive adsorption of other anions from solution.

3. *Objective:* Compare the impact of high silica concentrations in batch versus column systems.

   Hypothesis: High silica concentrations interfere differently and more severely in column versus batch systems due to the dynamics of silica preloading. These effects are most pronounced when comparing the quantity of arsenic adsorbed in

the head of the column (least pre-loading effect) versus deep within the column bed (greatest preloading effect).

Organization of thesis

The remainder of this introduction (Chapter 1) presents a history of the Guanajuato water supply, the initiation of the university-municipality collaboration, and the progression of research activities of the current work. Chapter 2 reviews the literature on select background information important for understanding this research and its place in the scientific body of knowledge. Chapter 3 gives details of the materials and methods used for the experimental results discussed in Chapter 4. Finally, Chapter 5 closes with a summary of research findings and recommendations for future work.

Overview of Collaboration with Guanajuato municipal water provider

Increasingly, cities in Mexico and Latin America are recognizing the importance that drinking water quality has on public health, hygiene, and even tourism. In 2008, city officials in Guanajuato, Mexico, began working with Rice University to assess and research new methods to improve drinking water quality. They provided a test-bed site for researchers with Rice's Center for Biological and Environmental Nanotechnology to develop nanomaterial-based water treatment technologies suited to address the water quality needs in Guanajuato. The present study addresses one problem area identified as part of an assessment of the Guanajuato municipal water supply: arsenic was present at levels above the Mexican contaminant limit for one of the municipal wells used for the public water supply. In prior work (Farrell 2009), laboratory adsorption isotherm and column experiments were used to estimate cost and understand design and operating

parameters for removal of arsenic by adsorption to magnetite nanoparticles in packed column reactors. From that point on, later work, as described in this report, focused on application to groundwater in Guanajuato. When promising results were obtained in the laboratory, pilot-columns were built for field-trials in Guanajuato in cooperation with local contacts to test various hypotheses with actual groundwater conditions, closest to the point of potential application. By interpreting laboratory and field experiments, modeling adsorption and transport, and researching the published literature, the factors that influence arsenic adsorption to magnetite-packed columns were investigated. This work evaluated methods to further enhance arsenic adsorption in natural waters.

Background on Guanajuato

Guanajuato, Mexico, is one of the most densely populated Mexican states with almost five million inhabitants and over 150,000 people living in the capital city, also named Guanajuato (Figure 1). Industrial production is focused on silver and gold mining, oil, clothing manufacturing, and tourism. Because of its beauty and its historical importance as the world's leading silver mining center in the 18th century, Guanajuato has been designated as a UNESCO World Heritage site.

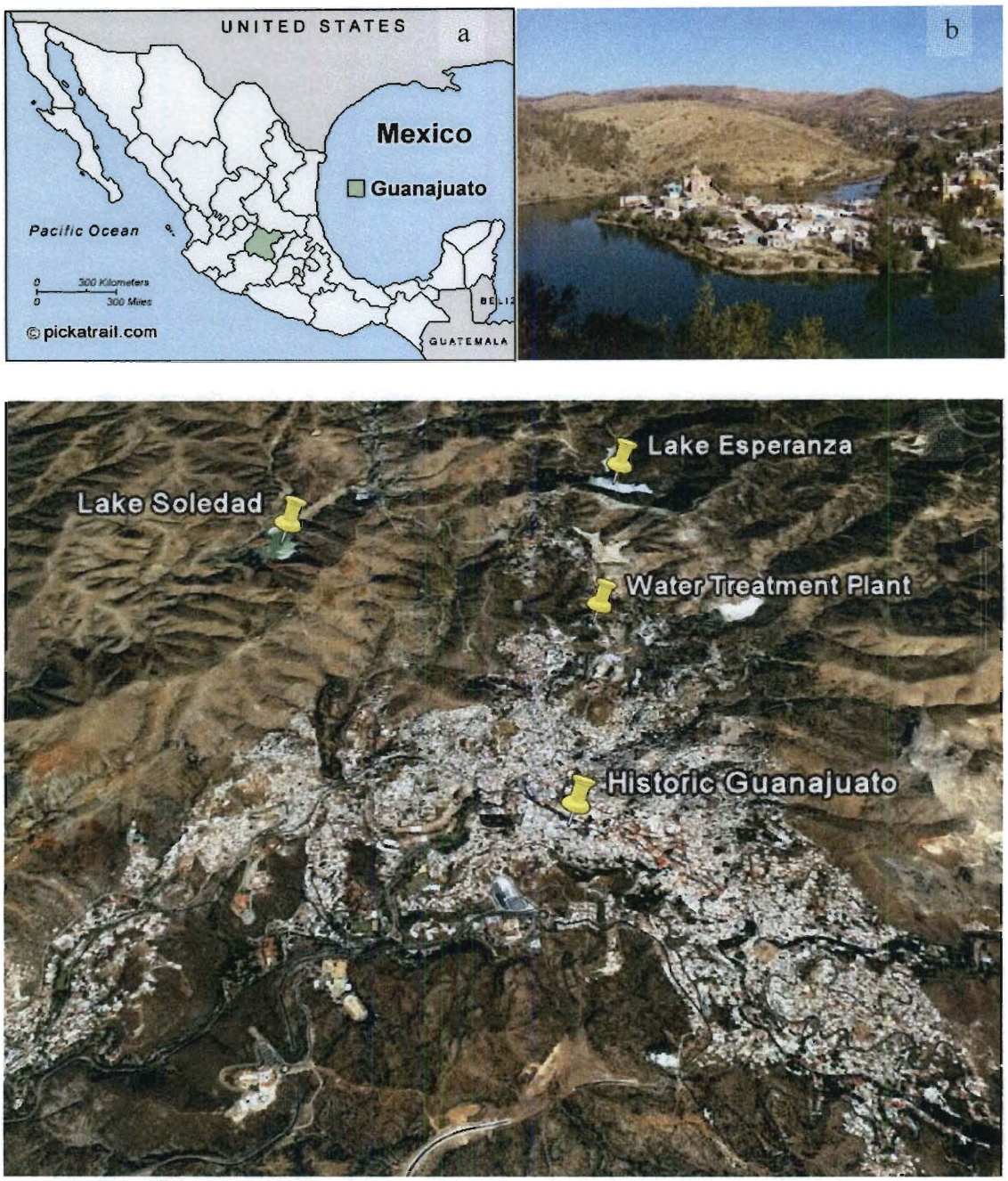

Figure 1 - (a) The state of Guanajuato, Mexico. (b) Lake Soledad. (c) Bird's-eye view of Guanajuato.

Before construction of their first dam in 1749, Guanajuato residents relied on an adjacent river for their water supply (Simapag 2009). During extremely dry seasons, the river would go dry, and the town residents resorted to drinking water from deep mines, which resulted in many fatalities. The first dam provided sufficient water supply year

round, and 100 years later, it was connected to 12 distribution fountains in the city where residents would come to purchase water (Figure 2a). In 1880, a large dam was built and named La Esperanza, meaning 'The Hope' in Spanish, which increased supply enough for residents to have running water in their homes (Figure 2b). The pipes supplied raw, untreated river water to city homes until the first water treatment plant was built in 1954. In 1983, deep groundwater wells were constructed to supplement the water supply in the city. While the city has spent millions over the last decade to improve water quality and supply, there are still concerns that heavy metals from the historic mines, microbial contamination, or other unknown hazards are present in the water that detrimentally affect the health of Guanajuato residents. City officials are also concerned with the elevated levels of arsenic in the municipal groundwater wells, from which 60% of the city now receives its water.

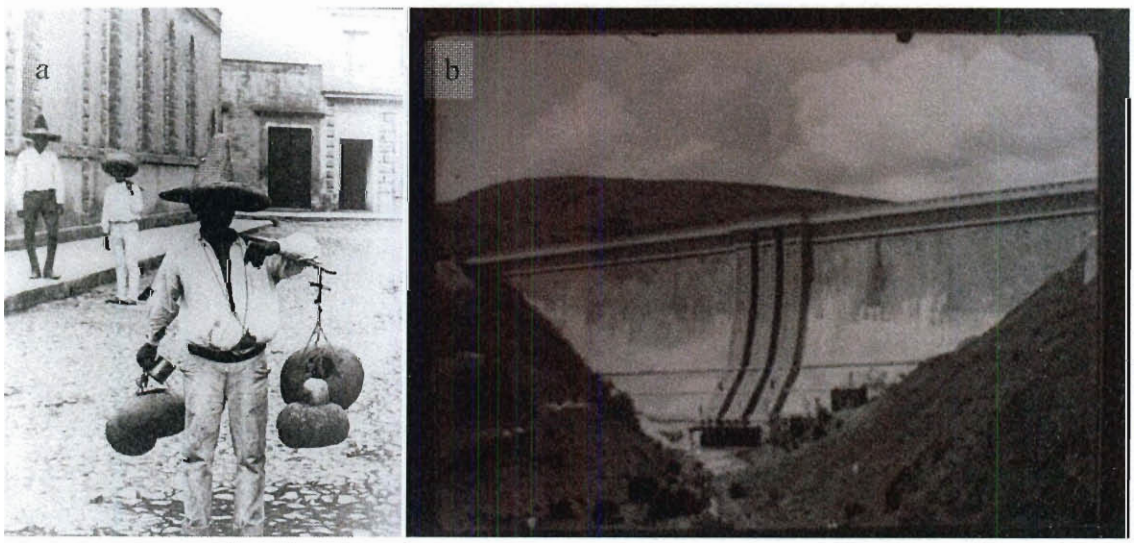

Figure 2 - Photos: (a) Carrying water in historic Guanajuato prior to 1880 and (b) the La Esperanza dam after completion (1880).

Collaboration established

In the summer of 2008, a delegation from the Center for Biological and Environmental Nanotechnology (CBEN) were invited to Guanajuato, Mexico, to understand health-related concerns related to the municipal water quality and to explore opportunities for collaboration using novel nanotechnologies developed at Rice. The delegation included Carlos Garcia and Jesse Farrell, and Drs. Vicki Colvin, Pedro Álvarez, Mason Tomson, and John Fortner. During the initial visit, city, state, and federal government officials as well as representatives from the local university expressed their support for collaboration with CBEN to assess water quality issues in Guanajuato and to develop and test appropriate, nanomaterial-based treatment options for water issues affecting Guanajuato. The director of the city water company, Simapag, agreed to make lab and office spaces available and to facilitate the test-bed work (Figure 3). The decision was made to move forward with an assessment of the city water system.

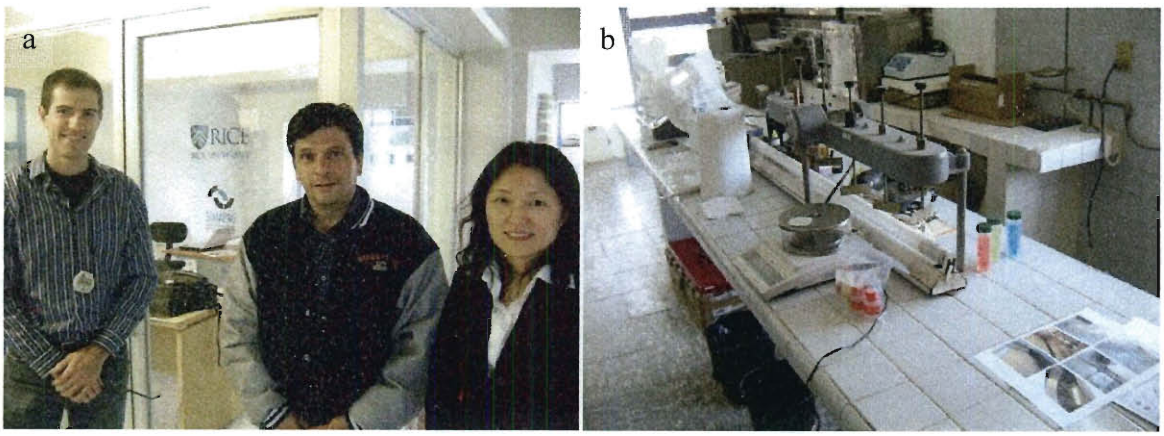

Figure 3 - Photos of the (a) office space and (b) lab space provided by Simapag. Pictured from left to right: Jesse Farrell (Rice student), Raphael Zárate-Araiza (Simapag director), and Dr. Qilin Li (Rice professor).

Water quality assessment

After an initial assessment of water samples (see Appendix A) sent to Rice University from Guanajuato in the summer of 2008, a field trip was made in January 2009 to conduct an extensive sampling of the city water system, from the lake and groundwater sources to every stage in the drinking water treatment plant and finally, to the city residents (Figure 4). For this assessment, water quality parameters were measured at each site, and samples were taken and preserved both for additional testing in the provided Guanajuato lab space and back at Rice University.

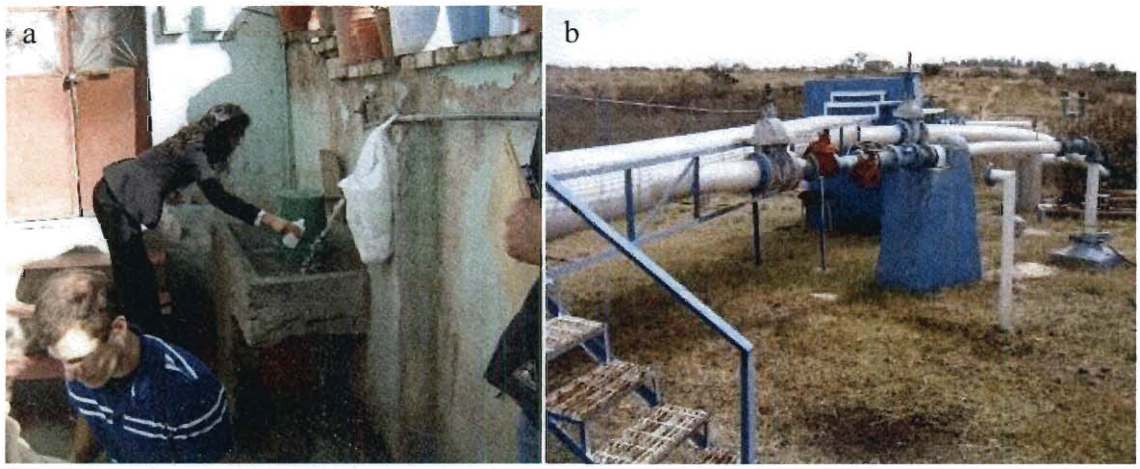

Figure 4 – Photos of (a) CBEN researchers Jesse Farrell and Dr. Qilin Li sampling at a home in Guanajuato, and (b) a groundwater well sampling site.

The water assessment from this trip (see Appendix B) highlighted three problem areas for the city.

The first issue identified was the groundwater contained elevated concentrations of arsenic and other heavy metals, and one well produced water at or above the current Mexican permissible contaminant level. Strictly as a health matter, removing arsenic from this groundwater would reduce the incidence of arsenic-related diseases. In addition, as a practical matter, removing arsenic from this groundwater would preserve the current water supply, because, if groundwater arsenic concentrations were to increase

or if Mexican regulators were to lower the acceptable limit to the current WHO standard, that well would have to be decommissioned. While arsenic and other heavy metals were also found in the river water and surrounding sediments, those concentrations were low enough not to be of concern.

A second issue identified relates to the local practice of routing all water through household-scale storage tanks on the rooftop of each building. The chlorine introduced at the municipal treatment plant is not sufficient to preclude biological contamination for the long holding periods in the tanks, so biological contamination is common, resulting in various health problems. This use of storage tanks in Guanajuato was copied from other communities in Mexico and Latin America where water utilities were unable to provide a continuous supply of water. Despite the fact that continuous water supply is not an issue in Guanajuato, such storage tanks are prolific in the city. Others at Rice (e.g. Alvarez and Colvin) are studying the use of novel nanomaterials to disinfect biologically contaminated water, but that is not within the scope of the present research.

A third issue relates to high iron concentrations and seasonal variability of turbidity in the surface water used in the city's water supply, which make dosing for effective coagulation and flocculation difficult at the treatment plant. When treatment of these surface waters is inadequate, turbid water can be released into the distribution system and pose health and aesthetic concerns. However, by retrofitting their coagulation/flocculation process and building an additional water treatment plant in 2010, Guanajuato officials have mitigated this third issue.

Research, development, and field testing with nanomagnetite packed-columns

In January 2009, engineering design and testing began at Rice to incorporate magnetite into sand-based columns to enable the removal of arsenic. Several variables were examined including, but not limited to: various water sources (synthetic, river water, groundwater), solution conditions, chemical additions, flow rates, residence times, sand to magnetite mixing ratios, column packing methods, and adsorbent selection (Farrell 2009). From the lessons learned, a pilot column experiment was designed and materials were acquired and shipped to Mexico for a field study. The selection of a commercially available, affordable, and food-grade nanomagnetite product made field testing more practical. A Houston-based plumbing company (C&B Plumbing) assisted in materials selection and design review of the pilot-columns.

In December 2009, researchers from Rice University spent eight days in Guanajuato building and testing a pilot-scale nanomagnetite column (Figure 5). Although the group originally planned to test the column directly connected to the arsenic-contaminated well, due to a malfunction in the submersible wellhead pump, water could not be provided from the intended well. Therefore, samples were brought from three other wells and water quality was assessed in an attempt to determine the groundwater with the most optimal conditions for arsenic adsorption. An alternate well was chosen (Municipal Well No. 8) based on its high arsenic concentration (Hach test), low phosphate interference, and high redox potential. To avoid the risk of another submersible pump failure, a 10,000 liter capacity truck was filled with groundwater from Well No. 8 and brought to the drinking water treatment plant lab for the pilot-column experiment. The first pilot column that was built leaked from an endcap seal and had to

be discarded. The second pilot column was water-tight and ran for three days, and water samples (treated and untreated) were brought back to Rice University for analysis. The results from the pilot-column experiment, as described later in the Results section, successfully demonstrated a proof-of-concept for arsenic removal by nanomagnetite.

Figure 5 - Rice University researchers John Fortner, Isabel Raciny, and Jesse Farrell inside the Guanajuato water treatment plant lab with the first nanomagnetite pilot column.

After the first field trial, parallel bench-scale columns at Rice University revealed that arsenic removal was over 10-fold greater for a column fed a synthetic feed solution than that fed an As-spiked groundwater solution. This disparity was investigated in batch systems both through the removal of groundwater components by various pretreatment methods and through addition of potentially interfering components to synthetic solutions. The interference was strongly correlated with the high concentration of silica found in Guanajuato groundwater. Secondarily, it was found that pH reduction improved adsorption, but to a lesser degree than the interference from silica. Activated alumina was tested as an adsorbent for silica; however, the use of the activated alumina as a pretreatment method would not complement arsenic adsorption to nanomagnetite for reasons discussed later in the Results section.

Given the limited options for silica removal, pH reduction was investigated as a means to improve upon arsenic removal and breakthrough in a column setting. In March of 2010, the research group traveled again to Guanajuato to perform a second pilot-scale column test. A 10,000 liter water truck was acidified to pH 5.5 with acetic acid; however after observing breakthrough within 24 hours, a second truck acidified with nitric acid was prepared and tested to eliminate the possibility of adsorption interference by acetate ion. However, neither pH adjustment method significantly altered or improved the arsenic retained by the pilot columns. The nine-day trip also included a demonstration of the pilot-scale columns for the benefit of the Canadian Broadcasting Company and the Guanajuato media. Jade Boyd from the Rice University Department of News and Media Relations traveled with the group and documented the trip by blog and video, which are posted online at http://guanajuato.blogs.rice.edu/ and http://www.youtube.com/watch?v=wKcE__MmzFY, respectively.

After pH adjustment did not improve the performance of the pilot columns in Guanajuato, research work at Rice University was directed to identify column-specific interference effects and how they could be mitigated. That work is described herein.

2. Background and Literature Review

This section summarizes the background and a review of the relevant literature on water treatment using a nanomagnetite adsorbent. The focus of this work has been on arsenic removal; however, as iron oxides are demonstrably effective adsorbents for a host of heavy metal contaminants of concern, this work has broader applications as well. Accordingly, background pertaining to the removal of various heavy metals of health and environmental concern are reviewed with a short summary of pertinent chemical information. Arsenic chemistry, occurrence, and health impacts are then discussed in more depth. The existing technologies for arsenic removal, which are largely shared as treatment methods for other heavy metals, are reviewed. Special attention is paid to literature concerning small scale treatment options, because drinking water contaminated by the highest levels of arsenic is most often found in rural areas with little infrastructure for large scale treatment. Also discussed are other references pertaining to surface complexation modeling, adsorption isotherms, and/or packed column adsorption. Then, arsenic adsorption to various adsorbents is discussed and the effect of other competing/interfering species in solution is examined. Due to the strong interfering effects exhibited by silica (as observed in the literature and in this work), background on silica chemistry, the mechanisms of interference, and various methods for removal are reviewed in depth. This section concludes with a brief review of media regeneration and disposal.

Heavy metal contaminants of concern for drinking water

Heavy-metals are regulated in the United States by the Environmental Protection Agency (EPA) due to their known health impacts even at trace levels from 1-100μg/l

(2002). The EPA has established primary drinking water standards for trace metals likely to occur in some drinking water supplies. These metals include antimony (6μg/l), arsenic (10μg/l), beryllium (4μg/l), cadmium (5μg/l), chromium (100μg/l), lead (15μg/l action level), mercury (2μg/l), selenium (50μg/l), and thallium (2μg/l), with current maximum contaminant levels (MCLs) displayed in parenthesis. The MCLs are enforceable by the US EPA and correspond to the highest level of contaminant allowed in drinking water. For some elements, health risks are known to be minimized further by reducing the concentration of these elements below the MCL but treatment is limited due to current technological limitations and overburdening costs.

As water becomes more and more of a precious resource, treatment processes are often called upon to address multiple treatment objectives. In this work, the removal of arsenic is emphasized due to the current public and scientific interest; however, reductions in other heavy metals are also monitored. Therefore, the nanomagnetite media described herein is not only an arsenic removal media, rather, it can be used as a media for the holistic treatment of various trace-heavy metals. Table 1 describes the heavy metals regulated by the US EPA. Each element will be discussed briefly below, while arsenic will be described in detail afterwards, as it is the primary focus in the present research. Background on the heavy metals is given, especially as it relates to adsorption to iron oxides.

Antimony (Sb), like arsenic, occurs in many different oxidation states (-3, 0, +3, and +5) typically in the form of sulfides or oxides. In natural waters, Sb(III) and Sb(V) occur in the hydroxyl complexes, $Sb(OH)_3$ and $Sb(OH)_5$; however the exact structure is

not known (Baes 1976). The control of Sb may be accomplished through sorption to Fe, Mn, and Al oxides and clay minerals as proposed by Callahan et al. (1979).

Beryllium (Be) is present in water in the +2 oxidation state primarily forming complexes of hydroxide ($BeOH^+$, $Be(OH)_2$, and $Be(OH)_3^-$) in typical environmental conditions or with fluoride when present in elevated quantities. Complexation also occurs with Cl^-, NO_3^-, and SO_4^{2-} but to a much lesser degree than with hydroxides (Rai, Zachara et al. 1984). Little is known about the sorption behavior of Be complexes (Bodek, Lyman et al. 1988).

Cadmium occurs primarily as Cd^{2+} in typical environmental conditions. Sunga and Engel et al. determined that it is the activity of the free Cd^{2+} ion that is important to toxicity (1978). Very little complexation with hydroxide occurs with conditions below pH 8. Complexes of chloride can form in highly saline waters and some organic ligand complexes can form in highly polluted waters, but these complexes are minimal in typical environmental conditions. Through adsorption to calcite and hydrous iron and aluminum oxides, cadmium concentrations in the natural aqueous environments typically remain very low. The adsorption of Cd is strongly impacted by pH, whereby very little Cd is adsorbed below pH 6 and almost all Cd adsorbs above pH 8 (Huang, Elliott et al. 1977; Callahan, Slimak et al. 1979). Besides pH effects, other species impact the adsorption of cadmium. For example, some species reduce cadmium adsorption, such as sulfate and chloride reducing adsorption to amorphous $Fe(OH)_3$ (Daviescolley, Nelson et al. 1984) and Ca^{2+} and Mg^{2+} reducing adsorption to Fe and Mn oxides (Rai, Zachara et al. 1984). Other anion species have been shown to enhance the adsorption of cadmium, such as thiosulfate, humic acid, nitriloacetate, glycine, tartrate, and phosphate (Huang, Elliott et

al. 1977; Kuo and McNeal 1984; Rai, Zachara et al. 1984; Koch 1985). Sorption constants for cadmium are well studied and reported in the literature (Rai, Zachara et al. 1984).

Chromium (Cr) is found commonly in the +2, +3, and +6 oxidation states, although Cr(II) is not stable in water above pH 6 and its hydrolysis products are not well understood (Baes 1976). The oxidation state of Cr matters greatly to human health as Cr(III) is classified as an essential nutrient, while Cr(VI) is classified as a carcinogen. The slow kinetics of polymerization of Cr(III) make it difficult to determine the precise distribution of hydrolysis products in solution. Mononuclear species of Cr^{3+} include $CrOH^{2+}$, $Cr(OH)_2^{+}$, $Cr(OH)_{3(aq)}$, and $Cr(OH)_4^{-}$, but these slowly convert to $Cr_2(OH)_2$ and $Cr_3(OH)_4^{5+}$ at 25°C. Cr(VI) is hydrolyzed in water to form the anionic species CrO_4^{2-}or $HCrO_4^{-}$ in natural waters, or $Cr_2O_7^{2-}$ at very high chromium concentrations that may occur in industrial contamination scenarios. The distribution of these species depends on pH, redox potential, and the concentration of other complexing ligands in solution, all of which also affect adsorption. Callahan et al reports that Cr(VI) does not adsorb significantly to hydrous metal oxides (1979), while James and MacNaughton et al. report that Cr(VI) adsorption decreases as pH increases (1977). Cr(VI) adsorption can be further reduced by competing species such as sulfate or phosphate ions or by formation of aqueous complexes such as calcium chromate (Rai, Zachara et al. 1984). Callahan et al. reports that Cr(III) is adsorbed 30 to 300 times more strongly than Cr(VI) onto clay minerals (Callahan, Slimak et al. 1979). In contrast to Cr(VI), Cr(III) adsorption increases as pH increases, and iron and manganese oxides are able to adsorb Cr(III) even at low pH (Rai, Zachara et al. 1984). Manganese oxides can convert Cr(III) to Cr(VI) in

soils, organic matter can reduce Cr(VI) back to Cr(III) (Bartlett and Kimble 1976). Anaerobic conditions can also rapidly convert Cr(VI) species to Cr(III) species which then may readily precipitate as hydroxides or oxides (Schroeder and Lee 1975).

In natural waters, lead typically only occurs as Pb(II). Lead(IV) and Pb(0) can be found, respectively, in extremely oxidizing and in strong reducing environments. Lead forms complexes with hydroxide significantly above pH 5, but is almost exclusively present as the Pb^{2+} ion in more acidic conditions. $PbOH^{+}$ is the predominant form of Pb in neutral pH conditions. Lead also forms complexes with other inorganic and organic constituents including but not limited to carbonate ion, chloride ion, humic acid, formic acid, and acetate. Lead is typically removed from solution by ion exchange, specific adsorption, co-precipitation with hydrous oxides, or adsorption to clay minerals and oxides of manganese and iron (Callahan, Slimak et al. 1979). Adsorption tends to increase with increasing pH (Rai, Zachara et al. 1984). In one study, the fraction of adsorbed lead to soil increased with the addition of humic acid (Huang, Elliott et al. 1977). Researchers of the study proposed two possible mechanisms of enhanced adsorption: humic acid anionic ligands may adsorb to surface sites and then complex with the cationic lead species in solution; or alternatively, lead first forms complexes in solution with anionic ligands, which then adsorb as a unit to specific surface sites.

Mercury can be present in natural environments in the oxidation state of 0, +1, and +2. Hg(II) hydrolyzes with water and functions as an acid with $Hg(OH)_{2(aq)}$ being the predominant form in neutral aerobic waters. Mercury is strongly adsorbed to hydrous iron and manganese oxides, clays, and organics as the primary environmental sinks in

natural systems (Perwak, Goyer et al. 1981). Adsorption of mercury is hysteretic[1]. Once adsorbed, desorption is negligible as one study found less than 1% removal after 70 hours of agitation of mercury contaminated sediments in deionized water (Ramamoorthy and Rust 1976). Not only is adsorption/desorption equilibrium partitioning different, but the kinetics are also shown to be much more rapid for adsorption than for desorption, with one study finding adsorption kinetics rate constants to be 10^3-10^5 times larger (Lockwood and Chen 1973). The approximate median value of literature data compiled by Bodek et al. for Hg sorption to iron oxides is given as 1,000 l/g (10^6 L/kg), indicating high affinity for iron-oxide surface sites (1988).

Selenium occurs in natural environments with the oxidation states of -2, 0, +4, and +6. The chemistry of selenium is similar to that of sulfur as might be expected as both appear in Group VI of the periodic table. Both form oxyanions in water, with the species depending on the Eh and pH conditions. Selenites (SeO_3^{2-}) and selenates (SeO_4^{2-}) are the most common forms of Se (IV) and Se(VI), respectively. The selenites can be rapidly reduced to the highly insoluble Se under mildly reducing conditions below pH 7 (Callahan, Slimak et al. 1979). In contrast to the rapid reduction, the oxidation of Se back to SeO_3^{2-} is a very slow process. Experimental evidence suggests that forms of silica, alumina, and iron(III) oxide control selenium adsorption. Selenite and selenate both adsorb strongly onto goethite (irreversible), amorphous iron (partially reversible), and gibbsite (reversible) in acidic conditions, and the degree of adsorption decreases with increasing pH (Rai, Zachara et al. 1984). The competing species of sulfate and phosphate contend for adsorption sites with selenium oxyanions and have been shown to desorb 90% of adsorbed selenite and selenate. Adsorption of selenate and selenite onto clays

[1] Hysteresis means the process of desorption does not follow the same path as adsorption.

and oxides follows Langmuir behavior and constants are available in the literature (Hingston, Posner et al. 1968; Little 1984). The removal of selenate can also be accomplished by ion exchange, and behaves similarly to sulfate in that regard (Rai, Zachara et al. 1984).

Thallium occurs in the oxidation states of +1 and +3 in environmental conditions. At the pH and Eh of natural waters, the Tl^+ species predominates. Tl^+ displays some similarities to alkali metals as TlOH is soluble in water and dissociates to form highly basic solutions. Tl^+ is also similar to Ag^+ in that it forms insoluble sulfides and light-sensitive halide complexes that are minimally soluble. Some affinity for adsorption to metal oxides has been suggested, although more work has focused on the great affinity of Tl^+ to clays (Callahan, Slimak et al. 1979).

Table 1 - Trace heavy metals regulated by the US EPA.

Species	EPA MCL	Health Effects	Potential sources into Drinking Water	Chemical form
Antimony	6 µg/l	Increase in cholesterol; decrease in blood sugar	Petroleum refinery discharge, fire retardants, ceramics, solder	$Sb(OH)_3$ $Sb(OH)_5$
Arsenic	10 µg/l	Skin and circulatory problems, elevated cancer risk	Release from natural deposits, runoff from orchards, glass work, or electronics production waste	H_3AsO_3, H_3AsO_4
Beryllium	4 µg/l	Intestinal lesions	Discharge from metal refineries, coal burning factories and from electrical, aerospace, and defense industries	$Be(OH)_2$
Cadmium	5 µg/l	Kidney damage; accumulated/retained in the human body	Corrosion/erosion from galvanized pipes, natural deposits; leaching from batteries and paints, discharge from metal refineries	Cd^{2+}
Chromium (total)	100 µg/l	Allergic dermatitis	Discharge from steel and pulp mills, erosion of natural deposits	$CrOH^{2+}$ and polymers; CrO_4^{2-}, $Cr_2O_7^{2-}$
Lead	15* µg/l Action level	Children: delays mental, physical development. Adults: kidney problems and high blood pressure	Corrosion of plumbing: pipes, solder, fittings; erosion from natural deposits	$Pb(OH)^+$
Mercury (inorganic)	2 µg/l	Kidney damage	Erosion of natural deposits, discharge from factories, refineries, runoff from landfills and cropland	$Hg(OH)_2$
Selenium	50 µg/l	Hair or fingernail loss, numbness in fingers and toes, circulatory problems	Discharge from refineries and mines, erosion of natural deposits	Se(IV), Se(VI), Se(0), Se(II-)
Thallium	2 µg/l	Hair loss; blood changes; kidney, intestine, or liver problems	Ore-processing sites, discharge from electronics, glass, and drug factories	Th(I), Th(III)

Arsenic chemistry, occurrence, uses

For the majority of the world's population, the primary route of arsenic exposure is through drinking water (Farrell 2009). Arsenic can occur in the –III, 0, +III, and +V oxidation states; however, inorganic As(V) predominates in the elevated redox conditions

of oxygenated waters. As pH increases, arsenate undergoes deprotonation from H_3AsO_4 to $H_2AsO_4^-$, $HAsO_4^{2-}$, and AsO_4^{3-} according to the pK_a values of 2.1, 6.7, and 11.2, respectively, similar to ortho-phosphate (H_3PO_4). In a reductive environment and below pH conditions of 9.1 As(III) predominates in the form of inorganic arsenite (H_3AsO_3). The pK_a values for the deprotonation of H_3AsO_3 to $H_2AsO_3^-$, $HAsO_3^{2-}$, and AsO_3^{3-} are 9.1, 12.1, and 13.4, respectively. The predominance diagram in Figure 6 displays the species of highest concentration in the common span of solution pH conditions and redox potentials for arsenic on top of an iron oxide template.

The region of pH and redox equilibrium encountered for all experiments in the present work conducted with Guanajuato well water measured between 200 to 300mV and between pH 5.5 to pH 8.7, and with the majority of experiments conducted between pH 7 to pH 8.5. As(V) species predominate in the entire region, and the surface of magnetite would be expected to oxidize to ferric hydroxide in the presence of water at the given redox potential.

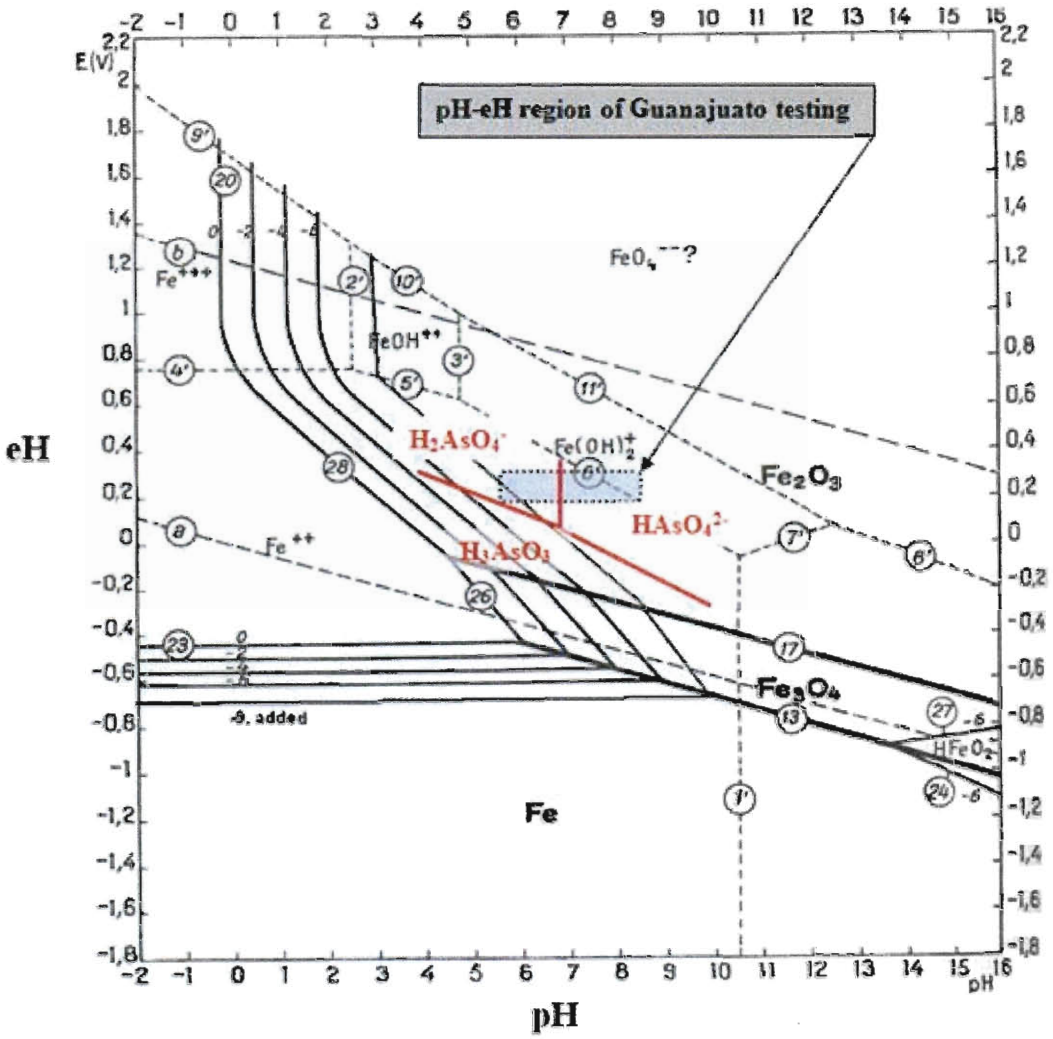

Figure 6 – A Pourbaix diagram for iron at 25°C and 1atm. The shaded region, enclosed by a dotted line, represents the conditions encountered in the present work for experiments with Guanajuato groundwater. The predominant arsenic speciation in that region is superimposed on the diagram in red (adapted from Pourbaix (1924)).

Given an average concentration of 1-1.8 ppm by weight, arsenic is the 20th most common element in the earth's crust (Matschullat 2000). Seawater also contains arsenic in concentrations between 1 and 2µg/l (Barbalace 1995-2009). Except for incidences of localized industrial contamination, arsenic usually enters the groundwater through interaction with the geological formation through natural processes of oxidation-

reduction, ligand exchange, adsorption, and precipitation (Ferguson and Gavis 1972). This is the case in the United States, where naturally occurring arsenic is present in elevated concentrations through parts of the southwest, midwest, northeast, and South Texas (Figure 7). In a 1997 review of US water supplies, arsenic above 0.5µg/l was present in 73% of surface water sources and 58% of groundwater sources. After treatment, it was estimated that 25% of all community water suppliers provided water with arsenic above 2µg/l, 6-17% provided water above 5µg/l, and 1-3% provided water above 20µg/l at the time of the survey (Frey and Edwards 1997).

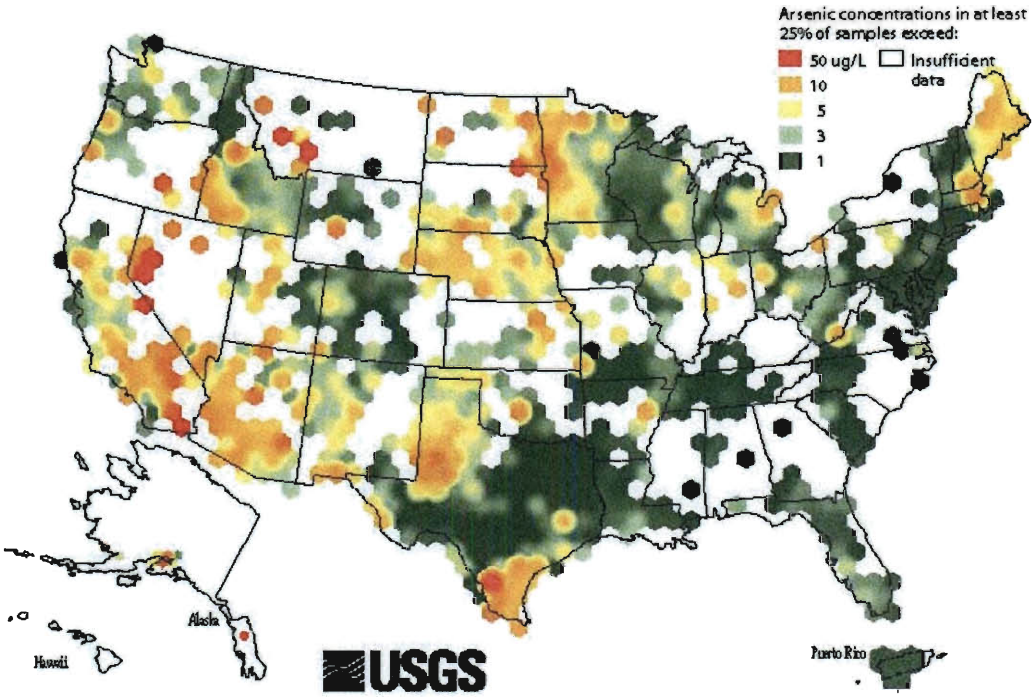

Figure 7 - Arsenic concentrations found in at least 25% of ground-water samples within a moving 50km radius (Ryker 2001).

Besides the United States, Mexico also has large regions of groundwater containing elevated arsenic concentrations above 10 and 50 µg/l (Hurtado-Jimenez and Gardea-Torresdey 2006; Armienta and Segovia 2008). In one such region, the

Transmexican Volcanic Belt, geothermal fluids have arsenic concentrations between 1 to 100 mg/l. Birkle and Bundschuh et al. found the arsenic concentrations were linked to geothermal species such as Si, Li, and B (2010), pointing to As dissolution from the host rock as the likely source. Arsenic concentrations in the geothermal waters is similar to the prediction of hot water-rock leaching experiments conducted with volcanic rock. These experiments showed leaching of arsenic in concentrations of 1.3 mg/kg directly from the rock, and thus direct interaction of magmatic fluid was determined not necessary to elevate arsenic concentrations to levels seen in geothermal reservoirs (Ellis and Mahon 1964). Evaporation of seawater would be another possible source if chloride and arsenic concentrations were correlated; however, this is not the case in the Transmexican Volcanic Belt (Birkle, Bundschuh et al. 2010). Drinking water is not typically produced directly from geothermal fluids; however, mixing with other groundwater and discharge to surface water can affect surrounding water quality. As an example, this is seen in Yellowstone National Park, USA, where geothermal springs containing over 1mg/l of arsenic (Ball 1998) contaminate downstream surface waters including the Madison River to 0.36mg/l (Nimick 1994). Where evidence of geothermal activity is present, the ground and surface water sources nearby may be affected.

The release of arsenic from anthropogenic sources in the industrial age has been primarily due to arsenic mining and combustion of coal and petroleum (Han, Su et al. 2003; Ongley, Sherman et al. 2007; Gutierrez, Alarcon-Herrera et al. 2009). Current production is around 47,000 metric tons per year. One study of mining areas in the Salamanca Province in Spain showed extreme arsenic contamination (>1000 mg/kg) in soils near mine tailings, but found that contamination plumes were limited to less than

500m (Garcia-Sandchez and Alvarez-Ayuso 2003). The authors believed that naturally occurring iron oxy-hydroxides in the soil prevented further transport. Mendoza-Amezquita and Armienta-Hernandez conducted leaching tests on mine tailings from the abandoned La Asuncion and Las Torres mines in Guanajuato, Mexico, and found the tailings did not release detectable amounts of arsenic (<2μg/l). Concentrations of arsenic were determined to be 21-25mg/kg and 36mg/kg for mine tailings from the La Asuncion and Las Torres mines, respectively (2006).

During the past 100 years, arsenic has served many uses in herbicides, fertilizers, wood preservatives, animal feed additives, corrosion inhibitors, paint pigments, semi-conductors, metal alloys, glass manufacturing, and medicine (Doyle 2009). In 2003, about 90% of arsenic produced was used as copper chromate arsenate for wood preservation treatment. Arsenic-bearing products are becoming less common as they are phased out with products more benign to health and the environment.

Knowledge of the prevalence of arsenic-containing groundwater is a recent phenomenon due to the historic scarcity of detection methods and high detection limits for arsenic. In Bangladesh and the bordering West Bengal area of India, UNICEF led an initiative with global support in the 1970s to drill millions of tube-wells which curbed one-quarter million fatalities per year which resulting from water-borne diseases transmitted through drinking the raw surface water in the area (Bagla 2003; Meharg 2005). By the 1990s, the number of tube wells grew to more than 10 million. In 1983, Dr. Saha noticed a large number of cases of peculiar skin diseases. One year later he published a study alerting of high levels of arsenic within the groundwater and its widespread effects within his region of Bangladesh (Garai, Chakraborty et al. 1984).

Tragically, it was not until 1996 that the scope of the problem was recognized by the world body, at which time WHO declared the arsenic problem a major public health issue. In Bangladesh, 59 of the nation's 64 districts and 9 districts in West Bengal have arsenic concentrations above the Bangladeshi standard of 50μg/l with some levels measured up to 4,000μg/l (Chowdhury, Biswas et al. 2000).

The primary route of arsenic intake for individuals is through food and beverages (WHO 2004). Arsenic shows up in food (rice, fish) in a less toxic, organic form which the body is better able to process. Organic species, mostly methylated arsenic is most often less than 1% of the total arsenic. Food can also be a route of exposure when cooked with arsenic-contaminated water (Monroy-Torres, Macias et al. 2009).

Arsenic health effects and regulatory limits

Long-term exposure to arsenic continues to be a topic of many epidemiology studies due to the overwhelming causal link to cancers of the skin, lung, bladder, and kidney in addition to skin pigmentation, skin thickening or hyperkeratosis, neurological disorders, muscular weakness, loss of appetite, and nausea (Jain and Ali 2000; Mandal and Suzuki 2002). The most comprehensive statistical study on human subjects was performed in an area of Taiwan where approximately 100,000 people had lived subsiding on groundwater for over sixty years with elevated arsenic concentrations (Tseng 1977). The study surveyed 40,421 inhabitants and follow-up was made with 1,108 cases of blackfoot disease, a form of gangrene. The overall rates of blackfoot disease were 8.9 in 1,000 and of skin cancer were 10.6 in 1,000 in the area. An increase in the adverse effects was correlated with the household groundwater sources with greater arsenic content.

In one study, elevated levels of arsenic exposure by mothers during pregnancy was correlated with increased alteration of gene expression, which may lead to higher risk of cancer for children later in life (Fry, Navasumrit et al. 2007). Even though the children may never drink contaminated water, their prenatal exposure may have lasting damage. This premise was confirmed in mice exposed to arsenite in-utero through maternal exposure. The adult offspring had high incidence of urinary bladder, lung, and liver cancers.

There is growing interest in the potential links between arsenic and type-2 diabetes (Coronado-Gonzalez, Del Razo et al. 2007), reduction in IQ (Rocha-Amador, Navarro et al. 2007; Rosado, Ronquillo et al. 2007), and Alzheimer's disease (Gong and O'Bryant 2010). Navas-Acien recently published a studying confirming statistically that those affected by type-2 diabetes had higher concentrations of arsenic in their urine, an indicator of arsenic exposure (2008).

Based on the growing body of knowledge, the US EPA reevaluated previous acceptable limits. In January of 2001, they agreed to modify the maximum contaminant limit from 50µg/l to 10µg/l and set a maximum contaminant level goal of 0µg/l. These limits were set in recognition of the balance between adverse health effects and the high cost of treatment that would be imposed, especially on small water systems. Compliance to the new rule became required in January 2006.

Methods of arsenic removal

There are, at least, four primary categories of arsenic removal methods: precipitation, membrane filtration, ion exchange, and adsorption (Feenstra, Erkel et al. 2007).

Precipitation is the most common technique, whereby iron or aluminum salts are used to co-precipitate arsenic and are then separated from solution. Only partial removal of As(III) is accomplished by this method so chlorine or permanganate is commonly used as a pretreatment to first oxidize As(III) to As(V). In the case of iron coagulation, hydrous ferric oxide (HFO) is formed during hydrolysis. HFO has high affinity for arsenic and extremely high surface area (estimated near 600 m^2/g) resulting in quick and effective removal. One drawback is that HFO is amorphous and therefore more difficult to separate from the treated water. Separation is usually accomplished through sedimentation and rapid sand filtration or microfiltration. Precipitation systems also require technical expertise for operation and maintenance, an ongoing supply of chemicals, and a method in place for disposal of the filtered waste. Although precipitation processes are economical at large scale and appropriate for centralized treatment systems, they are not easily scaled down for remote village wells where arsenic-contamination is often the worst.

Reverse osmosis, nanofiltration, and electrodialysis can be used to remove arsenic and at smaller-scale; however, these techniques generally require skilled operators and high operation and maintenance costs. Membrane technologies are among the most expensive of the treatment options (Mohan and Pittman 2007).

Ion exchange processes involve the exchange of arsenate anions in solution for anions electrostatically bound to a solid substrate. Nonionic arsenite must first be preoxidized to arsenate to enable removal by an anionic exchange resin. The substrate is often a synthetic exchange resin which can have some selectivity for arsenate, but there will always be other arsenic-like anions in solution that will compete for ion exchange

sites. Competition effects can be severe and regeneration is required to renew the system once it becomes saturated. The concentrated contaminant in the spent regeneration solution is a disposal issue.

Adsorption can be an effective method for arsenic removal. Adsorption processes typically involve passing water containing a certain adsorbate through a column packed with adsorbent media. The adsorbate partitions strongly to the adsorbent media and is removed from solution. High removal efficiencies are obtainable due to equilibrium partitioning at each incremental length through the column. Adsorption processes scale-down well as they require little capital infrastructure or technical expertise. However, solid adsorbents typically have low surface area ($<20 m^2/g$) in comparison to HFO ($\sim 600 m^2/g$), produced from dissociation and hydration of $FeCl_3$. Therefore, precipitation processes are more cost-effective for large water demands when infrastructure and technical support are available. Still, adsorptive materials are easier to separate from solution than HFO used in precipitation processes. Common adsorbents include iron oxide and oxy-hydroxide media such as granular ferric hydroxide (GFH), activated alumina, titanium dioxide, iron coated sand, polymer supported metals, and surface modified activated carbon (Huang and Fu 1984; Hristovski, Westerhoff et al. 2009).

Performance review of arsenic adsorbents

Direct comparison of arsenic adsorbents is complicated by the differing solution conditions and methods used in various studies.

Table 2 displays the published adsorption capacities of several arsenic adsorbents with corresponding solution conditions. Nanomagnetite (12nm) is by far the most competitive

adsorbent listed for As(III) on a surface area basis. In addition, these 12 nm particles are superparamagnetic, facilitating removal with a low field, permanent magnet (Yavuz, Mayo et al. 2006). On a weight basis, the iron oxides and the titanium dioxide adsorbents display the highest affinity for arsenic. There are many studies on low-cost, locally available materials that could act as appropriate adsorbents in some cases (Mohan and Pittman 2007; Abo-El-Enein, Eissa et al. 2009). A case-by-case review and analysis would be needed to select the most ideal adsorbent to accomplish water treatment objectives for a given scenario and water composition.

Table 2 – Comparison of As(III) and As(V) adsorbents. (Adapted from Shipley 2007)

Adsorbents			Valence State	Adsorption capacity		Solution Conditions	References
Mineral	Size (nm)	SSA* (m^2/g)		$\mu mol/m^2$	mmol/g		
HFO		600	AsIII	5.85	3.51	pH=8	Dixit and Hering, 2003
			AsV	4.47	2.68	pH=4	
Geothite			AsIII		0.173	pH=8	
			AsV		0.1730	pH=4	
Fe_3O_4			AsIII		0.332	pH=8	
$Fe(OH)_3$			AsIII		0.488	pH=7	Pierce and Moore, 1982
$Fe(OH)_3$			AsV		1.5	pH=4	
Fe_3O_4	300	3.7	AsIII	5.62	0.021	pH = 8.0	Yean et al., 2005
Fe_3O_4	20	60	AsIII	6.48	0.388	pH = 8.0	
Fe_3O_4	11.72	98.8	AsIII	18.22	1.800	pH = 8.0	
Fe_3O_4	300	3.7	AsV	3.89	0.014	pH = 4.8	*As_{eq}=34mg/l for entire study*
				2.70	0.010	pH = 6.1	
Fe_3O_4	20	60	AsV	2.54	0.152	pH = 4.8	
				1.69	0.101	pH = 6.1	
				1.32	0.079	pH = 8.0	
Fe_3O_4	11.72	98.8	AsV	23.30	2.300	pH = 8.0	
β-FeOOH	2.6	330	AsV	5.4	1.79	pH = 7.5	Deliyanni et

						IS = 0.1 M	al., 2003
Iron-oxide Coated Sand		10.6	AsIII AsV	0.05 0.05	0.00 0.00	pH = 7.6 As_{eq}=100µg/l	Thirunavuk-karasu et al., 2003
Activated Alumina		370	AsIII	0.01	0.00	pH = 7.6 As_{eq}=1mg/l	Singh and Pant, 2004
Activated Alumina		195	AsV	0.63	0.12	pH = 7.0 As_{eq}=50µg/l	Takanashi et al., 2004
TiO_2		334	AsIII AsV	2.39	0.80 0.50	pH = 4.0 As_{eq}=113mg/l	Dutta et al., 2004
TiO_2		251	AsIII AsV	1.50	0.43 0.55	pH = 7.0 As_{eq}=80mg/l	Bang et al., 2005
GFH			AsV		0.03	pH = 8-9 As_{eq}=100mg/l	Daus et al., 2004
GAC		1065	AsIII AsV	0.00 0.06	0.00 0.06	pH = 7.0 As_{eq}=1mg/l	Reed et al., 2000
Iron-oxide impregnated GAC		840	AsIII AsV	0.07 0.07	0.06 0.06	pH = 7.0 As_{eq}=1mg/l	Reed et al., 2000

Magnetite nanoparticles show particular promise as an arsenic removal media. As displayed in the chart above, Yean et al. and Mayo et al. found that by reducing nanomagnetite particle size from 300nm to 12nm, adsorption increased by almost 200 times, a more than proportional increase in relation to surface area (Yean, Cong et al. 2005; Mayo, Yavuz et al. 2007). Wiesner et al. interpreted this enhanced adsorption per unit area as an example of a true nano-effect (2009). Furthermore, Yavuz and Mayo et al. developed a low-cost batch method to synthesize the high surface area magnetite nanoparticles using common chemicals, potentially reducing the barriers to use as an

arsenic removal media in the developing world (2010). While most arsenic adsorbents are significantly less effective at removing As(III) than As(V), Shipley found that nanomagnetite adsorbs As(III) and As(V) similarly, consistent to the findings of other researchers for magnetite of larger particle size (Ohe K 2005; Gimenez, Martinez et al. 2007; Shipley, Yean et al. 2009). In addition, both As(III) and As(V) hysteretically adsorb to the magnetite surface, minimizing the risk of arsenic release (Yang 2009).

Small scale arsenic treatment methods

Even with advances in many small scale arsenic removal technologies, no solution has emerged as the 'magic bullet' for removing arsenic (Bundschuh, Litter et al. 2010). The complexity of designing appropriate, sustainable solutions for the water needs of differing areas makes this a difficult task. Appropriate solutions vary based on the water chemistry, water quantity and quality required, and cultural acceptability. Furthermore, some technologies are very effective at removing arsenic, but are dependent on a high capital investment, continuing costs, user training, user involvement, a continuous supply chain of materials, etc.

In 2007, the Grainger Challenge competition was held to award the most cost effective, culturally appropriate, and readily sustainable small-scale arsenic treatment system (Hussam 2007). Abdul Hussam won the prize for his work on the SONO filter (Figure 8), a dual-bucket filter that takes advantage of the high surface area of HFO generated from an iron composite for adsorption (Hussam and Munir 2007). It was based largely on the 3-kolshi (or bucket) system in which zero valent iron corrodes, generating HFO in-situ with high surface area for arsenic adsorption. The 3-kolshi filter is very effective at removing arsenic; however, it suffers from rapid decreases in flow rate as the

iron corrodes, forming iron oxy-hydroxide products such as goethite and akaganeite that reduce the porosity of the filter. The ratio of the volume of the corrosion products to the volume of iron before corrosion can range from 2.08 for magnetite to 6.40 for $Fe(OH)_3 \cdot 2H_2O$ (Care, Nguyen et al. 2008). The problem of reduced porosity can be minimized by mixing the zero valent iron with an inert filler material such as sand, gravel, or pumice (Noubactep 2009). The Grainger prize winner does not disclose the specific composition of the active adsorbent material referred to as a composite iron matrix (CIM) but does report that it is made from cast iron chips in a proprietary process.

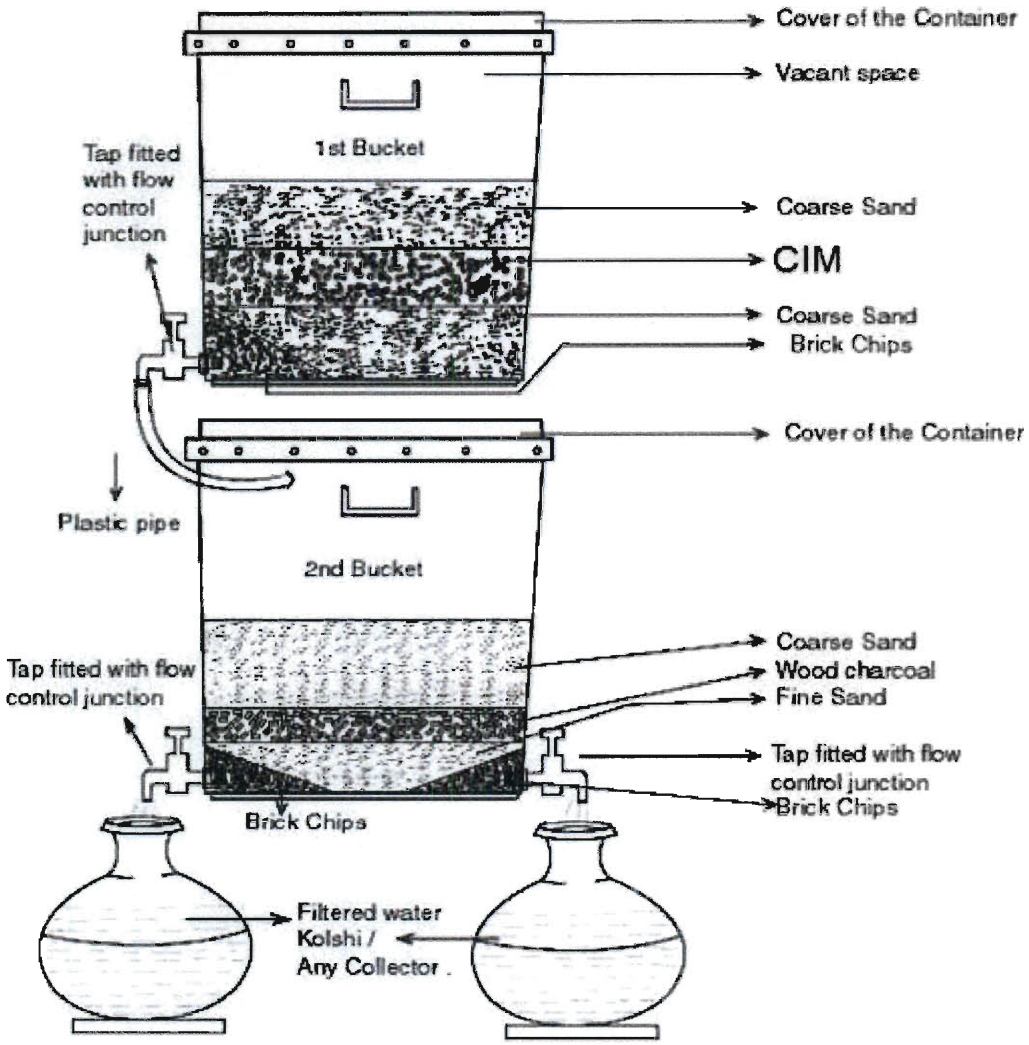

Figure 8 – Schematic diagram of a SONO Filter (Model SF-TWIN, Patent 1003935, 2002)

Still, the SONO filter has its drawbacks. The filter systems have a high capital cost of $45-50 USD, which is 10% of the annual income per capita in Bangladesh. A survey and review by Shafiquzzaman et al. of households with SONO filters after 2 years of use shows 28% were abandoned due to breakage (2009). Other complaints included low flow rates, problems with maintenance, insufficient guidance on disposal, and little sense of ownership. The filters may be one of the best options in use in Bangladesh

currently, but there is room for improvement on both the science and implementation sides.

Another approach, taken by Dr. David Manz from the University of Calgary, was to modify an existing small-scale water treatment process already in use in arsenic affected areas, thereby reducing the challenges of user acceptance and dissemination. The existing technology is sand filtration at the household scale which Dr Manz termed the biosand filter, now numbering over 200,000 in the developing world (Figure 9). Its popularity stems from its simplicity, versatility, low cost and health benefits. The biosand filter removes 95-99% of bacteria, viruses, and other organisms, but it does little to remove arsenic. Typical breakthrough of arsenic through sand occurs after 1-2 bed volumes of filtered water. Dr. Manz, the developer of this technology, endorses the method of extensive pretreatment by chlorination, to oxidize the As(III) to As(V), followed by addition of ferric sulfate for arsenic sorption to hydrous ferrous iron. The solution must be stirred to facilitate coagulation and flocculation and be allowed to settle for one hour. Dr. Manz recommends that the process be repeated twice before pouring the clarified water through the biosand filter. This is an effective method for producing drinking water within quality standards of the WHO, but the method is significantly labor and time intensive and does not easily produce large quantities of water.

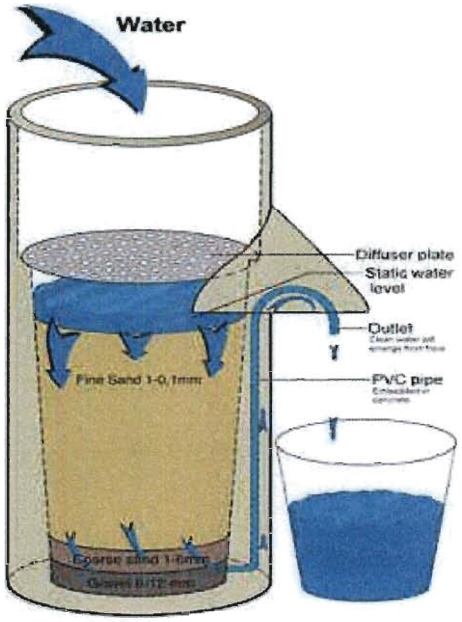

Figure 9 - Depiction of a biosand filter (www.biosandfilter.org)

Other researchers at MIT developed an alternative modification to the biosand filter to enable arsenic removal. Their method involved adding 5 kg of iron nails to the diffuser tray of the biosand filter (Ngai and Walewijk 2003; Ngai, Shrestha et al. 2007). As the iron nails rust and corrode in the presence of oxygen and water, the arsenic adsorbs to the iron-oxy-hydroxides that form, and 83% to 96% removal can be obtained. The study began in 2002 and is continuing in extensive field trials. There are several drawbacks however. The method is effective for As(V), but not for As(III), and performance has shown to be inconsistent in field trials. Chiew et al. found that for three source waters in Cambodia, only 40% to 75% of the arsenic was removed, which left arsenic concentrations in the effluent between 74 and 226µg/l (2009). The reduced effectiveness was attributed to short residence times in the diffuser basin and high concentrations of phosphate and low soluble iron in the influent water. Flow rate also decreased over time as significant amounts of iron deposited into the filters, requiring

frequent cleaning cycles. After each cleaning cycle, the disturbed biofilm layer required days to weeks to regain its effectiveness against harmful pathogens.

In contrast to the MIT work, the present work which applies to incorporating nanomagnetite directly into a sand bed would likely not affect pathogen removal in a biofilm layer above. Arsenic-contaminated water in contact with nanomagnetite mixed into a biosand filter would have a long residence time (>15 minutes) as it percolates through the 40-50cm sand layer. During intermittent pauses, the residence time would increase substantially, effectively eliminating any kinetic limitations to adsorption.

Conventional slow sand and rapid sand filtration

For larger scale operations, nanomagnetite may be compatible with slow or rapid sand filtration. Slow sand filtration (SSF) is recognized by the World Health Organization as one of the simplest, least expensive, and most effective technologies for water treatment. Use of SSF is widespread not only in developing areas, but also for large treatment works in many developed nations such as the United Kingdom, The Netherlands, Germany, and Switzerland (Ray 2002). A typical slow sand filter is displayed in Figure 10. Water is passed downward through approximately 0.9m of sand at flow rates between 0.1 to 0.4m/hr (Huisman 1974), giving a residence time of several hours. The average sand grain size used is approximately 0.3mm. A bed of 0.15-0.9m of gravel acts as a support for the sand. Head loss varies between 0.9 and 1.5m of water. Contact times within a rapid sand filter may be several minutes. After the initial 10-20 days of operation, a gelatinous layer, referred to as the Schmutzdecke or biofilm, develops on the top few millimeters of sand. Bacteria, fungi, and protozoa feed on potentially harmful pathogenic material in the raw water.

Based partially on analysis from the present work, there are several drawbacks foreseen to directly incorporate nanomagnetite into conventional slow sand filters. First, the nanomagnetite aggregates would likely cause an increase in pressure drop unless the aggregates were in the relative size range of the sand particles. Second, finer grain-size may increase the straining of finer particulates in the influent water and require an increased frequency of backwash. Third, backwash cycles may mobilize fine nanomagnetite particles or aggregates into the backwash water. These particles, being nanosize in nature and containing adsorbed arsenic, pose an unknown threat to health and environment wherever they may be disposed. Fourth, the surface adsorption sites of the nanoparticles may be more readily fouled in the presence of sands covered in organic matter, inorganic deposits, and microbial growth. Fifth, when the capacity of nanomagnetite is exhausted for the target contaminant of interest, high pH conditions would be required to regenerate the adsorbent, which may have the adverse affect of dissolving many other species into solution from the sand; this would also harm an advantageous biofilm layer. If nanomagnetite were to be added to conventional slow sand filters, these challenges would need to be addressed.

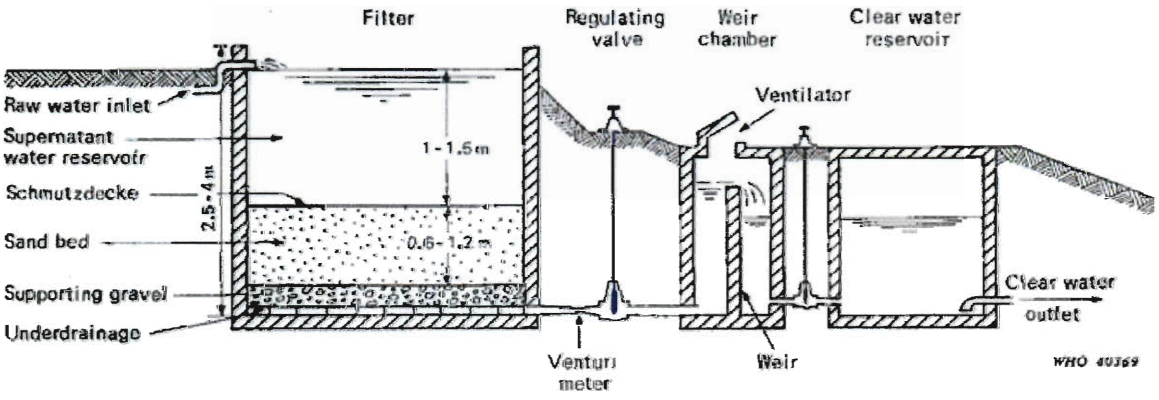

Figure 10 - Diagram of a slow sand filter (Huisman 1974).

Rapid sand filtration (RSF), as pictured in Figure 11, removes turbidity and allows physical adsorption to occur. Rapid sand filtration allows one to treat more water in less space than in slow sand filtration. Larger particle grain sizes are used, between 0.6-2mm, and rapid sand filters typically operate at flow rates between 4-21m/h (Huisman 1974). This results in residence times on the order of a few minutes, which would be sufficient for equilibrium-limited arsenic adsorption to nanomagnetite. However, given the short residence time, the media would reach saturation quickly and require frequent regeneration. Moreover, incorporation of nanomagnetite into rapid sand filters would result in the same set of challenges as described for slow sand filters.

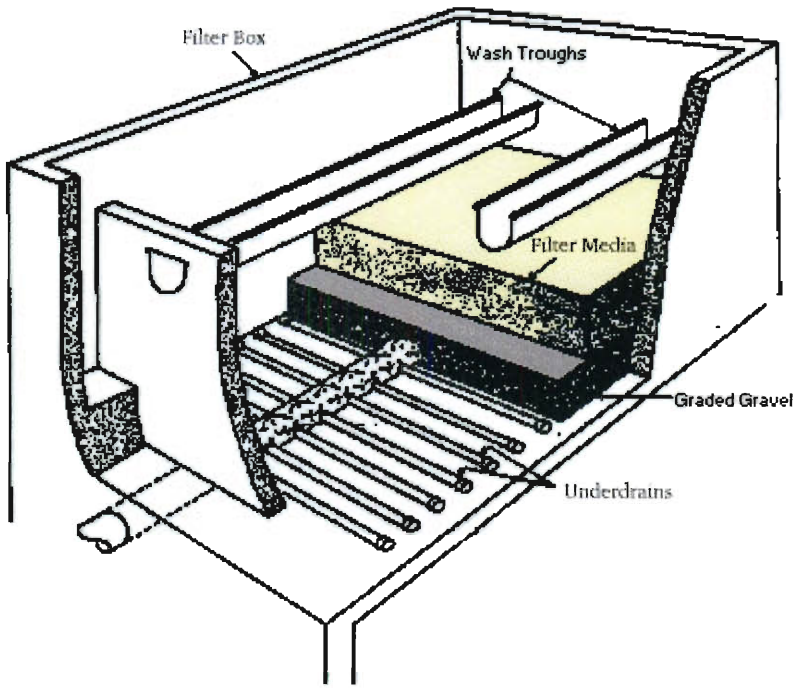

Figure 11 - Diagram of a rapid sand filter (MECC 2009).

CSTR versus packed column reactors

Continuous flow processes allow for increased throughput capacity, reduced capital and human operator requirements, and thus a lower overall cost compared to batch processes. An incremental upgrade from a batch system can be made by the addition of

inlet and outlet streams to a stirred tank reaction vessel. Also known as a continuous stirred-tank reactor (CSTR), the process allows for higher and continuous throughput of water, but it has several disadvantages: slow adsorption kinetics, high nanomagnetite requirements to accomplish the same arsenic removal as a batch process, a more complicated design, significant user involvement or electricity required, and potential for the treated water to contain traces of nanomagnetite with bound arsenic.

When nanomagnetite is incorporated into a plug flow reactor or, more specifically, a packed column reactor, many drawbacks of the SSF, RSF, and CSTR are avoided. From a reactor design perspective, the reduced capital, energy requirements, and mechanical complexity of a column provide clear advantages over a CSTR system. In a packed column reactor, the nanomagnetite is fixed in place as water percolates through the length of the column. Arsenic removal is achieved through the full length of the column because water at its highest arsenic concentration encounters the most saturated magnetite at the column entrance and then exits at its lowest arsenic concentration in equilibrium with the less saturated magnetite later in the column (Moel, Verberk et al. 2006). This produces an effluent with the lowest possible arsenic concentration in equilibrium with the least saturated magnetite at the exit of the column. Only a long series of CSTR reactors would be able to attain similar efficiency, but at a much higher cost and complexity. The packed column reactor may be operated until the nanomagnetite at the exit of the column has reached its loading capacity at the given inlet arsenic concentration, as described by the equilibrium partitioning of arsenic between the water and nanomagnetite solids (K_d). Once saturated, the nanomagnetite can be regenerated in place or removed for disposal.

Adsorption and surface complexation modeling: Chemical and electrostatic effects on K_d

The affinity of adsorbates to the surface of iron oxides can be affected by many aqueous and solid-solution properties. Regardless of system and solution conditions, the partitioning of any adsorbate between solid and aqueous phases can be represented by K_d, a value representing the concentration of an adsorbed species normalized by the solution concentration in contact with the adsorbent at equilibrium:

$$K_d\left(\frac{L}{g}\right) = \frac{q_e}{C_e} = \frac{[Total\ Arsenic\ Concentration]_{adsorbed}\left(\frac{\mu g}{g}\right)}{[Total\ Arsenic\ Concentration]_{in\ solution}\left(\frac{\mu g}{l}\right)}$$

The distribution coefficient, K_d, is important for transport modeling as it is a critical parameter for calculation of the retardation factor, R, as described later. Therefore, the ultimate goal of any adsorption, partitioning, or complexation modeling tool is to ultimately find K_d, the distribution value reflecting an adsorbate concentration on a solid phase versus concentration in a liquid phase for given conditions. The affinity and adsorption of a target species to surfaces involves chemical and electrostatic forces. A chemical interaction is typically the formation of a covalent bond which involves the merging of the electron clouds of two elements, only occurring over very short distances (Stumm and Morgan). Electrostatic forces can be felt over longer distances between ion-pairs of opposite or similar charge. The electrostatic influence can be accounted for in the adsorption partitioning coefficient by a correction factor, ψ, derived from the electrical double layer theory (Benjamin 2010). Complexation models, such as double-layer model and triple-layer model take this into account and are used by equilibrium modeling tools such as Visual Minteq and MINEQL.

Visual Minteq can be used to predict the adsorbed and aqueous concentrations of these species at equilibrium conditions; however, four parameters must be known: (1) the mass of solid in solution (mass/volume: g/l, etc), (2) the specific surface area of the solid (area/mass: m^2/g, etc), (3) the density of surface sites on in the solid (sites/area: sites/m^2, etc), and (4) the concentration of the adsorbate on the solid (mass/mass: mg/g, etc) (Tomson 2004).

Determination of adsorbed and aqueous concentrations is performed by Visual Minteq or other modeling software via equilibrium relationships between the activities of surface and solution species. Visual Minteq contains a database of equilibrium expressions for many solid phase surface reactions, including Dzombak and Morel's compilation (1990) for iron oxides, such as hydrous ferric oxide (HFO). The activity coefficient of all surface species is taken to be equal to one. Although a contested assumption, it is one taken by almost all equilibrium modeling software. The activities of the ions in solution are represented as a product of their concentration multiplied by an activity coefficient, γ: (Activity = Concentration$\cdot\gamma$). The activity coefficient is affected by both normal ion-ion interactions in solution (Debye and Huckel 1923; Davies and Malpass 1964) and surface charge interactions. To account for the electrostatic effects of surface charge on an ion in the bulk solution, its activity is multiplied by the Boltzmann factor, $e^{-\psi_0 F/RT}$, raised to the power of the ion's charge, which may be positive or negative. In the Boltzmann factor, ψ_0(Volts) is the potential of the charged surface, F is the Faraday's constant, R is the ideal gas constant, and T is the temperature in Kelvin.

Given that the electrostatic effects are dependent upon electrostatic forces, the effect of chemical interactions alone, the intrinsic chemical bond energy, can be

determined if the surface charge or charge of the aqueous species is zero. This elimination of charge can be accomplished when pH is equal to the point of zero charge (pzc), as described below, or if the pH renders an aqueous ion non-ionic (Sigg and Stumm 1980). Monosilicic acid, the primary silica species found in groundwater is predominantly nonionic sufficiently below the pKa_1 of 9.46, thus it effectively only adsorbs to surfaces via inner-sphere chemical bonds at neutral pH (Stumm and Morgan 1996).

The surface of an iron-oxide will have a positive, neutral or negative charge as pH increases in relation to the pH condition where the surface holds a net charge density of zero, the point of zero charge (pH_{pzc}). Below the pH_{pzc} excess H^+ ions in solution associate with the surface and result in a positive surface charge. At pH conditions equal to the pH_{pzc}, the surface sites are neutral and do not participate in electrostatic interactions. Above the pH_{pzc}, H^+ ions are released into solution resulting in a negatively charged surface species. The pH_{pzc} occurs between the pK_{a1} and pK_{a2} protonation constants and depends on the iron-oxide (see equations below). Similar equilibrium constants for other non-proton/hydroxyl adsorbates to the surface of iron oxides are compiled for various species on mineral surfaces. These not only can be affected by pH, as shown below for arsenite and arsenate, but also can affect the charge and point of zero charge for the surface. A selection of surface reactions are represented below, where ≡S corresponds to surface Fe (Westerhoff, Karanfil et al. 2006; Gustafsson 2009):

$\equiv SOH_2^+$	$\leftrightarrow$	$\equiv SOH + H^+$	$pK_{a1} = \sim 7.3$
$\equiv SOH$	$\leftrightarrow$	$\equiv SO^- + H^+$	$pK_{a2} = \sim 8.9$
$\equiv SOH + H_3AsO_4$	$\leftrightarrow$	$\equiv SAsO_4^{2-} + H_2O + 2H^+$	$\log(K_{eq}) = -0.50$
$\equiv SOH + H_3AsO_3$	$\leftrightarrow$	$\equiv SAsO_3^{2-} + H_2O + 2H^+$	$\log(K_{eq}) = 5.27$

Adsorption Isotherms

Adsorption isotherms are fitted models, based on experimental data which allow for prediction of partitioning behavior over a wide range of adsorbate concentration in solution. However, the value of the distribution coefficient, K_d, is only constant for linear isotherms whereby the adsorbate concentration on the solid, q_e, is linearly proportional to the adsorbate concentration in the liquid phase, C_e. More commonly, experimental determinations of partitioning fit better to Freundlich, Langmuir, or other non-linear isotherms. The K_d for linear, Freundlich, and Langmuir isotherms is equal to K_{linear}, $K_F \cdot C_e^{m-1}$, and $q_{max} \cdot K_{Langmuir}/(1+K_{Langmuir} \cdot C_e)$, respectively. The Freundlich and Langmuir isotherm models are described below.

The Freundlich isotherm contains only two adjustable constants, K_d and m, can be derived if it is assumed that the free energy of adsorption is linearly proportional to the logarithm of the adsorbed concentration (Morel and Hering 1993):

$$\Delta G^{\circ\prime} = \Delta G^{\circ} + \alpha RT ln_e[q_e]$$

Then after considerable rearrangement, it can be shown that

$$q_e = K_F C_e^m$$

or in linear form:

$$log q_e = log K_F + m log C_e$$

where

$$K_F = e^{-m\Delta G^{\circ}/RT}$$

And

$$m = 1/(1+\alpha)$$

The q_e represents the equilibrium arsenic concentration on the solid (µg/g), K_F is the adsorptive capacity constant (µg/g)/(µg/l)^m, C_e is the equilibrium arsenic concentration in the solution, and m is the adsorptive intensity constant. The exponent, m, is typically between 0.5 to 1. An exponent of 1 simplifies to a simple linear isotherm. An exponent value of less than one indicates a less favorable adsorption free energy associated with increasing sorbate concentration (Schwarzenbach, Gschwend et al. 2003). Values of K_F and m are often published for various soils, sediments, and minerals and vary greatly based on experimental conditions (Boulding and Ginn 2004). An example of a typical listing of Freundlich constants in the literature is given in Table 3.

Table 3 - Freundlich isotherm constants for $q_e = K_F C_e^m$ for adsorption of As(III) to various soils in West Virginia given q_e (mg/kg) and C_e (mg/l) (Bodek, Lyman et al. 1988).

Soil Location	K_F	m
Lily	28.3	0.399
Chavies	77.4	0.437
Gilpin	30.2	0.674
Pope	53.9	0.571
Upshur	33.6	0.545

One point of view is the Langmuir adsorption isotherm is the simplest isotherm model as it can be derived from simple reaction equilibrium (Morel and Hering 1993). If a constant free energy ($\Delta G^\circ_{ads} = constant$) can be assigned to the surface reaction:

$$\equiv X_{solid} + C_{aqueous} \rightarrow \equiv XC_{solid}$$

then the Langmuir constant can be expressed as

$$K_L = \frac{\{\equiv XC_{solid}\}}{\{\equiv X_{solid}\}\{C_{aqueous}\}} = e^{-\Delta G^\circ_{ads}/RT}$$

It is further assumed that the solid phase activity, {}, of the species is directly proportional to the solid phase concentration, [], and that the number of adsorption sites is constant:

$$[\equiv X_{solid}]_{total} = [\equiv X_{solid}] + [\equiv XC_{solid}]$$

$$[\equiv X_{solid}] = \frac{[\equiv XC_{solid}]}{K_L[C]}$$

$$[\equiv X_{solid}]_{total} = \left(\frac{1}{K_L[C]} + 1\right)[\equiv XC_{solid}]$$

$$\frac{[\equiv XC_{solid}]}{[\equiv X_{solid}]_{total}} = \frac{K_L[C]}{1 + K_L[C]}$$

This is the Langmuir isotherm, or written in more common convention,

$$q_e = \frac{q_{max} \cdot K_L C_e}{1 + K_L C_e}$$

where q_e (μg/g) is the concentration of adsorbate species on the solid, q_{max} (μg/g) is the maximum adsorbate concentration on the solid whereby no higher aqueous adsorbate concentration will increase its value, K_L is the Langmuir constant (L/g), and C_e (μg/l) is the aqueous phase equilibrium concentration. The Langmuir isotherm is characterized by a linear increase in concentration of adsorbed species on the solid at low concentrations of adsorbate in solution and a constant adsorbate concentration on the solid at high concentrations of adsorbate in solution. Langmuir constants for various soils and sediments can be obtained from many reference sources (Montgomery 2007).

Adsorption kinetics modeling

Shipley et al. developed a kinetics model for both As(III) and As(V) adsorption to nanomagnetite in a stirred tank batch reactor by empirical correlation based on least

squares analysis modeling (2009). The fraction of arsenic remaining in solution over time is represented by the equation:

$$\frac{C_t}{C_0} = \left(\frac{1}{1 + K_L r_{sw}}\right)(1 + K_L r_{sw} e^{-kt})$$

where C_t is the concentration of arsenic at time t, C_o is the initial arsenic concentration, K_L (l/g) is the partitioning constant for a linear portion of a Langmuir isotherm, r_{sw} is the solid-to-water concentration of magnetite (g/l), and k is the empirically determined rate constant (1/hr). A solution of 100µg/l As(III or V), 100mg/l bicarbonate, 0.01M THAM buffer, and pH of 8.00 were used to fit the empirical constant, k, for the experimental r_{sw} conditions: 0.05, 0.1, 0.2, and 0.5 g/l. The k value scaled linearly with r_{sw} in the range of values tested; however, packed colums have r_{sw} values several orders of magnitude higher than this range. For example, Guanajuato pilot column studies in this work had r_{sw} values of approximately 600 g/l as each column contained 456.6 grams of magnetite in contact with 0.768 liters of solution (1 pore volume). With an extrapolated rate constant of 8,500 hr^{-1}, or 2.3 s^{-1}, and a K_L value of 4L/g, the time required to reduce arsenic concentration from 30µg/l to 10µg/l would be approximately 0.5 seconds from the equation developed by Shipley et al. above. This would suggest that there is sufficient time in most column applications, which have a typical residence time of 1-4 minutes, for equilibrium partitioning to be established within a narrow mass-transfer window in the column. However, there are a few reservations with this estimate. The parameters were fit based on the given synthetic solution conditions, while interaction of other species and concentrations could affect the kinetics. Significant error may be introduced from extrapolating the rate constant correlation by over three orders of magnitude from the original study. In addition, the correlation was developed for stirred-tank batch reactors

where reactor kinetics are fundamentally different than for column reactors. In a column reactor the solution first comes in contact with saturated adsorbent, then moves to less saturated adsorbent. For batch reactors, the adsorbent is all in its virgin state at the beginning of the reaction period and all becomes saturated together as the reaction progresses.

In batch reactors, Shipley found that arsenate and arsenite partitioning equilibrium was established within approximately two hours for nanomagnetite sorbents, with 90% of the adsorption occurring within the first 30 minutes with a magnetite solids concentration of 0.5 g/l. The time to establish equilibrium partitioning between arsenic and magnetite was reduced, however, in the presence of competing species and was modeled for common competing species of HCO_3, SiO_2, SO_4, PO_4, DOM, Ca, Mg, and K by using a modification to the rate constant term, k, determined initially without interferences present:

$$k_{intf} = \frac{k_o}{1 + (\sum a_i C_i)/(r_{sw} SSA)}$$

The k_{intf} term is the rate constant with interfering species taken into account, k_o is the initial rate constant determined experimentally without interfering species present in solution, a_i is a coefficient fitted for each species based on least squares curve fitting of experimental data, C_i is the concentration of each interfering species in solution, r_{sw} is the concentration of magnetite, and SSA is the specific surface area of the magnetite particles (Shipley 2007). Based on the coefficients and the Guanajuato groundwater composition listed in Table 4, arsenic would be reduced from 30µg/l to 1µg/l in 1.7 seconds. This would suggest that even in the presence of interferences, equilibrium would be established almost instantaneously. The model predicts that the 52 mg/l silica would

have the largest effect in reducing the kinetics of adsorption, five times more of an effect than the next largest contributor from the bicarbonate (144 mg/l as $CaCO_3$). Nevertheless, silica's effect is still predicted to be very small given that any effect of ions is divided by the large solid to water ratio in the interference rate constant.

Beyond the findings of Shipley et al., some have reported longer equilibration times (2-7 days) for highly porous sorbents, such as activated alumina, where diffusion limitations exist (Rosenblum and Clifford 1983). In addition, the solution conditions can also have an impact on the time required to reach equilibrium. Waltham and Eick found that in the presence of 1mM silica at pH 8, arsenate adsorption to goethite increased slowly even after reaction times of 1 week, while at pH 4, equilibrium was established within 2 hours (Waltham and Eick 2002). This finding warrants attention from researchers working with varied solution conditions and could impact breakthrough results in column systems where kinetic limitations are a key factor.

Zhang and Selim modeled the kinetics of competitive sorption of phosphate and arsenic adsorption to various soils (2005; 2007). In their work they used a multi-reaction model approach that assumes some sites are dependent largely on kinetics, while others experience rapid or near instantaneous adsorption equilibrium. This biphasic system results in an initial rapid reaction, followed by a much slower reaction. On the contrary, Waltham and Eick found when arsenic was adsorbing without silica present, this biphasic behavior did not occur (2002).

Column filtration and advection dispersion modeling

Adsorption isotherms may represent the ultimate removal capacity of a column, but much variation is observed in real systems. Vaughan et al. observed similar

performance in isotherms and column experiments, with higher column residence times approaching the adsorbate concentration on the solid predicted by the adsorption isotherm (2007). However, this is not always the case as competitive interactions between adsorbing species, redox changes, fluid channeling, and restrictions in effective porosity among other factors can affect the capacity of adsorbents under dynamic conditions (EPA 1996) (Konikow 2010).

Commonly in packed column systems, partitioning of the adsorbate is sufficiently rapid to justify the assumption of local equilibrium needed to use the isotherm without a kinetic term. However, during the process in which the adsorbate must migrate from the bulk solution to the surface sites and adsorb there are four potential rate limiting steps (Seader 1998):

1. External mass transfer from the bulk fluid through a boundary layer to the external solid surface of the adsorbent,
2. Internal mass transfer from the external surface to within the pores of the adsorbent by pore diffusion,
3. Surface diffusion to sites of lower concentration, and
4. Adsorption onto surface sites.

For an ideal fixed bed adsorption column, adsorption occurs instantaneously and the adsorbate saturates the initial adsorbent completely before moving forward through the column. The concentration front represents the forward movement of the adsorbate as it saturates the column. The concentration front would appear as a sharp, step-like function, the stoichiometric front, in the absence of any dispersion (Figure 12). Upstream of the stoichiometric front the media is completely saturated with arsenic, while

downstream of the front the adsorbate concentration in the fluid is negligible and the media is completely unsaturated. The time for the stoichiometric front to travel the full column length is referred to as the stoichiometric time. The necessary assumptions for this behavior are:

1. Mass transfer resistances (both external and internal) are negligible
2. Plug flow is valid (constant velocity along cross any cross section of pipe and no momentum boundary layer adjacent to the inner wall of the pipe). Perfect plug flow is rarely the case for heterogeneous media where preferential flow paths exist (Silliman 1995).
3. Axial dispersion is negligible
4. Adsorbent media is initially free of the adsorbate
5. At the stoichiometric front, the adsorbate instantaneously reaches equilibrium between solid and liquid phases according to the adsorption isotherm.

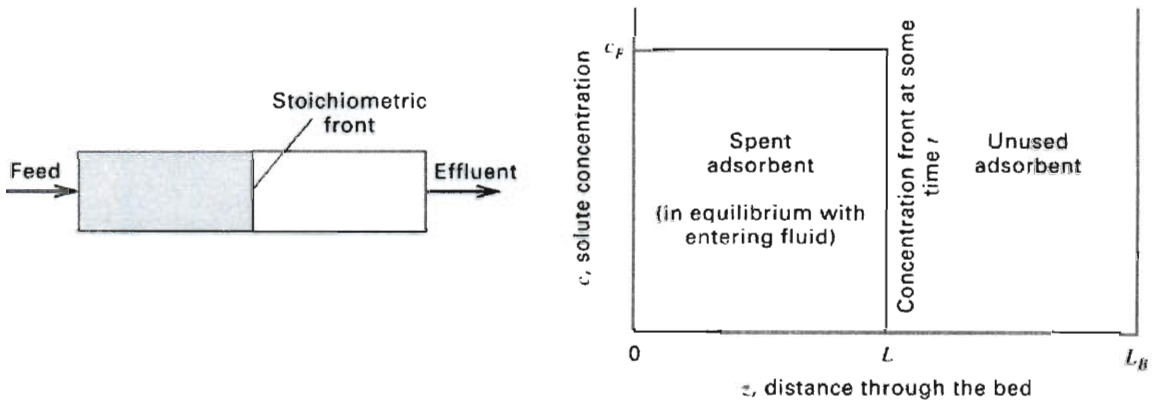

Figure 12 - Stoichiometric concentration front for ideal fixed-bed adsorpion column (Figure 15.27 from Seader 1998)

The retardation factor, R, describes the relative movement of the stoichiometric concentration front of a contaminant versus the flow of solution through a porous media.

Using the retardation factor, the theoretical maximum volume of water able to be treated can be calculated given the five assumptions from above. The retardation factor and the total treated volume are related as

$$R = {}^{1}/_{f_{ads}}$$

$$R = 1 + \frac{\rho_b}{\theta} K_d$$

$$V_{tot} = V_{PV} \times R$$

where f_{ads} is the fraction of the species that is adsorbed in the system, K_d is the distribution coefficient (L/g), ρ_b is the bulk density of the adsorbent (g/L), θ is the porosity of the column, V_{tot} is the theoretical maximum water treated before breakthrough, and V_{PV} is the pore volume within the column (Sontheimer 1988).

Transport in real systems, however, does not follow a strict step function type stoichiometric front and can deviate from the assumption of instantaneous local equilibrium. For real systems, breakthrough can be affected by diffusion, mechanical dispersion, kinetic limitations of mass transfer and reaction, irreversible sorption, and relaxation of the assumption of plug flow. The advection dispersion equation can be used to help represent the advective, dispersive, reactive, and kinetic adsorption components to transport. CXTFIT is a common modeling tool that uses a non-linear least-squares method (Kool, Parker et al. 1985) to fit user-specified forms of the advection dispersion equation (Toride, Leij et al. 1995). In this work, the following form of the 1-D advection dispersion equation for two-site, non-equilibrium transport of a linearly adsorbed solute, given steady-state flow in a homogeneous media was solved simultaneously with the subsequent differential equation describing change in adsorbate concentration on solid kinetic sites with time:

$$\left(1+f\frac{\rho_b}{\theta}K_d\right)\frac{\partial C}{\partial t}=D\frac{\partial^2 C}{\partial x^2}-v\frac{\partial C}{\partial x}-\frac{\alpha\rho_b}{\theta}[(1-f)K_dC-s_k]-\mu_lC-f\frac{\rho_b}{\theta}K_d\mu_{s,e}C$$

$$\frac{\partial s_k}{\partial t}=\alpha[(1-f)K_dc-s_k]-\mu_{s,k}s_k$$

given the following variables (definitions taken from Toride (1995)):

f - fraction of exchange sites assumed to be at equilibrium,

ρ_b - bulk density of the solid [ML^{-3}],

θ - volumetric water content (porosity),

K_d – distribution coefficient for linear adsorption [$M^{-1}L^3$],

C - volume averaged or resident concentration of the liquid phase [ML^{-3}],

t – time [T],

D_x - dispersion coefficient [L^2T^{-1}],

x – distance [L],

v - average pore water velocity [LT^{-1}],

α - first order kinetic rate coefficient [T^{-1}],

s_k - concentration of the adsorbed phase for kinetic sites [MM^{-1}],

μ_l - first order decay coefficient for the liquid phase [T^{-1}],

$\mu_{s,e}$ - first order decay coefficient for the adsorbed phase on equilibrium sites [T^{-1}], and

$\mu_{s,k}$ - first order decay coefficient for the adsorbate phase on kinetic sites [T^{-1}]

From left to right, the terms in the advection dispersion equation represent retardation with respect to equilibrium sites, Fickian dispersion, advection, transfer to kinetic sites, decay in the liquid phase, and decay on equilibrium sites. From left to right in the differential equation beginning with $\frac{\partial s_k}{\partial t}$, the terms represent change in the adsorbed

phase concentration of kinetic sites over time, transfer to kinetic sites, and decay of the adsorbate bound to kinetic sites.

The first order decay terms for the liquid phase, μ_l, and the for the adsorbed phase, $\mu_{s,e}$, on equilibrium sites are grouped into a combined decay term, μ_1, used by CXTFIT for fitting breakthrough data:

$$\mu_1 = \frac{L(\theta\mu_l + f\rho_b K_d \mu_{s,e})}{\theta v}$$

Arsenic is always conserved as opposed to an organic chemical, for example, which may decay over time. Thus, the liquid phase decay term, μ_l, for arsenic can be taken to be zero. For the adsorbed phase, however, the hysteretic adsorption of arsenic could potentially be modeled analogous to decay because it is essentially removed from equilibrium with solution.

If and only if K_d is linear with concentration, semi-analytical solutions to these differential equations can be obtained using Laplace transforms. The full semi-analytical solution for the set of differential equations above is given by Toride et al. for an initial value problem with an initial stepwise distribution (1995).

Given that arsenic is conserved in the system, the decay on the adsorbed phase may represent the transition of arsenate to hysteretic bonds on the surface of magnetite (Yean, Cong et al. 2005). As arsenate transitions from monodentate mononuclear to bidentate binuclear attachment (Figure 13), the arsenate could effectively be considered removed from the system, shifting the equilibrium to allow additional adsorption.

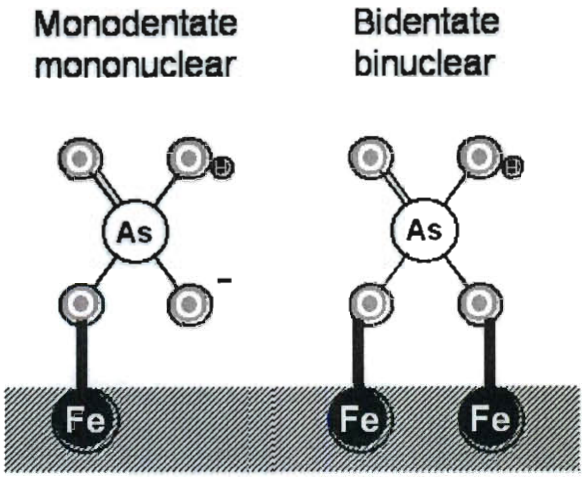

Figure 13 - Depiction of monodentate mononuclear and bidentate binuclear attachment of arsenate to an iron oxide surface (adapted from Weisner (2007)).

Given the large number of fitting parameters, a nonlinear least squares analysis may often not yield unique solutions to the advection dispersion equation. While mechanistically, decay in the solution phase is very different than decay on the equilibrium surface sites, a fitting routine would not be able to distinguish decay in solution from decay on the equilibrium solid sites as the two concentrations are always proportional, related by K_d. Therefore, modeling is limited in that it is not able to describe deterministically the mechanisms of transport, but it does aid in understanding the potential mechanisms.

Even with several fitting parameters associated with the advection dispersion equation (retardation, dispersion, kinetic rate coefficients), accurate modeling of column breakthrough in real systems is not trivial. In real systems, no matter the scale, the effects of unseen internal structure can hinder accurate modeling: heterogeneities may exist in the porous media, preferential flow paths can develop, dead-end pore space may be present which reduces the effective porosity, boundary effects may add complexity,

and the hydraulic conductivity may vary by direction among other effects. In addition, as included in the advection-dispersion model, mechanical dispersion is dependent on the second partial derivative of the concentration gradient as the driving force, which has no rigorous theoretical link. Given the complexities of real systems, some contend that the secret to successful modeling may be to lower expectations (Konikow 2010).

Some researchers such as Ko et al. model arsenic breakthrough in iron-based column media with an error function analytical solution to the advection dispersion equation neglecting any kinetic loss terms (Ko, Davis et al. 2007). They used a common analytical solution developed by Ogada and Banks (1961) to model arsenic transport through iron-coated sand columns. The fraction of contaminant released in solution past a distance, x, within the column at any time, t, can be represented as:

$$\frac{C(x,t)}{C_0} = \frac{1}{2}\left(erfc\left(\frac{Rx - v_x t}{\sqrt{4RD_x t}}\right) + exp\left(\frac{v_x Rx}{D}\right) erfc\left(\frac{Rx + v_x t}{\sqrt{4RD_x t}}\right)\right)$$

where C_0 is the initial concentration at x=0, erfc() is the complementary error function, R is the retardation factor, v_x is the linear velocity of the fluid through the column, and D_x is the dispersion coefficient.

Still other researchers model porous arsenic adsorbents using dimensionless scaling parameters to model larger scale columns by a technique originally developed for estimating full scale performance of activated carbon columns for organic removal (Sontheimer 1988). These rapid small scale column tests (RSSCTs) attempt to scale the hydrodynamics and mass transport for full scale columns using large granular size media down to small, bench scale columns with proportionally smaller media produced by

grinding. However nanomagnetite is not suitable for RSSCTs as it is a non-porous media, already in fine nanoparticle state.

In order to provide a working definition of breakthrough in real systems where sharp breakthrough does not typically occur, the concept of the mass transfer zone (MTZ) is used. The MTZ represents the concentration front where the arsenic concentration, C(x,t), in the fluid is between 5% and 95% of the feed concentration, represented as C_0 or C_F (Seader 1998). Inside the MTZ, the adsorbate is actively transferred from the liquid phase to the solid phase. Upstream of the MTZ, the adsorbate passes the saturated media unaffected, while downstream of the MTZ only minimal adsorbate is in solution available for adsorption. Figure 14 displays concentration profiles at different times through a column of length L_B. At time t_2 the MTZ is completely within the column, bound by L_s and L_f. The time t_b, displays the point of initial breakthrough, the point where the MTZ reaches the end of the column bed. Figure 15 is another representation of the observed breakthrough fraction as would be observed from the distance, L_B, at the end of the packed bed. This representation or similar, based on volume of water treated, is often referred to as the breakthrough curve. By modeling the mass transfer zone and the resulting breakthrough curve the time for an adsorbate to exceed a certain threshold concentration can be estimated, and thus the point of regeneration or replacement can be determined.

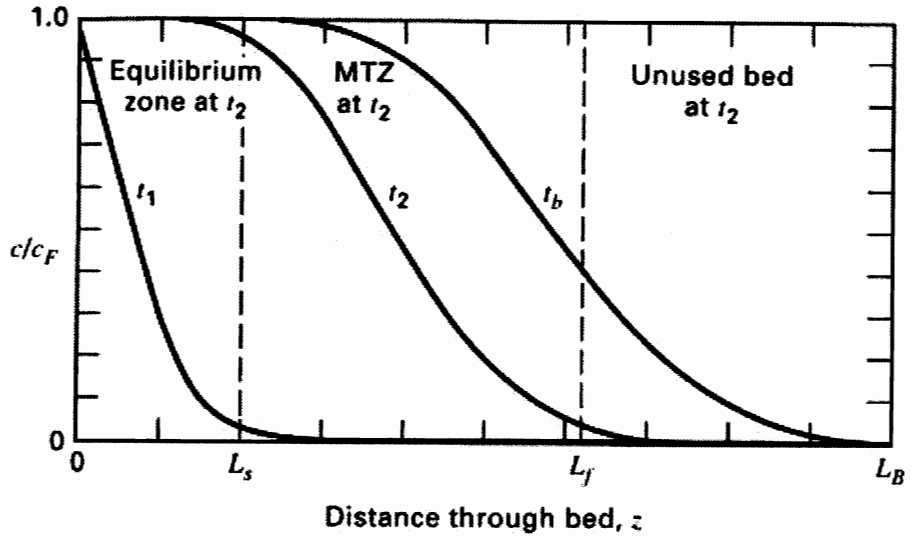

Figure 14 - Concentration fronts in a fixed-bed column with mass transfer effects (Figure 15.28a from Seader 1998).

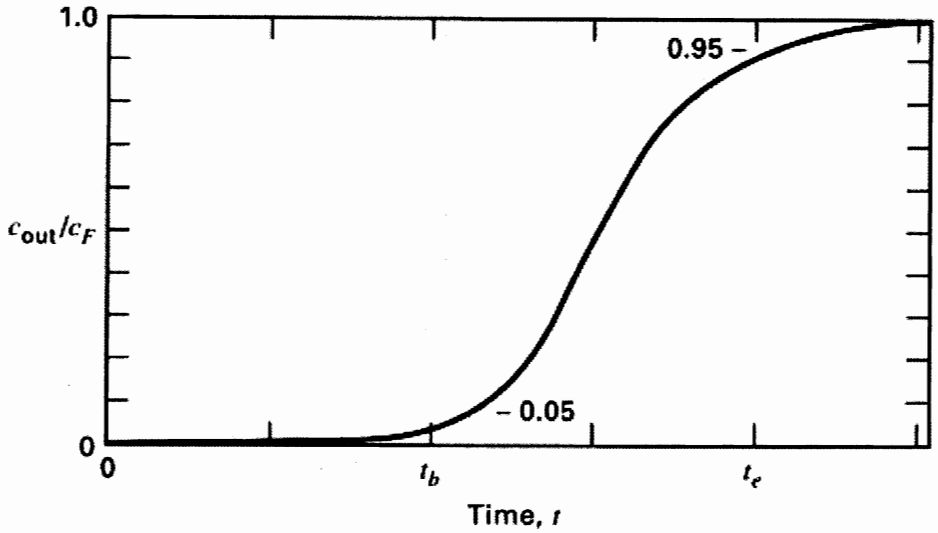

Figure 15 – Breakthrough curve on a time basis. (Figure 15.28b from Seader 1998)

Interfering species

Natural waters contain a matrix of chemical components that may interfere with arsenic adsorption to nanomagnetite. While the impact on arsenic adsorption is difficult to predict for the complex chemical make-up of a natural water source, insight to the relative effect of each component can be gained from a review of the effects of individual

contributing species. Among the interfering species commonly present in groundwater or surface water, the literature has given much attention to phosphate, sulfate, vanadium, carbonate, and silica, the primary subject of this study (Goh and Lim 2010). Silica is discussed in detail after an overview of the primary interfering species of interest.

Phosphates

Given its chemical similarity to arsenate, phosphate competes with arsenate for adsorption to nanomagnetite sites. Both have an oxyanion structure, both share a similar protonation scheme relative to pH, and both form bidentate complexes at the surface of iron oxides (Zeng, Fisher et al. 2008). Zhao et al. found that on the surface of goethite, phosphate reduces arsenic adsorption, and conversely, arsenic reduces phosphate adsorption; however, the sum of adsorption of arsenic and phosphate species is greater than either alone (2001). In addition, arsenic binds more strongly to iron-oxides than do phosphates (Pigna and Violante 2003). Jain and Loeppert found that the decrease in arsenic adsorption in the presence of phosphate was pH dependent (2000). Most research on the competition of phosphate is conducted at concentration ranges higher than those typically found in natural waters. That is to say, phosphate competition for nanomagnetite adsorption sites is minimal at concentrations typically found in natural waters.

Sulfates

Although commonly found in natural waters, sulfates minimally interfere with arsenic adsorption. Jain and Loeppert found in molar ratios of 50:1 (S:As), arsenate adsorption to ferrihydrite is not significantly affected and is, in fact, slightly improved at pH above 7 (2000). The increased adsorption may be due to the increase in ionic strength

which compresses the electrical double layer and minimizes repulsive forces approaching the surface of ferrihydrite. This may explain why there was no affect to the adsorption of arsenite, which has no charge at neutral pH, and therefore would not be affected by changes to the electrical double layer.

Bicarbonate

Bicarbonate is typically present in groundwater in the concentration range of 0.5-8mM (Stumm and Morgan 1996), and therefore have the potential to largely influence arsenic adsorption. Although bicarbonate ions can compete for adsorption sites on sufaces of iron oxides and oxyhydroxides, most studies show that they have have minimal impact compared to other competing ions, such as phosphate, in natural waters. Radu and Subacz et al. studied the mobilization and transport of arsenic by aqueous bicarbonate in iron oxide coated sand columns (Radu, Subacz et al. 2005). They determined that the concentration of bicarbonate had a negligible effect on As(V) adsorption at pH 7. By increasing the CO_2 partial pressure from $10^{-3.5}$ to $10^{-1.0}$, the adsorption of As(V) decreased minimally as compared to the relative effect that phosphate had at typical concentrations found in natural waters. In a separate study, Genc and Tjell examined the interferences of bicarbonate, phosphate, silicate, and sulfate on arsenic adsorption to red mud, of which hematite is the predominant component, and determined the bicarbonate was the species of least concern to arsenic adsorption (2003). They ordered the species from greatest to least interference on a molar basis to be phosphate > silicate > sulfate > bicarbonate.

In contrast to most studies showing no effect or a slight interference effect on arsenic adsorption by bicarbonate, one study, by Arai and Sparks et al., found that

bicarbonate actually enhanced adsorption of arsenic to hematite in the pH range of 4-8 depending on the timescale (2004). After an initial period of reduced adsorption capacity at short timescales, the adsorbed arsenic concentration increased beyond the baseline without bicarbonate after reaction times of 3 hours; although at equilibrium, the bicarbonate showed little effect. The authors hypothesized, based on FTIR studies that showed monodentate mononuclear species on the Fe polyhedron, that this behavior is due to an initial sorption of bicarbonate, followed by a replacement by arsenate ions. Adsorbed bicarbonate may be replaced more readily than surface hydroxyl groups as the shared charge[2] of bicarbonate is greater than that of hydroxide. The lower surface charge of bicarbonate results in weaker terminal surface Fe-O bonds which can be more readily be replaced by arsenate. This would contribute to enhanced adsorption of arsenate.

Silica

Silica is ubiquitous in the environment and binds strongly with iron oxides. The concentration of soluble silica (quartz) in groundwater is directly proportional to temperature and can be used as a geothermometer (Wright 1991). The TiO_2-based arsenic adsorptive media ADSORBSIA™GTO™ (Dow Chemical) is promoted to be the most resistant to the presence of silica compared to leading iron-based media. In a column study with ADSORBSIA™GTO™ media, by increasing silica concentration from 10mg/l to 40mg/l, breakthrough of 10% of the inlet arsenic concentration occured in one-fifth the time. The effect of silica on arsenic removal using iron oxides will be discussed below.

---

[2] Shared charge is the valence state of the central atom divided by the number of bonded oxygen atoms.

Vanadates

Vanadates have similar structure as arsenate and compete for adsorption sites on iron-based media. Aragon observed only a 10% reduction in adsorption capacity to iron-impregnated activated carbon in adsorption isotherms with NSFI-53 challenge water at pH 6.5 and 8.5 with 100µg/l vanadium as compared to 0µg/l vanadium (2005). Vanadium is typically present in natural waters in trace concentrations, rarely above 10µg/l, although several hundred µg/l are possible in thermal springs (Hem 1989). Guanajuato groundwater contained 13µg/l of vanadium, as measured in this study.

Zinc effect

Yang et al. found that zinc enhanced arsenic sorption to magnetite nanoparticles at pH 7 and above (2010). By adding less than 3 mg/l of Zn(II) to a 100µg/l As(V) solution at pH 8, sorption to magnetite increased from 66% to over 99% of the total arsenic. For a similar solution of As(III), adsorption improved from 80% to 95% removal in the presence of Zn(II). Yang proposed that the enhanced adsorption was due to the formation of a ternary surface complex between the magnetite surface, Zn^{2+} ions, and arsenic oxyanions. The enhanced adsorption only occurred for solutions with pH of 8 and had reduced effect at lower pH (4.5 and 6). Zn^{2+} was the only divalent cation that had this effect, while addition of Ca^{2+} slightly hindered adsorption.

Silica in the natural environment

Silicon is abundant in the natural waters and almost always present in parts per million levels except for highly treated waters. Silicon species are prolific in water supplies as they are sourced from the weathering and dissolving of silicate minerals which make up the majority of the Earth's crust (Iler 1979). Weathering can break down

silicate minerals to amorphous silica, a non-crystalline solid form of SiO_2, which can readily dissolve into water supplies. In contrast, little silica dissolves directly from quartz sources, such as sea sand. Dissolution of silica from quartz is negligible at room temperature, but high temperature and high pH conditions promote the rate of dissolution. Globally, if a mass balance of silicon is considered around the ocean, 80% of silicon input is from rivers, which have a mass-averaged concentration of 150µmol/l, or 9mg/l as SiO_2 (Tréguer, Nelson et al. 1995). The primary mechanism of removal from the ocean is biogeochemical, the formation of the cell walls of diatoms, a marine algae, which eventually deposit into sediments.

Silicon in water is most commonly found in the form of inorganic oxides. Silica hydrolyzes to form monosilicic acid, also referred to as orthosilicic or silicic acid. Silicic acid in solution is still often measured in molar equivalents of SiO_2 and is commonly referred to as silica. Silicic acid functions as a weak acid and is non-ionic in acidic and neutral conditions as can be inferred from the highly basic pKa_1 value.

$$SiO_2 + 2H_2O \leftrightarrow H_4SiO_4$$

$$H_4SiO_4 \leftrightarrow H^+ + H_3SiO_4^- \qquad pKa_1 = 9.46$$

$$H_3SiO_4^- \leftrightarrow H^+ + H_2SiO_4^{2-} \qquad pKa_2 = 12.56 \text{ (Stumm and Morgan 1996)}$$

The hydration of silicic acid is presumed to be four water molecules, giving a representative structure of $Si(OH{:}OH_2)_4$. In the neutral pH region of natural waters (pH 8.5 and below), soluble silicic acid tends to stay in nonionic monomeric form, as shown in Figure 16 for silica concentrations below 2mM (120mg/l as SiO_2). If the concentration of silica rises above 2mM, a portion of the silicic acid will polymerize rapidly especially at low pH. High pH is more ideal for retaining silicic acid in monomer form given high

silicic acid concentrations as shown by the elevated mononuclear wall in Figure 16. Davis and Knocke et al. determined that a 8,000mg/l SiO_2 solution at pH 12.8, made from dissolving Na_2SiO_3 in deionized water, gave approximately 85% monomers, as determined by the Hach silicomolybdate method (2001). A second solution at pH 6 of 1,200mg/l SiO_2 was found to give only 11-21% monomers. Therefore, if preparing stock solutions of high silica concentration, care must be taken to understand and control polymerization.

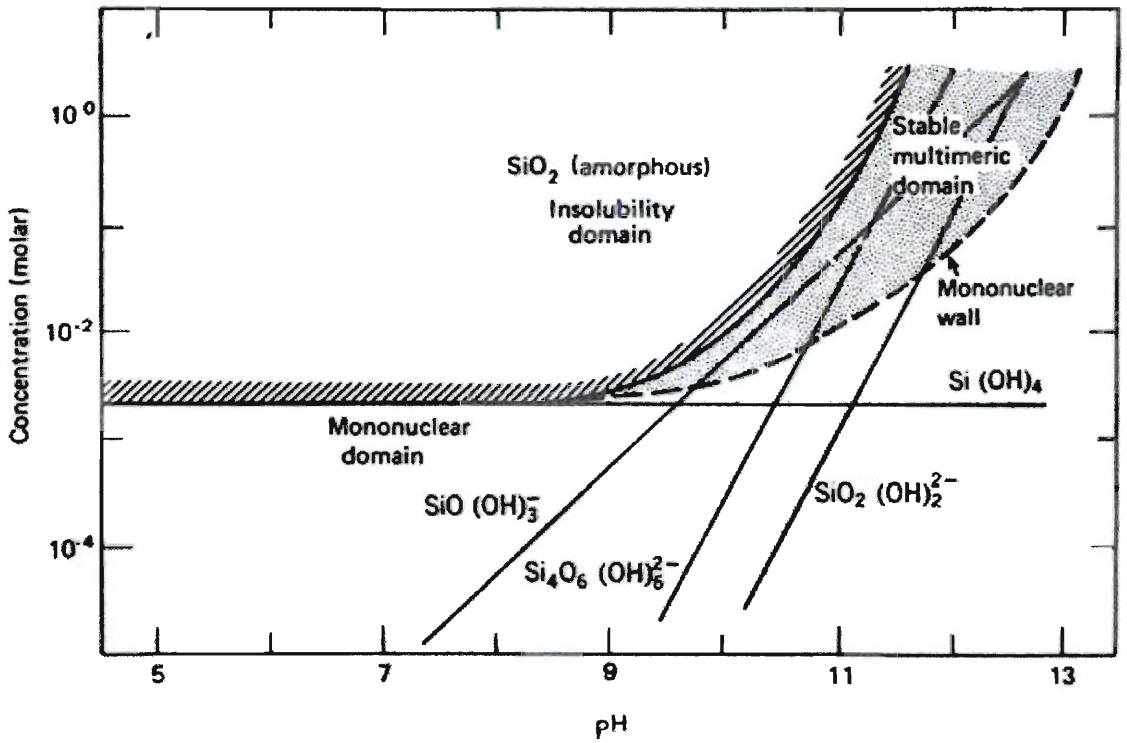

Figure 16 – Predominance diagram of silicate monomer/polymer species at various pH and silica concentrations (Stumm and Morgan 1996).

Dissolution of silica can be considered a depolymerization reaction by hydrolysis, while the solubility of silica represents the steady state of the depolymerization and polymerization reactions. The catalyst for the depolymerization reaction can be OH^- in basic solutions or HF in acidic solutions. Figure 17 is a schematic of the

depolymerization mechanism. To initiate the process, a catalyst (OH^- in this case) bonds with the silicon atom, increasing the coordination number of the silicon to more than four bonds. As a result, the strength of neighboring oxygen bonds is weakened and $Si(OH)_x^{(4-x)}$ is released.

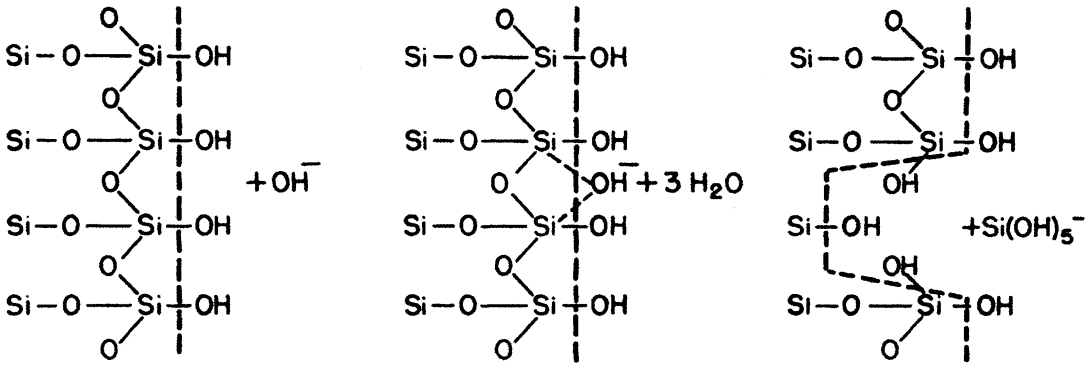

Figure 17 - Dissolution mechanism of silica: depolymerization by hydroxide ion (Iler 1979).

The solubility of quartz in neutral pH conditions at room temperature is 12 mg/l as silica. Quartz has a point of zero charge between pH 2-3. The rate of dissolution of quartz is slowest near this pH given the limited number of charged $S\text{-}OH_2^+$ or $S\text{-}O^-$ sites[3] occurring on the surface lattice. Given the low isoelectric point[4], quartz carries a negative charge when in contact with natural waters at neutral pH.

Solubility of silica is much higher with respect to amorphous silica. For a given sample of amorphous silica, the equilibrium solubility is reproducible and usually near 110-120mg/l (Iler 1979; Stumm and Morgan 1996); however, reported solubility ranges from 70mg/l to 150mg/l or more (Alexander, Heston et al. 1954; Elmer and Nordberg 1958). This wide range may be due to differences in particle size, state of internal hydration, and the presence of trace impurities. Given that the timescale of precipitation

[3] S represents the surface.
[4] The isoelectric point is the pH at which the solid surface carries no net electrical charge.

or dissolution of amorphous silica is much faster than the recrystalization of quartz, the effective solubility of silica is determined almost exclusively by the amorphous silica. Quartz will grow only when slightly supersaturated, and even then at very slow speed. Therefore, a solution containing up to 120 mg/l of silica could be quite stable in relation to quartz even over a long timescale (Iler 1979).

Polyvalent cations are shown to effect solubility and dissolution of silica. At pH 8, the presence of Al, Be, Fe, Ga, Ga, Gd, and Y can retard dissolution of silica. Ca and Mg are also shown to have this effect, but only above pH 9.5. As will be discussed in the silica removal section below, the polyvalent cations, Fe and Al, can be used to reduce the solubility of silica in water from 120 to less than 10 mg/l. F^- can also reduce solubility, but only in low pH conditions where SiF_6^{2-} forms. In contrast, the presence of other monovalent salts increases the ionic strength, thereby reducing the electrical double layer[5] and increasing the dissolution/recrystalization kinetics. However, the ionic strength does not significantly shift equilibrium solubility. Jones and Pytkowicz reported that silica solubility is affected somewhat by pressure. At 0°C, they measured soluble silica in seawater at 1atm, 150atm, and 1250atm as 65mg/l, 71mg/l, and 94mg/l, respectively (1973). Temperature, within a narrower range, has a much stronger influence on solubility.

The direct temperature correlation with silica solubility makes silica especially suitable as a geothermometer, useful for predicting reservoir temperatures (Truesdell and Fournier 1977). The silica-temperature[6] is used as an indicator for the temperature within

[5] The electrical double layer refers to the two parallel layers of charge surrounding the solid surface that acts to prevent collision of other charged particles to its surface by electrostatic repulsion.
[6] The silica-temperature is the reservoir temperature that can be assumed given the concentration of silica dissolved in solution.

the reservoir even after the water is brought to ambient temperature at the ground surface. It assumes equilibrium is established between quartz and dissolved silica in the formation with respect to its solubility at that temperature. Although groundwater will cool as it flows away from a hot source, the concentration of silica is conserved and can be readily preserved for analysis at a later time. Given the slow kinetics of quartz formation at room temperature, and as long as the concentration does not exceed the solubility of amorphous silica, the silica remains completely soluble in short timescales of days, weeks, or even months. Therefore, analysis of silica allows for simple estimation of reservoir temperatures. There are a few caveats to this method. The temperature may be in error if the groundwater flow converges with flow streams from a different temperature source. Also, if minerals present in a formation have significantly different solubilities than pure quartz, the validity of temperature estimates would also be in question.

Silica and other geothermometer markers were analyzed in several wells in Guanajuato and the surrounding cities in the present study. The silica-temperatures in Guanajuato and the surrounding region may indicate low level geothermal sources between 111-137°C (Appendix C). A second geothermometer correlation using Na-K-Ca ratios with a Mg correction factor (Fournier and Truesdell 1973; Fournier and Potter 1979) was used as a quality check, which predicted reservoir temperatures between 58-116°C. Therefore, both the silica and Na-K-Ca geothermometers confirm the existence of elevated reservoir temperatures in the region.

Several tools such as XRD, Raman, magic-angle spinning NMR, EXAFS, CTR and ATR-FTIR have been used to analyze silicates in solution and on solid surfaces.

Yang and Roonasi et al. examined bond stretching with total reflection Fourier transform infrared (ATR-FTIR) spectroscopy to analyze the speciation of dissolved silicates and silicates adsorbed to magnetite nanoparticles at various pH conditions and silicate concentrations (Yang, Roonasi et al. 2008). Two concentrations of silicates were examined: 1mM and 10mM (60mg/l and 600mg/l, respectively, as SiO_2). Given the case of lower surface loading (1mM silicate in solution), the infrared spectra indicated the presence of different types of complexes on the magnetite surface. They proposed a mechanism of adsorption by ligand exchange by which both monodentate and bidentate complexes could form, similar to adsorption of arsenate (Figure 18). The relative proportion of monodentate versus bidenatate complexes would depend on pH and silicate concentration in solution. The spectra indicated that at higher surface loading resulting from the 10mM silicate concentration, some oligomerization occurred. The 10mM concentration resulted in a range of silicate species even including some polymeric silica at low pH and some monomeric silica at high pH.

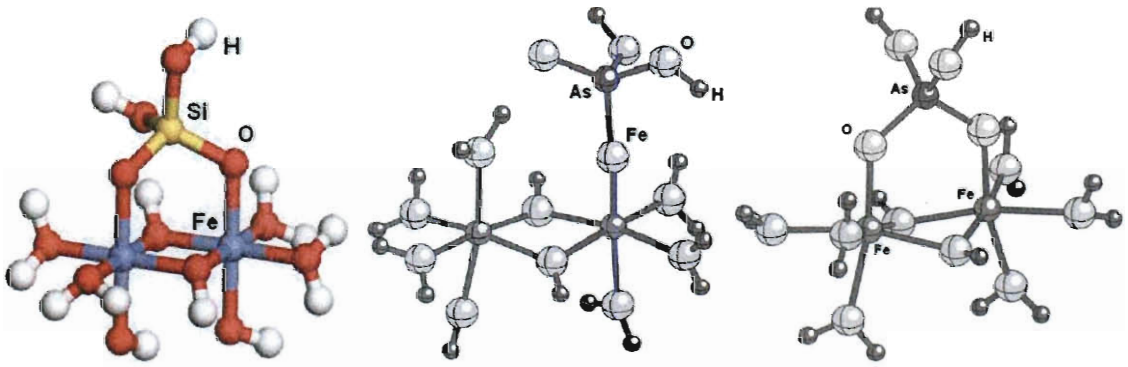

Figure 18 - Silicate chemically adsorbed to ferric oxide by bidentate binuclear attachment (adapted from Liao et al. (2009)) and arsenate chemically adsorbed to ferric oxide by mononuclear monodentate and binuclear bidentate attachment (adapted from Sherman and Randall (2003)).

Mechanism of silica interference

Silica has been shown to interfere significantly with arsenic adsorption to iron oxides. The mechanism of interference is likely time dependent, whereby silicates in solution first adsorb to surface sites via inner-sphere complexes (Figure 19). As mentioned earlier, silica is nonionic sufficiently below the pKa_1 of 9.46, thus it effectively only adsorbs to surfaces via chemical forces (Stumm and Morgan). Although arsenic has higher affinity than silica to iron oxides surfaces, the magnitude of silica interference can be significant as the silica:arsenate molar ratio can approach 15,000:1 in some natural waters. Silica may initially form inner-sphere complexes with iron-oxide through a rapid monodentate, mononuclear attachment followed by the slow formation of more stable bidentate, binuclear bonds. This transition results in occupation of two potential adsorption sites and increases the activation energy required for ligand exchange with arsenic. Once adsorbed, silica can form oligomers with adsorbed silicates of neighboring sites and, over days and weeks, coat the magnetite surface and severely hinder access to surface sites (Davis, Knocke et al. 2001; Smith and Edwards 2005). Depending on the pH in relation to the pKa_1 for silicic acid, the adsorbed silica may make the surface more negative, further reducing arsenate adsorption through electrostatic forces. Furthermore, silicates may display irreversible sorption due to surface diffusion and occupation of high energy sites, such as crystal defects and micropores.

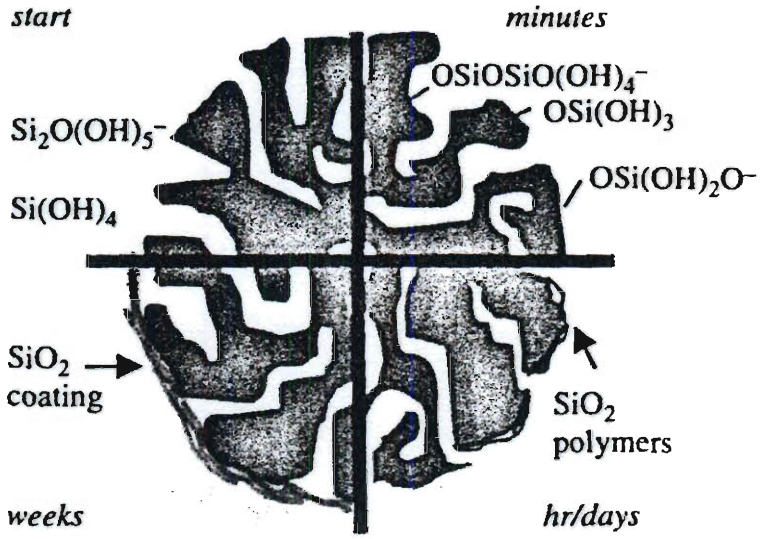

Figure 19 - Conceptualization of the stages of silica interference. Adapted from Smith and Edwards (2005).

Deposition of monomeric silica could form an impervious, glass-like layer, but only if solutions are slightly supersaturated. A 2-3 nm impervious layer formed by deposition was shown to make a Ni surface insoluble in acid (Iler 1979). Deposition to this full extent is not likely to occur in natural drinking water sources as they are typically undersaturated. Alternatively, at moderately supersaturated conditions, colloids would form in solution and deposit inefficiently, still leaving surface sites available for adsorption. Supersaturation can be caused by evaporation or a reduction in temperature.

Some studies have indicated that only the kinetics are affected by the presence of silica, while others observe a reduction in the total arsenic adsorbed at equilibrium as well (Swedlund and Webster 1999). The difference may be two-fold: first, the studies differ in pH conditions which can have a combined effect with silica on adsorption rates and second, the amount of time appropriated to allow the sorbent/sorbate system reach equilibrium varied from study to study. High pH conditions, result in a negative surface

charge due to similar protonation-deprotonation behavior for adsorbed silicates as for aqueous silicic acid near the pKa_1 of pH 9.46 (Anderson and Malotky 1979, Waltham and Eick 2002). The more negative the surface charge on the adsorbent surface, the more electrostatic repulsion that exists with the arsenate anions in solution, and the slower the approach to equilibrium. At pH conditions 7.5 and below, the concentration of negatively charged adsorbed silicates becomes much smaller, and therefore, the effects of silica become less significant. Second, many studies choose only one adsorption equilibrium time for the entire study but fail to observe if equilibrium is truly reached. If insufficient time is allowed for a system to reach equilibrium, then the kinetic limitations may be mistaken for equilibrium changes. For example, Moller and Sylvester conducted a study of two commercial sorbents in high pH conditions and high silica concentrations (2008). Their batch isotherms were only run for an overnight period and they reported significant changes to equilibrium sorption for both pH and silica concentration; however, equilibrium may not have been reached.

Silicic acid adsorbs to iron oxides and may reduce the surface potential of the adsorbent. Waltham and Eick found that the adsorption of silica to goethite followed biphasic kinetics (2002). An initial rapid adsorption was followed by a second much slower adsorption process, as shown in Figure 20a. The authors postulated that this behavior was due to changes in the type of surface complex. A study using EXAFS examined the attachment of arsenate to goethite to find monodentate attachment primarily at low surface coverage, bidentate mononuclear attachment at high surface coverage, and bidentate binuclear at the highest surface coverage scenario (Fendorf, Eick et al. 1997). The slower kinetics may have been associated with the formation of these

bidentate, binuclear bonds. Waltham and Eick found that surface precipitation or diffusion into interparticle spaces and intraparticle pores to be a less likely cause of the slower kinetics. The formation of amorphous silica through surface precipitation or polymerization was not probable as the solutions were undersaturated with respect to amorphous silica and the quantity of surface sites available exceeded the surface area that the silicic acid in solution could possibly cover. The biphasic kinetics of silica adsorption could also not be explained by interparticle diffusion as this is a physical process that would affect silicic acid and arsenate transport similarly. However, arsenate adsorption in the absence of silica did not have a second slow adsorption phase (not shown) unless silica was also present in solution (Figure 20b). This second slow adsorption phase for arsenic was attributed to slow replacement of adsorbed silicates with arsenate. As the experiment progressed, the system approached the condition of 1 mole of arsenic adsorbed per mole of silica desorbed, further confirming the replacement hypothesis.

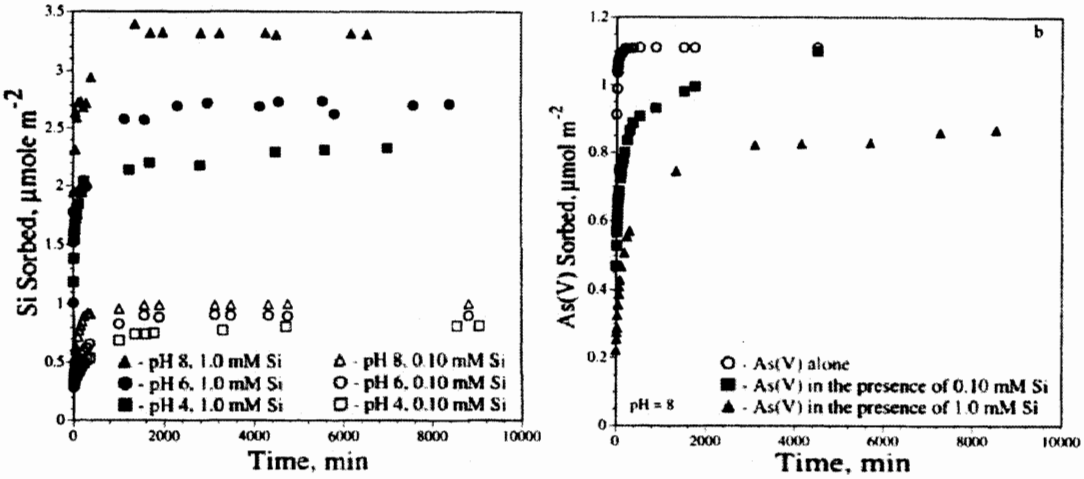

Figure 20 - a. Silica adsorbed to goethite at pH 4, 6, and 8 with 0.1 and 1.0mM Si. b. Arsenic adsorbed to goethite at pH 8 in the presence of 0.1mM and 1.0mM Si pre-equilibrated for 60h in solution (Waltham and Eick 2002).

Swedlund and Webster proposed a mechanism of silica polymerization on the surface of ferrihydrite (Figure 21). Through X-ray photoelectron spectroscopy (XPS), and Infrared (IR) spectroscopy, and differential thermal analysis (DTA) the presence of silicic acid monomers and polymers can be distinguished from those forming siloxane linkages. Polymerization began occurring when the mole ratio of $Si(OH)_4$ to Fe on the surface of ferrihydite was between 0.05-0.20. In addition, the characteristic Si-O-Si bond stretching, indicating siloxane linkages between two adsorbed silicates, occurred between mole ratios between 0 and 0.027. Although polymerization occurred at high molar ratios of Si to Fe (1.8:1), it was the adsorption of monomer silicates that still dominated the interference effect in relation to arsenic adsorption to the surface of ferrihydrite. This was hypothesized given the close alignment of experimental data with model prediction from the double-layer theory with the adsorption of silicate monomers. The molar Si:Fe ratio of 1.8:1 was established with solution conditions near the solubility of amorphous silica (108mg/l) and 56mg/l Fe in solution in the form of ferrihydrite.

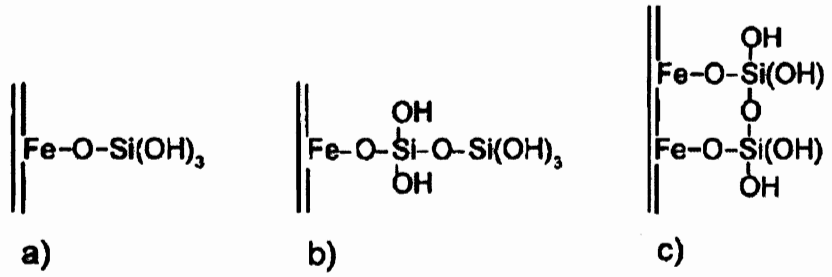

Figure 21 – Surface coverage depictions of silicic acid adsorbed on an iron-oxide surface: a. silicic acid monomer. b. polymerized silicic acid. c. adjacent silicic acid monomers forming a siloxane linkage (Swedlund and Webster 1999).

Waltham and Eick found that although the kinetics of arsenic adsorption to goethite decreased with increasing pH and silica concentration, the slower kinetics did

not result in less arsenic adsorbed at equilibrium except at the highest pH condition of pH 8 where a 21% reduction occurred Figure 20b. For each scenario, silica was pre-equilibrated for 60 hours before arsenic was added. When arsenic was introduced into the system, it caused desorption of silica approaching 1 mole of arsenic adsorbed per mole of silica desorbed after sufficient time given to reach equilibrium. This direct displacement indicates that the iron oxide surface has a stronger preference for bonding with arsenate than with silicate, and over time the silicate will be replaced by arsenate.

Silica has been shown to facilitate adsorption of some metals as is the case for Co, Ni, and Zn onto clays (Bodek, Lyman et al. 1988). Adsorption of these cationic metals is made more favorable in the presence of silica due to three mechanisms: by silica adsorbing on the surface making the surface charge more negative, by silica adsorbing to the surface and subsequently forming complexes with the metal species, and by complexing with the metal species in solution, then adsorbing as a unit. However, enhanced adsorption is the exception for most heavy metal species, including arsenates and arsenites, carrying a negative or neutral charge in water.

Mitigating the effects of silica

There is evidence that polyvalent cations not only partition to a greater extent onto adsorbent surfaces in the presence of silica, but they also reduce the competing effects that silica poses to adsorption of other heavy metals. Smith and Edwards found that above pH of 7.5, calcium ions in solution minimized the impact of silica on both the kinetics and equilibrium adsorption of arsenate to ferric hydroxide and activated alumina (2005).

The zeta potential[7] of preformed amorphous ferric hydroxide was shown to become more negative with the addition of silica in solution and with increase in pH; however, these affects were mitigated by the presence of calcium, as shown in Figure 22 (Smith and Edwards 2005). The positively charged calcium may increase the zeta potential by three different ways. First, the presence of divalent calcium in solution increases the ionic strength, causing the electrical double layer to compress. Second, the calcium may adsorb directly onto the iron hydroxide, directly making the surface charge more positive. Finally, the calcium may complex with the silica already adsorbed or with the silica in solution to later adsorb, either way counteracting the negative surface charge.

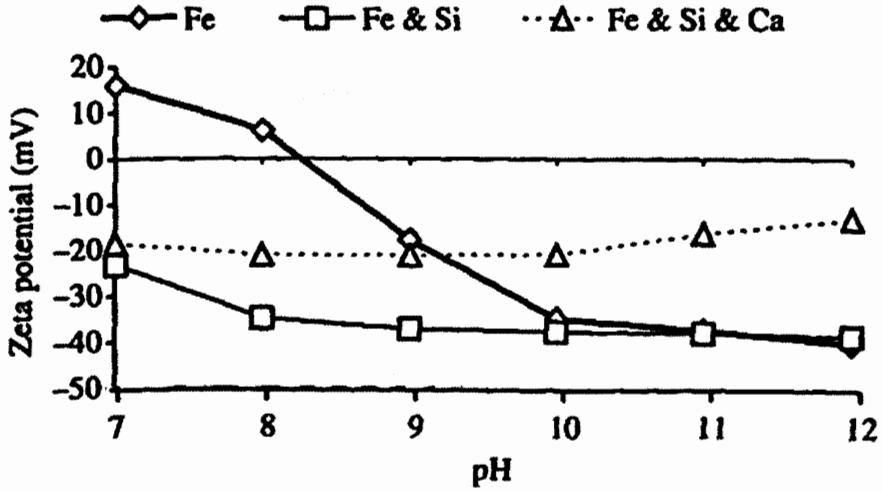

Figure 22 - Zeta potential of preformed ferric hydroxide versus pH in three solutions: Fe only, Fe and Si, and Fe, Si, and Ca. Fe = 20mg/l, SiO_2 = 40mg/l, Ca = 10mg/l (Smith and Edwards 2005).

The zeta potential is a key element in the rate of approach to equilibrium. In their experiments, Smith and Edwards found that if the zeta potential was equal to or more positive than -20 mV, then 80% of the quantity of arsenic adsorbed at 1365 hours was

[7] Zeta potential is the electric potential of electrical double layer at the location of the slip plane above the surface.

accomplished within the first 2 hours (Figure 23). Conversely, when the zeta potential was more negative than -35 mV, less than 50% of the 1365 hour quantity was adsorbed in 2 hours.

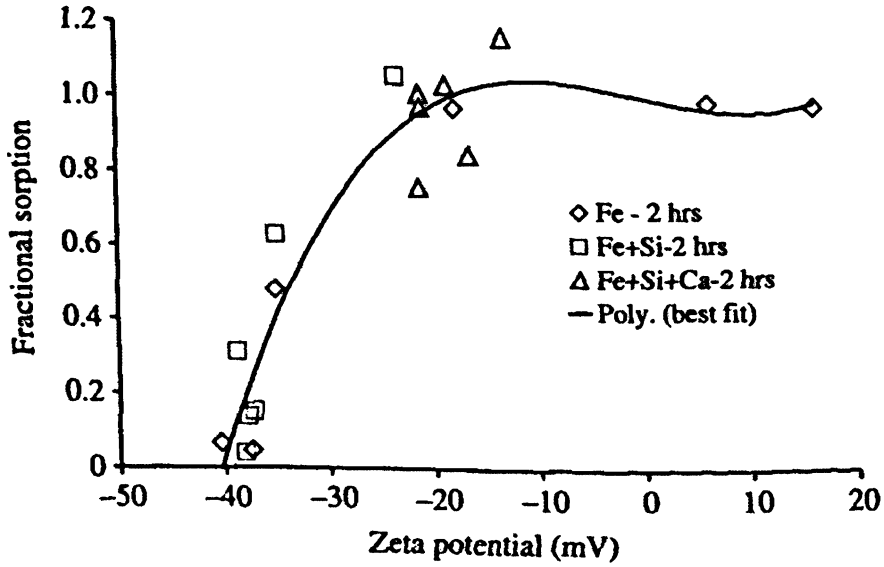

Figure 23 - Fractional sorption of arsenic (arsenic adsorbed in 2 hours divided by the arsenic adsorbed after 1368 hours) versus zeta potential. Initial conditions: As = 100µg/l, Fe = 20mg/l, SiO2 = 40mg/l, and Ca = 10mg/l. Zeta potential was varied by pH adjustment (Smith and Edwards 2005).

Waltham and Eick tested the hypothesis that zeta potential was the primary factor in adsorption kinetics (2002). They tested two silica concentrations (0.1 and 1.0 mM) at pH 8 and selected two pH conditions (pH 9 and 10) which would give similar zeta potentials on the surface of goethite without the presence of silica. Figure 24 shows the resulting adsorption and how the two solutions with silica aligned favorably with the pH adjusted solutions with similar zeta potential. Although the equilibrium sorption may have differed, the initial kinetics of sorption appeared to correspond closely with zeta potential.

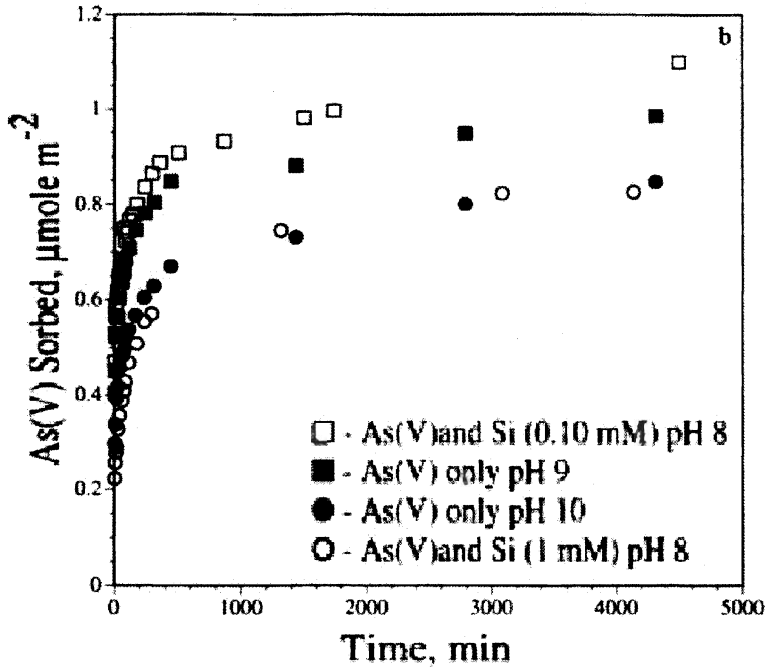

Figure 24 – Comparison of kinetics of As(V) adsorption to 1.0 g/l geothite in solutions of pH 8 with 0.10 and 1.0 mM $Si(OH)_4$ and in solutions of similar zeta potential without silicate at pH 9 and 10 (Waltham and Eick 2002).

In the Smith and Edwards study, the rate of arsenic sorption in a batch study was shown to vary greatly with concentration of silica and calcium. The solution with silica alone displayed the slowest initial adsorption rates to $Fe(OH)_3$, while calcium added to the solution with silica markedly improved initial sorption rates. One key observation is that the solutions including silica with and without calcium resulted in the same quantity of arsenic adsorbed for reaction periods above 100 hours. Calcium resulted in more arsenate adsorbed only at shorter residence times. This suggests that the overall effect of calcium is related to the kinetics, not the equilibrium state, of the system.

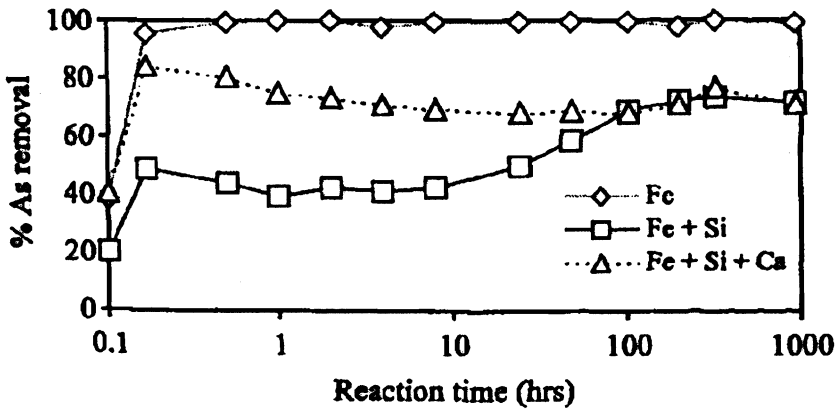

Figure 25 - Percent of initial arsenic removed from solution over time with amorphous $Fe(OH)_3$ at pH 8.5. Initial solution conditions: As(V) = 100µg/l, Fe = 20mg/l, SiO_2 = 40mg/l, and Ca = 10mg/l (Smith and Edwards 2005).

The batch study depicted in Figure 26 from Smith and Edwards demonstrates that the method of silica exposure to activated alumina can dramatically affect its capacity for arsenic removal (2005). The authors found similar results using granular ferric hydroxide although the results were not shown in their published work. Two sets of solutions of 2 g/l activated alumina were prepared with and without pre-exposure to 40 mg/l activated alumina. During the pre-exposure and reaction period with arsenic, silica was adsorbed. For one set of solutions the quantity of silica adsorbed was replaced daily with additional silica to reconstitute the initial 40 mg/l of SiO_2 in solution. Pre-exposure of activated alumina to a constant 40 mg/l of SiO_2 for 1 week caused the rate of arsenic adsorption (initial slope in Figure 26) to be 4 times slower than without pre-exposure. This pre-exposure scenario at constant concentration is similar to what is encountered in adsorptive media columns. That is to say, in column systems silica typically exhibits almost instantaneous breakthrough, establishing constant concentration throughout the column, while arsenic is completely removed initially in the front-end of the column. Later stages of the column will have pre-equilibrated with the inlet silica concentration

for some time before arsenic migrates to those stages. This batch study would suggest that the pre-equilibration time with constant silica concentration will minimize both the adsorption kinetics and final sorption density of arsenic in the later stages of the column.

The results of the Smith and Edwards study caution against the use of simple batch tests or rapid small scale column testing (RSSCT) for full-scale projections. The data indicates that batch and RSSCT tests will over predict the performance of full-size operations at pH 7.8 and above in waters with high silica concentrations. However, no other approach is yet available.

Interestingly, pre-equilibration with a solution with an initial silica concentration of 40mg/l had no adverse effect on adsorption. Only when the solution was replenished with silica to 40mg/l each day did the solution adversely interfere with arsenic sorption. This may be given the greater total mass of silica in the system for the silica-replenished experiment. Over the entire experiment 126 mg/l of silica were added for the solution replenished daily with silica versus only 40 mg/l of silica in total for the solution not replenished with silica.

Additionally, exposure to constant silica concentration concurrently with arsenic without the pre-equilibration period also did not impact adsorption of arsenic greatly. Arsenate was able to compete more readily with silica when it was introduced to the iron in the solution at the same time, despite the renewed silica concentration in solution over time. Except for the constant silica concentration experiment with 1 week pre-equilibration time, the arsenic adsorbed at equilibrium was largely the same; only the kinetics differed between the experimental conditions (Smith and Edwards 2005).

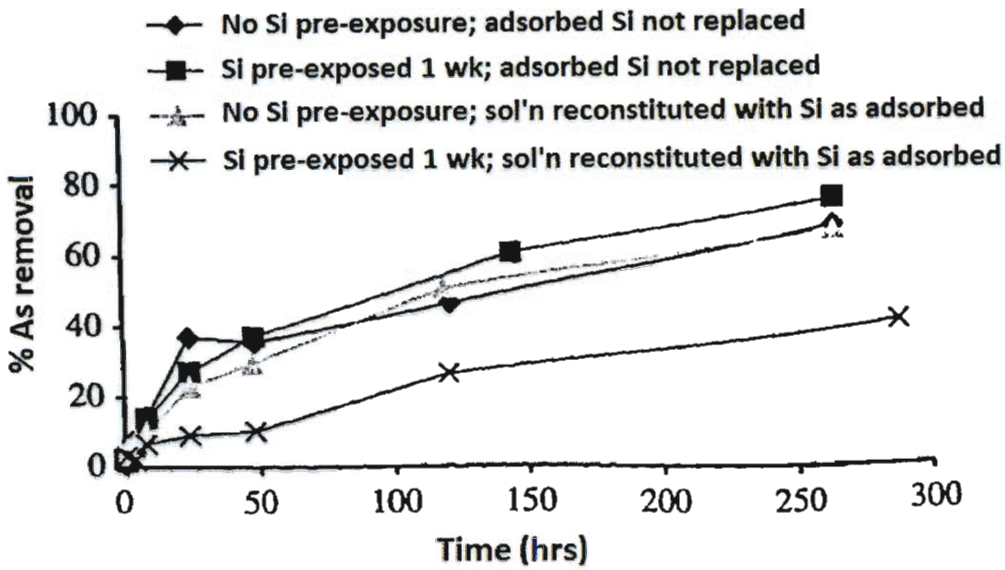

Figure 26 – Percent arsenic removal from batch experiments with 2g/l activated alumina given solutions prepared with 40mg/l SiO2, 500µg/l As, and 1mM $NaHCO_3$ (Smith and Edwards 2005).

Silica removal

High silica concentrations cause problems in the geothermal and power production industries, among others, due to formation of scale deposits. Silica scale can form on process equipment including turbine blades, cooling towers, and other heat exchange surfaces. Sometimes silica must be removed from industrial effluent waters to prevent the milky-appearance of colloidal silica in rivers and streams.

Removing silica from water is generally a two-step process. First, precipitation methods are used to bring silica concentrations down to approximately 2-3 mg/l. Then, adsorption or ion exchange processes can be used more economically to remove the remaining silica to the required level.

Silica can be precipitated from solution through the formation of calcium or magnesium complexes with silica above pH 9.5. When $MgCl_2$ or $CaCl_2$ is added to alkaline waters, it dissociates and forms Ca or Mg hydroxides. These metal hydroxides

can then complex with silicates lowering the solubility to at least those of pure quartz (Hast 1956; Garcia-Lara and Montero-Ocampo 2010). Lime, $Ca(OH)_2$, is often used to simultaneously add calcium and raise the pH. If the temperature of the solution is raised, the concentration of lime required can be reduced by half. In addition, Al, Be, Fe, Ga, Gd, and Y all retard dissolution and reduce the solubility of silica at neutral pH. Addition of Al had the greatest effect. Al^{3+} precipitates soluble silica in pH 5-11 but at least 4 moles of Al are required per mole of SiO_2. reducing soluble SiO_2 from 35mg/l to 15mg/l with 20mg/l Al from $AlCl_3$, to 5mg/l with 50mg/l Al, and to approximately 3mg/l with 100mg/l Al at pH 8-9 (Iler 1979). A corresponding correlation for molar concentration of Al and SiO_2 remaining in solution is approximately represented by:

$$C_{SiO_2} C_{Al} = (0.1 \pm 0.05) \times 10^{-12}$$

Adsorption to activated alumina in a packed column can reduce silica to very low levels. Bouguerra and Ali et al. found the pH range for maximum adsorption to be between 7-8.5 in batch testing (2007). The Barnstead silica removal unit used in the present work to produce highly pure, deionized water takes advantage of this maxima. The degree of adsorption from solution also correlated strongly with temperature between 10, 20, and 30°C with more adsorption occurring at higher temperatures. Common competing species (SO_4^{2-}, Cl^-, F^-, and NO_3^-) in concentrations of 250mg/l showed less than 6% reduction in adsorption of 50mg/l of SiO_2 as compared to the baseline without competing species.

Electro-coagulation with Fe or Al electrodes with copolymer can reduce silica concentrations to very low level (Abo-El-Enein, Eissa et al. 2009). However, the silica

must be ionized in alkaline solution before silica species will respond to an electric current.

Ion-exchange on a strong base resin is often used as a final polishing step to bring silica concentrations from 3mg/l to as low as 0.3mg/l. Like electro-coagulation, only silicate ions are adsorbed by strong-base ion exchange resins, so the solution must be alkaline before treatment.

Regeneration of iron-oxide adsorbents

Regeneration is often necessary to extend the life and reduce the cost of adsorptive media in packed columns. After adsorption to iron-oxide based media, several researchers have demonstrated the ability to successfully remove the arsenic and reuse the media for repeated adsorption cycles. Sylvester et al. reported that a warm caustic solution of NaOH effectively regenerated arsenic-saturated ion-exchange resins within 4 bed volumes (2007). The HFO-based adsorbent was regenerated by a 10% NaOH solution with a minimum empty bed contact time (EBCT) of 6 minutes. After regeneration, the bed was rinsed with 10-15 bed volumes of water sparged with carbon dioxide to return the column to neutral pH conditions. The arsenic removal capacity of the regenerated media actually increased over the first adsorption cycle. Huang and Fu found that strong acid or base desorbs As(V) from activated carbon media, but future adsorption capacity of the media was hindered (Huang and Fu 1984).

Pan et al. reported a 98% recovery of phosphate from an HFO nanoparticle-based sorbent by flushing with 10 bed volumes of a 5% NaOH, 5% NaCl solution by weight. The system showed no significant loss in capacity in successive adsorption cycles (2009). A saturated carbon-dioxide solution was used to return the system to neutral pH

following each regeneration cycle. Blaney et al. also observed over 95% recovery of phosphate with 12 bed volumes of a 2% NaOH, 2% NaCl regeneration solution by weight (2007).

Given a regeneration solution composed of NaOH in deionized water at pH of 13.5, Visual Minteq would predict that 25.8% of the arsenate in the system would be in the aqueous solution phase partitioning into 1 pore volume of the column, assuming an approximation of batch equilibrium. This prediction was generated using the HFO with DLM surface complexation modeling and assumed batch equilibrium. An iron-oxide concentration of $3000m^2/l$ was specified, which is the surface area of sites per liter inside one of the columns used in the present work, calculated from one bed volume containing 4.4ml of pore volume and 1.1g of magnetite with a surface area of $12m^2/g$. The regeneration solution would readily strip approximately one quarter of the arsenic from the adsorbent material with each pore volume through the column. If assuming batch regeneration with 8 regeneration solutions of one pore volume each, 90% of the adsorbed arsenic will have been removed from the media. Similarly, for 8 regeneration cycles with the same conditions, a Visual Minteq simulation predicts that 95% of the adsorbed silica would be removed from silica-saturated magnetite. A study by ATR-FTIR indicated that desorption of silicates from magnetite nanoparticles was facilitated by high pH conditions; however, the IR spectra also determined that a significant amount of adsorbed silicates were not desorbed (Yang, Roonasi et al. 2008). The authors hypothesized that inner-sphere complexes are formed between the silicate species and the magnetite surface.

Fate and transport of spent adsorbents and adsorbed contaminants

It is important to consider the fate and transport of spent nanomagnetite with adsorbed arsenic. The mobility of the nanomaterials, their toxicity on the environment and biota, and facilitated transport of heavy metals are areas of significant research and concern.

Saleh et al. found that unmodified zero-valent iron nanoparticles were immobile in porous media (2008). Only when a polymer or surfactant was added were the nanoparticles able to flow due to greater steric, electrostatic, or electrosteric stabilization. The mobility of the stabilized nanoparticles in sand columns depended on the ionic strength and cations present in solution as well as the physical and chemical heterogeneities of the media.

When nanomaterials are mobile, they may facilitate the transport of arsenic or other heavy metals through the environment and into biota. Sun et al. determined that the introduction of titanium dioxide nanoparticles into arsenic contaminated water increased the uptake of arsenic into carp by 132% during 25 days of exposure (2007).

In controlled lab environments, researchers have demonstrated cytotoxicity of some nanomaterials including carbon nanotubes and fullerenes (Sayes, Fortner et al. 2004; Jia, Wang et al. 2005), yet much more understanding is needed to consider the full impacts of the fate and transport of nanomaterials in the environment (Alvarez, Colvin et al. 2009).

In order to dispose of spent adsorbents in public landfills, the EPA requires the material be tested under the toxicity characteristic leaching procedure (TCLP). The TCLP leachate must comply with heavy metal limits including an arsenic limit of 5mg/l

in order to be considered non-hazardous (USEPA 2001). In California, more vigorous leaching tests are required in addition to the national TCLP tests. They include the TTLP and the California Waste Extraction Test (WET), which one researcher found to leach 10 times more arsenic than the TCLP test from 5 different spent adsorbents (Jing, Liu et al. 2005).

In addition to pH and direct chemical extraction, reducing conditions may also pose a risk to arsenic desorption and release. One study examined the redox transformation and mobility of spent media in reducing conditions (Jing, Liu et al. 2008). The spent media included granular ferric hydroxide, granular ferric oxide, titanium dioxide, and activated alumina from several pilot column filters. During the 65 day study, mixed reducing bacteria were used to reduce the electron activity (pE) from 1.7 to -7. In the reducing conditions, Fe(III) was reduced to Fe(II), As(V) to As(III), and sulfate to sulfide; however, less than 4% of the total arsenic was released from any of the iron-based materials. The titanium dioxide adsorbent, however, released up to 38% of the adsorbed arsenic at redox potentials below -6.

More complete understanding of the environmental fate and transport of the nanomaterials and adsorbed heavy metals as it relates to landfills may be needed to prove the applicability of the current regulations on disposal and leaching.

3. Materials and Methods

Solutions and chemicals

Raw groundwater from Guanajuato municipal well No. 8 was transported by personal vehicle in clean plastic 30 liter containers and placed in a refrigerated chamber at 4°C upon arrival to Rice University. Before conducting experiments with the Guanajuato groundwater, the water was allowed to warm to room temperature. Lab-purified water was Rice University groundwater that was first deionized by ion-exchange, then purified by either a Millipore Mili-Q water system (18.2 MΩ-cm) or by reverse osmosis followed by a 4-stage Barnstead filter. Untreated groundwater was also collected from the Rice University well, adjacent to the Mechanical Laboratory building, before the point of chlorination for use in laboratory studies. Unless otherwise noted, ACS-grade chemicals from Fisher and Sigma Aldrich were used. Generally, synthetic solutions were buffered with 2.5mM tris(hydroxymethyl)aminomethane (THAM) and brought to the desired pH with trace-metal-grade HNO_3 or 1.0 M NaOH. Ionic strength was adjusted with NaCl or $NaNO_3$. A concentrated solution of arsenate (50mg/l as As(V)), composed of arsenic(V) oxide hydrate ($As_2O_5 \cdot 3H_2O$) from Sigma Aldrich dissolved in deionized water, was used to spike experimental waters.

The properties and composition of groundwater from Guanajuato Well No. 8 and Rice groundwater are displayed in Table 4. Although conditions directly at Well No. 8 were measured at a temperature of 60°C, pH of 6.83, and redox potential of 200mV, the analysis displayed in Table 4 was taken of aerated groundwater at 25°C to be consistent with experimental conditions of the labwork conducted at Rice University with Guanajuato groundwater. Unless otherwise specified, the Rice University groundwater

was also brought to room temperature and aerated before experimental use. The pH was measured with an Orion-Research combination glass-reference electrode calibrated to pH 4, 7, and 10 using standard solutions from Fisher-Scientific. A Hach SensIon156 multimeter was used for conductivity and total dissolved solids (TDS) measurements. Total alkalinity was measured by Hach method, where phenolphthalein and bromocresol green-methyl red pillows were added to the solution and titrated with sulfuric acid to the pH 4.5 endpoint. Phosphate was measured by the Hach PhosVer methods. COD was determined by Hach reactor digestion method for ultra-low-range (0.7-40.0 mg/l) detection. The Hach FerroVer method was used to measure total Fe, which includes the particulate, as well as, dissolved Fe. Dissolved Ca, Mg, Fe, Si, Na, and K were determined by Perkin Elmer Optima 4300DV Inductively Coupled Plasma-Optical Emission Spectrometer (ICP-OES). Dissolved Ag, As, Be, Ca, Co, Cr, Cu, Pb, Se, U, V, and Zn were determined by Perkin Elmer Elan 9000 Inductively Coupled Plasma-Mass Spectrometer (ICP-MS) analysis as described in detail later in this section. Visual Minteq (Gustafsson 2009) was used to determine arsenic and iron speciation with the given redox potential and pH. At the conditions given in Table 4, 100% of the arsenic exists as As(V), with 97.8% in the form of $H_2AsO_4^-$, 2.1% in the form of $HAsO_4^{2-}$, 0.1% in the form of AsO_4^{3-}, and 0% in the form of H_3AsO_4. As for free iron and iron associated with aqueous complexes, 99.995% of the total was in the form of Fe(III) and the remainder being Fe(II).

Table 4 - Measured properties and components of aerated Guanajuato and Rice groundwater at 25°C

Parameter	Mexico GW	Rice GW	Units	Test Method
pH	8.55	8.55	-	Hach SensIon156 probe
Redox	291	184	mV	Hach probe
Conductivity	510	558	µS	Hach probe
COD	0	0	mg/l	Hach digestion ULR
Alkalinity	144	208	mg/l as $CaCO_3$	Hach titration
Hardness	39.7	40.4	mg/l as $CaCO_3$	Hach titration
Calcium	30.9	11.2	mg/l	ICP-OES
Magnesium	6.6	3.0	mg/l	ICP-OES
Zinc	0.1	0.0	mg/l	ICP-OES
Sodium	121.6	103.9	mg/l	ICP-OES
Potassium	1.3	1.4	mg/l	ICP-OES
Iron	0.7-1.7	0.12	mg/l as Fe	Hach FerroVer
Sulfate	15	6	mg/l	Hach SulfaVer
Phosphate	0.12	0.08	mg/l	Hach PhosVer
Chloride	<10	<10	mg/l	Hach titration
Silica	52	18	mg/l as SiO_2	ICP-OES
Arsenic	30	2	µg/l as As	ICP-MS
Vanadate	13	0	µg/l	ICP-MS

Property analysis of magnetite adsorbents

The degree of arsenic partitioning to several nanomagnetite products, listed in Table 5, was compared using adsorption isotherms to select an appropriate sorbent for large-scale pilot studies. The price per kilogram for each product was taken from sales quotes provided by each vendor. The specific surface areas listed are published from the product manufacturers. The high-purity rating certifies a product is of sufficient purity to

comply with FDA 21 CFR 73.2250 limits for As, Pb, and Hg (3, 10, and 3 mg/l, respectively), while the designation of safety for food-contact applications is based on regulations set out in the European Union Commission Directive 95/45/EC (EU 1995).

Table 5 - Summary of commercial magnetite nanoparticles screened by adsorption isotherms for use in subsequent arsenic removal batch and column studies. Values in parenthesis are estimated based on spherical geometry: $SSA(m^2/g) = 6\times10^9/(\rho \cdot D)$, where ρ is density (5×10^6 g/m^3) for magnetite and D is particle diameter (nm). †Indicates measurement by SEM or TEM at Rice. All other values and properties were provided by the manufacturer.

Product	Producer	Lot #	$/ kg	Particle Diameter (nm)	SSA m^2/g	21CFR Compliant	EC-Food Contact
Magnetite	Reade	-	260	(20)	60†	No	No
B22160	BioPigments	B22160	14	10	(120)	No	No
J8105	Rockwood	BE08043	5.5	200	(6)	No	No
BK5599	Rockwood	115075	5.5	300	(7)	No	No
78P	Rockwood	590C	5.5	(98)	12†	Yes	Yes
BK4799	Rockwood	17501292	5.5	(150)	8	Yes	No
845	Rockwood	S4242	5.5	90	(9.5)	No	No
850	Rockwood	S2648	5.5	110	(5.45)	No	No
848	Rockwood	S3827	5.5	90	(6.67)	Yes	Yes
BK5099	Rockwood	H504073	5.5	350	(6)	No	No
BK5000 HP	Rockwood	105081	5.5	300	(8)	Yes	No

The adsorption isotherms were conducted at room temperature and in aerated conditions. For each magnetite product, a series of masses (0, 4, 8, 17.5, 32.5, and 65 mg) were weighed into 60ml polyethylene vials (Environmental Express). It is understood that some associated water may contribute to the mass measured, however no attempt was made to normalize to adsorbent solid weight alone. The 50 mg/l As(V) stock solution was spiked into 2 liters of Rice groundwater, resulting in an arsenic concentration of 75µg/l. Triplicate samples of the spiked-groundwater were filtered

through 0.45μm polyethersulfone (PES) membrane filters from Whatman and acidified to 1%-by-weight with concentrated trace-metal-grade HNO_3 (Fisher) for analysis on ICP-MS. For the adsorption isotherms, vials with pre-weighed magnetite were filled with 50ml of the prepared solution, tightly capped, and rotated end-over-end at 3rpm for 24 hours. Afterwards the magnetite was let settle, aided by magnetic attraction to an N-52 grade, neodymium magnet (K&J Magnetics) placed below the vial. The magnet exhibited field strengths of 0.62 Tesla along its edges touching the vial and of 0.1 Tesla a distance of 1cm away from the magnet. Magnetic field was measured by a M1ST DC Gaussmeter (AlphaLab, Inc.), calibrated with an NIST certificate of accuracy. After magnetic-assisted settling, the vial caps were removed and 10ml of each solution was removed by 10ml plastic syringe (B-D, New Jersey, USA) and passed through a 0.45μm Whatman filter. Solutions were transferred to 15-ml centrifuge vials (Fisher) and acidified to 1%-by-weight with concentrated trace-metal-grade HNO_3 (Fisher). All samples were analyzed by ICP-MS and the adsorbed arsenic was calculated from the concentration of arsenic removed from solution.

The 78P magnetite used in the present work is formed by wet precipitation. The product is then dried and ground to reduce aggregate size. Because the product is stored dry in air, the surface layer is likely oxidized to maghemite (Rebodos and Vikesland 2010). Images of 78P were taken (Figure 27) via scanning electron microscopy (SEM), courtesy of Zuzanna Lewicka of the Dr. Vicki Colvin research group at Rice University. The instrument used was a Rice University Shared Equipment Authority (SEA) FEI Quanta 400F Field Emission Scope equipped with Secondary Electron (SE). Uncoated 78P powder was deposited dry onto carbon tape affixed to SEM aluminum stubs

(Electron Microscopy Sciences, Hatfield, PA). Stubs were tapped from the side to remove any loosely attached magnetite that could damage the instrument. Equipment settings included a working distance of 10mm, spot size of 3, accelerating voltage of 20 kV in high vacuum mode, and magnification levels of 5,000X, 20,000X, 50,000X, and 100,000X. The images suggest mostly spherical geometry with an upper size limit of about 400nm diameter to a lower boundary limited by image resolution on the SEM, much less than 100nm.

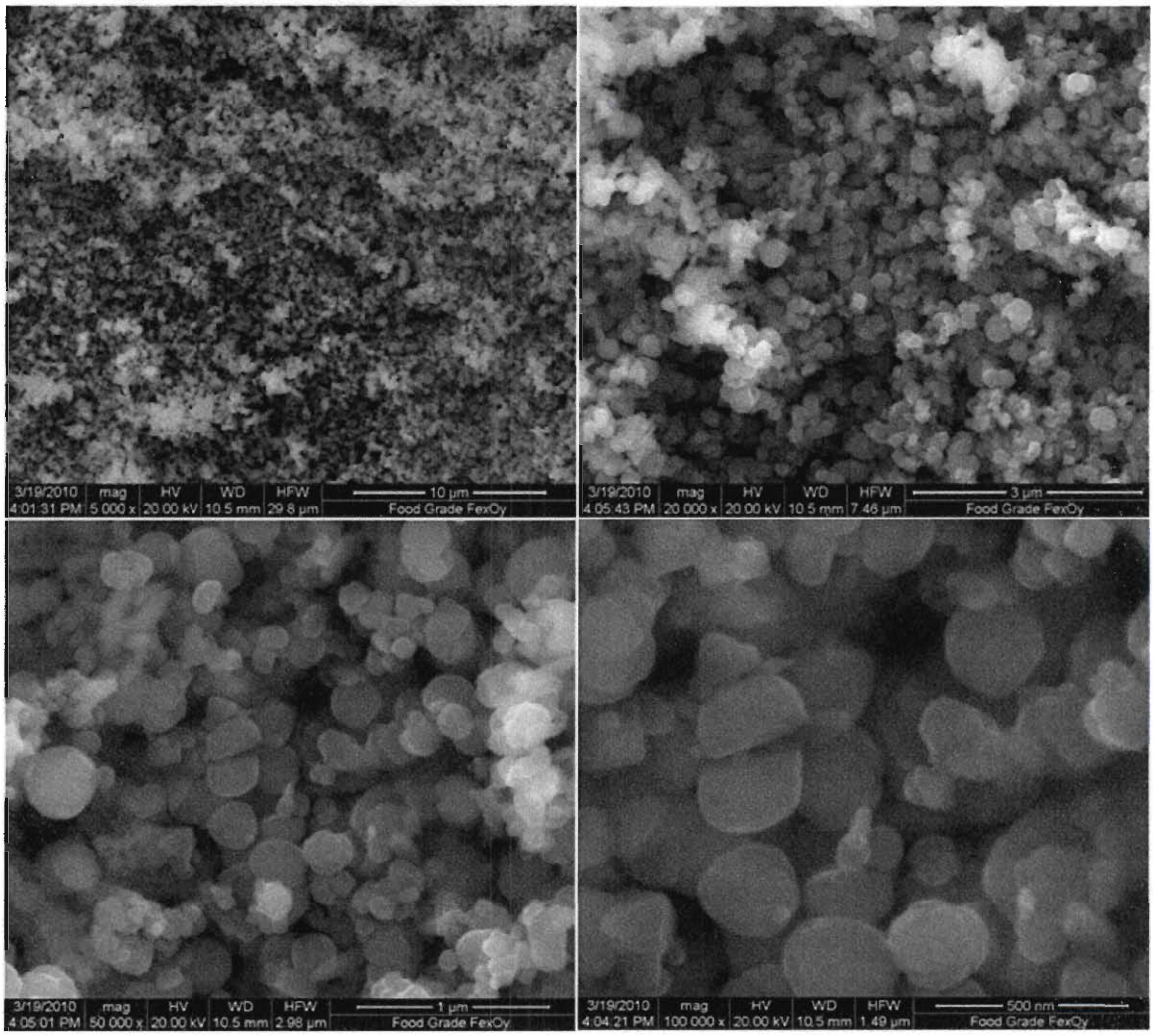

Figure 27 - SEM of Rockwood Pigments, Inc. 78P food-grade magnetite.

Brunauer-Emmett-Teller (BET) surface area analysis was conducted on 78P magnetite, courtesy of Zuzanna Lewicka, on a fully automated Quantachrome Autosorb 3B Surface Analyzer. As sample preparation, 0.3260g of 78P was introduced into a 6mm glass cell bulb (Qantachrome Instruments, Florida, USA). The sample was heated at 200 °C under vacuum for 8 hours to remove any contaminants adsorbed to the surface. The sample was then cooled with liquid nitrogen and the nitrogen adsorption was analyzed at specific pressures. Afterwards the pressure was decreased and the nitrogen desorption isotherm was assessed. The overlapping adsorption and desorption isotherms given in Figure 28 indicate that the material is non-porous; a hysteretic desorption profile would have indicate retention of nitrogen gas within pores. The BET equation coefficients were fit to the absorption curve between relative pressures of 0.07 to 0.32 P/P_0. This yielded a surface area of 12.13 m^2/g. Assuming smooth morphology, uniform particle size, and spherical geometry, the surface area measurement would give a particle diameter of 98.93 nm. This crude estimate of average diameter (nm) is estimated from the geometrical relationship:

$$D_{BET} = \frac{6}{SSA \times \rho} \times 1{,}000$$

where SSA is the specific surface area (m^2/g), and ρ is the solid density (g/cm^3), taken to be 5.0 g/cm^3 for magnetite (Walker 2009). The assumption of spherical shape underestimates the length dimensions of non-spherical particles as non-spherical particles have greater surface area to volume ratios. In addition, size heterogeneity and surface morphology result in many particle dimensions measuring above and below the given geometrical approximation.

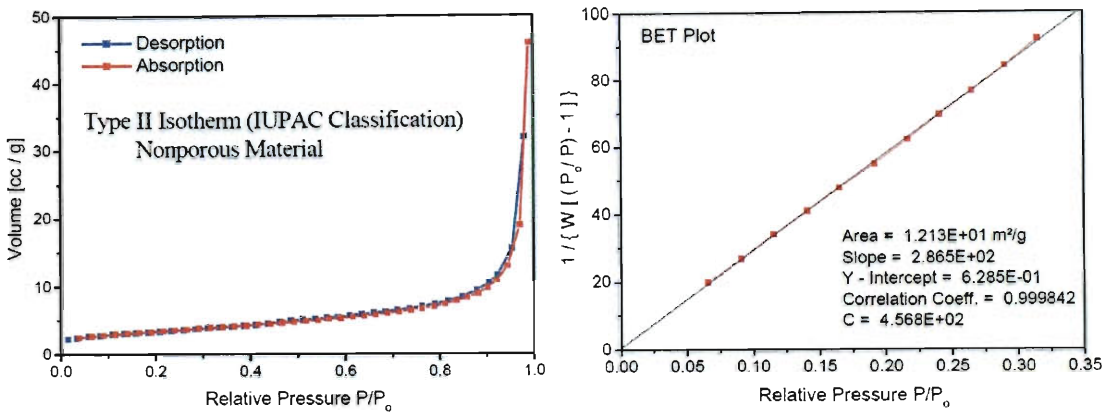

Figure 28 - BET surface area analysis of 78P food-grade magnetite.

ICP-MS elemental analysis

A Perkin Elmer ELAN 9000 Inductively Coupled Plasma-Mass Spectrometer (ICP-MS) was used to analyze for total arsenic and other trace elements in the parts per billion (µg/l) range. A daily performance analysis was performed before each batch of samples to ensure system parameters were within the acceptable range.

Certified multi-element atomic spectroscopy standard solutions from PerkinElmer were used to generate three to five point standard regressions for each element. The calibration solutions were acidified to 1% by volume with trace metal grade HNO_3. A 50 µg/l internal standard of germanium was prepared by volume dilution of a 1,000 mg/l Ge standard solution (Peak Performance) into Mili-Q water with 1% by volume trace-metal-grade HNO_3. The internal standard was mixed with the prepared elemental standards and samples through a static mixer as they were being injected into the ICP-MS. While the standard curve was developed and the samples were analyzed, the ICP-MS software adjusted the measured intensity of the sampled elements according to the internal standard intensity. The program assumed a constant germanium concentration, and therefore it normalized the variability in total mass of the target element bombarding the detector by the amount of germanium detected for each replicate and across the entire

sample-set. Due to this technique the prepared standards and samples, which were measured in triplicate, gave readings with relative standard deviations below 5%. Typical relative standard deviations ranged between 0.5 to 3% within the instrument measurement range for that particular element. The mean intensity of the blank standard was subtracted from the known germanium-adjusted intensities for the prepared known standards and a linear regression was forced through the origin and fitted by least-squares analysis. The resulting correlation coefficient, R^2, was typically greater than 0.9999, and when not, the prepared standards were remade. As an example, one standard series was prepared as 0, 0.26, 3.1, 12.4, and 27.0 µg/l of arsenic. The solutions were measured in triplicate giving a relative standard deviation of 3.7, 3.9, 1.2, 1.5, and 1.9% for each standard, respectively. The resulting R^2 coefficient of the linear regression was 0.999978, as shown in Figure 29. The minimum quantitation level (MQL) is defined as 10 times the standard deviation above the reagent water blank signal (1998). For the standard series mentioned above and shown in Figure 29, the blank intensity was 1752 counts with a relative standard deviation of 3.7%. The corresponding MQL would be 648 intensity units or 0.1 µg/l of arsenic, based on the slope of the standard regression.

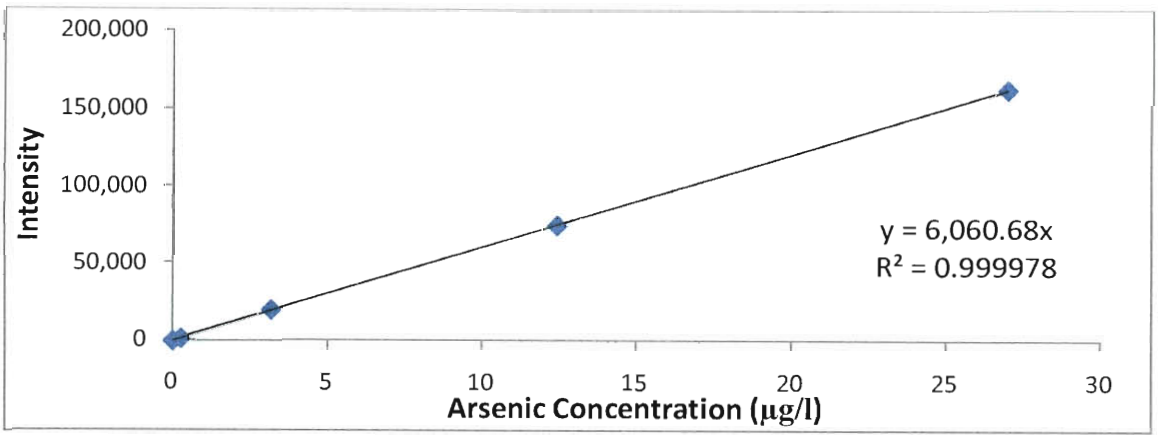

Figure 29 - ICP-MS calibration curve for arsenic.

After standard curve development, the concentrations of the target elements were determined for unknown samples arranged on a Perkin Elmer AS-93plus autosampler (Figure 30). Sample preparation before analysis included filtration through a 0.45µm PES membrane filter (Whatman) and acidification to 1% by volume with trace-metal grade HNO_3.

Figure 30 - Photo of the Perkin Elmer ELAN 9000 ICP-MS during a sample run with a sample set arranged on the Perkin Elmer AS-93plus autosampler.

Chloride interference on ICP-MS

Chloride is a known interference for arsenic (MW=75g/mol) measurement on ICP-MS due to its combination with argon to form ArCl (MW=75g/mol). An analytical balance was used to measure 40, 80, 206, and 412 mg of solid ACS-grade NaCl (Fisher) into 250ml Erlenmeyer flasks. Prior to the experiment, the glassware was washed and triple-rinsed with deionized water filtered by reverse osmosis and a 4-stage Barnstead unit. Approximately 215 ml of Guanajuato groundwater was weighed into each flask, yielding solutions with 112, 215, 595, and 1200 mg/l of chloride added. The

concentration of chloride in the raw Guanajuato groundwater was below the 10mg/l method detection limit of a silver nitrate titration (Hach Method 8207). The raw sample of Guanajuato groundwater without added chloride contained an initial concentration of 7.66μg/l as measured by ICP-MS. All samples were analyzed for arsenic by ICP-MS and the measured quantity above the concentration of arsenic in the raw water was considered to be due to the interference of chloride ions.

ICP-OES elemental analysis

A Perkin Elmer 4300 Inductively Coupled Plasma – Optical Emission Spectrometer (ICP-OES) was used for analysis of elements in the parts per million range (mg/l). This included Ca, Mg, Na, K, Si, S, and P. Certified multi-element atomic spectroscopy standard solutions from PerkinElmer were used to generate three to five point standard regressions for each element. The calibration solutions were acidified to 1% by volume with trace metal grade HNO_3. An internal standard of yitrium was prepared by volume dilution of a 1,000 mg/l Y standard solution (Perkin Elmer) into Mili-Q water with 1% by volume trace-metal-grade HNO_3. The internal standard was mixed with the standards and samples through a static mixer as they were being injected into the ICP-OES. While the standard curve was developed and the samples were analyzed, the ICP-OES software adjusted the measured intensity of the sampled elements according to the internal standard intensity. The program assumed a constant Y concentration, and therefore it normalized the variability in total mass of the target element based on the amount of Y detected for each replicate and across the entire sample-set. Due to this technique, the standard solution and samples, which were measured in triplicate, gave readings with relative standard deviations below 5%.

Typically, the relative standard deviations ranged between 0.25 to 1.5% within the instrument measurement range for each element. The standard curve was developed as a linear regression forced to cross the y-axis at the measured mean intensity of the blank and fitted by least-squares to the measured mean intensities of the known standards. However, before arithmetic means were calculated, each replicate measurement was first adjusted according to the internal standard intensity for that replicate. Standard solutions were remade whenever the correlation coefficient, R^2, dropped below 0.9999. An example standard series for silicon was prepared as 1.5, 9, and 28 mg/l. The solutions were measured in triplicate giving a relative standard deviation of 0.85, 0.61, and 0.29% for each standard, respectively. The resulting R^2 coefficient of the linear regression was 0.99996. The minimum quantitation level (MQL), defined as 10 times the standard deviation above the reagent water blank signal, was 0.019 mg/l (1998).

Sample preparation before analysis included filtration through a 0.45μm PES membrane filter (Whatman) and acidification to 1% by volume with trace-metal-grade HNO_3.

Arsenic isotherms and chromatographic breakthrough with synthetic solutions and groundwater

A high-purity synthetic solution and a groundwater solution were flowed through two identical columns (described below) to compare the effects of competing ions on arsenic breakthrough. The synthetic solution was formulated with Fisher HPLC-grade water, 29μg/l As(V), 2.5mM THAM buffer, 6.4 mM NaCl, and pH was adjusted to 8.5 with trace-metal grade HNO_3 in aerated conditions. The pH was measured by an Orion-Ross combination glass electrode. The groundwater solution was composed of

groundwater sampled from the Rice University well with As(V) added to result in 29µg/l of total arsenic, also in aerated conditions. Solutions were stirred by magnetic stir bar throughout the experiment in a 10 liter Pyrex glass container used as a feed tank.

Column packing media were made by combining 78P magnetite (Rockwood Pigments) and washed sea sand (Fisher) in a magnetite to sand ratio of 15:85. The magnetite and sand were weighed into a 60ml Environmental Express vial, capped, and blended together by shaking vigorously by hand for several minutes (Figure 31).

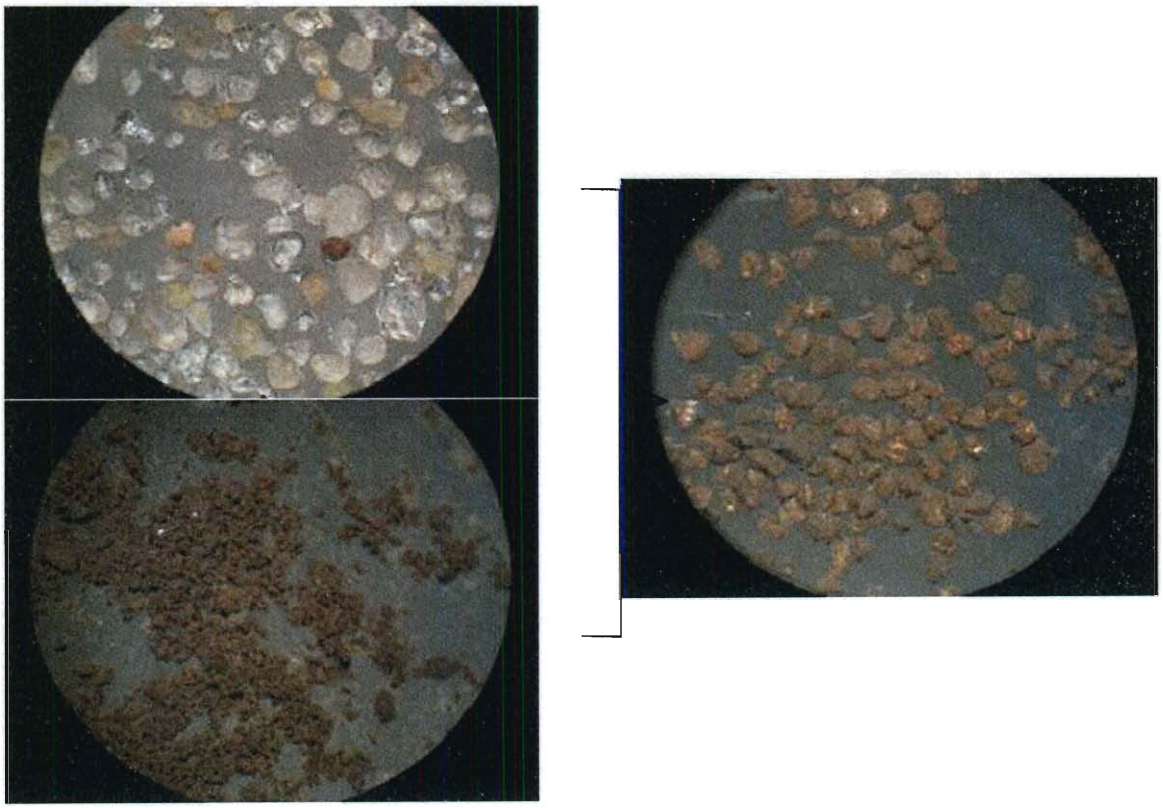

Figure 31 - Optical microscope image (3.5x magnification) showing sand and aggregated nanomagnetite individually and after shaking together vigorously for 1 minute. Upper left: sand; lower left: 78P magnetite; right: magnetite/sand blend.

The adsorbent blend was wet packed into a 10mm diameter, 40cm height Omnifit column. For the wet-packing procedure, HPLC-grade water was delivered in up-flow

mode through the column at a minimal flow rate of 0.5 ml/min using a Pharmacia P-500 pump. Column materials were all packed at a rate which kept the materials within 0.5-1 cm below the liquid level as the column filled. By slowly submerging materials in the standing water during packing, air pockets around the particles were greatly reduced as compared to dry-packing methods. Borosilicate glass beads (ChemGlass), 3mm in diameter, were loaded through a funnel at the top of the column. The beads rested at the base of the column to help disperse the dominant flow path from the center of the column and support the finer media that would be loaded above. Next, phosphoric acid-treated glass wool (Supelco) was rolled and compressed by hand into a tight ball, approximately 0.5cm in diameter and pushed down into the column, firm against the glass beads, with a metal rod. This supported a 2-3cm layer of pure sand. The column was tapped on the side of the column to level the sand layer before the next layer was added. The sand/magnetite adsorbent media were poured next into the column through a funnel and occupied 30cm of height within the column. Above the sand/magnetite material, the support materials were loaded in converse order (pure sand, glass wool, and finally glass beads) to contain the adsorbent media on both ends. The entire column contents were compressed slightly with an adjustable column endpiece. During the course of flow, if the media experienced compression and separation, leaving a water gap, the adjustable endpiece was used to remove the excess liquid space. During the experiments, the Pharmacia P-500 pump was used to keep a constant flow rate of 8.05 ml/min corresponding to a 1.1 minute residence time through the adsorbent media pore space of 8.90 cm^3. The flow rate was measured periodically with stop-watch and weigh dish but no significant change in flow rate was detected over the course of the experiments. In

addition to the residence time through the 8.90 cm^3 of pore space of the magnetite/sand blend, water also spent time in the column in the interstitial pores of the pure sand, glass bead, and glass wool support material. The residence time of the water in contact with the non-adsorbing support materials was not counted toward the residence time reported for the column. Neither was the interstitial pore space of the support material counted toward the column pore volume used in reporting breakthrough concentration profiles. In other words, the 1.1 minute residence time refers only to time the solution is in contact with the magnetite/sand blend portion of the column, and 1 pore volume (8.90 cm^3) is the water volume contained within the interstices of the magnetite/sand blend alone layer alone. However, the additional pore space of the interstices between the non-adsorbing support material sections (pure sand, glass beads, and glass wool) after the magnetite/sand blend section may have contributed to some dispersion of the actual arsenic concentration directly leaving the magnetite/sand blend portion of the column, due to mechanical dispersion and diffusion.

A sampling schedule was chosen to capture a high frequency of samples at the beginning of column flow, and the frequency was progressively reduced as time progressed. This improved the resolution for capturing the zone of mass transfer if arsenic breakthrough were to occur early. This also reduced the sampling burden in the case of delayed breakthrough -- in which case, lower sampling frequencies are required because the zone of mass-transfer spreads due to dispersion. Initial sampling frequency was every 5 minutes for the column fed the groundwater solution and it was gradually decreased until the sampling frequency at the end was every 70 minutes. These values were chosen based on estimates from arsenic adsorption isotherms in similar conditions.

Initial sampling frequency was every 40 minutes for the column fed the synthetic solution and it was gradually decreased until the sampling frequency at the end was every few hours; however, for some experiments longer sampling periods were used during overnight periods. Effluent samples were collected directly from the outlet tubing into a 10ml plastic syringe and then filtered by 0.45μm PES Whatman filter. Samples were acidified with 1% concentrated trace-metal-grade HNO_3 by volume and stored in 15ml Fisherbrand centrifuge vials until analysis.

Adsorption isotherms at high temperature, low oxygen wellhead conditions

Adsorption isotherms were conducted at the wellhead temperature (60°C) of the Guanajuato Municipal Well No. 8 (pictured in Figure 32) and in low oxygen conditions. A series of masses (9, 21, and 61 mg) of 78P magnetite were weighed into 60ml plastic vials. The final weight of the magnetite and vial were recorded for later use. A 2 liter glass beaker was filled with groundwater and spiked with stock As(V) solution (50mg/l) to 90μg/l as total arsenic. The solution was deoxygenated in a vacuum chamber over several hours, then capped and heated to 60°C in a laboratory oven (Fisher-Scientific). Approximately 55ml of groundwater was then poured into the pre-weighed vials containing the magnetite and weighed in an anaerobic chamber. The vial was capped, after wrapping the vial threads with Teflon tape, and attached securely to a plastic manifold. The manifold was submerged into a water, shaker bath (Julabo, SW22) which was preheated to 60°C.

After the mixing period, the magnetite was allowed to settle aided by magnetic attraction to an N-52 grade neodymium magnet (K&J Magnetics) placed below the vial. The vial caps were removed and 10ml of each solution was immediately removed by

10ml plastic syringe (B-D) and passed through a 0.45μm Whatman filter. Solutions were transferred to 15-ml centrifuge vials (Fisher) and acidified to 1%-by-weight with concentrated trace-metal-grade HNO_3 (Fisher). All samples were analyzed by ICP-MS and the adsorbed arsenic was calculated from the concentration of arsenic removed from solution.

Figure 32 - Guanajuato Municipal Well No. 8

Guanajuato groundwater adsorption isotherms at various pH conditions

Adsorption isotherms were conducted for series of pH conditions (5.5, 6.5, 7.5, and 8.5) in Guanajuato groundwater. Four 500ml portions of groundwater from the Guanajuato Municipal Well No. 8 were poured into 1 liter glass beakers and aerated at room temperature. The measured properties and composition of the groundwater is displayed in Table 4. Concentrated trace-metal-grade HNO3 was used to adjust the groundwater from 8.55 to the desired pH. The solutions were checked before and after the experiment to confirm that no significant change of pH occurred during the course of the experiment.

As(V) stock solution was spiked into each beaker to result in a total arsenic concentration of approximately 60 µg/l. Duplicate samples of each solution were filtered through a 0.45µm polyethersulfone (PES) membrane filter (Whatman) and acidified to 1%-by-weight with concentrated, trace-metal-grade HNO_3 (Fisher). These samples were set aside for analysis on ICP-MS and were defined as the initial arsenic concentration before adsorption. A series of 60ml vials (Environmental Express) with pre-weighed 78P magnetite (0, 4, 8, 17.5, 32.5, and 65 mg) were prepared for each pH condition. Approximately 50ml of the appropriate pH solution were poured into each vial and weighed. Two vials without magnetite were filled with solution as blanks for each pH condition. The vials were then tightly capped and rotated end-over-end at 3rpm for 24 hours. After the mixing period, the magnetite was allowed to settle aided by magnetic attraction to an N-52 grade neodymium magnet (K&J Magnetics) placed below the vial. The vial caps were removed and 10ml of each solution was removed by 10ml plastic syringe (B-D, New Jersey, USA) and passed through a 0.45µm Whatman filter. Solutions were transferred to 15-ml centrifuge vials (Fisher) and preserved with 1%-by-weight concentrated trace-metal-grade HNO_3 (Fisher). The samples were analyzed for arsenic by ICP-MS and the adsorbed arsenic was calculated from the concentration of arsenic removed from solution. In addition, the samples were analyzed on ICP-OES to measure Ca, Mg, Si, P, and S concentrations.

Pilot column studies in Guanajuato, Mexico

Three pilot column experiments were conducted in Guanajuato, Mexico, in December 2009 and March-April 2010, with groundwater from the Guanajuato Municipal Well No.8. The three pilot columns were built identically; however, the first

was tested with raw groundwater, while the second and third columns were tested with pH adjusted groundwater. For each pilot column, 10,000 liters of water were brought by city water truck (Figure 34a) to the municipal drinking water plant laboratory (Figure 34b). Piping was assembled to pump directly from the water truck into the pilot column stationed in the laboratory. A schematic of the piping and column system are shown in Figure 33.

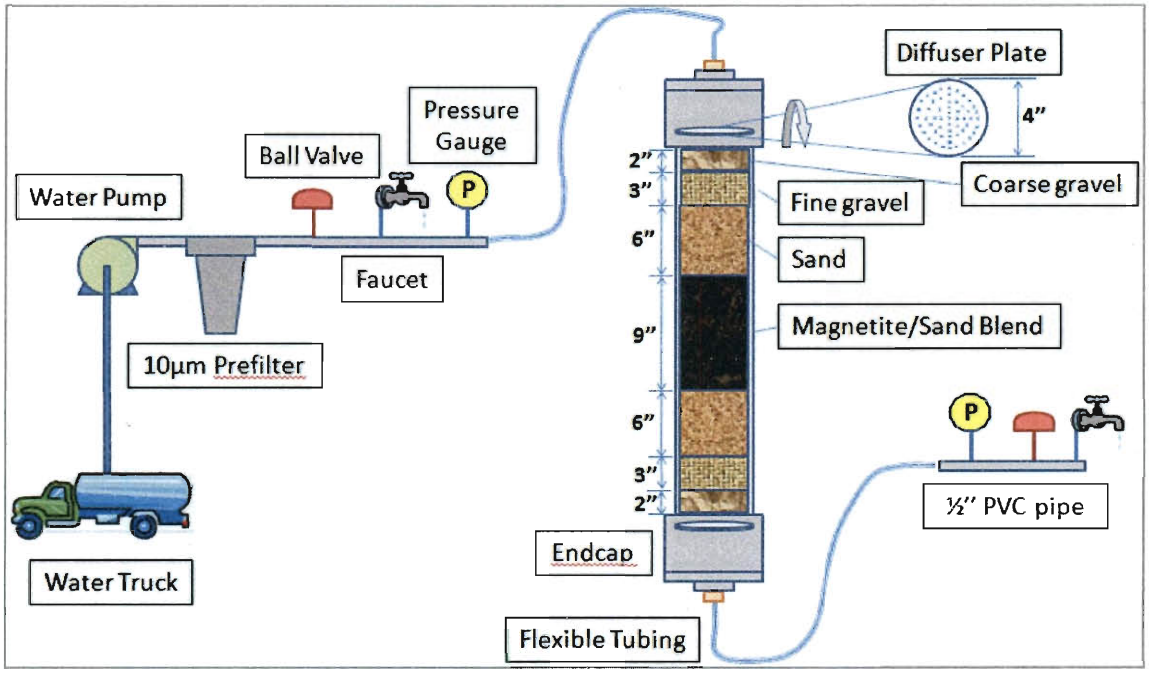

Figure 33 - Schematic of pilot column setup used in Guanajuato.

Figure 34 – a. Jesse Farrell and John Fortner setting up piping from the water truck to the laboratory through a window on the second floor of the water treatment facility. b. John Fortner monitoring the pilot column and Jesse Farrell performing arsenic testing in the laboratory space.

For the first experiment with raw groundwater, the Guanajuato municipal water company provided an industrial-sized pump to supply water to the column from the truck at a constant pressure (36psi). The fluid flow was regulated by the backpressure of a faucet valve at the end of the column. Over the span of several days, the pressure drop through the column increased due to compression of the media and particle straining. This effect is mediated in industry by frequent backwashing (Satterfield 2005); however the pilot columns were not backwashed in order to keep the magnetite/sand blend stationary. To mitigate the decreased flow rate in the pilot column with constant inlet pressure, the faucet valve at the column outlet was periodically adjusted to decrease the back-pressure at the end of the column, thereby maintaining the target flow rate. The flow rate issue was avoided for the pH adjusted experiments by using a positive displacement pump (QD Pump Drive, Q2CSC Pump Head, and Q485 precision adjustment dial; Fluid Metering, Inc.) which provided water at a constant flow rate to the columns, regardless of the pressure drop through the column. All columns were operated at a target rate of 1 liter per minute, which was measured periodically using a 500ml graduated cylinder and was adjusted as necessary. For all three columns, 456.6 grams of

Rockwood Pigments 78P magnetite was used in the active adsorption section of the column. The magnetite was dispersed by 2587.5 grams of washed sea sand (Fisher), making the magnetite to sand ratio 15:85 by weight, respectively. The mass of materials was measured with a triple beam balance. The sand and magnetite were combined in two 2-liter Nalgene, wide-mouth containers and were vigorously shaken by hand for approximately five minutes. Above and below the active adsorption section of the column, washed sea sand (Fisher), washed fine gravel, and washed course gravel was used to support and contain the media. Washing was accomplished by repeated rinse with deionized water until the wash water appeared clear. Diffuser plates (shown in Figure 33) were cut from a Plexiglass (PMMA) sheet, 0.5cm in thickness with holes drilled to permit fluid flow. The plates were carefully machined by the Facilities Engineering and Planning department at Rice University to fit between the column and the endcaps to support and contain the packing material. The column body was constructed with 4-inch internal diameter, pressure-rated transparent PVC pipe cut into 2.5-foot sections. Endcaps were assembled with 4-inch pressure-rated PVC couplings, 4-inch to 2-inch PVC reducers, and a 2-inch to ¾ inch thread reducers. Adapters were used to connect the ¾ inch thread to ½ inch PVC line or ¾ inch flexible, metal reinforced tubing which was rated for high pressure applications. PVC ball valves, pressure gauge dials, and metal faucet-valve sample ports were installed upstream and downstream of the columns. A 10 micron household prefilter (US Filter) was used before the column to prevent any sediments from entering the column. The PVC connections were sealed together with Harvey's PVC primer and quick-set PVC cement, while all threaded

connections were lined with Teflon tape. All column housing materials, fittings, pipe and auxiliary materials were purchased from C&B Plumbing Supplies (Houston, TX).

The column construction and assembly procedure began with cutting a 2.5 foot length of 4-inch diameter, clear PVC pipe (Figure 35a). Then, endcap components were bonded together with PVC primer and cement and let set for several hours as prescribed on the PVC cement container. When ready, one endcap was primed and glued onto the end of the 2.5-foot column with a diffuser plate in place and let set for another several hours before packing (Figure 35b). The column was placed over a y-fitting attached to a wide-base shower drain to stabilize the column upright and to allow an opening to connect flexible tubing to the column endcap. The column was further stabilized by a metal stand fitted with a 4 inch PVC clamp.

Figure 35 – Construction of the pilot columns in Guanajuato, Mexico.

A dry-pack method was used to prevent stratification of the media during construction. First, washed medium-coarse gravel was loaded with a gardening spade

until it occupied 2 inches of column height over the diffuser plate. This was followed by 3 inches of washed fine-gravel and 6 inches of washed sea-sand (Fisher). The target height for each material was marked on the column with a Sharpie before the column was loaded. Then the magnetite/sand blend was poured progressively into the column from the 2 liter Nalgene containers, tapping the column gently with a tool to promote a tight packing density (Figure 35c-d). The magnetite/sand blend occupied approximately 9 inches of height in the column. After the entire contents of the magnetite/sand blend containers were emptied into the column, an additional 5-6 inches of washed Fisher sand, 3 inches of fine gravel, and 2 inches of coarse gravel, respectively, were loaded over the magnetite/sand blend. Finally, a diffuser plate was compressed by hand over the top gravel layer to make the packing material flush with the end of the column. Using PVC primer and cement, an endcap was placed over the top of the diffuser plate and column to compress and seal the contents inside the column (Figure 35e). Flexible 6' washing-machine hose was attached to both endcaps which gave the ability to direct lines as needed during the setup and experimental run.

To prevent excessive air from being entrapped in the column, the packing material was wetted slowly in up-flow mode over the course of an hour. Deionized water (purchased from a lab supply company in Mexico) was funneled into flexible tubing connected to the bottom of the column. The funnel and tubing was lifted gradually to control the rise of fluid within the column to approximately 0.5 inch per minute (40ml/min). During wetting, leaks were detected in several of the columns built that could not be patched with various epoxy and silicon sealing methods. In those cases the columns were discarded and rebuilt. The various leaks were caused by a non-pressure

rated coupling in one of the endcaps and failure to use PVC primer before applying the PVC cement. After the wetting procedure, flow was reversed to down-flow mode while holding both ends of flexible tubing above the height of the column to maintain a water-lock in the column. Deionized water was used to rinse the column for 1 hour as a final wash. This was accomplished by pouring water through a funnel above the column in the first (raw groundwater) pilot column and using the positive displacement pump at 100 ml/min for the other pilot columns.

To begin the experiment, the column inlet tubing was connected to the pipes leading out of the water truck. A flow rate of 1 liter per minute was established using the Fluid Metering pump by the pH-adjusted experiments or by controlling the outlet flow rate of a faucet valve for the raw groundwater experiment with constant inlet pressure. 10ml samples were collected from a sample port before the column and from the outlet stream, normally directed down the drain when not being sampled. The samples were collected by 10ml plastic syringe (B-D, New Jersey, USA) and passed through a 0.45μm Whatman syringe filter. Solutions were transferred to 15-ml centrifuge vials (Fisher) and preserved with 1%-by-weight concentrated trace-metal-grade HNO_3 (Fisher). The samples were stored chilled in a cooler during air-transport back to Rice University. At Rice the samples were stored at 4 °C before analysis by ICP-MS for As, Co, Cr, Fe, Mn, P, Pb, Se, U, V, and Zn and by ICP-OES for Ca, Mg, Si, S, Na, and K. The quantity of each element adsorbed was calculated from its concentration removed from solution, the influent concentration minus the effluent.

A log book for recording sample ID, sample time, and comments was kept. Sample frequency was shortest at the beginning of the column experiment (1

sample/minute) and lengthened to every 1-2 hours or longer during overnight periods as the experiment progressed. For the pH adjusted experiments, night-staff at the water treatment plant were trained to take samples throughout the night. Although advanced instrumentation to monitor arsenic breakthrough was not available in Guanajuato, a portable arsenic test kit (Hach) was used to provide a qualitative value for the arsenic concentration of water flowing into and out of the column. The Hach kit uses a colorimetric method which reduces arsenic to arsine gas. The arsine gas is collected on a test strip and compared to a color chart to give an approximate concentration of arsenic in the sample (Figure 36). The Hach test results helped inform when to continue sampling and when to shut down the experiment at full breakthrough. Before using the Hach method in Guanajuato, the procedure was tested with known arsenic standards prepared to 0 and 30μg/l. By visual inspection, the color matched precisely with the appropriate concentration on the color chart. However the drawback of this method is when the test strip color is in between two colors on the chart, one only knows that the actual concentration in between that concentration range without additional quantitative certainty.

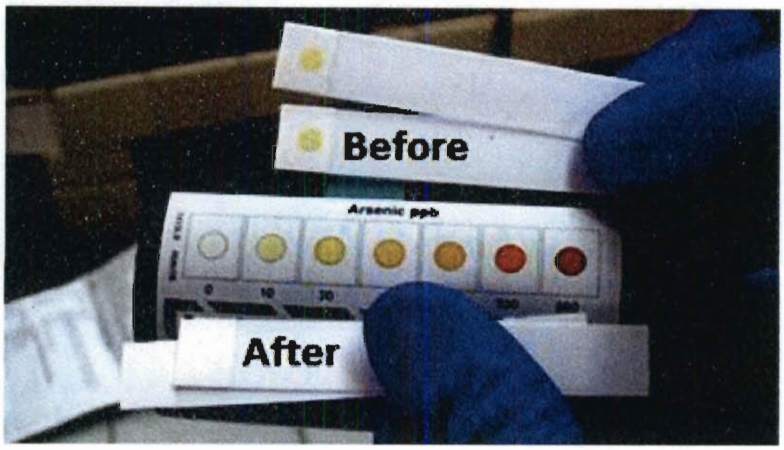

Figure 36 – In this photo the Hach test indicated that the Guanajuato groundwater contained between 10 and 30μg/l of arsenic before entering the column and was essentially free of arsenic after passing through the column.

The raw groundwater experiment required no special treatment. It was simply loaded directly into the water truck and brought to the water treatment plant for use. The pH-adjusted groundwater experiments, however, required the 10,000 liters of groundwater to be brought to an equilibrium pH of 5.5 from a pH condition of approximately 7 and supersaturated with $CO_{2(g)}$ (Figure 37).

To determine the approximate range of acid to be added, the buffering capacity of the groundwater was determined by Hach total alkalinity tiration (phenolphthalein, bromocresol green-methyl red) to the pH 4.5 endpoint. Then the calculated acid equivalent was added as concentrated glacial acetic acid or nitric acid to 500ml of groundwater to observe the pH change. A portable Hach SensIon156 multimeter was used to measure the pH of solution. The volume of acid addition was adjusted iteratively until the resulting solution equilibrated to a pH of 5.5±0.1. With each addition of acid, the solution was mixed turbulently for several minutes with the pH probe to ensure the carbonate system of the solution was at equilibrium with atmospheric CO_2. The solution

typically began at a pH within 1 pH unit below the target pH and rose slowly to a stable pH with mixing.

The eliptical tank dimensions of the water truck were measured to calculate the total water to be treated by acid-addition. The calculated volume of concentrated acid required to dilute the entire water tank was diluted with deionized water into clean 30 liter containers. The acid was diluted as a safety precaution for handling and to prevent the concentrated acid from dropping to the bottom of the tank due to density differences. As the water truck was being filled with a hose from the well, the diluted acid was poured progressively into the tank alongside. Mixing occurred with the pressurized hose stream and with the turbulent ride back to the water treatment plant. At the water treatment plant, the pH of the tanks were monitored daily. The pH of the tank acidified with acetic acid began at 5.4 and rose approximately 0.1 pH unit each day for the 3.5 day experiment. For the tank acidified with HNO_3, the pH began at 5.79 and rose to 6.16 after 3 days of the experiment.

Figure 37 – Rice researchers and Guanajuato water staff preparing Well No. 8, testing the buffering capacity of the groundwater, and distributing groundwater and dilute acid into a water truck.

Pretreatment for removal of interfering species

Single point adsorption isotherms were conducted to examine effects of an array of different pretreatment options for Guanajuato groundwater. Before dosing of 78P magnetite adsorbent, various pretreatment methods (described in detail below) were used to modify the chemical composition of Guanajuato groundwater. After pretreatment, the solutions were isolated and adjusted to pH 7.5 as necessary with trace-metal-grade HNO_3 or 1M NaOH (Fisher) and spiked with As(V) to approximately 60µg/l. 50 ml of each pretreated solution were added to 60ml vials (Environmental Express), each containing 17.5mg of 78P magnetite. Headspace in the vials promoted convective mixing during a 24 hour period, during which the vials were rotated end-over-end at 3 rpm. Afterwards the magnetite was let settle, aided by magnetic attraction to an N-52 grade, neodymium magnet (K&J Magnetics) placed below the vial. 10ml of each solution was removed by 10ml plastic syringe (B-D, New Jersey, USA) and passed through a 0.45µm Whatman filter. Solutions were transferred to 15ml centrifuge vials (Fisher) and acidified to 1%-by-weight with concentrated trace-metal-grade HNO_3 (Fisher). These samples as well as samples taken before the mixing period with magnetite were analyzed for As, Cr, Fe, Se, Tl, U, V, and Zn on ICP-MS and for Ca, Mg, Si, P, and S on ICP-OES.

The pretreatment methods included filtration (0.025µm, 0.22µm, and 0.45µm filters), batch adsorption to activated alumina (0.1, 1, 2.5, and 10 g/l), batch adsorption to magnetite (0.1, 1, and 10 g/l), cation exchange column (Amberlite 120-120 Plus, Mallincrodt), anion exchange column (Dowex 1-X8 20-50 mesh), both cation and anion exchange columns, ferrous sulfate coagulation, flocculation, and sedimentation (Proctor and Gamble, PUR packet), removal of carbonates and dissolved CO_2 (first by vacuum,

then sparged with argon), and aeration. The pretreatment solutions are shown in Figure 38 before dosing with 78P magnetite.

Figure 38 - Glassware containing an array of pretreated water solutions before 24-hour isotherms.

For the filtration pretreatment, three sets of raw Guanajuato groundwater solutions were passed through Millipore filters of 0.025μm, 0.22μm, and 0.45μm using vacuum filtration. The solutions were then spiked to 60μg/l of arsenic with a 50mg/l As(V) stock solution, adjusted to pH 7.5, and used to produce single point adsorption isotherms with magnetite as described above.

For the activated alumina pretreatment, powdered activated alumina (Aldrich Chemical Company) was dosed in concentrations of 0.1, 1, 2.5, and 10 g/l into raw Guanajuato groundwater in 250ml Erlenmeyer flasks. The activated alumina adsorbent was neutral in pH, standard grade, Brockman I, 150 mesh, and had a surface area of $155 m^2/g$. Solutions were stirred at room temperature for 1 hour by a magnetic stir plate and then filtered by 0.45μm Whatman PES syringe filter to remove the activated alumina. The solutions were then spiked to 60μg/l of arsenic with a 50mg/l As(V) stock solution,

adjusted to pH 7.5, and used to produce single point adsorption isotherms with magnetite as described above.

Magnetite (78P, Rockwood Pigments) was used as its own pretreatment before the single point isotherms. A series of 500ml beakers containing 0.1, 1, and 10 g/l of magnetite in raw Guanajuato groundwater was stirred/agitated for 1 hour using an overhead propeller (The Agitator; Arrow Engineering) at room temperature. Afterwards the magnetite was let settle, aided by magnetic attraction to an N-52 grade, neodymium magnet (K&J Magnetics) placed below the vial. The solutions were then filtered by 0.45μm Whatman PES syringe filter, spiked to 60μg/l of arsenic with a 50mg/l As(V) stock solution, adjusted to pH 7.5, and used to produce single point adsorption isotherms with magnetite as described above.

A column of cation exchange beads was used to remove cationic species from the raw groundwater solution. To set up the column, the top end of a 15ml plastic pipet (Falcon) was snapped off and glass wool (Supelco) was pushed down into the shaft to support the cation exchange beads. 10 grams of Amberlite IR-120 Plus, strongly acidic, medium porosity, cation exchange beads (Mallincrodt) were loaded into the column with a funnel. Once packed in the column, the beads were preconditioned with 10 pore volumes of a 1M HNO_3 solution, then 10 PV of deionized water. After conditioning, 50ml of raw Guanajuato groundwater was poured through a funnel into the column and the water slowly percolated through the packing material into a collection beaker. After collection the pH was brought back to pH 7.5 with 0.1M NaOH.

Anion exchange was also conducted as pretreatment to arsenic adsorption to determine the effect of removing competing anionic species from solution. The top end

of a 15ml plastic pipet (Falcon) was snapped off to produce a column and glass wool (Supelco) was pushed down into the shaft as a media support. 10 grams of Dowex 1-X8 anionic resin (Dow Chemical) rated at 1.4 meq/ml were loaded into the column with a funnel. Once packed in the column, the beads were preconditioned with 10 pore volumes of a 1M NaOH solution, then 10 PV of deionized water. After conditioning, 60ml of raw Guanajuato groundwater was poured through a funnel into the column and the water slowly percolated through the packing material into a collection beaker. After collection the pH was brought back to pH 7.5 with 0.1M HNO_3.

In addition to testing anion and cation exchange separately as pretreatment methods, they were also used in combination to remove both cationic and anionic species from water. The cationic exchange process and the anionic exchange process were performed in series as described individually above.

Ferrous sulfate coagulation was conducted as prescribed by the Proctor and Gamble PUR packet treatment method used in the developing world for cleaning household drinking water. A 750ml of raw Guanajuato groundwater was poured into a 1 liter beaker and 0.3 grams of a 4 gram PUR packet designed to treat 10 liters of water was added to the beaker. The PUR packet consisted of $FeSO_4$ and 0.542% of $Ca(OCl)_2$ resulting in an Fe concentration of 0.146 g/l in solution for the coagulation/flocculation treatment. As prescribed, the water was stirred for 5 minutes with a scupula, then let stand for 5 minutes while the floc settled. The supernatant was then filtered by 0.45μm Whatman PES syringe filter, spiked to 60μg/l of arsenic with a 50mg/l As(V) stock solution, adjusted to pH 7.5, and used to produce single point adsorption isotherms with magnetite as described above.

Raw Guanajuato groundwater and a synthetic solution were degassed to observe the effect of reducing carbonate species on adsorption. The synthetic solution was used as a baseline of comparison for the groundwater as the synthetic solution did not have the naturally occurring constituents that were present in the groundwater. The synthetic solution was made by adding 2.5mM THAM buffer and 2.5mM NaCl to Milli-Q water (Millipore). The groundwater and synthetic solutions were poured into 500ml beakers, then trace-metal grade HNO_3 (Fisher) was used to reduce the pH to 4.5 while stirring with a magnetic stir plate. When H^+ was added, the equilibrium was shifted to the right to evolved $CO_{2(g)}$ according to the following equilibrium:

$$H^+_{(aq)} + CO_3^{2-}{}_{(aq)} \leftrightarrow HCO_3^-{}_{(aq)} \quad \log K_{a1} = 10.3$$

$$H^+_{(aq)} + HCO_3^-{}_{(aq)} \leftrightarrow H_2CO_{3(aq)} \quad \log K_{a2} = 6.4$$

$$H_2CO_{3(aq)} \leftrightarrow H_2O_{(l)} + CO_{2(g)} \quad H = 10^{1.46} \text{ atm/(mol/L)} \text{ (Sawyer, McCarty et al. 2003)}$$

A Visual Minteq simulation confirmed that for the synthetic solution in contact with atmospheric $CO_{2(g)}$ at pH 4.5, the carbonates would essentially all be in the form of H_2CO_3 (Figure 39).

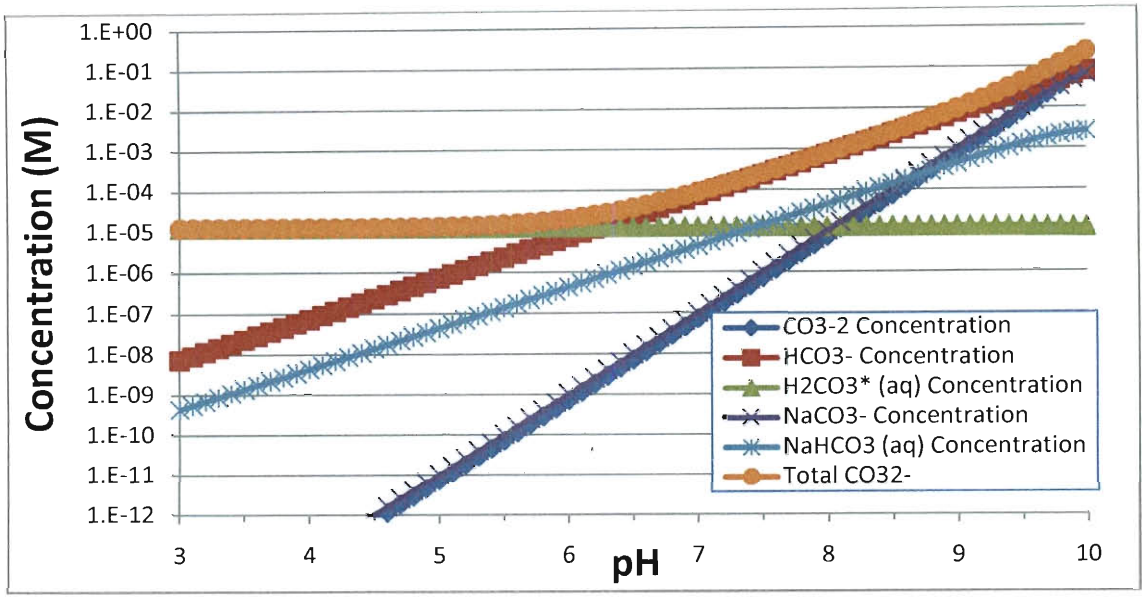

Figure 39 - Carbonate speciation in equilibrium with atmospheric CO_2 ($10^{-3.42}$ atm) at room temperature (Gustafsson 2009).

After reducing the pH, the $CO_{2(g)}$ was driven out of solution by sparging with argon and stirring. Plastic wrap covered the top of the beaker to leave an argon blanket over the solution and exclude $CO_{2(g)}$ from reentering the solution. After sparging, 1M NaOH was carefully added to raise the solution pH back to 7.5. The solutions were then filtered by 0.45μm Whatman PES syringe filter, spiked to 60μg/l of arsenic with a 50mg/l As(V) stock solution, and used to produce single point adsorption isotherms with magnetite as described above.

For the aeration pretreatment, synthetic and Guanajuato groundwater solutions were stirred rapidly with a magnetic stir plate as the pH was reduced to 7.5 with trace-metal grade HNO_3 (Fisher). After acid addition, the pH tended to depress quickly and then slowly uptake the free H+ ions as $CO_{2(g)}$ was evolved. Several iterations of acid addition were required to lower the pH to remain stable at 7.5. To ensure equilibration with atmospheric $CO_{2(g)}$, the pH was monitored over an hour period to ensure a change of

less than 0.05 pH units from pH 7.5. The solutions were then filtered by 0.45μm Whatman PES syringe filter, spiked to 60μg/l of arsenic with a 50mg/l As(V) stock solution, and used to produce single point adsorption isotherms with magnetite as described above.

Adsorption isotherms of synthetic water with silica addition

Adsorption isotherms were conducted with synthetic waters to examine the effect of silica concentration on arsenate adsorption to nanomagnetite. The solutions were prepared at room temperature and in aerated conditions. A range of masses (8, 18, and 65 mg) of 78P nanomagnetite were weighed into 60ml polyethylene vials (Environmental Express). An initial solution was made by dissolving 2.9mM NaCl (Fisher), 5mM tris-buffer (Fisher), the required Na_2SiO_3 (Fisher) into Milli-Q water (Millipore). The sodium silicate powder was dissolved directly into solution in 0, 0.17, 0.94, 2.0, and 4.25 mg/l concentrations. Dissolving a low concentration of silica salt directly helped prevent polymerization, which occurs at high silica concentrations. The highest concentration solution of silica (4.25mg/l) was also repeated with the addition of 13μg/l of V(V) to observe the combined effects of two competing species. The V(V) was dosed from a stock solution made from dissolving Na_3VO_4 (Fisher) into Milli-Q water. The solutions were dosed to 66μg/l As(V) from a 50 mg/l As(V) stock solution and adjusted to pH 7.5 with trace-metal grade HNO_3 (Fisher) or 0.1M NaOH as needed. Samples of each initial solution were filtered through 0.45μm polyethersulfone (PES) membrane filters (Whatman) and acidified to 1% by weight with concentrated trace-metal-grade HNO_3 (Fisher) for analysis on ICP-MS. For the adsorption isotherms, vials with pre-weighed magnetite were filled with 50ml of the prepared solution, tightly capped, and rotated end-

over-end at 3rpm for 24 hours. Afterwards the magnetite was let settle, aided by magnetic attraction to an N-52 grade, neodymium magnet (K&J Magnetics) placed below the vial. After magnetic-assisted settling, the vial caps were removed and 10ml of each solution was removed by 10ml plastic syringe (B-D, New Jersey, USA) and passed through a 0.45μm Whatman filter. Solutions were transferred to 15-ml centrifuge vials (Fisher) and acidified to 1%-by-weight with concentrated trace-metal-grade HNO_3 (Fisher). All samples were analyzed by ICP-MS and the adsorbed arsenic was calculated from the concentration of arsenic removed from solution.

Removal of silica and arsenic with activated alumina: batch and column studies

Given activated alumina as an effective silica removal media (Bouguerra, Ali et al. 2007), adsorption isotherms with powdered activated alumina (PAA) in Guanajuato groundwater were conducted to assess removal of both silica and arsenic. A pH of 7.5 was selected as it corresponded to the pH of the Guanajuato groundwater used in the first pilot column experiment. The pH of the groundwater immediately out of the well is approximately 6.8, but the pH rises 0.1-0.2 pH units per day as $CO_{2(g)}$ evolves from solution and equilibrates with the atmospheric partial pressure. Bouguerra and Ali et al. also found that a pH of 7.5 was in the range of maximum silica adsorption (pH 7-8.5) to activated alumina. Various weights (4, 8, 18, 33, and 65 mg) of PAA (Aldrich Chemical Company) were added to 50ml vials of Guanajuato groundwater spiked to 70μg/l of As(V). The activated alumina adsorbent was neutral in pH, standard grade, Brockman I, 150 mesh, and had a surface area of $155 m^2/g$. The vials were rotated end-over-end for 24 hours. The supernatant of each vial was filtered through a 0.45μm Whatman filter and acidified to 1% by volume trace-metal-grade HNO_3 (Fisher). The arsenic concentration

was analyzed before and after the mixing period by ICP-MS and the difference was used to calculate adsorption to the PAA surface. In addition, the samples were analyzed for Ca, Mg, Si, P and S by ICP-OES before and after mixing.

A column loaded with granular activated alumina was used to assess breakthrough of silica and arsenic simultaneously. A 40cm Omnifit column (Diba Industries) was loaded with 18.8 grams of granular activated alumina (mesh size) from Fisher to a height of 30.5 cm (Figure 40). Raw Guanajuato groundwater (pH 7.65) from Municipal Well No. 8 was delivered through the column at 8.3 ml/min with a Pharmacia P-500 dual-syringe pump. This resulted in a 2.3 minute residence time through the 19.1 ml of pore volume. The groundwater contained 47.9 mg/l of silica as SiO_2 and 8.8 μg/l of arsenic. Samples were collected every 30 minutes to 2 hours during daytime and every 4 hours overnight. The solution was analyzed for silicon and arsenic by ICP-OES and ICP-MS, respectively, before and after passing through the column. Adsorption to the granular activated alumina was calculated from the difference in inlet and outlet concentrations.

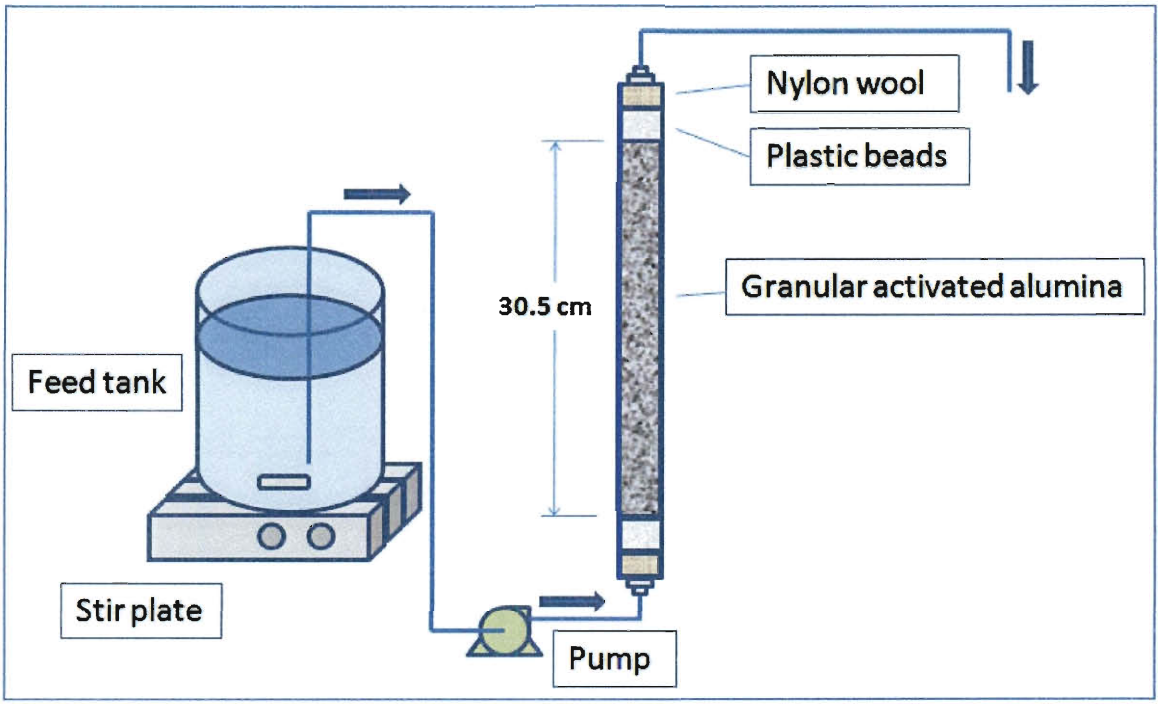

Figure 40 - Schematic for the column setup used to test granular activated alumina.

Mid-column sampling used to monitor the migration of silica and arsenic

All column experiments performed previously were solely able to illuminate concentrations of adsorbates at the influent and effluent positions alone. However, insight into the migration of the mass-transfer zone within the column was lacking. In order to observe this migration behavior, columns were constructed that facilitated the extraction of samples from various points within the column.

The column shaft was designed with flexible, transparent, Tygon tubing punctured with syringe needles for sampling along the length of the packed bed (Figure 41). Tygon R3603 tubing was used with an internal diameter of 7.9mm and was composed of PVC and plasticizers. Plastic parts and packing materials were used to reduce any interaction with silica in the water, especially during regeneration testing in high pH conditions.

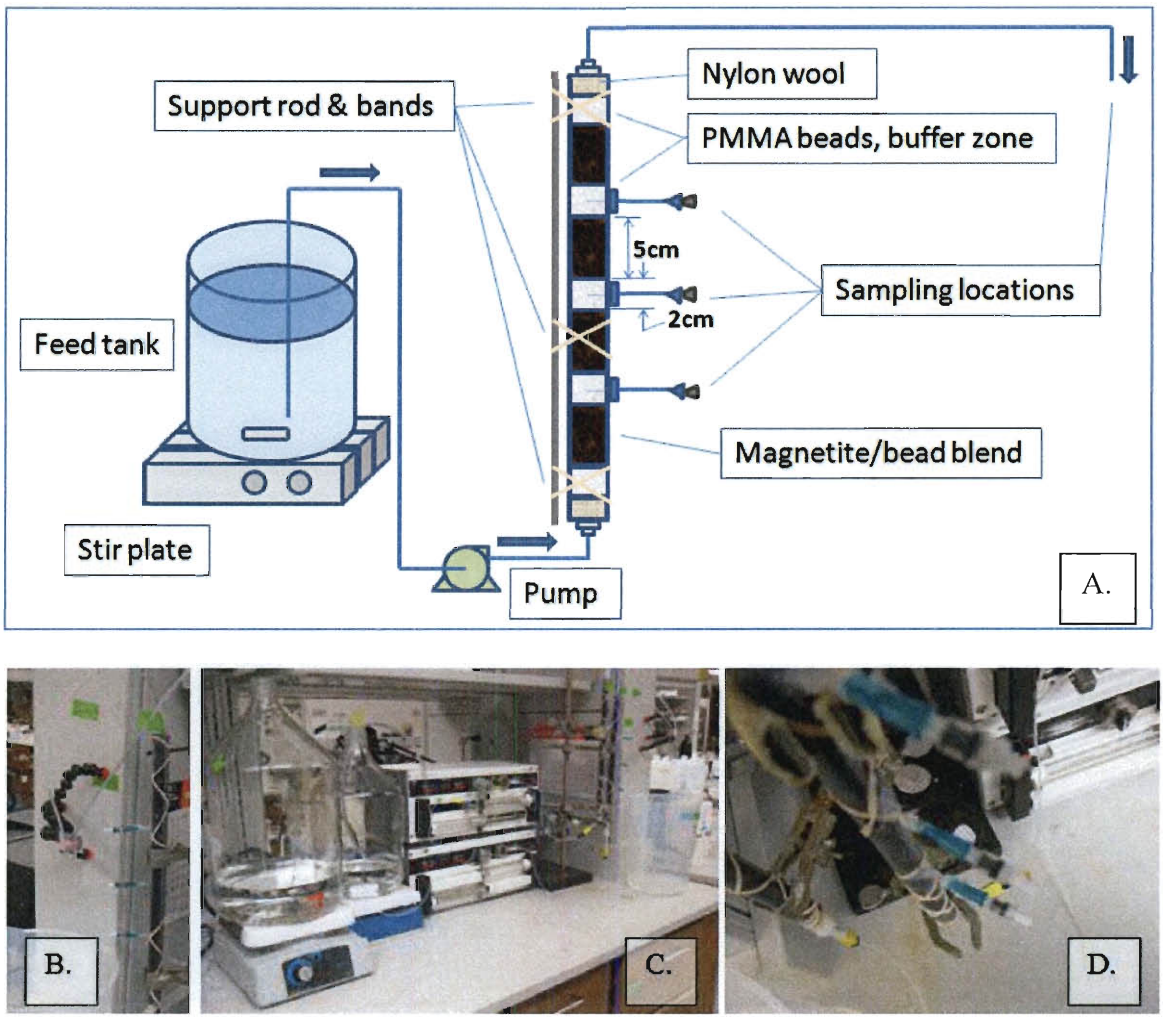

Figure 41 - Columns constructed with sampling ports along their length. A. Schematic of the system design. B. Picture of the outlet tubing with adjustable discharge height. C. From left to right: Feed tanks (with and without silica), dual-syringe pumps, columns with sample ports, and collection beaker. D. Close-up of luer sample ports with plugs.

The active adsorptive media of the column was composed of 78P magnetite (Rockwood Pigments), making up 15% by weight, and 200μm diameter polymethyl-methacrylate (PMMA) beads (Polysciences, Inc), making up the remaining 85% by weight. Four portions of adsorptive media were prepared, each containing 0.285g of magnetite and 1.56g of PMMA beads, measured by analytical balance (0.1mg resolution) into 60ml vials (Environmental Express). The vials were shaken to mix and disperse the

magnetite among the PMMA beads. In addition, a wooden end of a cotton swab was used to crush larger aggregates in the vials and mix until no larger aggregates could be seen. Each portion of adsorbent media occupied a 5cm section within the column, separated by a 2cm buffer zone of 200μm PMMA beads. BD syringe needles were pierced through the Tygon tubing into each buffer zone to enable sample extraction from within the column. The buffer zone prevented magnetite from migrated out or clogging the syringe needle. When not in use, each syringe sample port was closed off with a luer plug. The plugs were made by cutting off the tip of a 1ml BD syringe and gluing the stopper in place with super glue gel (Super Glue Corp.). PMMA beads also contained and compressed the media on both ends. A Pharmacia continuous, dual syringe pump was used to keep a constant flow rate of 0.885 ml/min corresponding to a 1.25 minute residence time through the pore space (1.11 cm^3) of each section, or cumulatively 5 minutes through the entire column. The PMMA buffer zones represent a time offset of 30 seconds each, but they do not retard migration of adsorbates; therefore, they are not included in the reported residence time. Solutions were pumped in up-flow mode to reduce the amount of time required to flush air bubbles from the system. Both feed solutions were made with Millipore 18.2 MΩ-cm water, 100 μg/l As(V), 2.5 mM THAM buffer, and pH adjusted to 7.0 with trace-metal grade HNO_3. In addition, sodium meta-silicate nonahydrate was added to one feed solution to yield 50 mg/l as SiO_2. The pH of 7 was selected to closely match the Guanajuato Well No. 8 conditions directly out of the well.

Samples from the four sampling locations were extracted progressively starting with the top, effluent location and working toward the bottom, column inlet. This order

was maintained so as not to disturb the residence time of the downstream sample locations immediately before they would be sampled. During a sampling event, the plug of a sample port was removed and the flow rate through the sample port was controlled by hydrostatic pressure by raising or lowering the elevation of the effluent tubing. Enough flow was directed through the sample port to provide a 2ml sample over a period of 3-10 minutes typically. However, only a fraction of the total inlet flow was drawn from the sample port to still maintain flow out the effluent of the column during sampling events. This ensured the flow direction did not reverse in the column, drawing water from later stages of the column. Before each sample was collected, three volumes of fluid filling the syringe (approximately 0.1ml) were drained with a Kimwipe to flush stagnant fluid from the sample port and ensure a representative sample from the column. After the flush, approximately 2ml were collected into pre-weighed vials and diluted with 6ml of 1.33% trace-metal grade HNO_3 in deionized water. This preserved the sample and ensured sufficient volume for analysis of arsenic on ICP-MS and silica on ICP-OES.

4. Results and Discussion

Magnetite product selection

A selection of commercial magnetite products was assessed in batch to determine suitability for laboratory and field-study column experiments for arsenic removal (Farrell 2009). The selection criteria included the arsenic solid/liquid partitioning coefficient (K_d), product safety certifications, and cost. The materials with the strongest arsenic partitioning to the solid phase were BioTransB22160, Reade, J8105, BK5599, and 78P in order of decreasing arsenic concentration on the solid (µg/g) given an arsenic concentration in solution of 30µg/l (Figure 42). The greater adsorption by BioTransB22160 and Reade could be attributed to their reduced particle size (10-20nm), therefore, yielding the greatest surface area on a mass basis in comparison to the other adsorbents (90-350nm). Adsorption of arsenic on a surface area basis resulted in a moderate range between 4-12 µg/g for the given conditions based mostly on manufacturer reported particle diameters. However, the particle size of commercial magnetite can be very heterogeneous and vary from batch to batch, so the calculated surface areas may have been cause for the greatest variation in arsenic adsorption density. For Reade magnetite and 78P magnetite, for which surface areas were measured by BET the adsorbed arsenic concentration was very similar (6.33 and 6.15 µg/g, respectively) when normalized by surface area indicating surface area may be an excellent predictor of adsorption capacity. Arsenic also partitioned strongly to J810, but the product left an iron residual in solution (>3mg/l; Hach FerroVer method) most likely a result of oxidation of the magnetite surface and subsequent adsorption to ferric hydroxides. A cost versus performance analysis was conducted as described below.

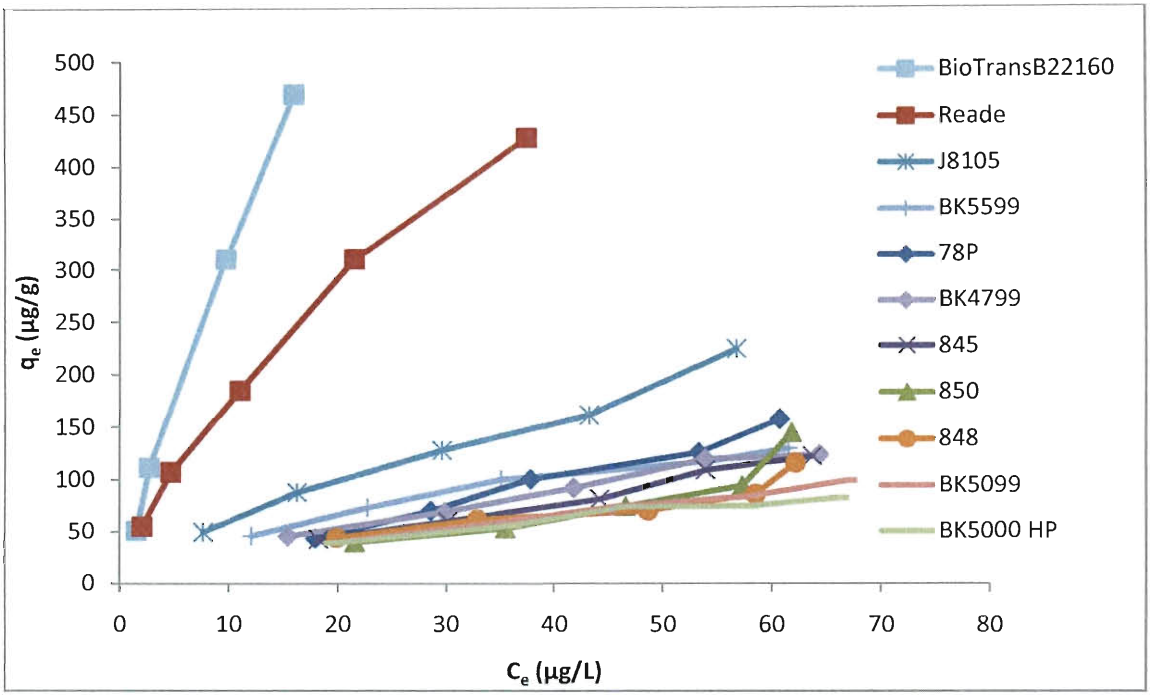

Figure 42 - As(V) adsorption isotherms for commercial magnetite particles in Rice groundwater at pH 8.00.

In the absence of pilot and full-scale column testing, an initial cost analysis of the magnetite adsorbents was conducted based on batch adsorption isotherms alone. However, laboratory experiments are limited for their ability to predict full scale treatment in that: (1) interfering species may affect column systems differently than in batch processes, (2) mass transfer kinetics may not scale proportionally from bench-scale to pilot and full-scale, (3) regeneration conditions may also differ with scale, (4) fluctuations in inlet water chemistry such as inlet arsenic concentration, pH, temperature, and seasonal variations may occur in the field that affect removal and (5) fouling or plugging may occur more readily in full-scale columns and require backwash cycles which perturb the mass-transfer zone within a column.

Due to these limitations, several simplifying assumptions were made to derive the adsorbent media costs listed in Table 6 for the treatment of arsenic by column filtration: (1) Given kinetic and preloading limitations, the magnetite in the column was taken to adsorb only a fraction (0.75 used for values in Table 6) of the 24-hr adsorption isotherm concentration on the solid (μg/g) in equilibrium with the corresponding arsenic concentration of the feed water. (2) Feed water containing 30μg/l As(V) would be treated by columns arranged in series and blended with raw water to a target concentration of 25μg/l, the Mexican contaminant limit for arsenic. (3) Only adsorption of As(V) was considered given the high redox potential of Guanajuato groundwater, although if it were to be present in another scenario, As(III) has been shown to adsorb similarly to magnetite nanoparticles (Shipley 2007). (4) Two regeneration cycles were assumed to enable recovery of all adsorbed arsenic and return media to its initial state for a subsequent adsorption step (Sylvester, Westerhoff et al. 2007). (5) Costs for auxiliary materials, construction, labor, operation, regeneration, and disposal were not considered. As kinetic limitations, effects of interfering species, regeneration capabilities, product availability, and operating requirements may be different for each material, the lowest cost adsorbent may not always result in the most economical treatment process (Chen, Frey et al. 1999). Adsorbent costs, in dollars per cubic meter of treated water, were calculated based on the following equation:

$$\text{Cost}\left[\frac{\$}{m^3}\right] = \frac{\text{Media Cost}\left[\frac{\$}{kg}\right]}{q_e\left[\frac{\mu g}{g}\right] \times \text{Fraction of Isotherm} \times 1000\left[\frac{g}{kg}\right]} \times \left(C_{As,initial}\left[\frac{\mu g}{l}\right] - C_{As,target}\left[\frac{\mu g}{l}\right]\right)$$

$$\times 1000\left[\frac{l}{m^3}\right] \div (1 + \text{No. of Regeneration Cycles})$$

Table 6 – 24-hr adsorption isotherm parameters and cost estimates for commercial magnetite products treating As-spiked Rice groundwater from 30µg/l to 25µg/l at pH 8.0. The q_e listed corresponds to equilibrium with 30µg/l of As(V) in solution. Fraction of isotherm is 0.75 and 2 regeneration treatments are assumed.

Adsorbent	Food Grade	Cost $/kg	SSA m^2/g	K_F L/g	m	R^2	q_e µg/g	q_e $µg/m^2$	$/m^3
BioTrans B22160	no	14	120†	37.8	0.92	0.98	874‡	7.3	0.04
Reade magnetite	no	260	60	33.8	0.71	1.00	380	6.3	1.52
J8105	no	5.5	6†	11.4	0.72	0.99	132	22	0.09
BK5599	no	5.5	7†	9.95	0.63	0.99	84.5	12	0.14
78P	yes	5.5	12	2.26	1.03	0.99	74.5	6.2	0.16
BK4799	no	5.5	8†	5.98	0.74	0.99	72.9	9.1	0.17
845	no	5.5	9.5†	3.40	0.86	0.98	62.8	6.6	0.19
848	yes	5.5	6.7†	4.97	0.72	0.89	57.5	8.6	0.21
BK5099	no	5.5	6†	4.22	0.75	0.99	53.5	8.9	0.23
BK5000 HP	no	5.5	8†	6.30	0.62	0.97	52.5	6.6	0.23
850	no	5.5	5.5†	1.20	1.10	0.88	51.2	9.3	0.24

† indicates value estimated from the manufacturer reported particle diameter.
‡ indicates extrapolation from isotherm curve fit.

From the batch analysis, Table 6 suggests that BioTrans B22160 is the most economical adsorbent media resulting in an adsorbent cost of $0.04 per thousand liters (USD/m^3). However, BioTransB22160 could not be used for further studies as it was discontinued by the manufacturer. The well defined, size controlled Reade magnetite nanoparticles used in previous experiments and publications (Yean, Cong et al. 2005; Shipley 2007; Shipley, Yean et al. 2009) yielded treatment costs an order of magnitude than the majority of the 100-200nm products. The J8105 adsorbent was unacceptable due to the iron residuals left in the water. The fourth and fifth strongest adsorbents, BK5599 and 78P, yielded similar treatment costs of $0.14/$m^3$ and $0.16/$m^3$, respectively. Therefore, beyond initial laboratory tests conducted with Reade magnetite as described

later, 78P was selected for subsequent lab and field experiments given the factors of treatment cost, commercial availability, and safety for food-contact applications.

Residence time and magnetite blending ratio

Early work conducted with Reade magnetite examined several design and operating parameters in column trials to determine effect on arsenic removal. These included: ratio of magnetite to sand, flow rate, residence time, and gentle versus vigorous mixing of magnetite within the sand media. The mass fraction of magnetite in the column seemed to be the most important design factor by far. In addition, short residence times were able to shift the inception and shape of the breakthrough curve significantly but made little difference in the total retention of arsenic in the column at full saturation. The experiments that examined magnetite mass percentage and residence time are discussed below.

Figure 43 compares the effects of magnetite mass percentage and residence time on arsenic breakthrough in the packing media for columns 5cm in height that were fed equivalent solutions of Rice groundwater spiked to 100µg/l with As(V).

A two site nonequilibrium model was used within CXTFIT to simultaneously model the retardation (R), dispersion (D cm^2min^{-1}), 1st order decay coefficient (μ_1 min^{-1}) for equilibrium sites, the fraction of equilibrium sites (f), the first order kinetic rate coefficient (α, min^{-1}), and the 1st order decay coefficient for kinetic sites ($\mu_{s,k}$ min^{-1}). When fit to all six parameters simultaneously, the correlation matrix showed high correlation between model parameters, suggesting that they were not unique. Given that the fraction of kinetically slow sites were nearly always less than 3%, and usually <0.1 ($f \geq 0.999$), unless otherwise noted, the kinetic sites were excluded from the model

equation. This is consistent with the findings of Shipley et al. suggesting rapid equilibrium (1.7 seconds calculated for high silica Guanajuato groundwater) at these solid-solution ratios (2007). However, the model assumption of rapid and reversible equilibrium is not completely satisfying as the adsorption of arsenic to nanomagnetite has been shown to display strong hysteresis (Yavuz, Mayo et al. 2006). Nevertheless, using three parameters (R, D, and μ_1) most of the breakthrough data could be modeled with $r^2 >$ 0.99 and with reasonable standard deviations. To demonstrate the fit of the model to the experimental data, one breakthrough curve (20% magnetite column) is shown in Figure 44 giving a coefficient of determination of 0.9955.

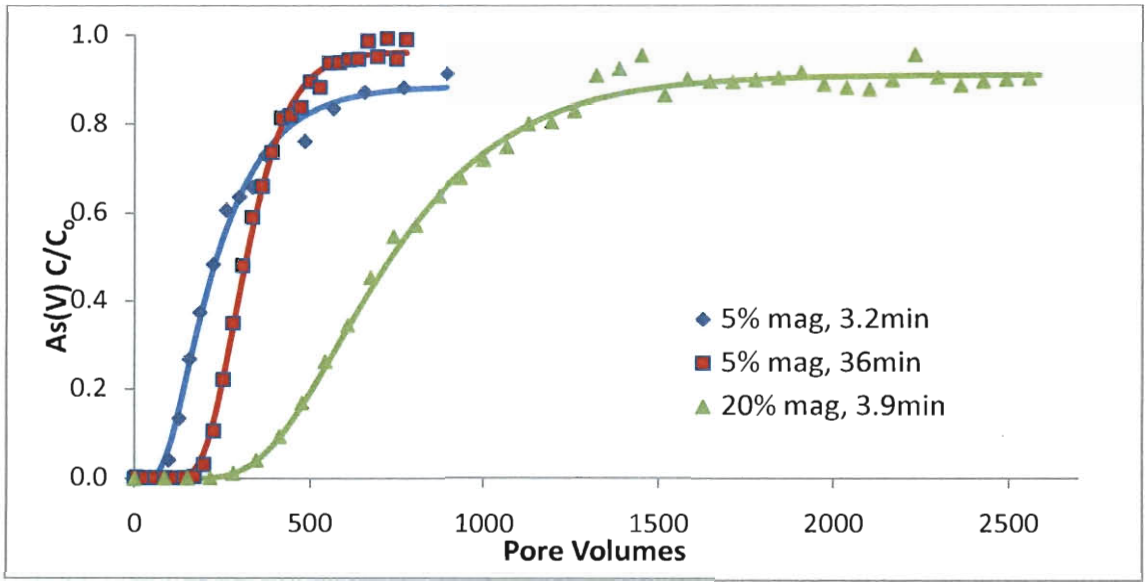

Figure 43 - Breakthrough of 100µg/l As(V)-spiked Rice GW, pH 8.5, in 1cm diameter sand columns of 5% and 20% Reade nanomagnetite by weight with varied residence times. Solid lines are fitted with CXTFIT.

Table 7 - CXTFIT model parameters with standard deviations are listed for the breakthrough curves displayed in Figure 43.

	R	D (cm^2/min)	μ_l (min^{-1})	r^2
5% mag; 3.2min res. time	261±9	1.47±0.19	0.038±0.006	0.996
5% mag; 36min res. time	329±3	0.033±0.002	0.001±0.000	0.998
20% mag; 3.9min res. time	769±10	0.585±0.047	0.024±0.009	0.996

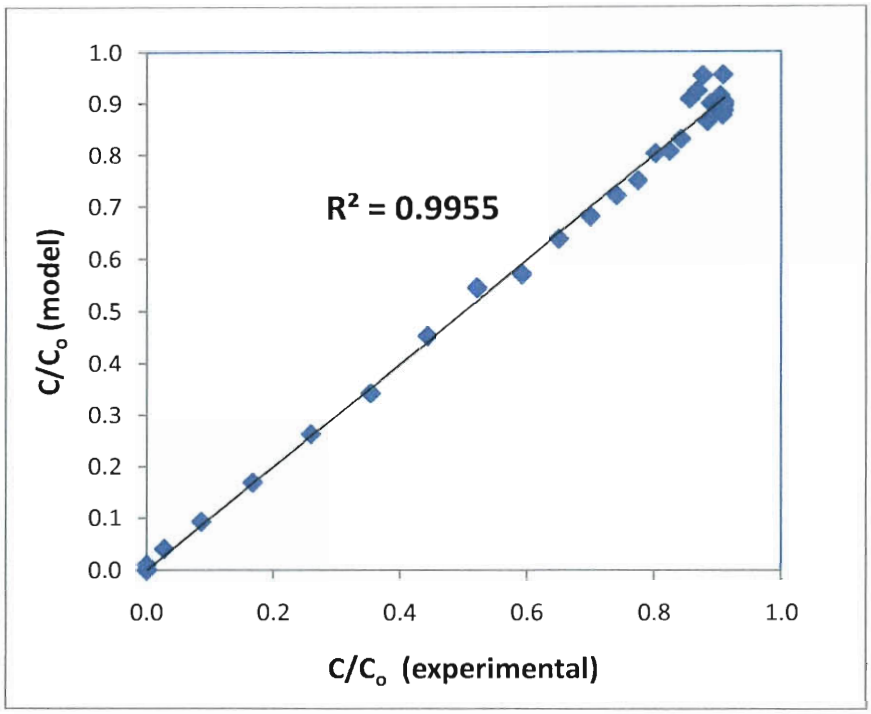

Figure 44 - Model versus experimental C/C_0 values for As(V) breakthrough in a column of 20% magnetite with residence time of 3.2 minutes.

The retardation factor for the column with 20% magnetite was approximately 3 times larger than that of the 5% magnetite column with similar flow rate. Although, a retardation factor of 4 times larger than that of the 5% magnetite column might have been expected, the result can still be reasonable given the changes to the dynamics of flow and dispersion as a result of the additional magnetite in the 20% column. For example, the dispersivity (characteristic length) of the 20% magnetite column was half that of the 5% magnetite column given the larger percentage of fine nanomagnetite aggregates.

Furthermore, by the termination of both experiments, the total arsenic adsorbed per gram of magnetite was quite similar (Figure 45). The 5% column adsorbed 205μg/g and the 20% column adsorbed 175μg/g. The breakthrough curves for both columns, given their short residence times, had a tailing effect near C/C_0=0.9. A mass balance can be considered over the column during this period with constant arsenic removal. This removal of arsenic from equilibrium sites is represented in the CXTFIT with a decay term. Mechanistically, the decay may correspond to adsorbed arsenate species going from monodentate mononuclear to hysteretic bidentate binuclear attachment. Once arsenate is bound hysterically, it no effectively longer is part of the system and additional arsenate may adsorb to magnetite with monodentate mononuclear attachment. When residence times are shorter than the characteristic time of the decay term, the breakthrough would be expected to level off at a rate equivalent to this decay term. In this case, the inverse of the decay term for the 20% magnetite column yielded a characteristic time of 41 minutes. Given this characteristic time, as would be expected, the column with residence time of 36 minutes approaches a C/C_0 value of 1 at much earlier pore volumes than either column with short residence time.

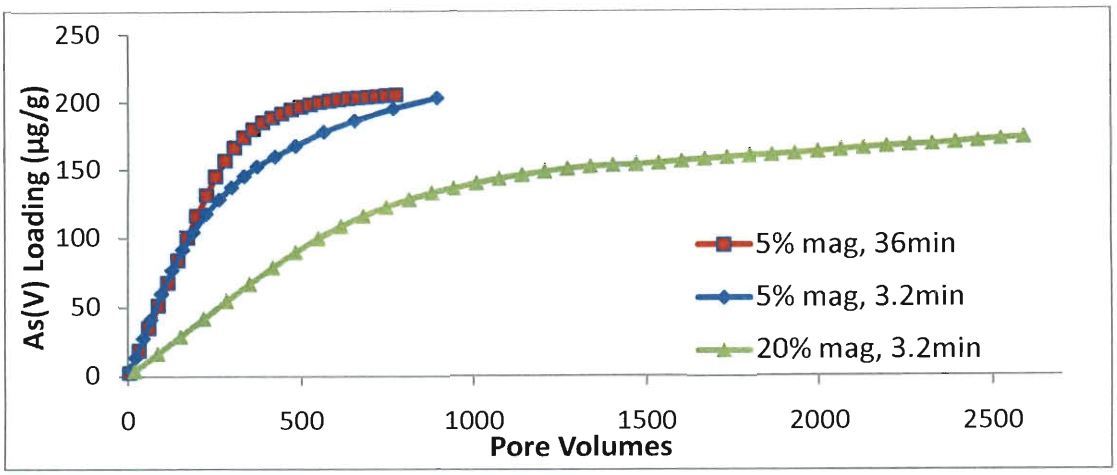

Figure 45 - Cumulative mass of As(V) adsorbed to Reade nanomagnetite calculated from experimental data in Figure 43. Solid lines are for visualization only.

Also in Figure 43, the effect of residence time between the two columns of 5% magnetite was examined. The two columns were packed identically with sand media containing 5% nanomagnetite by weight, but the pumping rate was varied to yield hydraulic residence times of 3.2 and 36 minutes. The column with longer residence time had initial arsenic breakthrough (C/C_0= 0.10) delayed by a factor of 1.9, retardation was extended from 261 to 329, and the dispersion was reduced from 1.477 to 0.033 cm^2/min. The increase in retardation was not very large, while much of the decrease in dispersion could be expected due to the decrease in flow-rate by approximately $1/10^{th}$. As can be seen in Figure 45, the change in dispersion and retardation factor had significant impact on the quantity of arsenic adsorbed between about 200 to 800 pore volumes. Eventually the cumulative arsenic adsorbed in both columns approached the same value, near 205µg/g, with time, regardless of residence time. This cumulative maximum is somewhat below the experimental adsorption isotherm value of 349µg/g given Reade magnetite in contact with 100µg/l As(V) in Rice groundwater at pH 8.5, but is not

unexpected due to column-specific effects such as preloading of competing species that may have been occurring as examined by later experiments.

Given the temporal effects of residence time on effluent concentration and cumulative arsenic removed, a system can be designed appropriately. For a home-scale drinking water system where less treated water is required per day and extended operation is needed before initial breakthrough, a single filter with a residence time above 40 minutes would be ideal. Alternatively, for a large-scale system, where maximum throughput is desired with the smallest footprint, shorter residence times could be used without loss of cumulative capacity for arsenic. Large-scale, modular columns could be arranged in series, allowing the full capacity of the initial column to be exhausted while columns downstream ensure an effluent quality with near non-detectable levels of arsenic. At exhaustion, the initial column could be taken offline for regeneration or replacement and be put back online as the final column in the treatment train. In this work, targeting arsenic removal in Guanajuato municipal water, short residence times were used.

Arsenic breakthrough in synthetic solutions versus groundwater

Two identical columns were prepared and arranged as shown in Figure 46 to monitor arsenic breakthrough for two feed solutions: a laboratory-synthesized solution and a groundwater solution. The synthetic solution was made with Fisher HPLC-grade water, 2.5mM tris buffer, 6.4mM NaCl, pH adjusted to 8.5 with 0.1M NaOH and trace metal grade HNO_3, and 30μg/l As(V). The groundwater was from the Rice University well with composition given in Table 4.

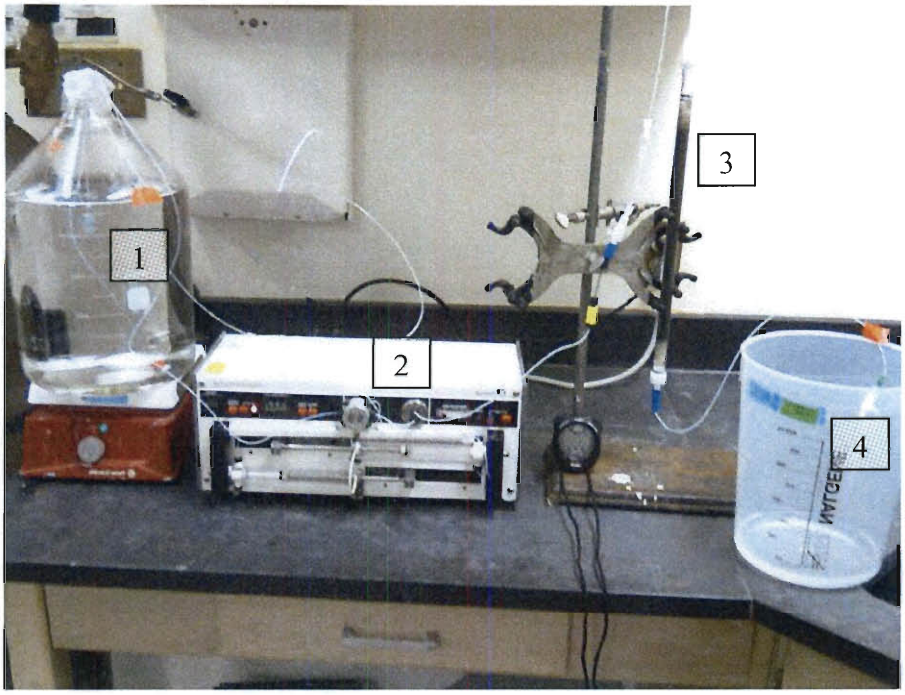

Figure 46 – Experimental setup for 15% food-grade magnetite columns used to monitor arsenic breakthrough in synthetic and groundwater solutions. (1) Feed Tank, (2) Pharmacia P-500 Pump, (3) Nanomagnetite/sand packed column, and (4) sample port and collection beaker.

The column with the synthetic feed water retained arsenic for 4,732 pore volumes before initial breakthrough ($C/C_0 = 0.05$) occurred (Figure 47). The zone of mass transfer ($0.05 < C/C_0 < 0.95$) left the column between 4,732 and 8,108 pore volumes. During the experiment, all effluent water was collected in either 10ml sample vials or 2-4 liter collection beakers and each sample fraction was weighed and analyzed for arsenic. From a mass balance encompassing the complete experiment, the arsenic retained in the column totaled 1,428µg, or alternatively 277.4µg per gram of magnetite. Given the inlet arsenic concentration of 30.3µg/l, an equivalent K_d value of 9.15 L/g was obtained. The K_d value signifies that, on average, the quantity of arsenic contained within 9.15 liters of feed water was adsorbed to each gram of magnetite.

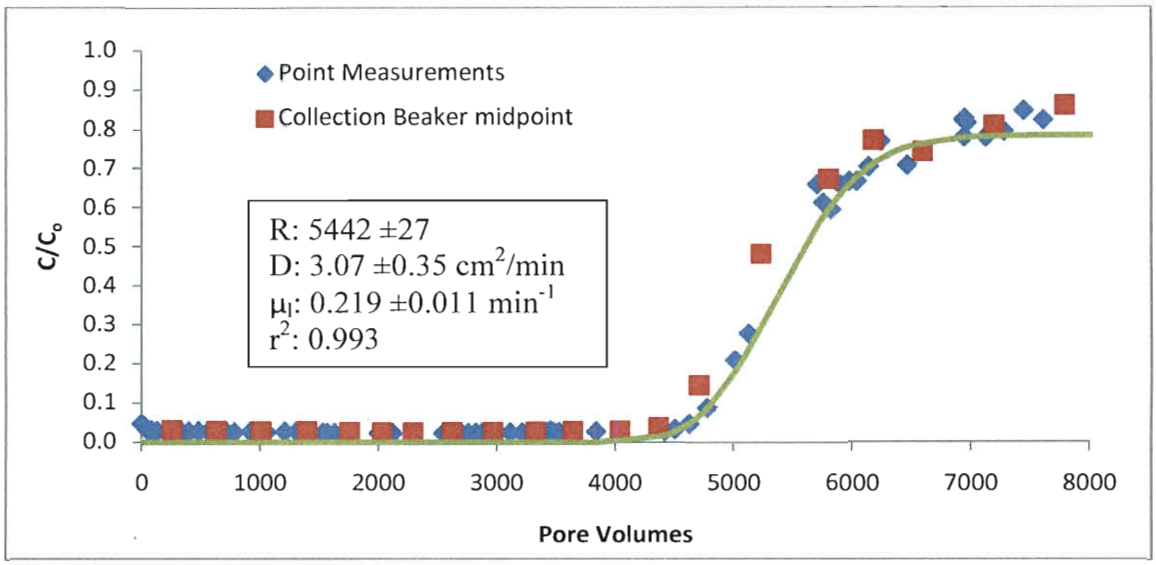

Figure 47 – Arsenic breakthrough for lab synthesized feed water (HPLC-grade water, pH 8.50, 30.3μg/l As(V), 6.4mM NaCl, and 2.5mM THAM) pumped with a residence time of 1.1 minutes through a 26cm packed-column bed composed of 15% magnetite, 85% sand.

As a quality control, the concentration of effluent water collected in the 2-4 liter collection beakers was plotted alongside the 10ml grab samples. The grab samples aligned well with samples taken from the collected beakers, confirming that the effluent arsenic concentration did not fluctuate significantly from minute to minute (Figure 47). Accordingly, grab samples were considered sufficiently representative to observe breakthrough in subsequent experiments.

For the identical column delivered groundwater with arsenic spiked to 29.2μg/l, the initial breakthrough ($C/C_0 = 0.05$) occurred at 231 pore volumes (Figure 48). The total arsenic adsorbed through the column (119μg or 23μg/g) was calculated from the cumulative arsenic measured from grab samples and collection beakers. With a feed water concentration of 29.2μg/l, the degree of arsenic partitioning to the magnetite yielded a K_d of 0.79 L/g by the termination of the experiment at 80% breakthrough.

Comparing the respective breakthrough results in Figure 47 and Figure 48, arsenic in the synthetic feed solution had more than an order of magnitude more affinity to magnetite than in the groundwater feed solution. This was apparent from the initial breakthrough (4,732 versus 231 pore volumes), the modeled retardation (5442 versus 412), and the mass of arsenic bound to magnetite by the end of the experiment (277.4 µg/g versus 23.1 µg/g). The large acceleration in breakthrough and reduction in arsenic adsorbed were hypothesized to be effect of interfering species present in the groundwater.

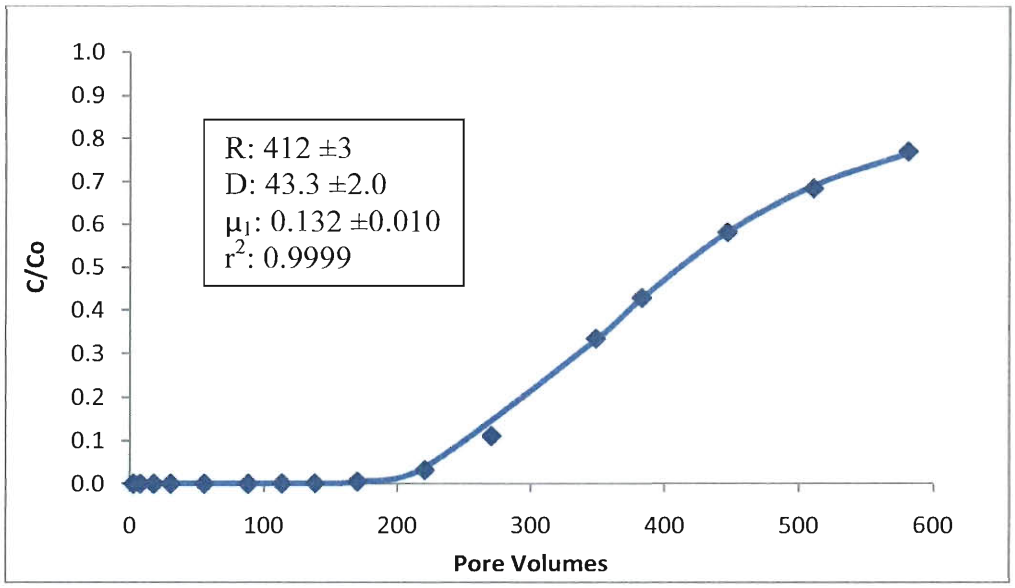

Figure 48 – Arsenic breakthrough for spiked groundwater (Rice groundwater, pH 8.50, 29.2µg/l As(V)) pumped with a residence time of 1.2 minutes through a 30cm packed column bed of 15% magnetite, 85% sand. Solid line is fitted with CXTFIT.

Chloride is known to interfere with arsenic measurement by ICP-MS, due to association of chloride with the carrier gas, argon. The mass spectrometer is unable to distinguish between the reaction product, ArCl, from As, as they both have a molecular weight of 75g/mol. To determine the significance of the ArCl interference in groundwater, a series of Guanajuato groundwater samples each containing 7.5µg/l As

was spiked with known masses of a chloride standard. The increase in the As observed in Figure 49 was due to an increase in ArCl concentration alone. The interference proved to be linear in proportion to the chloride concentration added. According to this correlation determined by known addition, the Guanajuato groundwater which has a chloride concentration of <10 mg/l (measured as underrange by Hach titration) would register only 0.03 µg/l of additional arsenic due to chloride. This assumes 5mg/l of chloride. The 0.03µg/l of false positive error incorporated into each groundwater measurement is not significant as it is below the range of detection on the ICP-MS.

However, when NaCl or other sources of chloride are added to synthetic solutions or groundwater, the chloride interference can have a significant effect. For the synthetic solution used for the column experiment displayed in Figure 47, 6.4mM of NaCl would result in an arsenic reading of over 1 µg/l due to chloride. This explains what was observed in the column effluent before the initial breakthrough of arsenic at 4,500 pore volumes. The chloride tracer broke through the column immediately and elevated the reading for arsenic by approximately 1 µg/l from the first pore volume onward.

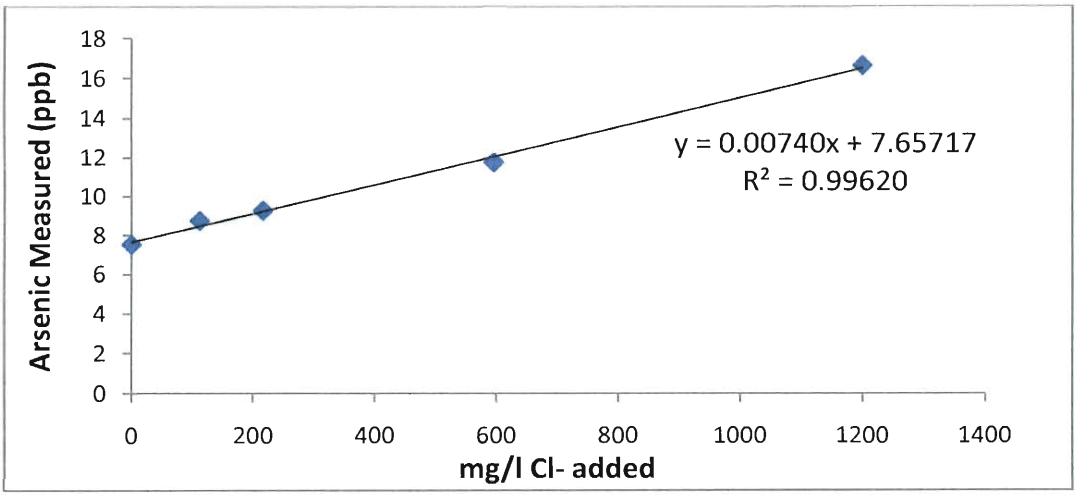

Figure 49 - Chloride Interference to arsenic measurement on ICP-MS.

Adsorption isotherms in high temperature, low oxygen conditions

Adsorption isotherms were conducted at 60°C in an oxygen-limited environment to consider the impact of operating an arsenic removal system at wellhead conditions in Guanajuato. At wellhead conditions, arsenic adsorption showed minimal change or slight improvement from the aerated, room temperature conditions (Figure 50). Typically warm conditions are used for desorption of adsorbates during regeneration cycles (Sylvester, Westerhoff et al. 2007); however, the current result suggests that the increased temperature may improve adsorption as well. The issue may be one of kinetics if the 24-hour isotherms do not allow sufficient time at room temperature to accurately represent equilibrium. Higher temperature solutions would allow a more rapid approach to equilibrium distribution.

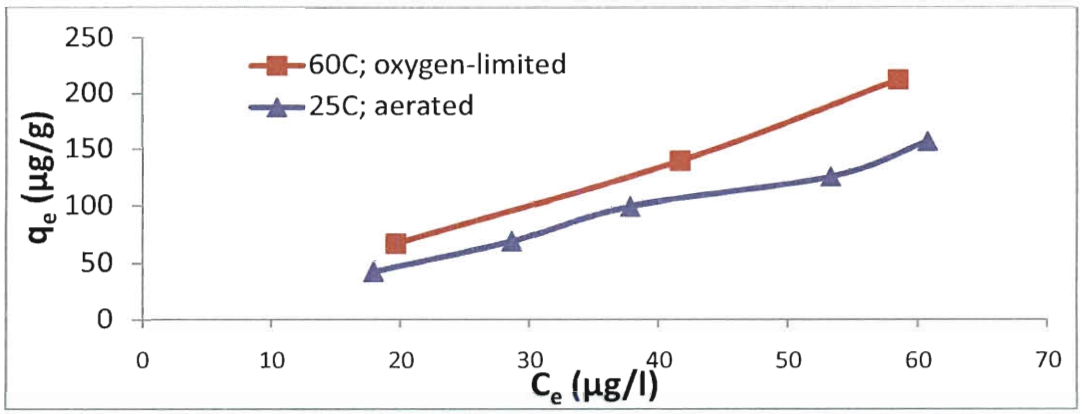

Figure 50 - Arsenic adsorption to 78P magnetite at Guanajuato wellhead conditions (60°C, oxygen-limited) and at room temperature in an aerated environment. Experiments conducted in Rice groundwater, buffered with 10mM THAM and adjusted to pH 8.00. Lines are for visualization only.

Single-point adsorption isotherms with pretreated groundwater

To investigate the large difference in arsenic adsorption behavior between synthetic water and Guanajuato groundwater, a selection of pretreatment methods were

employed to the groundwater. The purpose in using a breadth of pretreatment operations was to understand the primary interfering species in Guanajuato groundwater. By removing an individual constituent or a group of constituents from the groundwater, the major interfering species could be identified. The pretreatments used in this work included membrane filtration, activated alumina adsorption, powdered activated carbon adsorption, magnetite adsorption, anion and cation exchange, flocculation, degasification, and pH treatment processes.

The groundwater initially contained 8μg/l of background arsenic before pretreatment. After pretreatment As(V) was spiked into each solution to approximately 60 μg/l and trace-metal grade HNO_3 or NaOH was used to bring the solution to pH 7.5, unless otherwise stated. The prepared solutions were then dosed with 0.35g/l of 78P magnetite and the arsenic removed from solution was measured to calculate the arsenic adsorbed to magnetite. The arsenic distribution between adsorbed phase on magnetite and aqueous phase is shown in Figure 51 for the solutions prepared with different pretreatment methods.

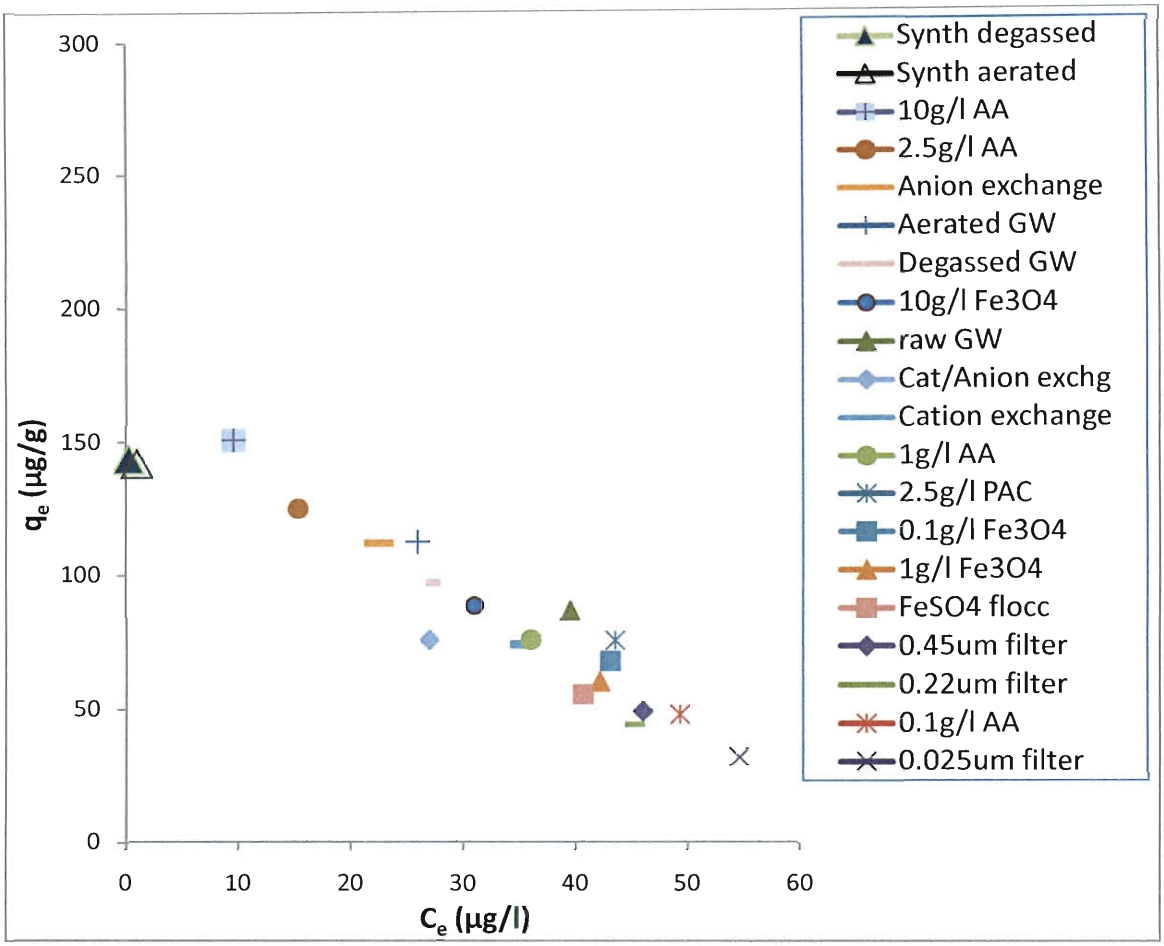

Figure 51 – Single point 24-hr adsorption of As(V) from various pretreated solutions to 78P magnetite. Pretreatments in legend are listed in order of their effect on subsequent arsenic adsorption to magnetite from most adsorption to least adsorption.

Pretreatments by membrane filters of 0.45µm, 0.2µm, and 0.025µm were used to determine if filterable particles were the cause of reduced adsorption to magnetite. Filtering the groundwater caused the opposite effect. The distribution coefficient, K_d, for arsenic adsorbing to magnetite was reduced 51%, 55%, and 73% by the 0.45µm, 0.2µm, and 0.025µm filters, respectively. This may suggest suspended solids (>0.45µm) and colloids (>25nm) facilitate arsenic adsorption. Alternatively, the decrease in adsorption could be unrelated, caused by some other parallel process such as residue released from the filters.

Likewise, the impact of trace organics or oil from the wellhead pump might have been a complicating factor in the groundwater via fouling of magnetite surfaces. Sorption of organics is assumed to occur through dynamic interaction between organic functional groups (primarily COOH and OH) and surface hydroxyl groups including ligand exchange reactions, hydrogen bonding, and electrostatic interaction (Yean, Cong et al. 2005). To investigate the possibility, powdered activated carbon was used as a pretreatment to scavenge trace organics from the groundwater. After the pretreatment arsenic adsorption to magnetite was hindered slightly (K_d=1.73 versus K_d=2.19 without treatment). At least at concentrations present in the groundwater, organics did not appear to adversely affect adsorption.

The synthetic solutions provided the most ideal conditions for arsenic adsorption to magnetite. The synthetic solution was composed of Rice groundwater treated by reverse-osmosis and 4-stage Barnstead filter, then spiked with arsenic, dosed with 2.9mM NaCl to increase ionic strength, buffered with 2.5mM THAM, and adjusted to pH 7.5 with trace-metal grade HNO_3. One synthetic solution was aerated while another was degassed to remove bicarbonate ions. Degassing may have minimally improved arsenic adsorption, but not significantly. Therefore, dissolved CO_2 as HCO_3^- was not shown to strongly affect adsorption in highly pure solutions.

To examine the effect of carbonates in natural waters, a groundwater sample was acidified, degassed, and sparged with argon to remove the bicarbonate ions from solution. Afterwards, argon was used to blanket the solution and the solution pH was brought back to 7.5 with 0.1M NaOH. Adsorption of arsenic from the degassed solution was compared to adsorption in an aerated groundwater solution. Contrary to expectations, the aerated

sample resulted in slightly improved adsorption. This may be due to a parallel increase in redox with vigorous mixing making the solution conditions more oxidizing, which could result in oxidation of the magnetite to create $Fe(OH)_3$ with high surface area. Alternatively, the bicarbonate may have facilitated adsorption of arsenate. Arai et al. proposed a mechanism by which bicarbonate first adsorbs and is then replaced by arsenate through ligand exchange (2004). The adsorbed bicarbonate may be replaced more readily than surface hydroxyl groups as the shared charge of bicarbonate is greater than that of hydroxide. The lower surface charge of bicarbonate results in weaker terminal surface Fe-O bonds which can be more readily be replaced by arsenate.

The synthetic solution prompted slightly less adsorption when aerated than when degassed while the groundwater solution yielded the opposite effect. Therefore, no clear observation can be made on the effect of bicarbonate, except that its magnitude is minor. Bicarbonate seems to have little influence on arsenic adsorption.

Beyond the extensive reverse osmosis and Barnstead filter pretreatment, the 10g/l activated alumina pretreatment caused the greatest increase in arsenic adsorption to magnetite. Arsenic adsorption increased with increasing dose of activated alumina (from 0.1g/l to 10g/l). A dose of 0.1g/l slightly reduced adsorption to magnetite, 1g/l had a neutral effect, and 2.5g/l and 10g/l was highly beneficial. Silica may be the primary factor as the distribution coefficient, K_d, appears to show dependence on the silica concentration in solution (Figure 52). There also appears to be a threshold silica concentration near 20mg/l of silica below which the K_d increases dramatically. The effect of activated alumina when concentrations of silica are left above this value appears almost negligible. At low activated alumina doses, the cause for reduced arsenic removal

is not readily apparent. A reduction in the concentration of divalent cations would be a likely cause of less arsenic adsorption to magnetite; however, the major cations Ca^{2+} and Mg^{2+} were only reduced by 2.3% and 4.4%, respectively, from the raw groundwater by 0.1g/l activated alumina.

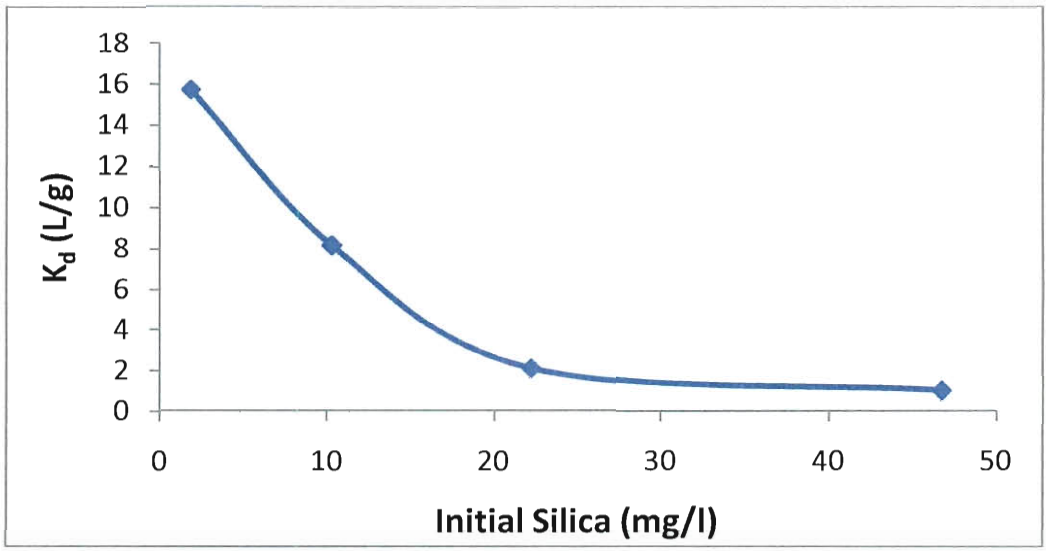

Figure 52 - Arsenic partitioning to magnetite given initial silica concentrations in solution resulting from pretreatment with activated alumina. From left to right, the concentrations of activated alumina used in the pretreatment to reduce the silica concentration from 51 mg/l to the value shown were 10 g/l, 2.5 g/l, 1 g/l, and 0.1 g/l of activated alumina.

By passing the groundwater through an anion exchange resin the resulting solution conditions facilitated greater arsenic adsorption to magnetite than the raw groundwater conditions. A cation exchange resin had a neutral effect, and when groundwater was passed through both cation and anion exchange resins, the subsequent arsenic adsorption was between the result for the individual cation and anion treatments. The anion exchange resin significantly removed Cr from 9.9 to 2.3µg/l, V from 13.6 to 1.5µg/l, and S from 5.0 to 1.3mg/l. No significant changes were made to the divalent cations. The cation exchange resin significantly removed Fe from 87µg/l to 0.0, U from

2.9 to 0.1μg/l, Zn from 102 to 6.3μg/l, Ca from 30.9 to 0.1mg/l, and Mg from 6.6 to 0.0mg/l. The combination of anion and cation exchange reduced all measured concentrations on the ICP-OES and ICP-MS to near trace levels, except for silica which remained constant at 51mg/l and sulfur which was only reduced from 5.0 to 2.1mg/l. The positive effect that anion exchange exhibited was likely two-fold. First, the concentrations of anionic species that compete for adsorption sites with arsenic were reduced. Secondly, the divalent cations were left in solution, thereby improving the electrostatics of arsenate adsorption via electrical double layer compression, surface adsorption, or surface complexation.

Magnetite was also used as its own pretreatment. The goal of this pretreatment was to determine if magnetite itself could remove species that compete with arsenic adsorption. This pretreatment targeted the potential for a trace, strongly adsorbing constituent in solution that would foul the magnetite surface but then be removed from solution, therefore unable to foul additional magnetite. However, only with a large solids concentration pretreatment of 10 g/l magnetite did the groundwater facilitate slightly improved arsenic removal. Lower concentrations of magnetite in the pretreatment showed no change or a negative effect for the second adsorption cycle with magnetite. The competing or fouling constituents were thus determined to not be significantly removed from solution by magnetite.

Ferrous sulfate was added to raw groundwater to initiate coagulation. The solution was then stirred to facilitate flocculation, and flocs were let settle. The supernatant water was filtered through a 0.45μm PES filter (Whatman), adjusted to pH 7.5. Significant changes to solution as a result of this pretreatment included the reduction

of V from 13.6 to 0.1µg/l, the reduction of Si from 24.0 to 20.4mg/l, and the increase of S from 5.0 to 40.8mg/l. The large increase in sulfur could be attributed to residual sulfate from the $FeSO_4$ coagulant. After the pretreatment, the resulting arsenic adsorption to magnetite was slightly lower (K_d = 1.4L/g) than for adsorption in raw groundwater (K_d = 2.2L/g). The reduction in adsorption may have been due to the increased interference by sulfate.

Due to the well reviewed electrostatic effects of pH on adsorption, full isotherms were conducted for pH adjusted groundwater as described below.

Adsorption isotherms with pH-adjusted Guanajuato groundwater

Adsorption isotherms were developed using pH-adjusted Guanajuato groundwater and modeled with corresponding solution conditions in Visual Minteq. Although the modeling showed significant deviation from experimental data, the model predictions encompassed the experimental data on both the high and the low end. In addition, both data sources were in agreement that pH reduction would strongly increase the amount of arsenic adsorbed to magnetite (Figure 53). The deviation of model predictions from experimental data may be due to ability of the surface complexation modeling to account for the simultaneous interactions of all species in solution. In addition, the assumption was made that arsenic adsorption to hydrous ferric oxide (HFO) is equivalent to adsorption to magnetite when normalized for surface area. HFO was used given the large body of equilibrium data available from Dzombak and Morel (1990). The reduction in arsenic adsorption is largely due to the more positive magnetite surface charge at lower pH. As the magnetite adopts more hydrogen into its surface species, the net charge of the surface becomes more positive, resulting in electrostatic attraction of arsenate anions.

Arsenate species remain predominantly negatively charged at all pH conditions above the pKa_1 of 2.19. At the pKa_2 of magnetite, the predominant arsenate species changes from $HAsO_4^{2-}$ to $H_2AsO_4^-$ as pH decreases below the pKa_2 of 6.94. The magnetite surface charge becomes more positive as pH is reduced in relation to the pH_{pzc} of magnetite at 6.8 (Yean 2008). In addition, the silica species adsorbed to magnetite go from negatively charged to neutral as pH decreases in relation to the pKa_1 of silicic acid (9.46). Both the modeled and the experimental isotherms shift from Freundlich behavior (curved) to linear as the pH increases. At low pH, adsorption of the arsenate species adsorbs so significantly that the surface charge on the magnetite becomes more negative as the arsenic concentration in the system increases. At higher adsorbed concentrations, the electrostatic interaction becomes less favorable which results in a bend in the adsorption isotherm. This is observed much less in the isotherms for higher pH conditions because the concentration of arsenic on the solid is sufficiently low.

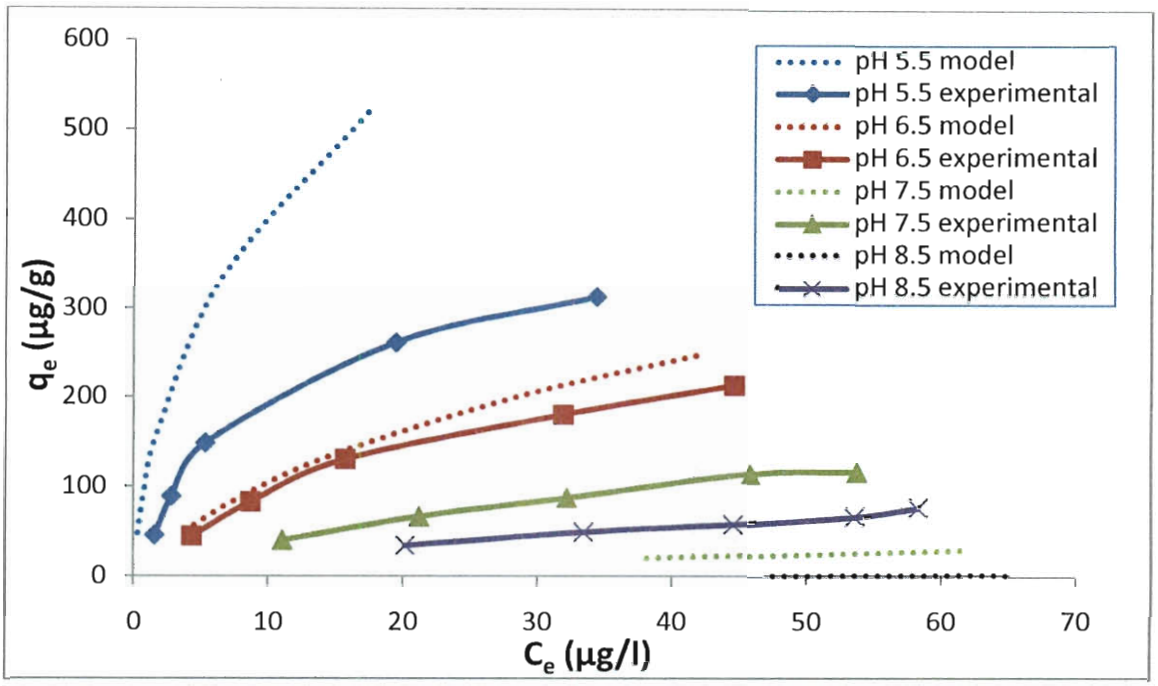

Figure 53 - pH effect on arsenic adsorption to 78P magnetite in batch for Guanajuato groundwater compared with predictions from Visual Minteq (Gustafsson 2009).

Arsenic breakthrough with raw and pH-adjusted Guanajuato groundwater

In contrast to its effect on batch isotherm experiments, pH reduction did not improve arsenic adsorption in column experiments conducted in the field with Guanajuato groundwater. Pilot-scale columns were constructed in a Guanajuato lab to test arsenic breakthrough with raw and pH-adjusted groundwater. Approximately 5,000 liters of groundwater were passed through each column over the course of 3-4 days with a residence time of 0.75 minutes. The column fed the raw groundwater removed 99% of the influent arsenic for approximately 1,000 pore volumes before initial breakthrough (Figure 54). By numeric integration between the influent and effluent concentration curves over the entire experiment, magnetite in the column had adsorbed, on average, 20.3µg of arsenic per gram of magnetite. Given a final influent concentration of 6.8µg/l of arsenic, this corresponded to a K_d of 3.0 L/g. Near 1,900 pore volumes the arsenic

breakthrough remained constant for 500 pore volumes below dropping at approximately 2,500 pore volumes. The effluent concentration then steadily increased immediately beyond 2,500 pore volumes and trended toward convergence with the influent concentration with some oscillation. The drop at 2,500 occurred almost immediately following an anomalous spike in Cr, Zn, and V, all suggesting that the As disp is an artifact of the pumping system. This might be correlated with magnetite surface oxidation within the column. Although no definitive evidence is available, for the given the pH (7.3) and redox potential (237 mV) conditions, the magnetite surfaces were not thermodynamically stable and could have slowly oxidized to ferric hydroxide over time (Figure 6). The in-situ formation of ferric hydroxides would create additional surface area for adsorption, and corrosion from the magnetite surface and would allow for additional adsorption sites from where the corrosion product was cleaved.

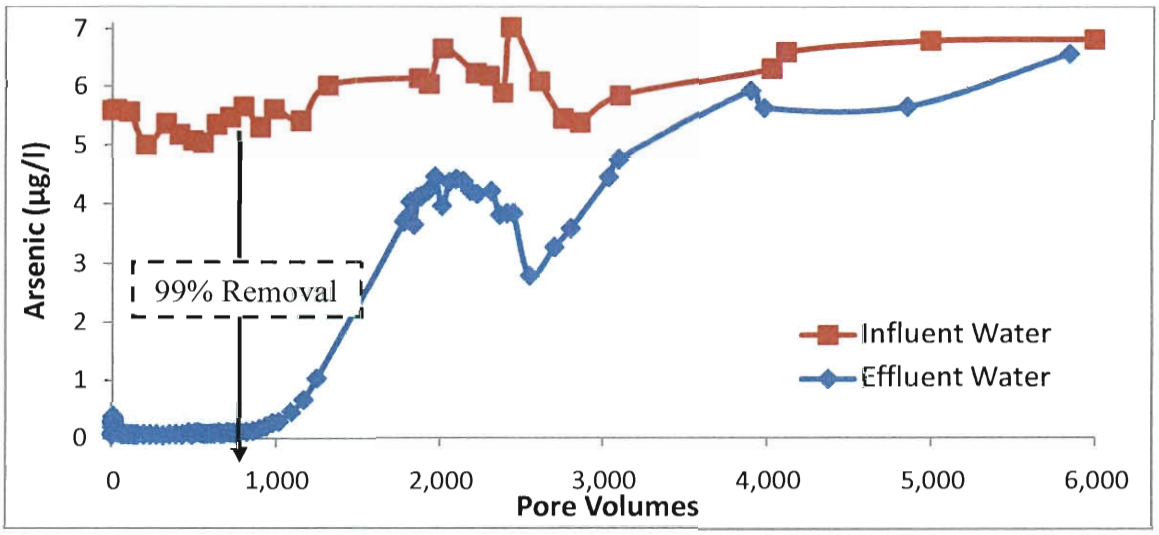

Figure 54 - Guanajuato pilot column fed raw groundwater from Municipal Well No. 8; pH 7.3.

The effects of iron were most certainly a large factor in the raw groundwater pilot experiment, as the metal pipe released red rust during an initial flush of the piping system

before the column experiment. The pipes were flushed for several hours before starting the experiment; however, the arsenic concentration in the inlet water just before the column was only 5-6 μg/l by the beginning of the experiment as compared to 9.7 μg/l in the water truck feed tank. The inlet arsenic concentration rose from 5 μg/l to 7 μg/l by the end of the experiment. For later pilot-column experiments, clean PVC lines were installed to connect the water truck feed tank to the pilot-column without the issue of oxidized iron from the system.

Acetic acid was used for its self-buffering capacity to adjust the pH of another water truck feed tank to the desired level of 5.5; however, after observing no significant improvement in breakthrough from the raw groundwater case and considering that acetate ion may compete for adsorption sites, nitric acid was used to condition another feed tank to pH 5.5. Figure 55 shows that both the pH-adjusted feed solutions were ineffective in significantly improving arsenic adsorption from the raw groundwater case. Initial breakthrough was similar for all three columns, each occurring near 1,000 pore volumes. For the feed tank adjusted with acetic acid, the effluent arsenic concentration rose to over 140% breakthrough after 2,000 pore volumes of treated water. The cause of the excess arsenic released is not readily apparent; however, the behavior may again be related to iron in solution. Given the inlet and outlet iron concentrations shown in Figure 56, the hematite would be highly supersaturated (Saturation Index (SI) =12), and at the initial inlet phosphate concentrations, strengite ($FePO_4 \cdot 2H_2O$) and several forms of calcium phosphate would be supersaturated near an SI of 2 (see also Figure 6). The interaction of these supersaturated species with the disappearance of phosphorus (Figure 57) from the inlet feed water, and the breakthrough of arsenic, vanadium, and uranium is

likely related given their simultaneous occurrence near 2,000 pore volumes. Inlet and outlet concentrations of other elements are displayed in Appendix D. These simultaneous occurrences suggest that the unexpected rise in As at about 2,000 pore volumes is probably related to some field artifact and not a systematic reaction of As and magnetite.

The final K_d obtained for the acetic acid adjusted experiment rose to a maxima of 2.6L/g before dropping to 1.9L/g by the end of the experiment. The K_d for the nitric acid adjusted experiment reached 3.1L/g by the end of the experiment. These compare similarly to the K_d of 3.0L/g obtained in the raw groundwater experiment. The pH adjustment did not have a discernable impact on the total quantity of arsenic removed by the columns.

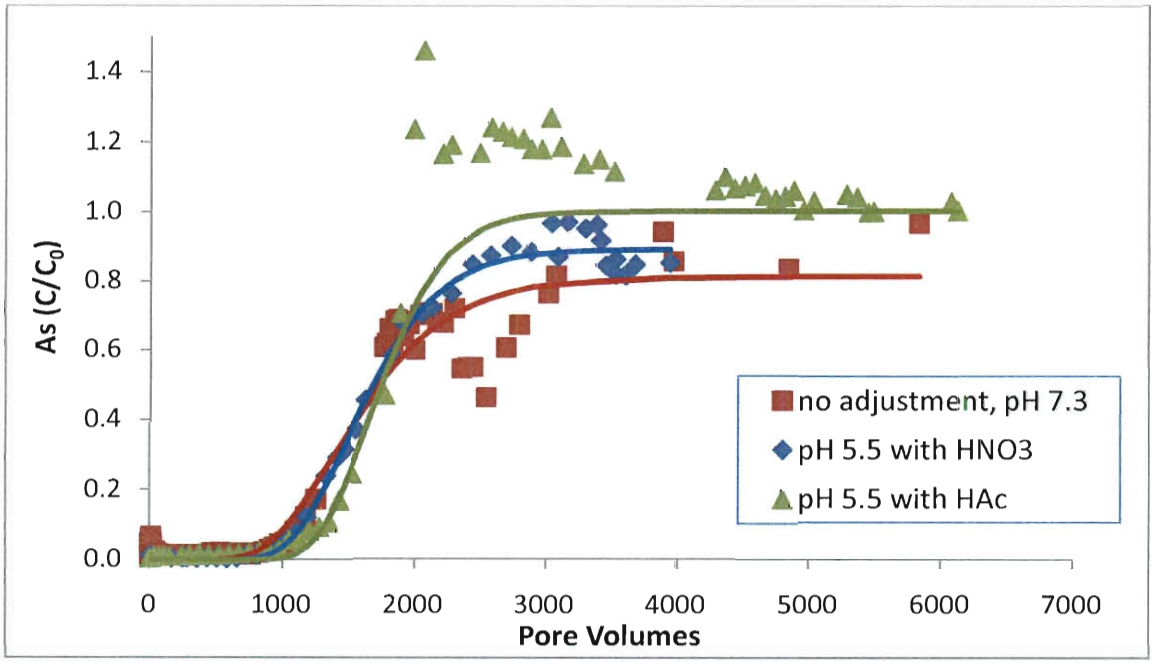

Figure 55 - Arsenic breakthrough in pilot column studies in Guanajuato with raw and pH-adjusted groundwater. Solids lines are fitted by CXTFIT.

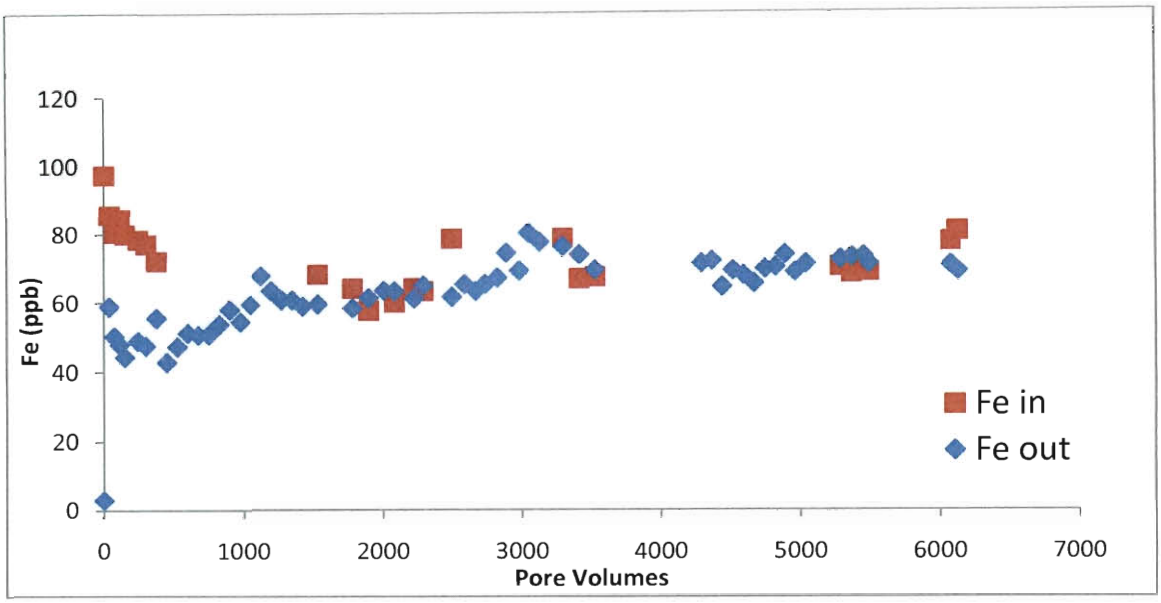

Figure 56 - Inlet and outlet iron concentrations for pilot column delivered Guanajuato groundwater with pH adjusted to 5.5 with acetic acid.

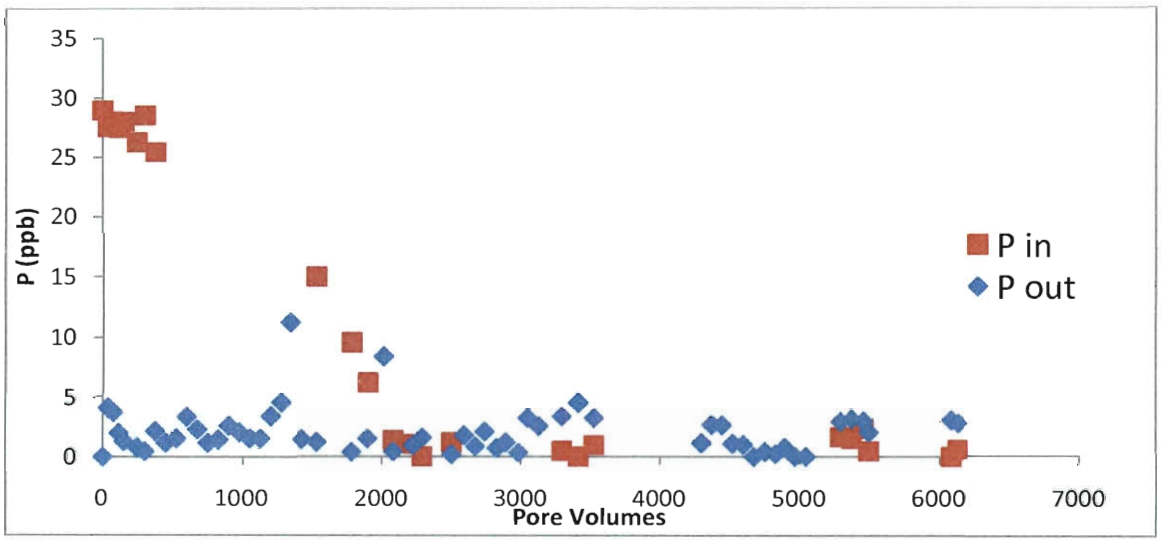

Figure 57 - Inlet and outlet phosphate concentrations for pilot column delivered Guanajuato groundwater with pH adjusted to 5.5 with acetic acid.

Batch isotherms improved significantly with a reduction in pH, but column studies showed no significant change. The difference may have been due to dynamic effects of competitive species via preloading and altered adsorption kinetics or of redox processes likely involving iron. The pH 7.5 isotherm gave similar K_d (2.9 L/g) to that

calculated from the column data at pH 7.3 (3.0 L/g), while at pH 5.5 the isotherm adjusted by HNO_3 was much higher (10 L/g) than the corresponding pilot-column experiment adjusted by HNO_3 (3.1 L/g). Preloading is one contributor to the lack of improvement in arsenic removal for the column studies with pH reduction. Preloading refers to the situation that occurs when arsenic is retained in the first portion of the column, but other constituents pass through and are exposed to later portions of the column for extended time periods. Pre-exposure to these constituents can foul adsorbent media, and reduce its effectiveness for later arsenic adsorption. It has been postulated that fouling occurs by reorientation of the fouling species on the adsorbent surface over time, potentially by polymerization (Knappe, Snoeyink et al. 1997). As silica transitions from monodentate mononuclear to bidentate binuclear, the adsorption becomes more irreversible. Also since actual Guanajuato water was used in the lab, it is possible that the Ca and Mg may have formed metal silicate colloids that removed the inhibiting impact of the silica. Appendix D shows the breakthrough profiles of silica and other elements through the two pH-adjusted columns. Due to the immediate breakthrough of silica, the magnetite towards the outlet of the column may show a reduced capacity for other target species, including arsenic, than magnetite at the inlet of the column. This possibility was investigated in later experiments.

Table 8 - CXTFIT model parameters with standard deviations listed for the breakthrough curves displayed in Figure 55.

	R	D (cm^2/min)	μ_l (min^{-1})	r^2
Raw Groundwater	1709 ±92	42.1 ±12.9	0.273 ±0.066	0.937
pH-adjusted with HAc	1798 ±191	15.0 ±7.4	0.000 ±0.467	0.906
pH adjusted with HNO_3	1698 ±23	24.1 ±2.9	0.146 ±0.014	0.992

Due to the fine size of the magnetite aggregates (~0.3μm-0.6μm; see Figure 27), pressure was required to pass water through the sand/magnetite column at the flow rate of 1 liter/min. The pressure loss was observed to increase with time as the media became more compact and sediment straining occurred. After conducting the pilot-column experiment with the raw groundwater, on the fourth day the flow rate was varied by opening and closing the resistance valve at the outlet of the column and inlet and outlet pressures were monitored by pressure gauges (Figure 58). Figure 59 displays the linear pressure loss profile observed for the range of flow rates tested. Although not a focus of this work, pressure drop is an important factor in column design and operation as it influences the depth of filter and suitability for gravity flow.

If pressure losses associated with entrance and exit effects is neglected, the hydraulic conductivity of the media was calculated to be 22.7 ft/day from Figure 59 if pressure loss through the whole length of sand bed (with and without magnetite) is taken into account. Alternatively, the lowest possible conductivity of the sand/magnetite section alone would be 15.4 ft/day if pressure loss from entrance and exit effects is neglected and the support sand is neglected. Both hydraulic conductivities are within the range (10-1,000 ft/day) of a well sorted sand or sand and gravel mixture (Bear 1988).

Figure 58 - Inlet and outlet pressure gauges of a pilot column in Guanajuato, Mexico.

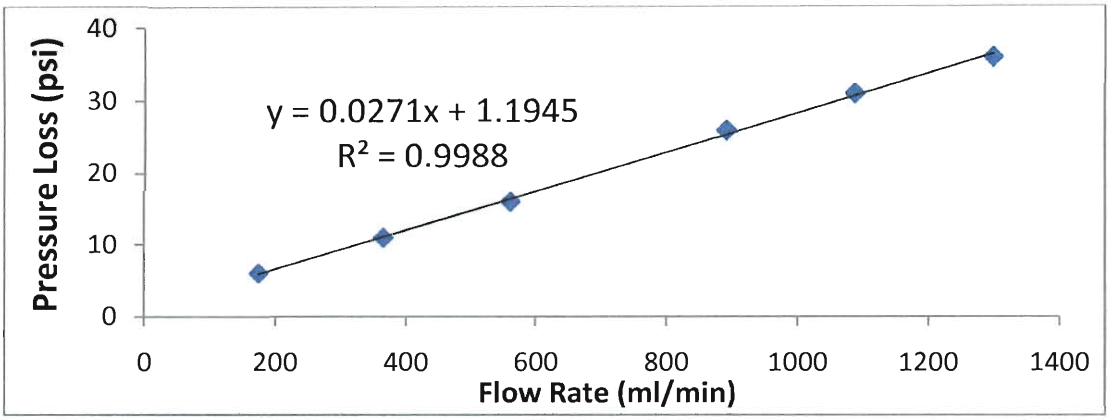

Figure 59 - Pressure loss in a Guanajuato pilot column versus flow rate.

Influence of silica removal on adsorption

Given the significant improvement to arsenic adsorption to magnetite after activated alumina pretreatment, compositional changes to the water were analyzed from before and after the treatment. From that analysis, it was determined that activated alumina removed silica much more effectively than any other pretreatment. The arsenic distribution between magnetite and solution (K_d) is plotted against the silica concentration remaining in solution after each pretreatment with activated alumina in Figure 52. The smooth inverse relationship between silica concentration and K_d can be clearly seen. The K_d was 15.7 L/g in the water with the lowest silica concentration as

compared to 2.2 L/g in the raw groundwater. In Figure 60, all the pretreatment methods are plotted against initial silica concentration, showing that only minimal improvement in arsenic adsorption was obtained in other pretreatments as compared to the activated alumina method that removed significant quantities of silica. Besides activated alumina, only the pH reduction and anion exchange pretreatments improved partitioning to magnetite significantly, yielding K_d values of 9.1 L/g and 5.0 L/g, respectively. This suggests that the most significant improvement to adsorption would likely be related to silica removal.

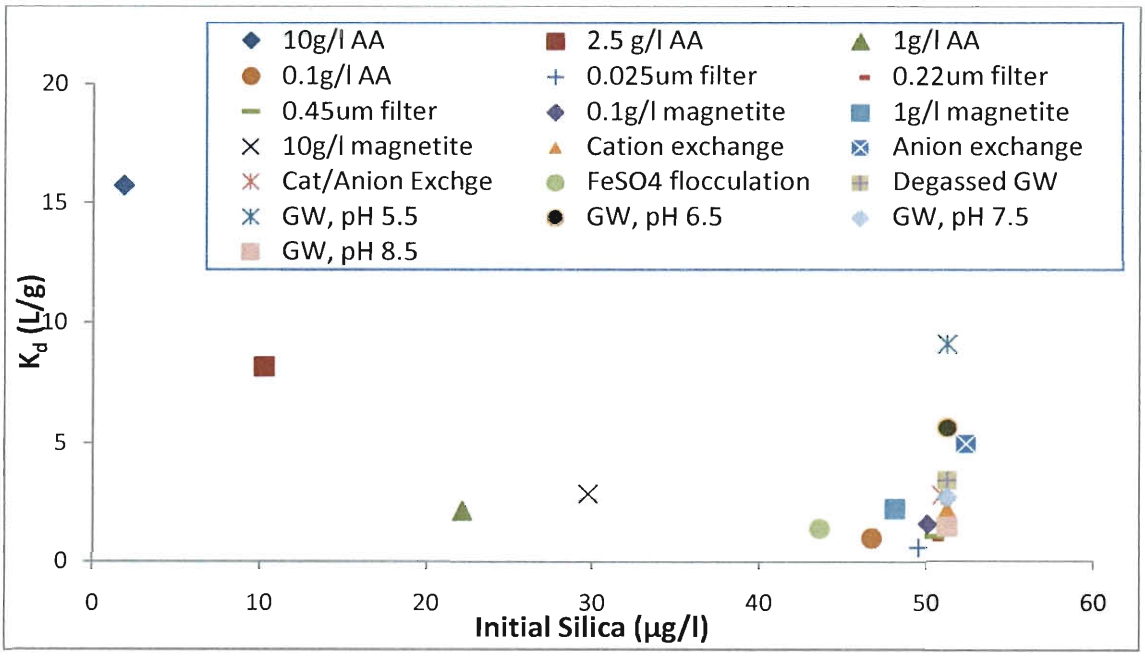

Figure 60 – Distribution of arsenic, K_d (L/g) for single point adsorption isotherms to magnetite given the initial silica concentration yielded by the indicated pretreatment.

Table 9 is a summary of the water components potentially found in natural groundwater that were investigated as part of the pretreatment survey. The impacts inferred for each component are qualitatively assessed based on change to the partitioning coefficient (K_d) for their respective treatment.

Table 9 –The impact of groundwater components on arsenic adsorption to magnetite inferred from the single-point adsorption isotherms conducted with pretreated Guanajuato groundwater.

Component	Impact on adsorption	Indicator Treatment	K_d (L/g)
Raw groundwater		No treatment	2.2
Decreased pH	Moderate-highly positive	Acidification (pH 6.5–5.5)	5.6–9.1
High redox potential	Moderately positive	Aeration with vigorous mixing	4.3
Colloids (>25nm)	Slightly positive	0.025 µm filters	0.6
TSS (>0.2 and 0.45µm)	Slightly positive	0.20 and 0.45µm filters	1.0–1.1
Divalent cations	No clear effect	Cation exchange	2.2
Trace organics	No clear effect	Granular activated carbon	1.7
Bicarbonate ions	Slightly negative	Vacuum and argon sparge	3.4
Anionic species	Moderately negative	Anion exchange	5.0
Silica	Highly negative	Activated alumina (2.5–10g/l)	8.2–15.7
Sum of components	Very highly negative	RO/Barnstead 4-stage filter	83

The impact of silica addition to synthetic solutions

Removal of silica by activated alumina had a direct correlation with the subsequent quantity of arsenic adsorbed to magnetite (Figure 52); however, silica was not the only component removed by activated alumina. With 10 g/l of activated alumina, other species were removed such as calcium (from 31 to 17 mg/l), magnesium (from 7 to 4 mg/l), sulfate (from 15 to 11 mg/l), vanadium (from 13 to 2 µg/l), and uranium (from 2.9 to 0.2 µg/l) alongside the reduction in silica (from 51 to 2 mg/l). While other pretreatments were able to remove a variety of the potentially interfering species,

activated alumina was the only pretreatment that significantly removed silica. To further verify the effect of silica alone, adsorption isotherms were conducted with synthetic solutions with added silica (Figure 61). Adsorption to magnetite was severely reduced by silica. As calculated from the highest point on the isotherm in Figure 61, K_d was reduced from 64 L/g to 16.1 L/g when 4.2 mg/l of SiO_2 was added to the synthetic solution. Even though the reduction was severe, it was slightly less than predicted, given the K_d value of 15.7 mg/l from the groundwater treated with 10 g/l of activated alumina which contained only 1.9 mg/l of silica. The lower K_d value for the treated groundwater may be a result of other interfering species still remaining in solution after treatment with activated alumina. Addition of vanadium into synthetic solution with silica at the concentration present in the groundwater gave a slightly depressed adsorption isotherm, which may or may not be significant. The compound effect of other competing ions may further reduce arsenic adsorption.

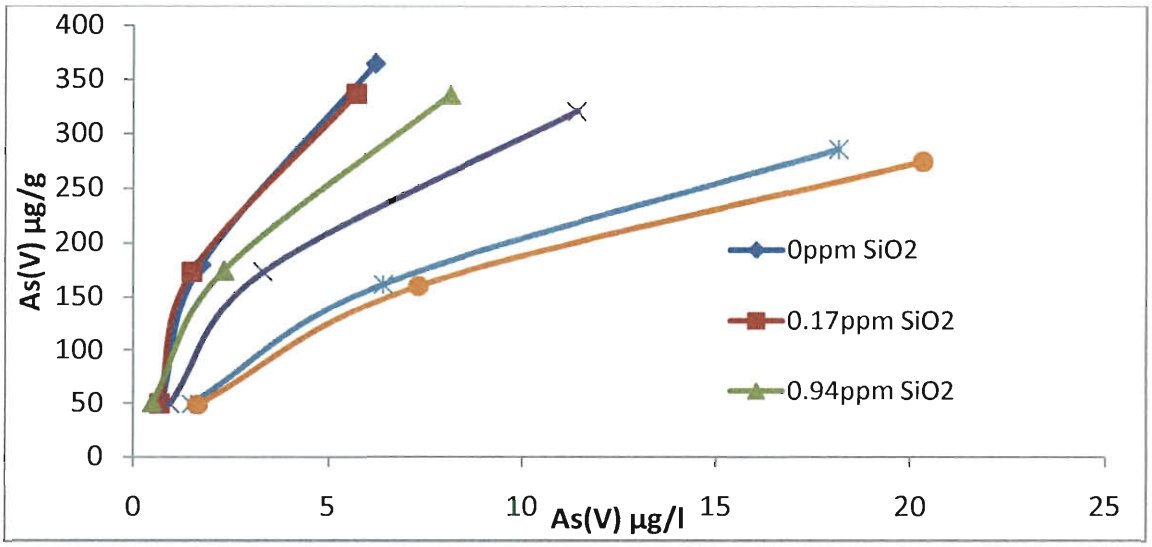

Figure 61 - 24-hour adsorption isotherms displaying the effects of silica and vanadium addition to synthetic solution containing 66µg/l As(V), 2.9mM NaCl, and 2.5mM THAM buffer adjusted to pH 7.5.

Figure 62 puts into perspective the effect of silica on arsenic adsorption as it displays the K_d values for the synthetic solutions with silica added (calculated from point of highest arsenic concentration for each curve in Figure 61) and the most effective pretreatments both with and without appreciable silica removal. Only limited improvement in arsenic removal, such as through anion exchange or pH adjustment, can be obtained without silica removal. However with silica removal, arsenic partitioning to magnetite can be increased from 2 L/g to 16 L/g or more as evidenced by treatment with activated alumina.

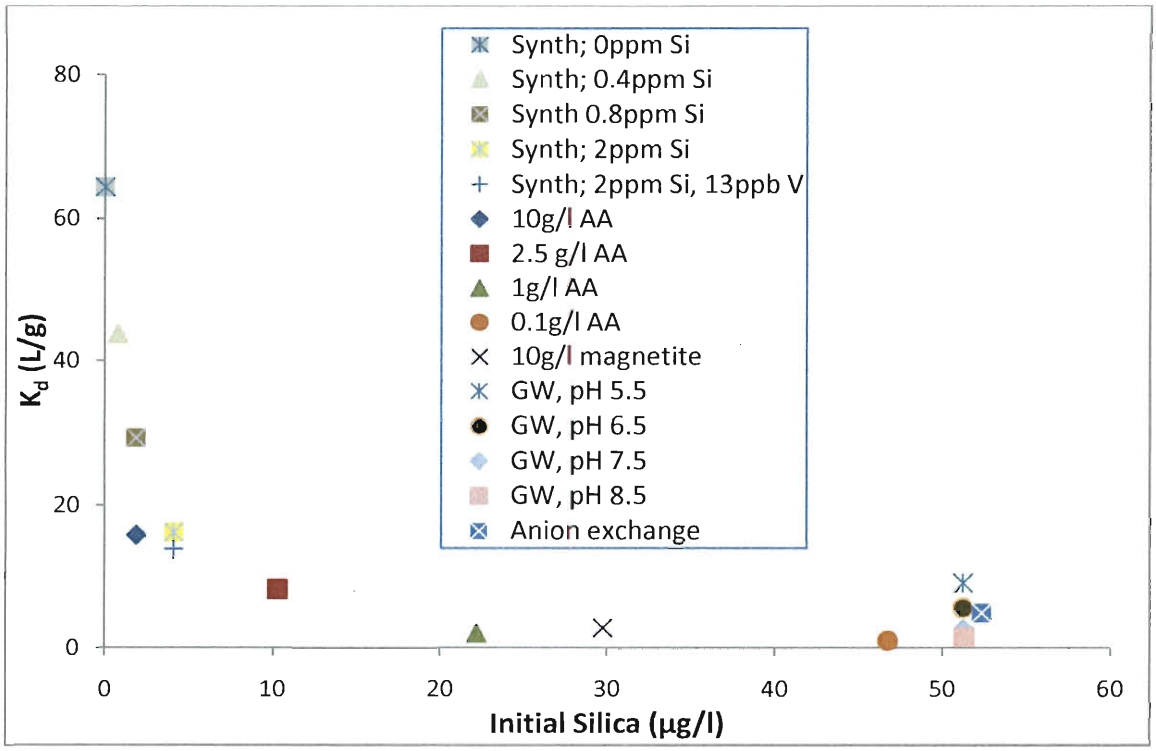

Figure 62 – The K_d values of single-point adsorption isotherms for arsenic to magnetite resulting from pretreated solutions with the given initial silica concentrations.

Removal of silica by activated alumina

A survey of groundwater from Guanajuato and surrounding areas was conducted, and all groundwater contained high levels of silica, indicating low-level geothermal

Preceding a process of arsenic adsorption to magnetite, an ideal pretreatment method would remove silica preferentially over arsenic, decreasing the ratio of silica to arsenic. The activated alumina did the opposite as Si:As ratios were higher in the effluent water than in the influent. The silica interference to a column of magnetite would, therefore, be more substantial in water pretreated with activated alumina than in non-pretreated water. An alternative pretreatment method would be needed to reduce silica to beneficial levels for arsenic removal by nanomagnetite.

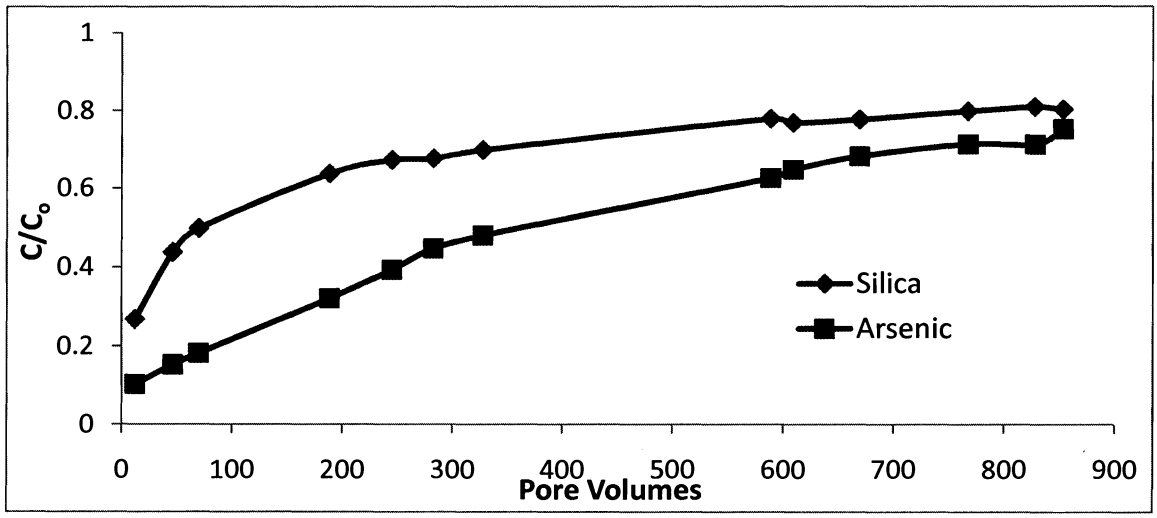

Figure 63 - Silica and arsenic removal through a 30.5cm packed column of activated alumina. Feed water composed of Guanajuato groundwater containing 48 mg/l SiO_2 and 8.8 µg/l As(V) at pH 7.9 was pumped with a 2.3 minute residence time.

Preceding a process of arsenic adsorption to magnetite, an ideal pretreatment method would remove silica preferentially over arsenic, decreasing the ratio of silica to arsenic. The activated alumina did the opposite as Si:As ratios were higher in the effluent water than in the influent. The silica interference to a column of magnetite would, therefore, be more substantial in water pretreated with activated alumina than in non-pretreated water. An alternative pretreatment method would be needed to reduce silica to beneficial levels for arsenic removal by nanomagnetite.

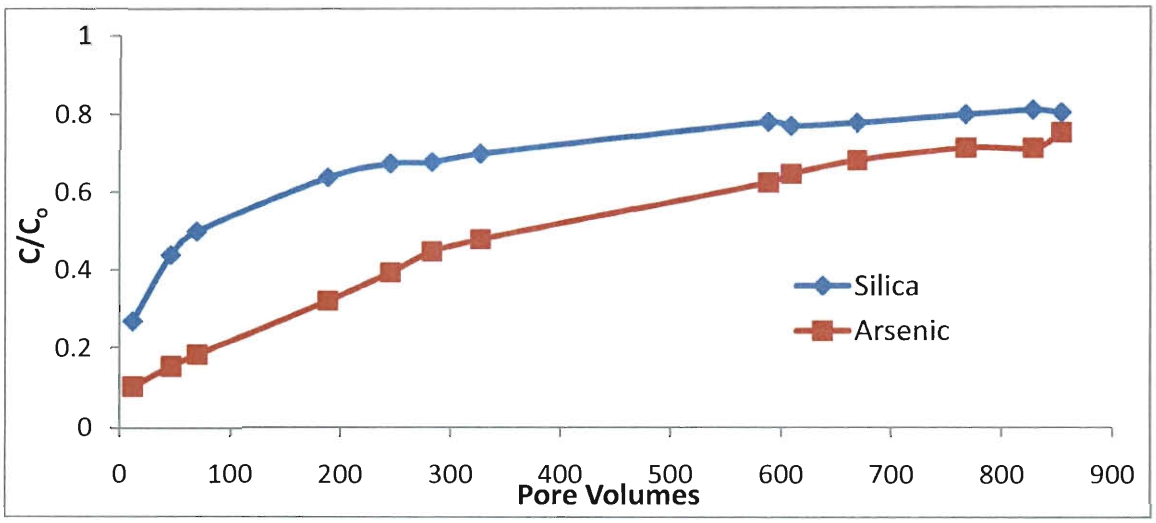

Figure 63 - Silica and arsenic removal through a 30.5cm packed column of activated alumina. Feed water composed of Guanajuato groundwater containing 48 mg/l SiO_2 and 8.8 µg/l As(V) at pH 7.9 was pumped with a 2.3 minute residence time.

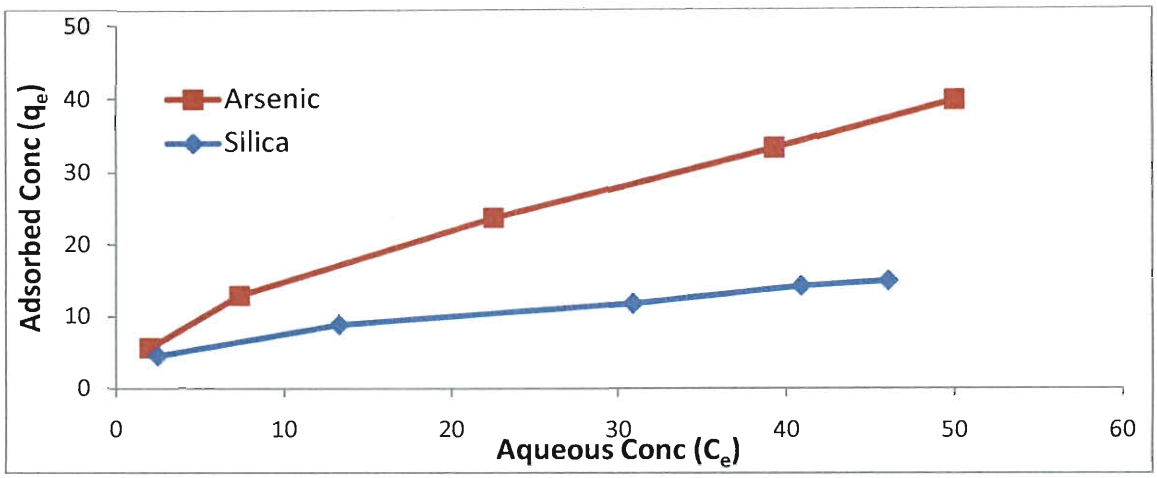

Figure 64 - Arsenic and silica adsorption to Activated Alumina. Units for aqueous concentrations for arsenic and silica are µg/l and mg/l, respectively. Units for adsorbed concentrations for arsenic and silica are µg/g and mg/g, respectively. The solution was composed of Guanajuato groundwater with As(V) added to 61µg/l; pH 7.7.

Silica and arsenic migration through the length of a column

To better understand the effects of silica on arsenic breakthrough, arsenic and silica concentrations were monitored in columns built with four sample ports, equally spaced along a column. Two identical columns, 13% magnetite by-weight dispersed among plastic beads, were run side-by-side with synthetic feed solutions, one with silica and one without. The base synthetic solution was composed of Milli-Q water, 100µg/l As(V), 2.5mM THAM buffer, and pH adjusted to 7.0 with HNO_3. The progressive breakthrough across each quarter-section of the column was monitored from each sample port. If later sections of the column adsorbed less arsenic than earlier sections of the column in the presence of silica, then a fouling effect by silica could be deduced. As shown in Figure 65 for the column feed solution containing silica, complete breakthrough of silica to the effluent of each column section was obtained by the second set of sample points near 150 pore volumes. Arsenic, however, saturated the media preceding each

sample port gradually over time for both the column with silica (Figure 66) and the column without silica (Figure 67). Breakthrough is displayed in terms of time (minutes) for clarity as the pore volume of each section is ¼ of the total pore volume of the column.

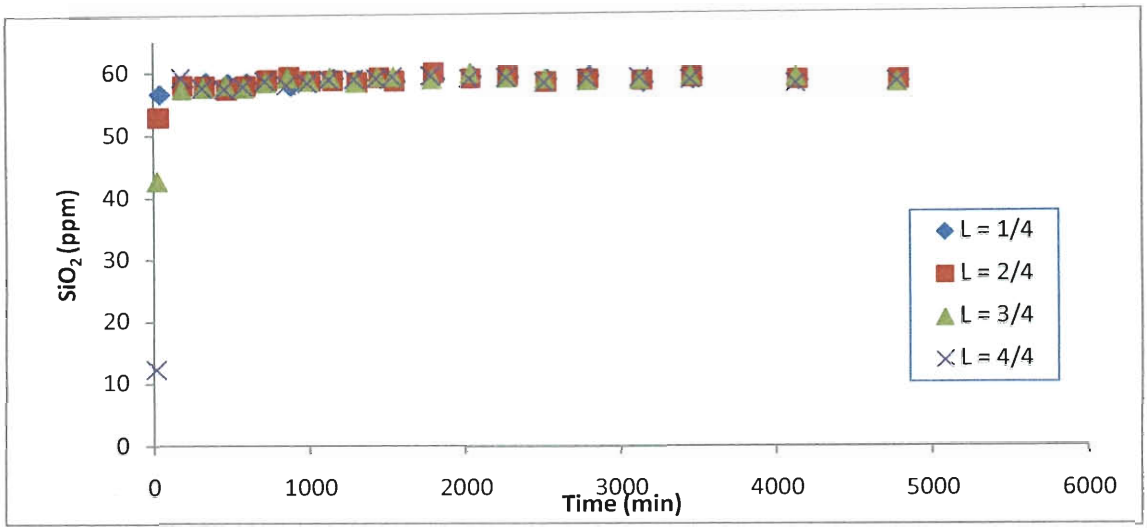

Figure 65 - Breakthrough of silica for synthetic water feed water (50mg/l as SiO_2, 100µg/l As(V), 2.5mM THAM buffer, pH adjusted to 7.0 with HNO_3) through each quarter of a column packed 13% by-weight with 78P magnetite and 87% by-weight with plastic beads.

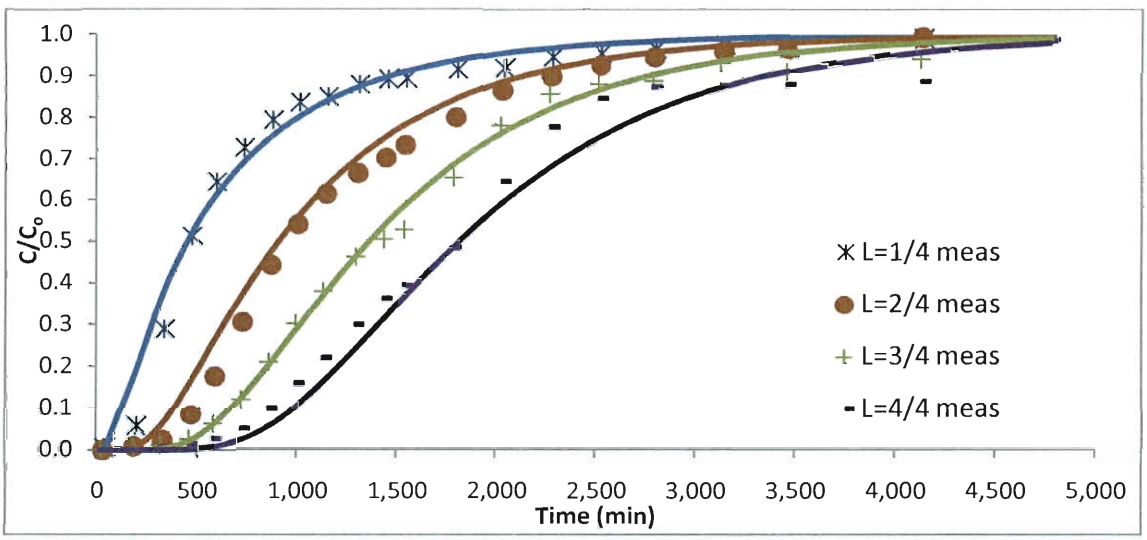

Figure 66 - Arsenic breakthrough for synthetic feed water containing silica (see description in Figure 65) shown through each quarter of a magnetite-packed column. Solid lines are the fitted model.

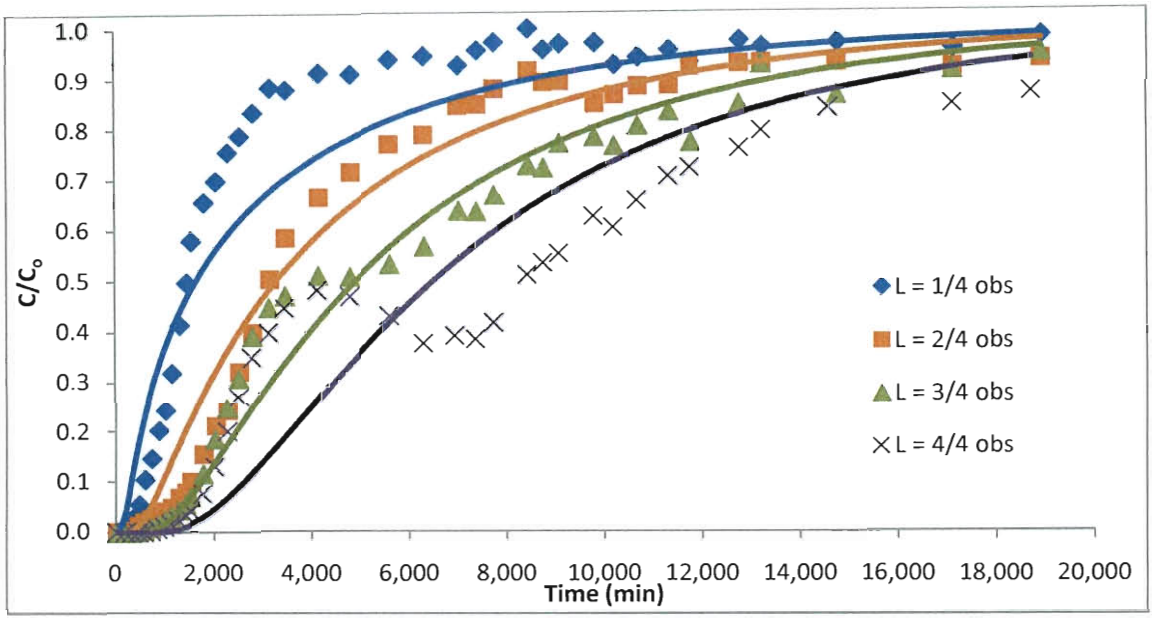

Figure 67 - Arsenic breakthrough for synthetic water feed water not containing silica shown through each quarter of a magnetite-packed column. Solid lines are the fitted model.

The hydraulic residence time within the 4 sections of the column was 5 minutes, cumulatively. For each column, the arsenic measurements from all four sample ports were fitted simultaneously to the advection-dispersion equation. The fitted parameters and applicable statistics generated using SolvStat (Billo 2001) are shown in Table 10. The presence of silica in the feed solution reduced the retardation factor of arsenic through the column by a factor of 3.6, from 1298 to 362. The synthetic solution without silica was reported to give more than double the dispersion; however, this was largely an artifact of the poor model fit around the irregular breakthrough curve in the 3rd and 4th sections of the column without silica.

Table 10 – Summary of transport parameters for the arsenic breakthrough curve displayed in Figure 66 and Figure 67, fitted simultaneously for all 4 sections of each column.

	R	D (cm^2/min)	μ_l (min^{-1})	r^2
With silica	362 ±5	9.46±0.53	0 ±0.015	0.989
Without silica	1298 ±34	21.0 ±1.8	0 ±0.0	0.941

The synthetic solution with silica resulted in a well-behaved breakthrough; however, irregular breakthrough occurred with the solution without silica. For the column without silica during the first 3,000 minutes, the 3rd and 4th quarter sections of the column did not significantly adsorb any arsenic. Arsenic essentially passed through these sections into the effluent. At 3,000 minutes, the 3rd section began adsorbing arsenic and held the arsenic concentration steady out of the 3rd quarter of the column. Then at 5,000 minutes the 4th section began to significantly adsorb arsenic and even reduced the effluent arsenic concentration to below the concentration released from the column at 3,000 minutes (C/C_0 <0.4). After 7,000 minutes, the arsenic breakthrough began to steadily rise through the end of the experiment. The irregular breakthrough behavior could be due to unseen mechanical or chemical processes. Mechanically, preferential flow paths may have existed in the 3rd and 4th sections initially that could have collapsed near 3,000 pore volumes resulting in more even saturation of the magnetite media from that point forward, but this scenario is less likely an issue in these laboratory experiments.

Chemically, the column without silica might be more susceptible to redox processes such as oxidation of magnetite to $Fe(OH)_3$ that might occur in later portions of the column. Over the range of conditions tested, in the lab and field, magnetite is not thermodynamically stable at the given pH and redox conditions (Figure 6). Oxidation of

the mixed Fe(II)·Fe(III) iron-oxide, magnetite can occur by reaction water alone ($Fe_3O_4 + 5H_2O \rightarrow 3Fe(OH)_3 + \frac{1}{2}H_{2(g)}$) or by other redox-active species in solution. By inhibiting the transport of oxidants to the magnetite surface, silica can prevent the oxidation of magnetite, as is reported elsewhere for other surfaces coated silica (Koh, Choi et al. 2000). The leveling and decrease in arsenic breakthrough observed with the synthetic solution without silica from 4,000 to 7,000 minutes (67 to 125 hours) closely resembled the dip observed in the pilot-column study conducted with raw groundwater (pH 7.3) from 23 to 32 hours. Although silica was present in the raw Guanajuato groundwater, oxidation could have been more aggressive due to other redox active species present in the groundwater.

The area above each breakthrough curve was numerically integrated using the trapezoidal rule to determine the arsenic adsorbed in each column section. Given no preloading effects, at full breakthrough one would expect the same quantity of arsenic to be adsorbed in each section. However for the silica-fed column, at full breakthrough the total arsenic adsorbed in the first section was significantly greater than that adsorbed in later sections (Figure 68). In contrast, the silica-free water did not show a large reduction from section to section. The 2nd section adsorbed an equal mass of arsenic as the 1st, while the 3rd and 4th sections trailed closely behind (Figure 69). In addition, the 3rd and 4th sections would have continued to adsorb more arsenic if the experiment had continued as breakthrough had only reached 87% and 93%, respectively.

A bar chart of the final mass of arsenic adsorbed to each section at the conclusion of the two column experiments is shown in Figure 70. The steady decline in arsenic adsorption capacity in later column sections confirms that silica results in column-

specific interference on arsenic adsorption that would not be predicted by batch adsorption isotherms. Moreover, the cumulative arsenic adsorbed through the entire column was reduced from 725µg/g to 161µg/g in the presence of silica. The results show that silica has a large effect on reducing arsenic adsorption capacity and that those effects amplify with time after pre-exposure to 50mg/l silica in a column scenario. For areas with high silica concentrations, column systems of short bed length (short residence times) may be ideal.

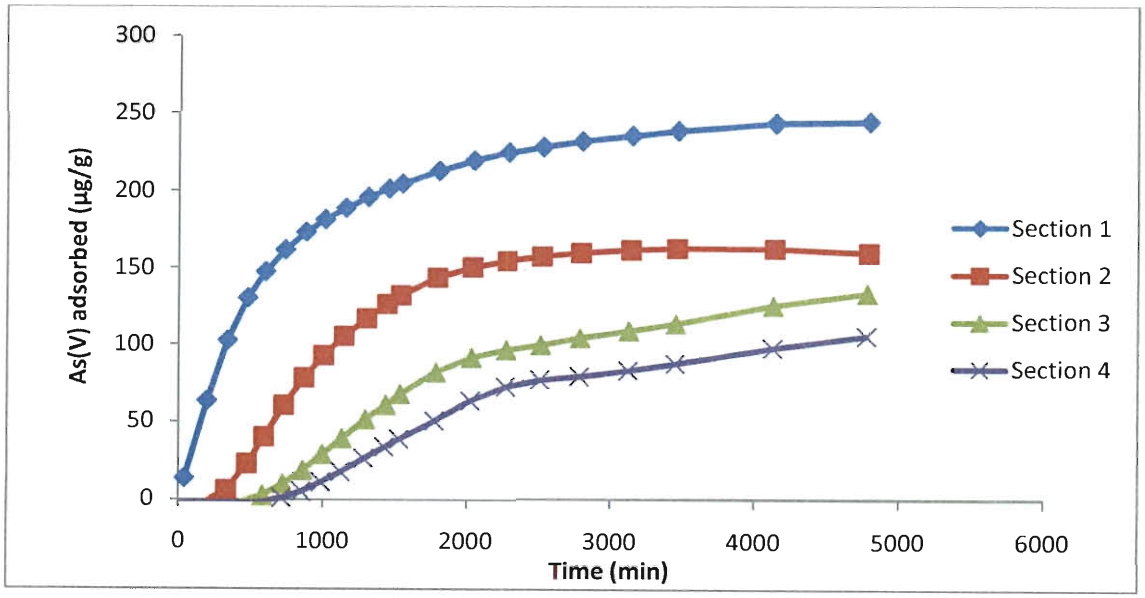

Figure 68 – The cumulative arsenic adsorbed per gram of magnetite in each quarter-section is shown over time for a column delivered a synthetic feed solution containing silica.

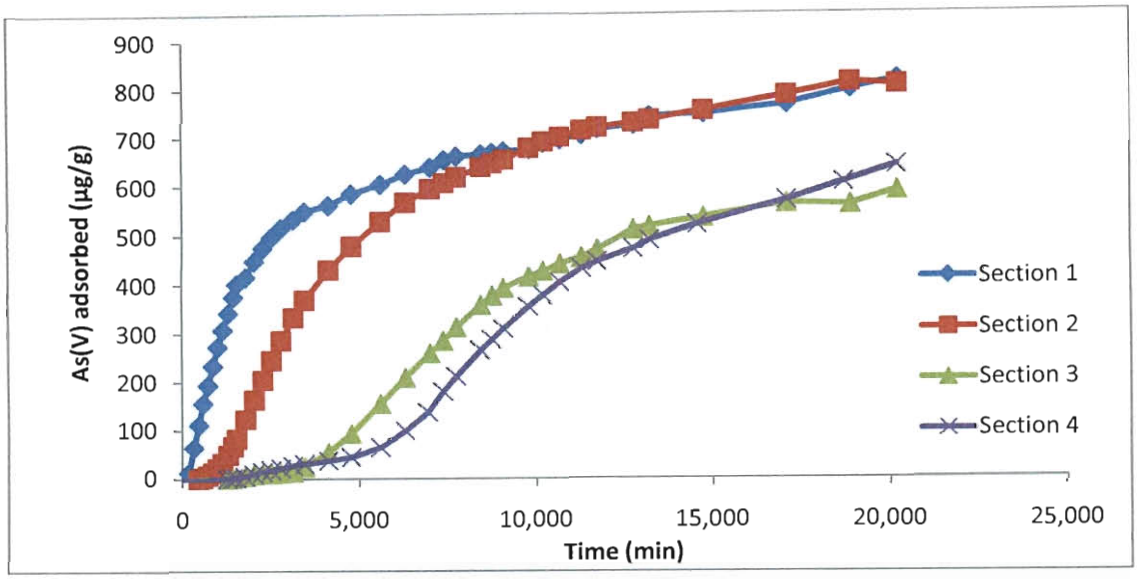

Figure 69 - The cumulative arsenic adsorbed per gram of magnetite in each quarter-section is shown over time for a column delivered a synthetic feed solution not containing silica.

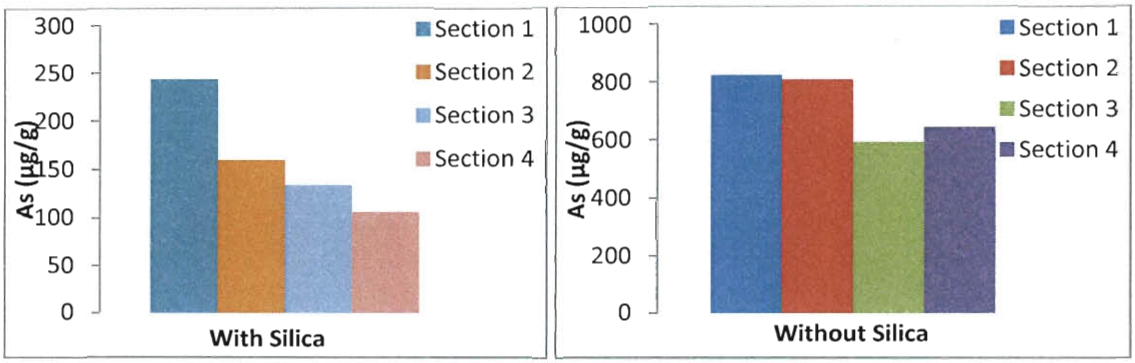

Figure 70 – The total arsenic adsorbed per gram of magnetite in each quarter section of the packed column by the end of the mid-column sampling experiment for feed solutions with silica and without silica.

Calcium effect on arsenic breakthrough in high silica feed water

In batch systems, Waltham and Eick showed that silica pre-equilibrated with goethite for 60 hours significantly reduced arsenic adsorption kinetics in proportion to silica concentration. With no silica in solution, equilibrium partitioning was established rapidly within 4 hours after arsenic was dosed into solution. However, when 6 and 60

mg/l of SiO_2 were pre-equilibrated for 60 hours, the time required to reach equilibrium was extended to 75 and >150 hours, respectively. This suggests that silica preloading in a column could slow the kinetics of arsenic adsorption, and potentially alter operation from equilibrium-limited to kinetically-limited operation. Smith and Edwards found calcium to improve the kinetics of arsenic adsorption to $Fe(OH)_3$ in the presence of silica interferences in batch systems but not change the quantity of arsenic adsorbed at equilibrium (2005). Projecting from the observation of Smith and Edwards, it could be postulated that calcium would have no effect on a column operating at equilibrium conditions with silica. To verify, batch adsorption was modeled in Visual Minteq and column experiments with identical solution conditions were conducted to observe the effect of calcium on arsenic adsorption in the presence of silica.

Visual Minteq modeling was conducted with and without the addition of calcium and silica species to solution. Simulation conditions were 100µg/l of As(V), ionic strength of 3mM, pH of 8, 0.04g/l (this produces the equivalent surface area) of hydrous ferric oxide adsorbent, and without and without 20mg/l of calcium ions and with and without 50mg/l of SiO_2. Table 11 displays the percentage of each species that adsorbed in the given conditions. When calcium was added to solution of arsenic and silica, the total arsenic adsorbed increased from 23.9 to 33% sorbed, a 38% increase. Calcium had minimal effect on arsenic adsorption when silica was not in solution, even at lower HFO concentrations where arsenic was not 99% adsorbed (not shown). When calcium is in solution, it competes for adsorption sites with silica, and increases the surface charge of the iron-oxide surface. This increases the electrostatic interaction with arsenate anions

and results in more adsorption. Contrary to Smith and Edwards observations, the Visual Minteq model suggests more adsorption of As(V) at equilibrium conditions.

Table 11 – Visual Minteq simulation giving the percentage of species adsorbed for the given species in solution

Species in solution	As (% sorbed)	Ca (% sorbed)	Si (% sorbed)
As(V)	99.991	-	-
As(V) + Ca	99.996	0.912	-
As(V) + Si	23.877	-	4.553
As(V) + Si + Ca	33.037	0.791	4.472

Column experiments were conducted to observe the Visual Minteq model predictions given the addition of calcium to a synthetic solution of arsenic and silica. Differing from the Visual Minteq conditions, the solids concentration of magnetite in the column was equivalent to 4 g/l of HFO. Figure 71 shows breakthrough of arsenic through identical columns with one synthetic solution containing 20mg/l of calcium and one without calcium. The calcium increased retardation within the column from 146 to 257 pore volumes and the dispersion from 157 to 232 cm^2/min (Table 12). The increase in the retardation is almost proportionate to the increase in predicted by Visual Minteq. Given that the columns were constructed identically and were fed solution at the same flow rate, the apparent change in dispersion may have been due to an inhibition of the silica preloading effect rather than a true change in the dispersivity of the media. In addition, the quantity of arsenic adsorbed by the termination of each experiment was 74 μg/g for the column without calcium and 138 μg/g for the column with calcium added, an 87% increase (Figure 72). This large increase with calcium addition indicates that calcium has a greater effect in column operation than predicted by equilibrium modeling. The additional increase may be due to calcium improving the kinetics of adsorption

within the column or mitigating the preloading effect of silica downstream of the arsenic mass transfer zone. Adsorbed calcium alongside the preloaded silica would increase the surface charge of magnetite and enhance electrostatic attraction with arsenate anions; i.e, the Ca^{2+} ions act as bridging ions. The larger electrostatic interaction could result in more rapid ligand exchange with adsorbed silicates and adsorption of arsenate species. The assumption that breakthrough can be predicted by equilibrium assessment alone is not valid for both for solutions with high silica or with high silica and calcium. The projection of arsenic adsorption capacity of a column from adsorption isotherms may only represent a best-case scenario and require significant adjustment to account for dynamic processes associated with column operation. At the same time, these differences from theory can be used to enhance future experimental designs.

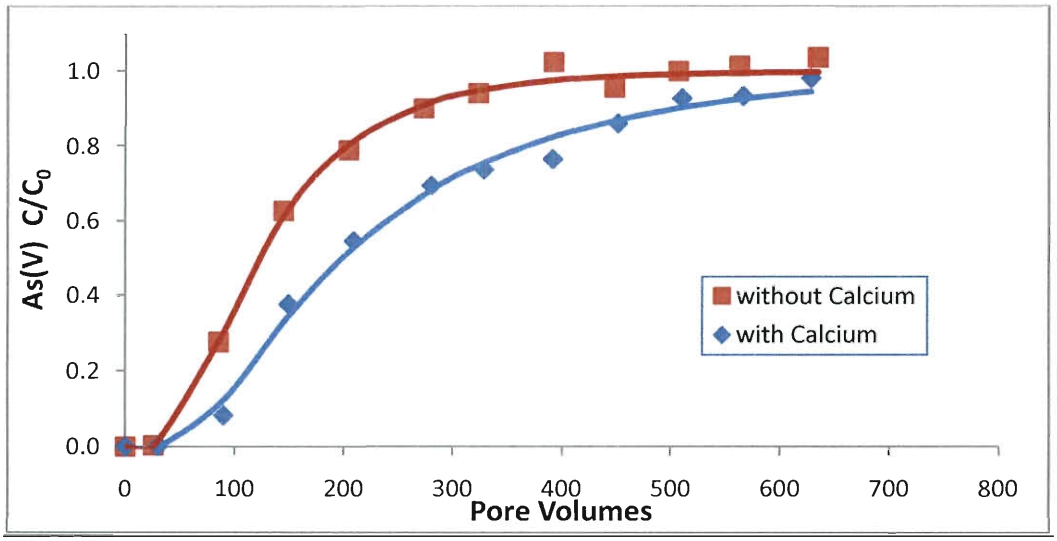

Figure 71 – Arsenic breakthrough with synthetic feed solutions with and without calcium. Feed solutions were formulated with 100 µg/l As(V), 50 mg/l as SiO_2, 2.5mM THAM buffer, trace-metal grade HNO_3 to reduce the pH to 8.0, sufficient $NaNO_3$ to raise the conductivity to 750µS/cm, and with or without 20mg/l of Ca^{2+} from $CaCl_2$. Lines are fitted using CXTFIT.

Table 12 - Fitted parameters to the column breakthrough described in Figure 71.

	R	D (cm^2/min)	μ_l (min^{-1})	r^2
Without Calcium	146 ±5	157 ±25	0 ±0.014	0.997
With Calcium	257 ±21	232±57	0 ±0.050	0.994

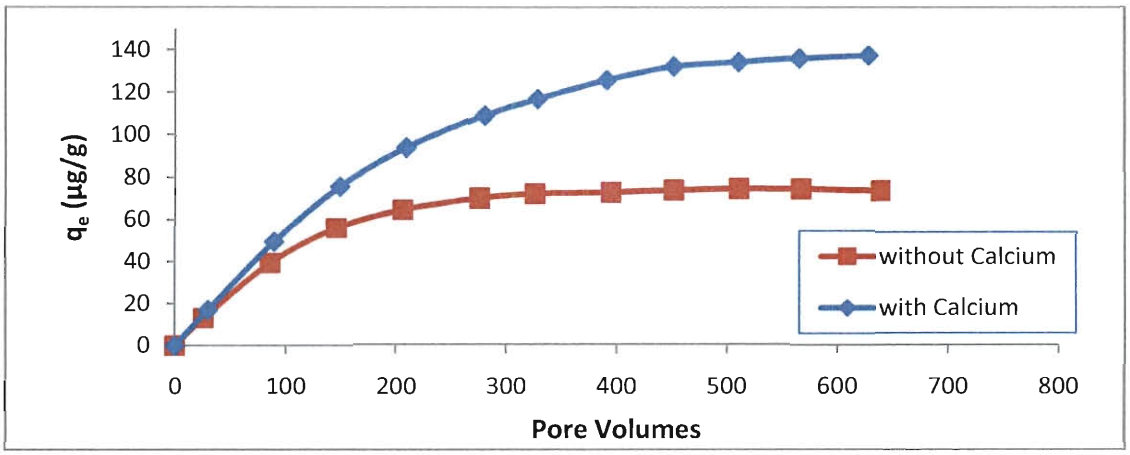

Figure 72 - Cumulative arsenic adsorbed in columns with synthetic feed solutions as described in Figure 71. Lines are for visualization only.

5. Conclusions and Recommended Future Work

Food-grade magnetite (78P) was selected for field and laboratory studies regarding arsenic removal from groundwater based on arsenic adsorption isotherms, cost analysis, and consumer-safety considerations. On a surface area basis, 78P magnetite (12.16m^2/g) was shown to adsorb a similar amount of arsenic as Reade magnetite (60 m^2/g) near 6 μg/m^2 in equilibrium with 30 μg/l As(V) in Rice groundwater at pH 8.0. Given simplifying assumptions, 78P was estimated to treat 1,000 liters of Rice groundwater from 30 μg/l to 25 μg/l of As(V) for $0.16 US. Column trials were used to determine ideal design and operating conditions. Increased magnetite to sand ratios delayed breakthrough of arsenic, but yielded an elongated mass transfer zone with the greater percentage of magnetite. Long residence time reduced the slope of the breakthrough curve through reduced dispersion caused by the lower flow rates. Notably, neither magnetite percentage nor residence time appeared to significantly alter the total mass of arsenic adsorbed to magnetite at saturation. Arsenic breakthrough approached a plateau of C/C_0=0.9 through the end of a 3.9 minute residence time experiment, indicating steady state adsorption, proposed to be due to arsenate surface species going from monodentate mononuclear attachment in rapid equilibrium with solution to the hysteretic bidentate binuclear attachment. A first-order decay term represented the data well with a characteristic time of 41 minutes. This time appeared to be accurate as a column with a similar residence time of 36 minutes converged readily to full breakthrough with only a negligible rate coefficient for decay (μ_1=0.001).

Breakthrough of arsenic in columns of the food-grade magnetite and sand was delayed greater than 10 times with a synthetic feed solution (R = 5442) as compared to a

groundwater feed solution (R = 412) at the same pH. Adsorption isotherms conducted with Guanajuato groundwater treated by various means were used to assess the effect of naturally occurring species from greatest benefit to most severe interference for adsorption. In the Guanajuato groundwater, beneficial species and conditions included low pH, high redox potential, and colloids and suspended solids. Minimal or neutral effects were observed for divalent cations, bicarbonate, and trace organics. Negative effects were observed for competing anions and silica. The species with the greatest interference for arsenic adsorption in the Guanajuato groundwater was silica. With silica removed from groundwater by activated alumina or with the addition of silica to synthetic solutions, adsorption isotherms confirmed silica's strong effect. Low-level geothermal waters with high silica concentrations are common throughout central Mexico and other parts of the world, presenting a major challenge for arsenic adsorbents. In areas such as Guanajuato, silica cannot be avoided as silica concentrations were consistently found to be between 48-100mg/l (Appendix C).

The adsorption of arsenic from Guanajuato groundwater in batch experiments was highly dependent on pH. However, contrary to batch experiments, equilibrium modeling in Visual Minteq, and literature consensus, pilot-scale column experiments showed no improvement in breakthrough behavior with pH reduction of the same groundwater source. It was suspected that column-specific effects of silica preloading and redox processes were largely responsible for the lack of improvement in arsenic retention. Silica can be expected to adsorb similarly to magnetite sufficiently below its first pKa value of 9.46 due to the formation of inner-sphere chemical bonds in neutral and pH-reduced groundwater. In addition, redox conditions were favorable for oxidation of

magnetite to Fe(III) corrosion products which would have created more surface area for arsenic adsorption during the column experiment.

Deep bed effects were observed more closely from laboratory columns sampled from 4 locations along their length. A synthetic feed solution with silica gave a more significant decrease in arsenic adsorption to magnetite (244, 160, 134, and then 105 μg/g) with each segment deeper within the column bed than a synthetic solution without silica (822, 807, 591, and then 643, μg/g). In batch systems, silica has been shown to reduce both the equilibrium distribution and the kinetics of arsenic adsorption to iron oxides; those affects appear to be amplified in columns where deep bed preloading can reduce arsenic adsorption. When calcium was present in feed water it had almost immediate breakthrough, similar to silica, and therefore likely acted to mitigate the effects of preloading. By increasing the surface charge of magnetite, adsorbed calcium facilitates greater electrostatic interaction with arsenate. The preloading effects of silica and calcium and the deep-bed redox effects observed to occur in several of the magnetite columns would not be realized from adsorption isotherms alone.

This research provides several avenues for future work regarding deep bed effects of magnetite in packed columns. Research is needed to identify the oxidation rates of magnetite for varied solution conditions, model the rates of silica preloading and ligand exchange kinetics for arsenic adsorption on the surface of magnetite with and without the presence of calcium, and further study into other species, such as Zn or Mg, that may facilitate the arsenic adsorption on magnetite in the presence of silica. For example, Zn has been shown in batch studies to increase the rate of arsenic adsorption in synthetic

waters without silica (Yang, Kan et al. 2010), but its beneficial effect have not been clearly studied for waters containing of silica and for its surface effect in column systems.

Research activities are recommended for point-of-use applications relevant to the developing world. Field application in household sand filters with long residence times (30-45 minutes) would likely delay arsenic breakthrough for longer than modeled in the short residence time columns (0.75-4 minutes) in this work. If assessed in areas with typical silica concentrations (5-10 mg/l as SiO_2), column filtration would likely be more effective as the current research suggests significantly less silica interference when silica is present at those levels below 20 mg/l.

Arsenic adsorption by magnetite in columns is complex due to the competitive species present in natural water and the deep-bed preloading and redox-active nature of the magnetite surface and species in solution.

References

(1998). Standard Methods for the Examination of Water and Wastewater, APHA, AWWA, WEF.

"ADSORBSIA™ As500 Titanium Based Media " Form No. 177-02163-0609, 1-4.

(1998). Standard Methods for the Examination of Water and Wastewater, APHA, AWWA, WEF.

(2002). 40 CFR Title 40. EPA, United States. **19**.

Abo-El-Enein, S. A., M. A. Eissa, et al. (2009). "Removal of some heavy metals ions from wastewater by copolymer of iron and aluminum impregnated with active silica derived from rice husk ash." Journal of Hazardous Materials **172**(2-3): 574-579.

Alexander, G. B., W. M. Heston, et al. (1954). "THE SOLUBILITY OF AMORPHOUS SILICA IN WATER." Journal of Physical Chemistry **58**(6): 453-455.

Alvarez, P. J. J., V. Colvin, et al. (2009). "Research Priorities to Advance Eco-Responsible Nanotechnology." ACS Nano **3**(7): 1616-1619.

Aragon, J. C. N. (2005). DRINKING WATER QUALITY IN NORTHERN MEXICO AND ARSENIC TREATMENT WITH IRON IMPREGNATED GAC. Civil and Environmental Engineering. Tempe, AZ, ASU. **MS:** 234.

Arai, Y., D. L. Sparks, et al. (2004). "Effects of dissolved carbonate on arsenate adsorption and surface speciation at the hematite-water interface." Environmental Science & Technology **38**(3): 817-824.

Armienta, M. A. and N. Segovia (2008). "Arsenic and fluoride in the groundwater of Mexico." Environmental Geochemistry and Health **30**(4): 345-353.

Auffan, M., J. Rose, et al. (2009). "Towards a definition of inorganic nanoparticles from an environmental, health and safety perspective." Nat Nano **4**(10): 634-641.

Baes, C. F. (1976). The hydrolysis of cations. New York, John Wiley.

Bagla, P. (2003, June 5, 2003). "Arsenic-Laced Well Water Poisoning Bangladeshis." Retrieved November 12, 2009, from http://news.nationalgeographic.com/news/2003/06/0605_030605_arsenicwater.html.

Ball, J. W., Nordstrom, D.K., Jenne, E.A., Vivit, D.V. (1998). Chemical Analysis of Hot Springs, Pools, Geysers, and Surface Waters from Yellowstone National Park, Wyoming and its Vicinity. U. O.-F. Report**:** 98-182.

Bang, S., M. Patel, et al. (2005). "Removal of arsenic from groundwater by granular titanium dioxide adsorbent." Chemosphere **60**(3): 389-397.

Barbalace, K. L. (1995-2009). "Periodic Table of Elements - Arsenic – As." Retrieved 9/12/2009, from http://environmentalchemistry.com/yogi/periodic/As.html.

Bartlett, R. J. and J. M. Kimble (1976). "BEHAVIOR OF CHROMIUM IN SOILS .2. HEXAVALENT FORMS." Journal of Environmental Quality **5**(4): 383-386.

Bear, J. (1988). Dynamics of Fluids in Porous Media Courier Dover Publications.

Benjamin, M. M. (2010). Water Chemistry, Waveland Press, Inc.

Billo, E. J. (2001). Excel for Chemists: A Comprehensive Guide. Second Edition. New York, John Wiley and Sons, Inc.

Birkle, P., J. Bundschuh, et al. (2010). "Mechanisms of arsenic enrichment in geothermal and petroleum reservoirs fluids in Mexico." Water Res **44**(19): 5605-5617.

Blaney, L. M., S. Cinar, et al. (2007). "Hybrid anion exchanger for trace phosphate removal from water and wastewater." Water Research **41**(7): 1603-1613.

Bodek, I., W. J. Lyman, et al. (1988). Environmental Inorganic Chemistry. Properties, Processes, and Estimation Methods. New York, Pergamon Press.

Bouguerra, W., M. B. Ali, et al. (2007). "Equilibrium and kinetic studies of adsorption of silica onto activated alumina." Desalination **206**(1-3): 141-146.

Boulding, R. and J. S. Ginn (2004). Practical handbook of soil, vadose zone, and ground-water contamination. New York, Lewis Publishers.

Bundschuh, J., M. Litter, et al. (2010). "Emerging mitigation needs and sustainable options for solving the arsenic problems of rural and isolated urban areas in Latin America - A critical analysis." Water Research **44**(19): 5828-5845.

Callahan, M. A., M. Slimak, et al. (1979). Water-related environmental fate of 129 priority pollutants / by Michael A. Callahan ... [et. al.]. Washington, D.C. :, Office of Water Planning and Standards, Office of Water and Waste Management, U.S. Environmental Protection Agency.

Care, S., Q. T. Nguyen, et al. (2008). "Mechanical properties of the rust layer induced by impressed current method in reinforced mortar." Cement and Concrete Research **38**(8-9): 1079-1091.

Chen, H. W., M. M. Frey, et al. (1999). "Arsenic treatment considerations." Journal American Water Works Association **91**(3): 74-85.

Chiew, H., M. L. Sampson, et al. (2009). "Effect of Groundwater Iron and Phosphate on the Efficacy of Arsenic Removal by Iron-Amended BioSand Filters." Environmental Science & Technology **43**(16): 6295-6300.

Chowdhury, U. K., B. K. Biswas, et al. (2000). "Groundwater arsenic contamination in Bangladesh and West Bengal, India." Environmental Health Perspectives **108**(5): 393-397.

Coronado-Gonzalez, J. A., L. M. Del Razo, et al. (2007). "Inorganic arsenic exposure and type 2 diabetes mellitus in Mexico." Environmental Research **104**(3): 383-389.

Daus, B., R. Wennrich, et al. (2004). "Sorption materials for arsenic removal from water: A comparative study." Water Research **38**(12): 2948-2954.

Davies, C. W. and V. E. Malpass (1964). "ION ASSOCIATION + VISCOSITY OF DILUTE ELECTROLYTE SOLUTIONS .I. AQUEOUS INORGANIC SALT SOLUTIONS." Transactions of the Faraday Society **60**(503P): 2075-&.

Daviescolley, R. J., P. O. Nelson, et al. (1984). "COPPER AND CADMIUM UPTAKE BY ESTUARINE SEDIMENTARY PHASES." Environmental Science & Technology **18**(7): 491-499.

Davis, C. C., W. R. Knocke, et al. (2001). "Implications of Aqueous Silica Sorption to Iron Hydroxide: Mobilization of Iron Colloids and Interference with Sorption of Arsenate and Humic Substances." Environmental Science & Technology **35**(15): 3158-3162.

Debye, P. and E. Huckel (1923). "The theory of electrolytes I. The lowering of the freezing point and related occurrences." Physikalische Zeitschrift **24**: 185-206.

Deliyanni, E. A., D. N. Bakoyannakis, et al. (2003). "Sorption of As(V) ions by akaganeite-type nanocrystals." Chemosphere **50**(1): 155-163.

Dixit, S. and J. G. Hering (2003). "Comparison of Arsenic(V) and Arsenic(III) Sorption onto Iron Oxide Minerals: Implications for Arsenic Mobility." Environmental Science & Technology **37**(18): 4182-4189.

Doyle, D. (2009). "Notoriety to respectability: a short history of arsenic prior to its present day use in haematology." British Journal of Haematology **145**(3): 309-317.

Dutta, P. K., A. K. Ray, et al. (2004). "Adsorption of arsenate and arsenite on titanium dioxide suspensions." Journal of Colloid and Interface Science **278**(2): 270-275.

Dzombak, D. A. and F. M. M. Morel (1990). Surface Complexation Modeling: Hydrous Ferric Oxide. New York, John Wiley and Sons.

Ellis, A. J. and W. A. J. Mahon (1964). "Natural hydrothermal systems and experimental hot-water/rock interactions." Geochimica et Cosmochimica Acta **28**(8): 1323-1357.

Elmer, T. H. and M. E. Nordberg (1958). "SOLUBILITY OF SILICA IN NITRIC ACID SOLUTIONS." Journal of the American Ceramic Society **41**(12): 517-520.

EPA (1996). ICR Manual for Bench- and Pilot-Scale Treatment Studies. EPA 814/B-96-003. T. S. Division. Cincinnati, OH**:** 2-6.

EU (1995). COMMISSION DIRECTIVE 95/45/EC; Laying down specific purity criteria concerning colours for use in foodstuffs.

Farrell, J. (2009). Nanomagnetite enhances sand filtration for removal of arsenic from drinking water. Department of Civil and Environmental Engineering. Houston, TX, Rice University. **M.S.:** 122.

Feenstra, L., J. v. Erkel, et al. (2007). Arsenic in groundwater: Overview and evaluation of removal methods. Utrecht, The Netherlands, International Groundwater Resources Assessment Centre. **2**.

Fendorf, S., M. J. Eick, et al. (1997). "Arsenate and chromate retention mechanisms on goethite .1. Surface structure." Environmental Science & Technology **31**(2): 315-320.

Ferguson, J. F. and J. Gavis (1972). "A review of the arsenic cycle in natural waters." Water Research **6**(11): 1259-1274.

Fournier, R. O. and R. W. Potter (1979). "MAGNESIUM CORRECTION TO THE NA-K-CA CHEMICAL GEOTHERMOMETER." Geochimica et Cosmochimica Acta **43**(9): 1543-1550.

Fournier, R. O. and A. H. Truesdell (1973). "An empirical Na---K---Ca geothermometer for natural waters." Geochimica et Cosmochimica Acta **37**(5): 1255-1275.

Frey, M. M. and M. A. Edwards (1997). "Surveying arsenic occurrence." Journal American Water Works Association **89**(3): 105-117.

Fry, R. C., P. Navasumrit, et al. (2007). "Activation of inflammation/NF-kappa B signaling in infants born to arsenic-exposed mothers." Plos Genetics **3**(11): 2180-2189.

Garai, R., A. K. Chakraborty, et al. (1984). "Chronic arsenic poisoning from tube-well water." J Indian Med Assoc **82**(1): 34-35.

Garcia-Lara, A. M. and C. Montero-Ocampo (2010). "Improvement of Arsenic Electro-Removal from Underground Water by Lowering the Interference of other Ions." Water Air and Soil Pollution **205**(1-4): 237-244.

Garcia-Sandchez, A. and E. Alvarez-Ayuso (2003). "Arsenic in soils and waters and its relation to geology and mining activities (Salamanca Province, Spain)." Journal of Geochemical Exploration **80**(1): 69-79.

Genc, H. and J. C. Tjell (2003). "Effects of phosphate, silicate, sulphate, and bicarbonate on arsenate removal using activated seawater neutralised red mud (bauxsol)." Journal De Physique Iv **107**: 537-540.

Gimenez, J., M. Martinez, et al. (2007). "Arsenic sorption onto natural hematite, magnetite, and goethite." Journal of Hazardous Materials **141**(3): 575-580.

Goh, K.-H. and T.-T. Lim (2010). "Influences of co-existing species on the sorption of toxic oxyanions from aqueous solution by nanocrystalline Mg/Al layered double hydroxide." Journal of Hazardous Materials **180**(1-3): 401-408.

Gong, G. and S. E. O'Bryant (2010). "The Arsenic Exposure Hypothesis for Alzheimer Disease." Alzheimer Disease & Associated Disorders **24**(4): 311-316.

Gustafsson, J. P. (2009). Visual MINTEQ. Stockhom, Sweden.

Gutierrez, M., M. T. Alarcon-Herrera, et al. (2009). "Geographical distribution of arsenic in sediments within the Rio Conchos Basin, Mexico." Environmental Geology **57**(4): 929-935.

Han, F., Y. Su, et al. (2003). "Assessment of global industrial-age anthropogenic arsenic contamination." Naturwissenschaften **90**(9): 395-401.

Hast, N. (1956). "A REACTION BETWEEN SILICA AND SOME MAGNESIUM COMPOUNDS AT ROOM TEMPERATURE AND AT +37-DEGREES-C." Arkiv for Kemi **9**(4): 343-360.

Hem, J. D. (1989). Study and Interpretation of the Chemical Characteristics of Natural Water. U. S. G. Survey. Alexandria, VA, UNITED STATES GOVERNMENT PRINTING OFFICE.

Hingston, F. J., A. M. Posner, et al. (1968). "ADSORPTION OF SELENITE BY GOETHITE." Advances in Chemistry Series(79): 82-&.

Hristovski, K. D., P. K. Westerhoff, et al. (2009). "Effect of synthesis conditions on nano-iron (hydr)oxide impregnated granulated activated carbon." Chemical Engineering Journal **146**(2): 237-243.

Huang, C. P., H. A. Elliott, et al. (1977). "INTERFACIAL REACTIONS AND FATE OF HEAVY-METALS IN SOIL-WATER SYSTEMS." Journal Water Pollution Control Federation **49**(5): 745-756.

Huang, C. P. and P. L. K. Fu (1984). "TREATMENT OF ARSENIC .5. CONTAINING WATER BY THE ACTIVATED CARBON PROCESS." Journal Water Pollution Control Federation **56**(3): 233-242.

Huisman, L. W., W.E. (1974). Slow Sand Filtration. Geneva, World Health Organization.

Hurtado-Jimenez, R. and J. L. Gardea-Torresdey (2006). "Arsenic in drinking water in the Los Altos de Jalisco region of Mexico." Rev Panam Salud Publica **20**(4): 236-247.

Hussam, A. (2007). Clean Drinking Water: Solving Arsenic Crisis through a Sustainable Local Filtration Technology. Fairfax, Virginia, Department of Chemistry & Biochemistry, George Mason University.

Hussam, A. and A. K. M. Munir (2007). "A simple and effective arsenic filter based on composite iron matrix: Development and deployment studies for groundwater of

Bangladesh." Journal of Environmental Science and Health Part a-Toxic/Hazardous Substances & Environmental Engineering **42**(12): 1869-1878.

Iler, R. K. (1979). The Chemistry of Silica: Solubility, Polymerization, Colloid and Surface Properties, and Biochemistry. New York, John Wiley & Sons, Inc.

Jain, A. and R. H. Loeppert (2000). "Effect of competing anions on the adsorption of arsenate and arsenite by ferrihydrite." Journal of Environmental Quality **29**(5): 1422-1430.

Jain, C. K. and I. Ali (2000). "Arsenic: Occurrence, toxicity and speciation techniques." Water Research **34**(17): 4304-4312.

James, R. O. and M. G. Macnaughton (1977). "ADSORPTION OF AQUEOUS HEAVY-METALS ON INORGANIC MINERALS." Geochimica et Cosmochimica Acta **41**(11): 1549-1555.

Jia, G., H. Wang, et al. (2005). "Cytotoxicity of Carbon Nanomaterials: Single-Wall Nanotube, Multi-Wall Nanotube, and Fullerene." Environmental Science & Technology **39**(5): 1378-1383.

Jing, C., S. Liu, et al. (2008). "Arsenic remobilization in water treatment adsorbents under reducing conditions: Part I. Incubation study." SCIENCE OF THE TOTAL ENVIRONMENT **389**(1): 188-194.

Jing, C. Y., S. Q. Liu, et al. (2005). "Arsenic leachability in water treatment adsorbents." Environmental Science & Technology **39**(14): 5481-5487.

Jones, M. M. and R. M. Pytkowicz (1973). "SOLUBILITY OF SILICA IN SEA WATER AT HIGH PRESSURES." Bulletin de la Societe Royale des Sciences de Liege **42**(3-4): 118-120.

Knappe, D. R. U., V. L. Snoeyink, et al. (1997). "The effect of preloading on rapid small-scale column test predictions of atrazine removal by GAC adsorbers." Water Research **31**(11): 2899-2909.

Ko, I., A. Davis, et al. (2007). "Arsenic Removal by a Colloidal Iron Oxide Coated Sand." JOURNAL OF ENVIRONMENTAL ENGINEERING **133**(0): 891.

Koch, R. (1985). "W. SALOMONS and U. FÖRSTNER: Metals in the Hydrocycle. Berlin — Heidelberg — New York — Tokyo: Springer Verlag, 1984, 349 S., 149 Abb., DM 98.—." Acta hydrochimica et hydrobiologica **13**(2): 267-267.

Koh, Y.-H., J.-J. Choi, et al. (2000). "Strengthening and Prevention of Oxidation of Aluminum Nitride by Formation of a Silica Layer on the Surface." Journal of the American Ceramic Society **83**(2): 306-310.

Konikow, L. F. (2010). "The Secret to Successful Solute-Transport Modeling." National Ground Water Association.

Kool, J. B., J. C. Parker, et al. (1985). "Evaluation of soil hydraulic properties by nonlinear least-squares parameter analysis." Trans. Am. Geophys. Union **66**(274).

Kuo, S. and B. L. McNeal (1984). "EFFECTS OF PH AND PHOSPHATE ON CADMIUM SORPTION BY A HYDROUS FERRIC-OXIDE." Soil Science Society of America Journal **48**(5): 1040-1044.

Liao, Z., Z. Gu, et al. (2009). "Treatment of cooling tower blowdown water containing silica, calcium and magnesium by electrocoagulation." Water Science and Technology **60**(9): 2345-2352.

Little, A. D. (1984). Full-Scale Evaluation of Waste Disposal from Coal-Fired Generating Plants. Appendix F (Part 4). EPA. Washington DC, Office of Research and Development.

Lockwood, R. A. and K. Y. Chen (1973). "ADSORPTION OF HG(II) BY HYDROUS MANGANESE OXIDES." Environmental Science & Technology **7**(11): 1028-1034.

Mandal, B. K. and K. T. Suzuki (2002). "Arsenic round the world: a review." Talanta **58**(1): 201-235.

Matschullat, J. (2000). "Arsenic in the geosphere -- a review." The Science of The Total Environment **249**(1-3): 297-312.

Mayo, J. T., C. T. Yavuz, et al. (2007). The effect of nanocrystalline magnetite size on arsenic removal. SCIENCE AND TECHNOLOGY OF ADVANCED MATERIALS.

MECC. (2009). "Types of Filters." Water/Wastewater Distance Learning Retrieved November 4, 2009, 2009, from http://water.me.vccs.edu/concepts/filters.html.

Meharg, A. A. (2005). Venomous Earth. New York, Macmillan.

Mendoza-Amezquita, E., M. A. Armienta-Hernandez, et al. (2006). "Potential lixiviation of trace elements in tailings from the mines La Asuncion and Las Torres in the Guanajuato Mining District, Mexico." Revista Mexicana De Ciencias Geologicas **23**(1): 75-83.

Moel, P. J. d., J. Q. J. C. Verberk, et al. (2006). Drinking Water Principles and Practice. New Jersey, World Scientific Publishing Co. Pte. Ltd.

Mohan, D. and C. U. Pittman (2007). "Arsenic removal from water/wastewater using adsorbents - A critical review." Journal of Hazardous Materials **142**(1-2): 1-53.

Möller, T. and P. Sylvester (2008). "Effect of silica and pH on arsenic uptake by resin/iron oxide hybrid media." Water Research **42**(6-7): 1760-1766.

Monroy-Torres, R., A. E. Macias, et al. (2009). "Arsenic in Mexican Children Exposed to Contaminated Well Water." Ecology of Food and Nutrition **48**(1): 59-75.

Montgomery, J. H. (2007). Groundwater Chemicals Desk Reference. Boca Raton, FL, CRC Publishers.

Morel, F. M. M. and J. G. Hering (1993). Principles and applications of aquatic chemistry New York, Wiley.

Navas-Acien, A., E. K. Silbergeld, et al. (2008). "Arsenic Exposure and Prevalencce of Type 2 Diabetes in US Adults." JAMA **300**(7): 814-822.

Ngai, T. and S. Walewijk (2003). THE ARSENIC BIOSAND FILTER (ABF) PROJECT: DESIGN OF AN APPROPRIATE HOUSEHOLD DRINKING WATER FILTER FOR RURAL NEPAL.

Ngai, T. K. K., R. R. Shrestha, et al. (2007). "Design for sustainable development - Household drinking water filter for arsenic and pathogen treatment in Nepal." Journal of Environmental Science and Health Part a-Toxic/Hazardous Substances & Environmental Engineering **42**(12): 1879-1888.

Nimick, D. A. (1994). "Arsenic hydrogeochemistry in an irrigated river valley: a reevaluation." Ground Water **36**: Ground Water.

Noubactep, C. (2009). "Comment on "Effect of Groundwater Iron and Phosphate on the Efficacy of Arsenic Removal by Iron-Amended BioSand Filters"." Environmental Science & Technology **43**(22): 8698.

Ogata, A. and R. B. Banks (1961). A solution of the differential equation of longitudinal dispersion in porous media. Professional Paper 411-A. U.S.G.S. Washington DC.

Ohe K, T. Y., Nakamura S, Oshima T, Baba Y (2005). "Adsorption behavior of arsenic(III) and arsenic(V) using magnetite." JOURNAL OF CHEMICAL ENGINEERING OF JAPAN **38**(8): 671-676.

Ongley, L. K., L. Sherman, et al. (2007). "Arsenic in the soils of Zimapan, Mexico." Environmental Pollution **145**(3): 793-799.

Pan, B. J., J. Wu, et al. (2009). "Development of polymer-based nanosized hydrated ferric oxides (HFOs) for enhanced phosphate removal from waste effluents." Water Research **43**(17): 4421-4429.

Perwak, J., M. Goyer, et al. (1981). An Exposure and Risk Assessment for Mercury. EPA. Washington, D.C., Offic of Water Regulations and Standards.

Pierce, M. L. and C. B. Moore (1982). "ADSORPTION OF ARSENITE AND ARSENATE ON AMORPHOUS IRON HYDROXIDE." Water Research **16**(7): 1247-1253.

Pigna, M. and A. Violante (2003). "Arsenate fixation in soils and variable-charge minerals in the presence of polycarboxylic organic acids and phosphate." Agrochimica **47**(3-4): 103-111.

Pourbaix, M. (1924). Atlas of Electrochemical Equilibrium in Aqueous Solutions, NACE.

Radu, T., J. L. Subacz, et al. (2005). "Effects of dissolved carbonate on arsenic adsorption and mobility." Environmental Science & Technology **39**(20): 7875-7882.

Rai, D., J. Zachara, et al. (1984). Chemical Attenuation Rates, Coeffiecients, and Constants in Leachate Migration. Vol I: A Critical Review. Richland, WA, Pacific Northwest Laboratories (Battelle Institute). **1**.

Ramamoorthy, S. and B. R. Rust (1976). "MERCURY SORPTION AND DESORPTION CHARACTERISTICS OF SOME OTTAWA RIVER SEDIMENTS." Canadian Journal of Earth Sciences **13**(4): 530-536.

Ray, C. G. M. R. B. L. (2002). Riverbank Filtration: Improving source-water quality. The Netherlands, Kluwer Academic Publishers.

Rebodos, R. L. and P. J. Vikesland (2010). "Effects of Oxidation on the Magnetization of Nanoparticulate Magnetite." Langmuir **26**(22): 16745-16753.

Reed, B. E., R. Vaughan, et al. (2000). "As(III), As(V), Hg, and Pb removal by Fe-oxide impregnated activated carbon." Journal of Environmental Engineering-Asce **126**(9): 869-873.

Rocha-Amador, D., M. E. Navarro, et al. (2007). "Decreased intelligence in children and exposure to fluoride and arsenic in drinking water." Cadernos De Saude Publica **23**: S579-S587.

Rosado, J. L., D. Ronquillo, et al. (2007). "Arsenic exposure and cognitive performance in Mexican schoolchildren." Environmental Health Perspectives **115**(9): 1371-1375.

Rosenblum, E. and D. Clifford (1983). The Equilibrium Arsenic Capacity of Activated Alumina. EPA. Cincinnati, OH.

Ryker, S. J. (2001). "Mapping Arsenic in Groundwater." Geotimes **46**(11): 34-36.

Saleh, N., H. J. Kim, et al. (2008). "Ionic strength and composition affect the mobility of surface-modified Fe-0 nanoparticles in water-saturated sand columns." Environmental Science & Technology **42**(9): 3349-3355.

Satterfield, Z. (2005) "Filter Backwashing." Tech Brief **5**, 4.

Sawyer, C., P. McCarty, et al. (2003). Chemistry for Environmental Engineering and Science, 5th Ed. New York, McGraw Hill.

Sayes, C. M., J. D. Fortner, et al. (2004). "The Differential Cytotoxicity of Water-Soluble Fullerenes." Nano Letters **4**(10): 1881-1887.

Schroeder, D. C. and G. F. Lee (1975). "POTENTIAL TRANSFORMATIONS OF CHROMIUM IN NATURAL-WATERS." Water Air and Soil Pollution **4**(3-4): 355-365.

Schwarzenbach, R. P., P. M. Gschwend, et al. (2003). Environmental Organic Chemistry. Hoboken, NJ, John Wiley & Sons, Inc.

Seader, J. D. H., E. J. (1998). Separation Process Principles. New York, John Wiley & Sons, Inc.

Shafiquzzaman, M., M. S. Azam, et al. (2009). "Technical and Social Evaluation of Arsenic Mitigation in Rural Bangladesh." Journal of Health Population and Nutrition **27**(5): 674-683.

Sherman, D. M. and S. R. Randall (2003). "Surface complexation of arsenic(V) to iron(III) (hydr)oxides: Structural mechanism from ab initio molecular geometries and EXAFS spectroscopy." Geochimica et Cosmochimica Acta **67**(22): 4223–4230.

Shipley, H. (2007). Magnetite Nanoparticles for Removal of Arsenic from Drinking Water. Civil and Environmental Engineering. Houston, TX, Rice University. **PhD:** 145.

Shipley, H. J., S. Yean, et al. (2009). "ADSORPTION OF ARSENIC TO MAGNETITE NANOPARTICLES: EFFECT OF PARTICLE CONCENTRATION, pH, IONIC STRENGTH, AND TEMPERATURE." Environmental Toxicology and Chemistry **28**(3): 509-515.

Sigg, L. and W. Stumm (1980). "The Interaction of Anions and Weak Acids With the Hydrous Goethite (alpha-FeOOH) Surface." Colloids and Surfaces **2**(2): 101-117.

Silliman, S. E. (1995). "Particle transport through two-dimensional, saturated porous media: influence of physical structure of the medium." Journal of Hydrology **167**(1-4): 79-98.

Simapag (2009) "RESEÑA HISTÓRICA DEL SUMINISTRO DE AGUA POTABLE EN LA CIUDAD DE GUANAJUATO."

Singh, T. S. and K. K. Pant (2004). "Equilibrium, kinetics and thermodynamic studies for adsorption of As(III) on activated alumina." Separation and Purification Technology **36**(2): 139-147.

Smith, S. D. and M. Edwards (2005). "The influence of silica and calcium on arsenate sorption to oxide surfaces." Journal of Water Supply Research and Technology-Aqua **54**(4): 201-211.

Sontheimer, C., Summers (1988). Activated Carbon for Water Treatment. Karlsruhe, Germany, DVGW-Forschungsstelle.

Stumm, W. and J. Morgan (1996). Aquatic Chemistry. New York, John Wiley & Sons, Inc.

Sun, H., X. Zhang, et al. (2007). "Enhanced Accumulation of Arsenate in Carp in the Presence of Titanium Dioxide Nanoparticles." Water, Air, & Soil Pollution **178**(1): 245-254.

Sunda, W. G., D. W. Engel, et al. (1978). "EFFECT OF CHEMICAL SPECIATION ON TOXICITY OF CADMIUM TO GRASS SHRIMP, PALAEMONETES-PUGIO - IMPORTANCE OF FREE CADMIUM ION." Environmental Science & Technology **12**(4): 409-413.

Swedlund, P. J. and J. G. Webster (1999). "Adsorption and polymerisation of silicic acid on ferrihydrite, and its effect on arsenic adsorption." Water Research **33**(16): 3413-3422.

Sylvester, P., P. Westerhoff, et al. (2007). "A hybrid sorbent utilizing nanoparticles of hydrous iron oxide for arsenic removal from drinking water." Environmental Engineering Science **24**(1): 104-112.

Takanashi, H., A. Tanaka, et al. (2004). "Arsenic removal from groundwater by a newly developed adsorbent." Water Science and Technology **50**(8): 23-32.

Thirunavukkarasu, O. S., T. Viraraghavan, et al. (2003). "Arsenic removal from drinking water using iron oxide-coated sand." Water Air and Soil Pollution **142**(1-4): 95-111.

Tomson, M. B. (2004). Tutorial on Visual Minteq 2.30, adsorption. RiceUniversity. Houston, TX.

Toride, N., F. J. Leij, et al. (1995). The CXTFIT Code for Estimating Transport Parameters from Laboratory or Field Tracer Experiments. Version 2.0. Riverside, CA, US Salinity Laboratory.

Tréguer, P., D. M. Nelson, et al. (1995). "The Silica Balance in the World Ocean: A Reestimate." Science **268**(5209): 375-379.

Truesdell, A. H. and R. O. Fournier (1977). "PROCEDURE FOR ESTIMATING TEMPERATURE OF A HOT-WATER COMPONENT IN A MIXED WATER BY USING A PLOT OF DISSOLVED SILICA VERSUS ENTHALPY." Journal of Research of the Us Geological Survey **5**(1): 49-52.

Tseng, W. P. (1977). "EFFECTS AND DOSE-RESPONSE RELATIONSHIPS OF SKIN CANCER AND BLACKFOOT DISEASE WITH ARSENIC." Environmental Health Perspectives **19**(AUG): 109-119.

USEPA (2001). Federal Register. **66:** 6976-7066.

Vaughan, R. L., B. E. Reed, et al. (2007). "Modeling As(V) removal in iron oxide impregnated activated carbon columns." Journal of Environmental Engineering-Asce **133**(1): 121-124.

Walker, R. (2009). "SI Metric Density of Materials." Retrieved 2/4/2011, from http://www.simetric.co.uk/si_materials.htm.

Waltham, C. A. and M. J. Eick (2002). "Kinetics of arsenic adsorption on goethite in the presence of sorbed silicic acid." Soil Science Society of America Journal **66**(3): 818-825.

Weisner, M. and J.-Y. Bottero (2007). Environmental nanotechnology: applications and impacts of nanomaterials. New York, McGraw Hill.

Westerhoff, P., T. Karanfil, et al. (2006). Aerogel & Iron-Oxide Impregnated Granular Activated Carbon Media For Arsenic Removal. Denver, CO, Awwa Research Foundation and Arsenic Water Technology Partnership.

WHO (2004). Guidelines for Drinking-water Quality. Geneva, Switzerland.
Wright, P. M. (1991). Direct Use Engineering and Design Guidebook. Geochemistry. Salt Lake City, UT.
Yang, W. (2009). Unpublished work in Mason Tomson's laboratory, Rice University.
Yang, W., A. T. Kan, et al. (2010). "pH-dependent effect of zinc on arsenic adsorption to magnetite nanoparticles." Water Res **44**(19): 5693-5701.
Yang, X. F., P. Roonasi, et al. (2008). "A study of sodium silicate in aqueous solution and sorbed by synthetic magnetite using in situ ATR-FTIR spectroscopy." Journal of Colloid and Interface Science **328**(1): 41-47.
Yavuz, C. T., J. T. Mayo, et al. (2010). "Pollution magnet: nano-magnetite for arsenic removal from drinking water." Environmental Geochemistry and Health **32**(4): 327-334.
Yavuz, C. T., J. T. Mayo, et al. (2006). "Low-field magnetic separation of monodisperse Fe3O4 nanocrystals." Science **314**(5801): 964-967.
Yean, S., L. Cong, et al. (2005). "Effect of magnetite particle size on adsorption and desorption of arsenite and arsenate." Journal of Materials Research **20**(12): 3255-3264.
Yean, S. J. (2008). Arsenic Removal Using Iron Oxides: Application of Magnetite Nanoparticles and Iron Salts. Department of Civil and Environmental Engineering. Houston, TX, Rice University. **Doctor of Philosophy:** 224.
Zeng, H., B. Fisher, et al. (2008). "Individual and competitive adsorption of arsenate and phosphate to a high-surface-area iron oxide-based sorbent." Environmental Science & Technology **42**(1): 147-152.
Zhang, H. and H. M. Selim (2005). "Kinetics of arsenate adsorption-desorption in soils." Environmental Science & Technology **39**(16): 6101-6108.
Zhang, H. and H. M. Selim (2007). "Modeling competitive arsenate-phosphate retention and transport in soils: A multi-component multi-reaction approach." Soil Science Society of America Journal **71**(4): 1267-1277.
Zhao, H. S. and R. Stanforth (2001). "Competitive adsorption of phosphate and arsenate on goethite." Environmental Science & Technology **35**(24): 4753-4757.

Appendices

Appendix A –Assessment of water samples shipped from Guanajuato to Rice University Summer of 2008

Sample #	Sample Description
1	Guanajuato municipal groundwater; sampled from a home
2	Lake Esperanza water
3	Lake Soledad water
4	Lake Soledad water; sampled at entrance to Water Treatement Plant (WTP)
5	Effluent from WTP
6	Effluent from WTP; sampled from a home

Parameter	Test Method	1	2	3	4	5	6	Guideline	Units
pH	Electrode	7.80	7.59	7.45	7.50	6.70	7.05	6.5 - 8.5	
Conductivity	Electrode	302	152	173	168	171	183		µS
Hardness	ICP (Mg + Ca)	66	63	69	69	74	75		mg/l as $CaCO_3$
Alkalinity	Hach titration	144	32	46	46	27	26		mg/l as $CaCO_3$
Fluoride	Electrode	0.45	0.20	0.23	0.22	0.20	0.20	1.5	mg/l
Phosphate	Hach PhosVer	0.27	0.1	0.12	0.13	0.11	0.06		mg/l as PO_4^{3-}
Ammonia	Hach method	0.02	0.13	0.42	0.42	0.07	<0.02		mg/l as NH_3-N
TDS	Electrode	204	83	95	94	110	110	500	mg/l
COD	Hach digestion	3.1	22.2	9.0	8.0	11.3	6.0		mg/l
Chloride	Hach titration	4.5	2.0	3.0	3.0	19.0	22.3	250	mg/l
Sulfate	Hach turbidity	24	38	34	37	29	32	250	mg/l
Nitrate	Hach	1.9	9.4	3.5	3.2	0.5	0.9	10	mg/l as NO_3^{1-}-N
Turbidity	Turbidity Meter	1	184	730	700	10	4		NTU
Color (True)	Hach Spectr	5	37	18	19	7	9	15	Pt-Co units
Color (Apparent)	Hach Spectr	31	>500	>500	>500	96	57	15	Pt-Co units
ICP - Total Dissolved Metals - Filtered									
Ca	ICP	20.78	12.18	11.83	11.81	13.73	14.08		mg/l
Fe	ICP	0.00	0.18	0.05	0.05	0.00	0.00	0.3	mg/l
Mg	ICP	3.31	7.98	9.51	9.60	9.64	9.70		mg/l
Si	ICP	31.39	8.06	5.62	5.67	5.06	5.04		mg/l
ICP - Total Extractable Metals - Unfiltered									
Ca	ICP	20.21	13.37	14.93	14.57	14.49	14.88		mg/l
Fe	ICP	0.09	10.96	35.24	35.04	0.47	0.17	0.3	mg/l
Mg	ICP	3.52	10.11	17.73	17.19	10.35	10.52		mg/l
Si	ICP	27.73	22.63	49.24	46.34	5.57	4.99		mg/l
ICP/MS - Total Dissolved Metals - Filtered									
As	ICP/MS	16.32	0.85	0.23	0.25	0.35	0.40	10	µg/l
Al	ICP/MS	2.21	55.52	7.55	8.43	10.47	13.37	50 - 200	µg/l
Be	ICP/MS	0.03	0.02	0.01	0.01	0.01	0.01	4	µg/l
Cd	ICP/MS	0.01	0.01	0.00	0.00	0.06	0.01	3	µg/l
Co	ICP/MS	0.04	0.13	0.07	0.07	0.17	0.19		µg/l
Cr	ICP/MS	7.94	2.25	1.65	2.48	0.47	0.45	50	µg/l
Cu	ICP/MS	40.64	5.63	1.89	2.15	1.14	3.87	1,300	µg/l
Mn	ICP/MS	0.06	2.06	0.31	0.35	37.54	26.31	50	µg/l
Mo	ICP/MS	1.27	0.37	0.75	0.77	0.76	0.55	70	µg/l
Pb	ICP/MS	0.11	0.05	0.00	0.00	0.00	0.01	10	µg/l
Sb	ICP/MS	0.32	0.33	0.18	0.19	0.45	0.23	6	µg/l
Se	ICP/MS	1.20	0.57	0.52	0.60	0.71	0.59	10	µg/l
Th	ICP/MS	0.41	0.59	0.17	0.18	0.86	0.34	2	µg/l
Tl	ICP/MS	0.00	0.01	0.00	0.00	0.02	0.00		µg/l
U	ICP/MS	4.55	0.04	0.02	0.02	0.05	0.02	15	µg/l
V	ICP/MS	8.30	1.28	1.09	1.07	0.84	0.87		µg/l
Zn	ICP/MS	156.34	0.00	0.00	0.00	259.95	180.76	5,000	µg/l
ICP/MS - Total Extractable Metals - Unfiltered									
As	ICP/MS	8.61	2.88	1.50	2.78	-0.11	-0.25	10	µg/l
Be	ICP/MS	0.03	0.17	0.26	0.44	0.01	0.01	4	µg/l
Cd	ICP/MS	0.01	0.08	0.04	0.06	0.05	0.01	3	µg/l
Co	ICP/MS	0.06	2.20	5.08	7.82	0.30	0.25		µg/l
Cr	ICP/MS	0.46	10.17	22.70	36.59	1.16	0.77	50	µg/l
Cu	ICP/MS	31.84	12.85	14.22	21.93	2.40	6.08	1,300	µg/l
Mn	ICP/MS	3.75	0.89	0.86	0.96	46.38	27.53	50	µg/l
Mo	ICP/MS	0.85	0.43	0.77	1.33	0.51	0.53	70	µg/l
Pb	ICP/MS	1.45	2.57	2.97	4.90	1.05	0.63	10	µg/l
Sb	ICP/MS	0.32	0.55	0.31	0.43	0.35	0.87	6	µg/l
Se	ICP/MS	0.26	0.14	0.11	0.33	0.43	0.39	10	µg/l
Th	ICP/MS	0.02	0.41	0.77	1.30	0.08	0.05	2	µg/l
U	ICP/MS	2.76	0.101	0.18	0.26	0.015	0.013	15	µg/l
Organics: GC/MS Results Summary									

Only compounds with a fit value in excess of 90% were considered. Standards were not available yet for comparison; therefore, the report must be considereed preliminary. Probably the only compound of significance is diphenyl ether. Several C10+ alkanes plus numerous silanes and siloxanes were identified by the mass spectrometer, most likely from either grease in the sample or in the laboratory equipment as a contaminant. In addition, diphenyl ether was identified in samples 2 and 3. Although no standards for diphenyl ether are available, based upon relative peak abundance with a naphthalene standard, the concentration is clearly less than 1 mg/l. Also, 4-nitro-4'-chlorodiphenylsulfoxide was identified in sample No. 5, but since no standards are available and as it is not reported in standard references, it is probably not the correct compound identity. The compound is similar in structure to common flame retardants.

Appendix B – Analysis from Guanajuato water assessment trip; January 2009

Guanajuato Water Sampling -- January 2009		mV	°C	NTU	ppm						
Description	pH	Eh	Temp	Turbidity	TDS	DO	Free Cl2	Total Cl2	Ammonia	Nitrate-N	Nitrite-N
Esperanza Dam unfiltered	7.20	159	12.2	60.4	225	5				0	0
Esperanza Dam unfiltered											
Esperanza Dam filtered											
Esperanza Dam filtered											
Soledad Dam unfiltered	8.53	156	14.0	0.74	338	6			0.11	0	0
Soledad Dam unfiltered											
Soledad Dam filtered											
Soledad Dam filtered											
WTP inlet unfiltered	8.49	123	14.1		346	7	0	0			
WTP inlet unfiltered											
WTP inlet filtered											
WTP inlet filtered											
Coag tank with Cl_2 unfiltered	8.30	335			352	8	1.45	1.52			
Coag tank with Cl_2 unfiltered											
Coag tank with Cl_2 filtered											
Coag tank with Cl_2 filtered											
1st sedimentation stage effluent											
Sand filter influent	7.80	628	14.9	0.20	376	5.5	1.23	1.43			
Sand filter influent											
Sand filter effluent	7.07	586	15.1		375	7.5	0.45	0.95			
Sand filter effluent											
Effluent of WTP (with chlorination)	7.85	619	15.1		371	5.5	0.82	1.01			
Effluent of WTP (with chlorination)											
GW at well before chlorination	7.60	292	29.2		315	4				1.5	0
GW at well before chlorination											
household tap directly from distribution system	7.87	484	14.8		364	5	0.74	0.91		0	0
Effluent of black household storage tank	8.08	301	15.7		360	5	0.07	0.07		0	0
GW storage tank (3 Star Tank)	7.23	653	29.1		253	4	1.95	2.04		1.5	0
GW storage tank (3 Star Tank)											
arsenic suspect well (well #1)		291									
arsenic suspect well (well #1)											
arsenic suspect well (well #1)											
arsenic suspect well (well #1)											
MCL's by WHO/EPA (Secondary standards denoted by an asterisk)					500*					10	

Guanajuato Metals Analysis -- Jan 2009	ppm				ppb																							
Description	Fe	Ca	Mg	Ba	Ag	Al	As	Be	Bi	Cd	Co	Cr	Cs	Cu	Ga	Hg	In	Mn	Ni	Pb	Rb	Se	Sr	Tl	U	V	Zn
Esperanza Dam unfiltered	1.77	34	20	0	0	313	4	0	0	0	1	1	0	3	2	0.1	0	1	11	1	1	1	34	0	0	3	154
Esperanza Dam unfiltered	1.68	34	20	0	0	23	3	0	0	0	1	1	0	2	2	0.1	0	1	8	1	0	1	9	0	0	3	224
Esperanza Dam filtered	0.04	34	20	0	0	82	2	0	0	0	1	2	0	2	2	0.2	0	1	1	1	1	1	1	0	0	1	6
Esperanza Dam filtered	0.00	33	20	0	0	73	2	0	0	0	1	2	0	2	2	0.2	0	1	1	1	1	0	1	0	0	1	5
Soledad Dam unfiltered	0.06	43	33	0	0	103	1	0	0	0	0	2	0	2	1	0.6	0	20	1	1	1	2	1	0	0	2	345
Soledad Dam unfiltered	0.04	42	33	0	0	108	2	0	0	0	0	1	0	1	1	0.2	0	19	1	1	1	1	1	0	0	2	379
Soledad Dam filtered	0.03	42	33	0	0	106	2	0	0	0	0	3	0	2	2	0.3	0	11	1	1	1	1	1	0	0	2	8
Soledad Dam filtered	0.03	42	32	0	0	80	1	0	0	0	0	1	0	1	1	0.2	0	8	1	0	0	2	1	0	0	2	9
WTP inlet unfiltered	0.01	42	33	0	0	120	2	0	0	0	0	1	0	11	2	0.2	0	38	1	1	1	2	1	0	0	2	336
WTP inlet unfiltered	0.00	42	33	0	0	86	2	0	0	0	0	1	0	2	1	0.2	0	33	1	1	1	2	1	0	0	2	266
WTP inlet filtered	0.00	42	32	0	0	160	2	0	0	0	0	2	0	2	2	0.2	0	18	1	1	1	2	1	0	0	2	11
Coag tank with Cl_2 unfiltered	0.01	41	32	0	0	0	2	0	0	0	0	1	0	2	1	0.3	0	35	1	1	1	2	1	0	0	2	297
Coag tank with Cl_2 unfiltered	0.01	41	32	0	0	0	2	0	0	0	0	1	0	2	1	0.5	0	34	1	1	1	2	1	0	0	2	349
Coag tank with Cl_2 filtered	0.06	42	32	0	0	160	2	0	0	0	0	2	0	2	1	0.6	0	14	1	1	1	1	1	0	0	2	8
Coag tank with Cl_2 filtered	0.00	41	32	0	0	223	2	0	0	0	0	2	0	1	1	0.7	0	13	1	1	1	1	1	0	0	2	8
1st sedimentation stage effluent	0.00	41	32	0	0	94	1	0	0	0	0	2	0	1	0	0.4	0	3	0	0	0	2	1	0	0	2	8
Sand filter influent	0.00	42	32	0	0	0	2	0	0	0	0	2	0	2	2	0.7	0	24	1	1	1	1	1	0	0	2	232
Sand filter influent	0.00	41	32	0	0	0	2	0	0	0	0	1	0	2	1	0.9	0	23	1	1	1	1	1	0	0	2	303
Sand filter effluent	0.00	40	31	0	0	0	2	0	0	0	0	1	0	3	2	0.7	0	14	1	1	1	2	1	0	0	2	280
Sand filter effluent	0.00	42	32	0	0	0	1	0	0	0	0	1	0	3	1	0.6	0	14	1	1	1	1	1	0	0	2	385
Effluent of WTP (with chlorination)	0.00	41	32	0	0	0	2	0	0	0	0	1	0	2	1	0.7	0	12	1	1	1	2	1	0	0	2	245
Effluent of WTP (with chlorination)	0.00	41	32	0	0	0	2	0	0	0	0	1	0	2	2	0.7	0	12	1	1	1	2	1	0	0	2	344
household tap directly from distribution system	0.00	40	31	0	0	0	2	0	0	0	0	1	0	2	1	0.4	0	17	1	1	1	2	1	0	0	2	405
Effluent of black household storage tank	0.00	41	32	0	0	292	2	0	0	0	0	1	0	4	1	0.3	0	15	1	1	1	2	1	0	0	2	355
GW at well before chlorination	0.00	16	2	0	0	92	11	0	0	0	0	2	2	2	1	0.5	0	7	0	1	12	1	94	0	5	18	293
GW at well before chlorination	0.00	16	2	0	0	93	11	0	0	0	0	2	2	1	1	0.4	0	7	0	1	12	2	96	0	5	18	196
GW storage tank (3 Star Tank)	0.00	18	3	0	0	99	16	0	0	0	0	1	7	2	1	0.3	0	7	0	1	15	1	116	0	4	8	349
GW storage tank (3 Star Tank)	0.00	18	3	0	0	73	15	0	0	0	0	1	7	2	1	0.3	0	6	0	1	15	1	114	0	4	8	276
Arsenic suspect well (well #1)	0.07	15	2	0	0	105	17	0	0	0	0	2	4	15	1	0.5	0	8	1	17	13	2	86	0	11	11	353
Arsenic suspect well (well #1)	0.17	9	1	0	0	134	25	0	0	0	0	2	4	13	2	0.6	0	12	1	8	9	2	50	0	7	8	236
Arsenic suspect well (well #1)	0.08	17	2	0	0	112	17	0	0	0	0	3	4	18	1	0.5	0	11	1	9	13	3	91	0	11	11	613
Arsenic suspect well (well #1)	0.10	12	1	0	0	110	22	0	0	0	0	2	4	13	2	0.5	0	9	1	8	11	2	64	0	8	8	520
WHO/EPA mcl's (* denotes 2ndary standard)	0.3*			2	100*	200*	10	4		3		50		1.3k*		1		50*	20	10		10			15		5k*

Appendix C – Geothermometer temperatures for groundwater wells in Guanajuato and surrounding areas

Town	Well Name	SiO_2	Na	K	Ca	Mg	Silica Temp*	Na-K-Ca-Mg Temp**
		(mg/l)	(mg/l)	(mg/l)	(mg/l)	(mg/l)	(°C)	(°C)
Guanajuato	Well 3	96.3	95.6	8.1	25.4	3.5	135	107.0
Guanajuato	Well 8	63.7	52.9	3.9	12.6	2.2	114	91.1
San Miguel	Lomas	91.7	1.8	0.2	24.9	4.6	132	***
San Miguel	Ejido	69.4	436.3	9.1	10.5	1.0	118	***
San Miguel	Meiquito	61.0	471.9	22.1	47.2	8.3	111	***
San Miguel	San Luis Rey	68.3	458.0	25.8	62.2	12.4	117	***
San Miguel	Nigromante	67.2	444.2	11.4	25.5	1.7	116	***
Irapuato	Well 58	99.5	88.0	11.3	23.2	8.6	137	57.8
Irapuato	Well 58A	71.0	353.8	10.6	6.6	0.4	119	***
Irapuato	Aldama well	78.3	259.1	8.7	8.9	0.4	124	***
Irapuato	Los Arcos well	92.2	49.1	10.5	53.0	13.5	133	68.6

* Silica geothermometer correlation: Truesdell (1976)

** Na-K-Ca-Mg geothermometer correlation: Fournier and Potter (1979)

*** Some samples were marked as preserved by Na_2SO_3. As a result, artificially high Na concentrations were present and the Na-K-Ca-Mg geothermometer results were not calculated.

Appendix D –Guanajuato pilot-column breakthrough curves by element

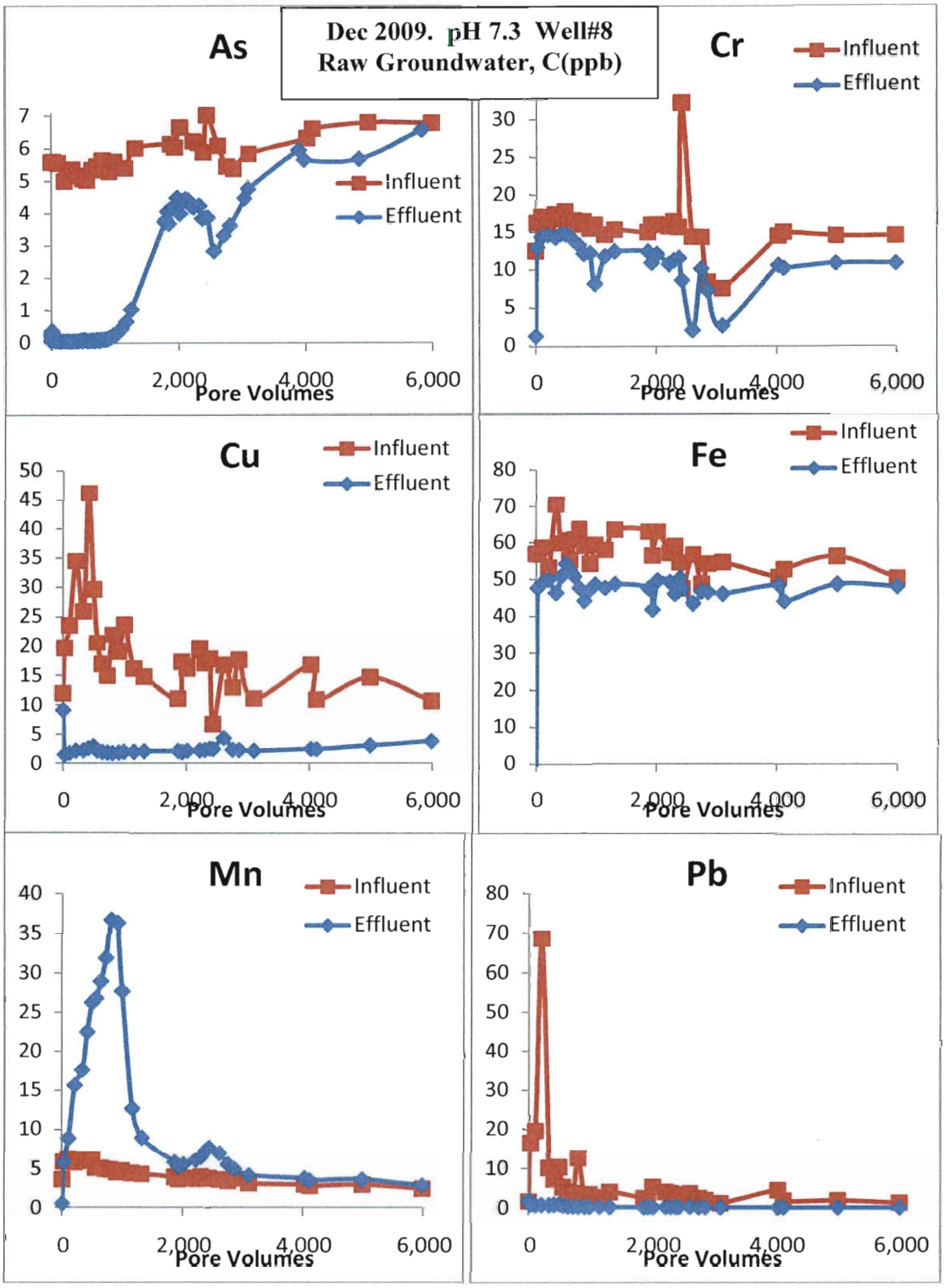
Dec 2009. pH 7.3 Well#8
Raw Groundwater, C(ppb)
As
Cr
Cu
Fe
Mn
Pb
Influent
Effluent
Pore Volumes
0
2,000
4,000
6,000

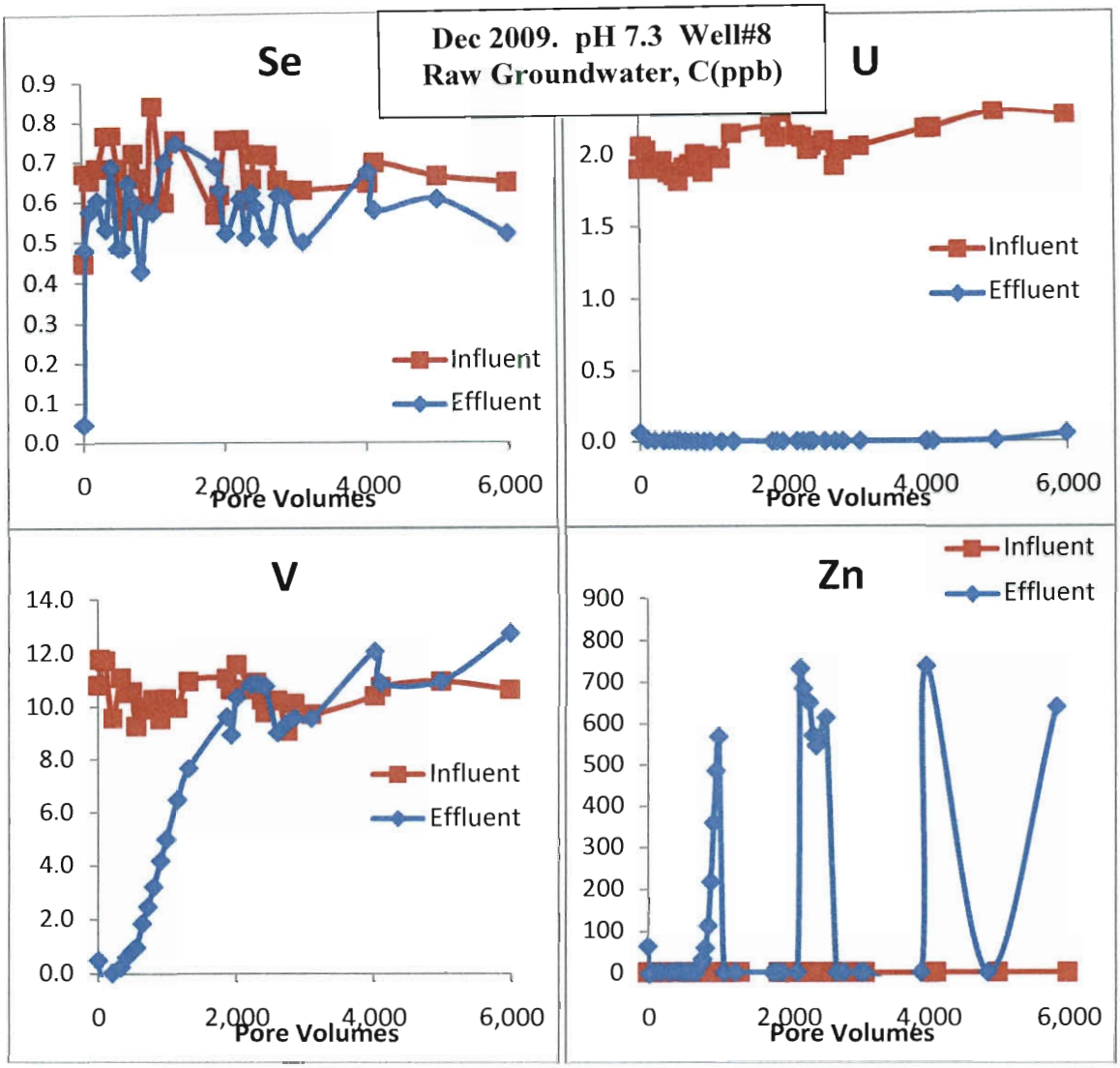
Dec 2009. pH 7.3 Well#8
Raw Groundwater, C(ppb)
Se
0.9
0.8
0.7
0.6
0.5
0.4
0.3
0.2
0.1
0.0
Influent
Effluent
0
2,000
4,000
6,000
Pore Volumes
U
2.0
1.5
1.0
0.5
0.0
Influent
Effluent
0
2,000
4,000
6,000
Pore Volumes
V
14.0
12.0
10.0
8.0
6.0
4.0
2.0
0.0
Influent
Effluent
0
2,000
4,000
6,000
Pore Volumes
Zn
900
800
700
600
500
400
300
200
100
0
Influent
Effluent
0
2,000
4,000
6,000
Pore Volumes

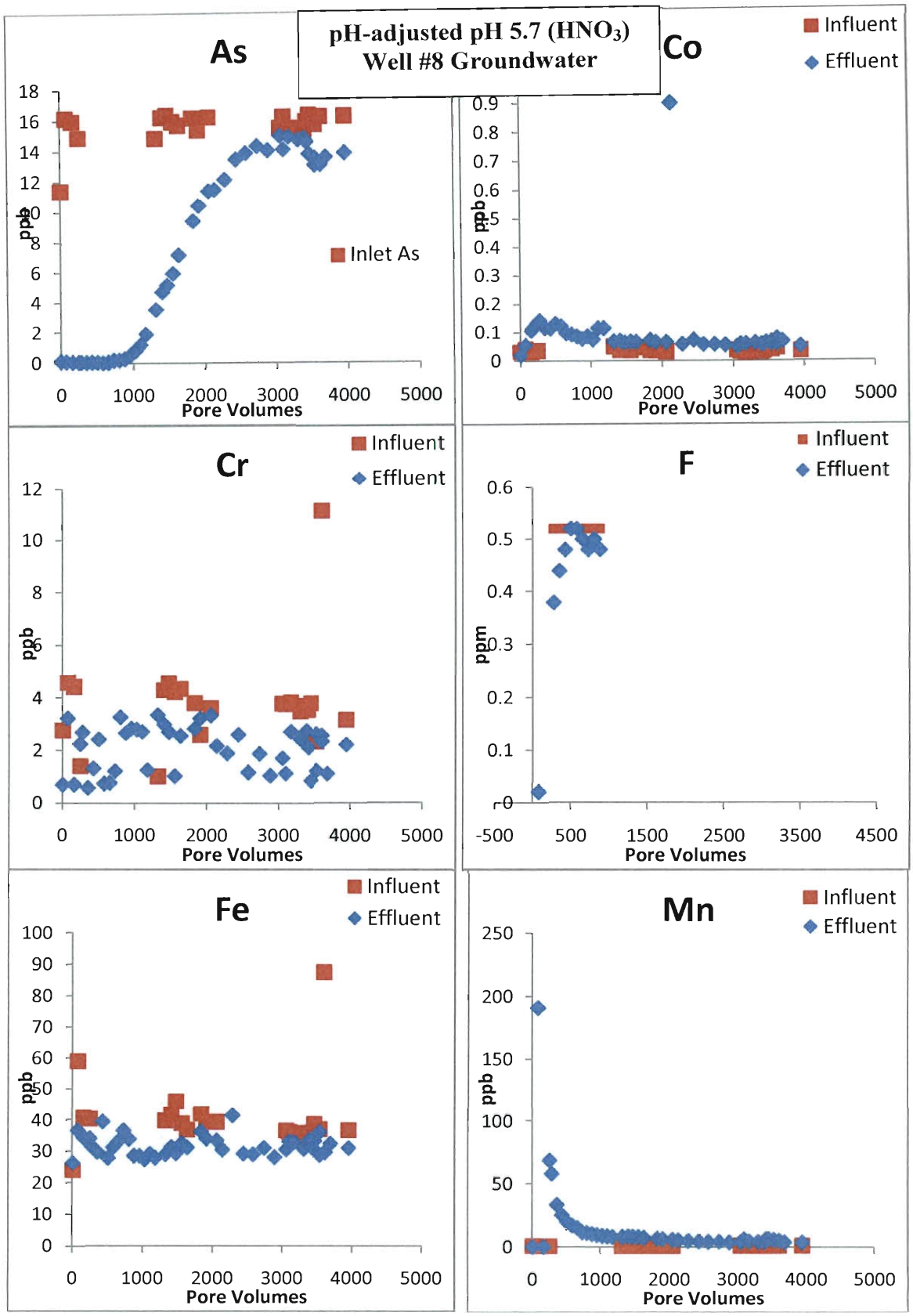
pH-adjusted pH 5.7 (HNO_3)
Well #8 Groundwater
As
Inlet As
ppb
Pore Volumes
Co
Influent
Effluent
ppb
Pore Volumes
Cr
Influent
Effluent
ppb
Pore Volumes
F
Influent
Effluent
ppm
Pore Volumes
Fe
Influent
Effluent
ppb
Pore Volumes
Mn
Influent
Effluent
ppb
Pore Volumes

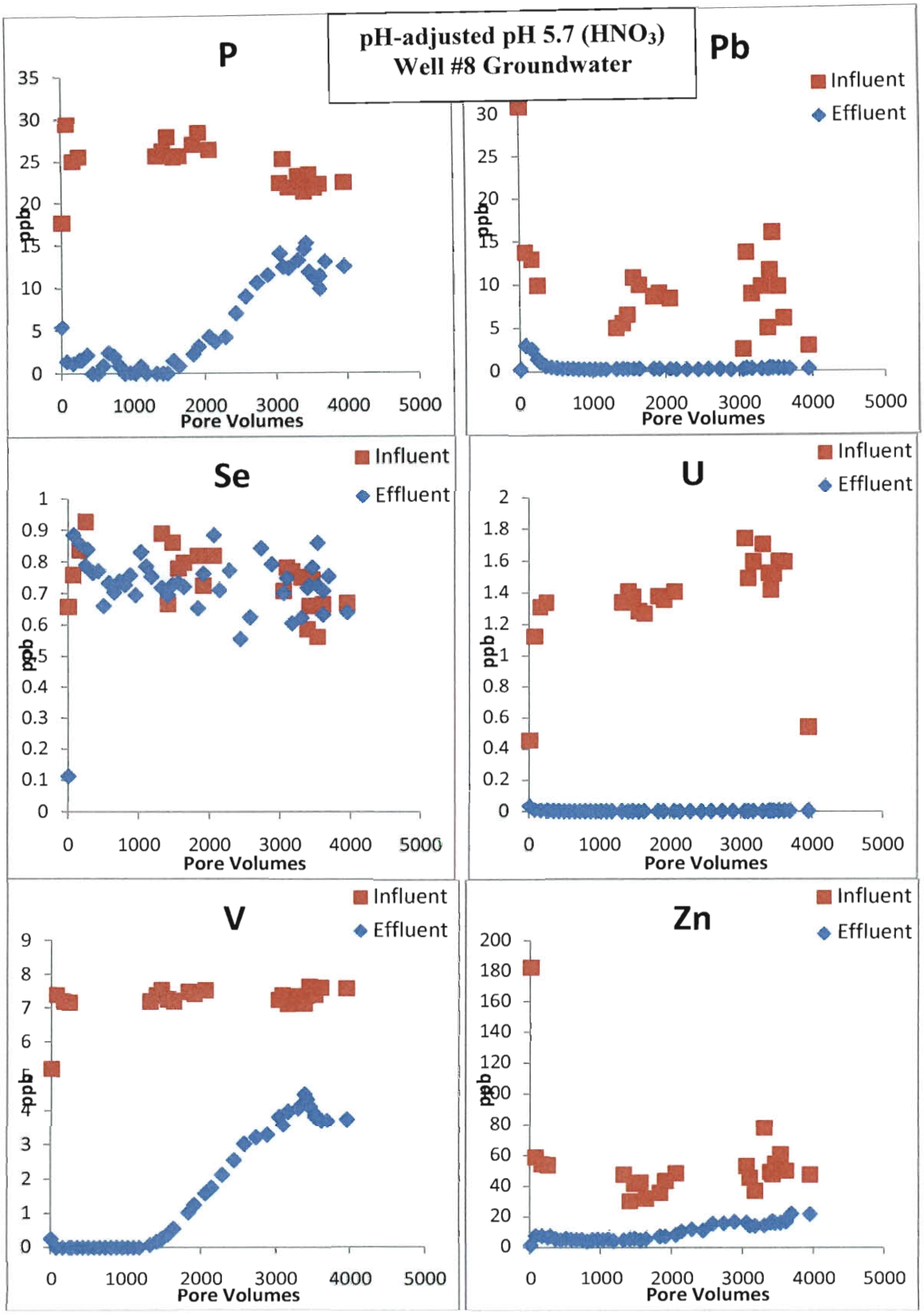
pH-adjusted pH 5.7 (HNO_3)
Well #8 Groundwater
P
Pb
Se
U
V
Zn
Influent
Effluent
ppb
Pore Volumes
0
1000
2000
3000
4000
5000

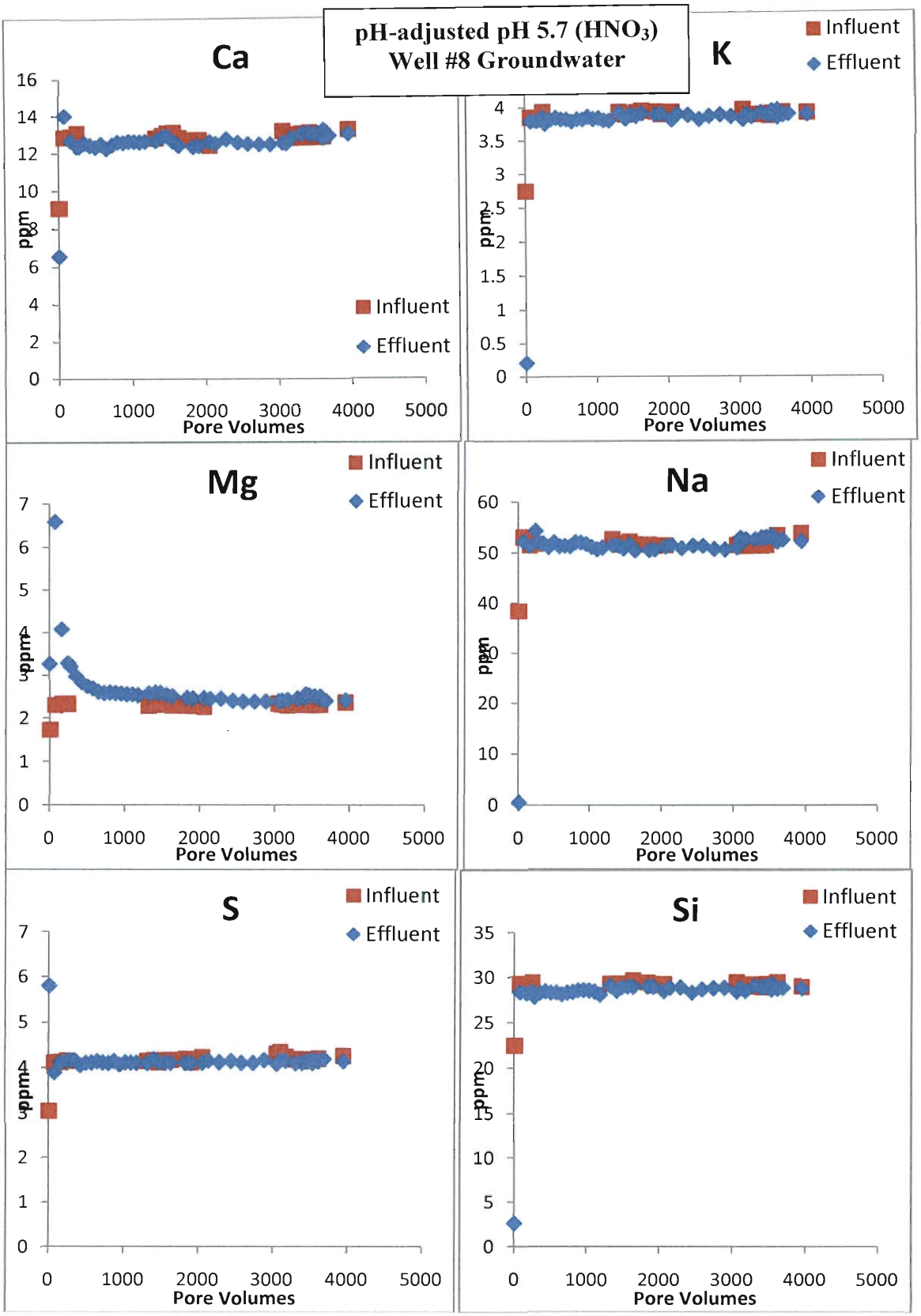
pH-adjusted pH 5.7 (HNO_3)
Well #8 Groundwater
Ca
K
Mg
Na
S
Si
Influent
Effluent
ppm
Pore Volumes
0
1000
2000
3000
4000
5000

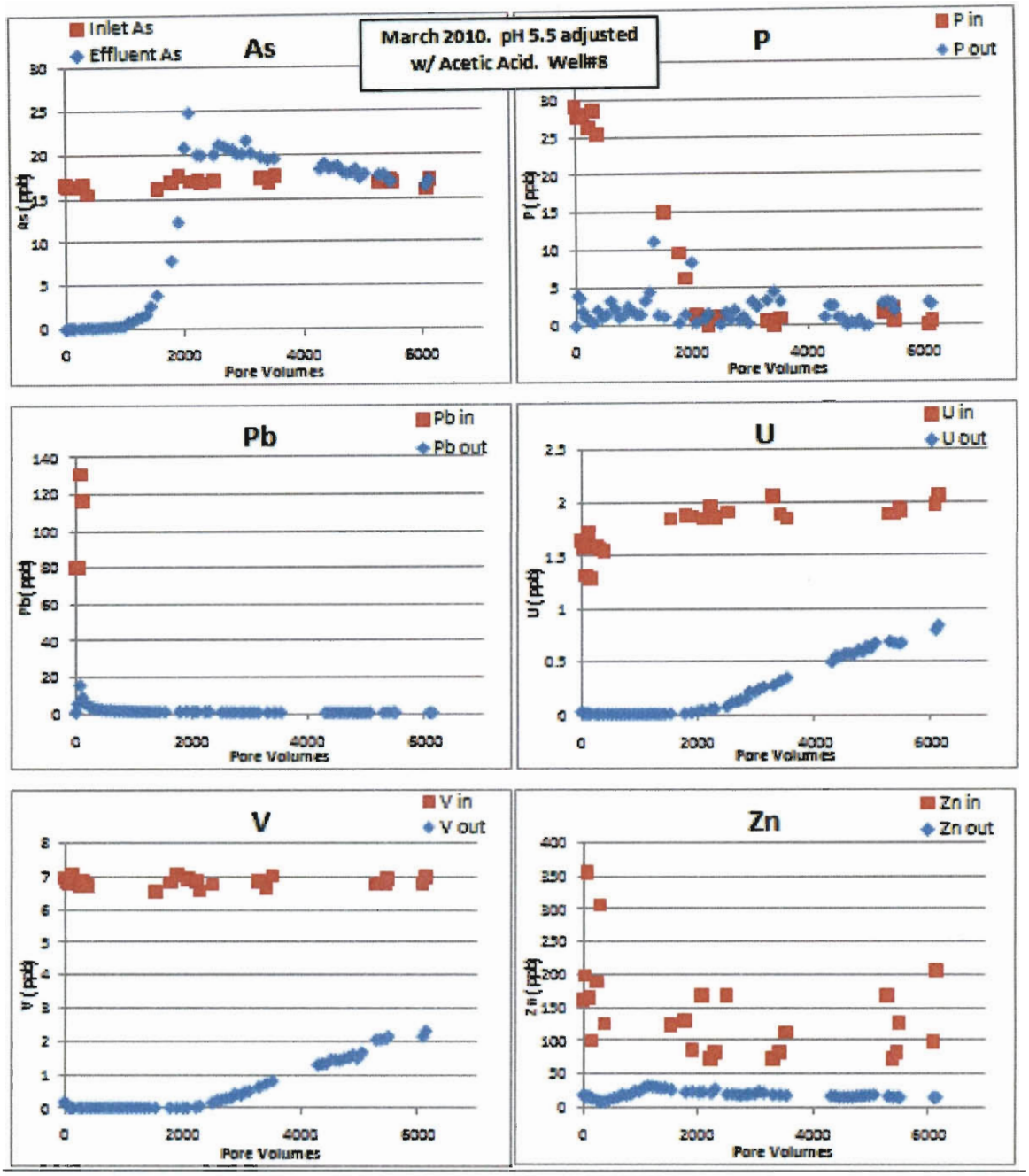
March 2010. pH 5.5 adjusted w/ Acetic Acid. Well#8
As
Inlet As
Effluent As
As (ppb)
Pore Volumes
P
P in
P out
P (ppb)
Pb
Pb in
Pb out
Pb (ppb)
U
U in
U out
U (ppb)
V
V in
V out
V (ppb)
Zn
Zn in
Zn out
Zn (ppb)

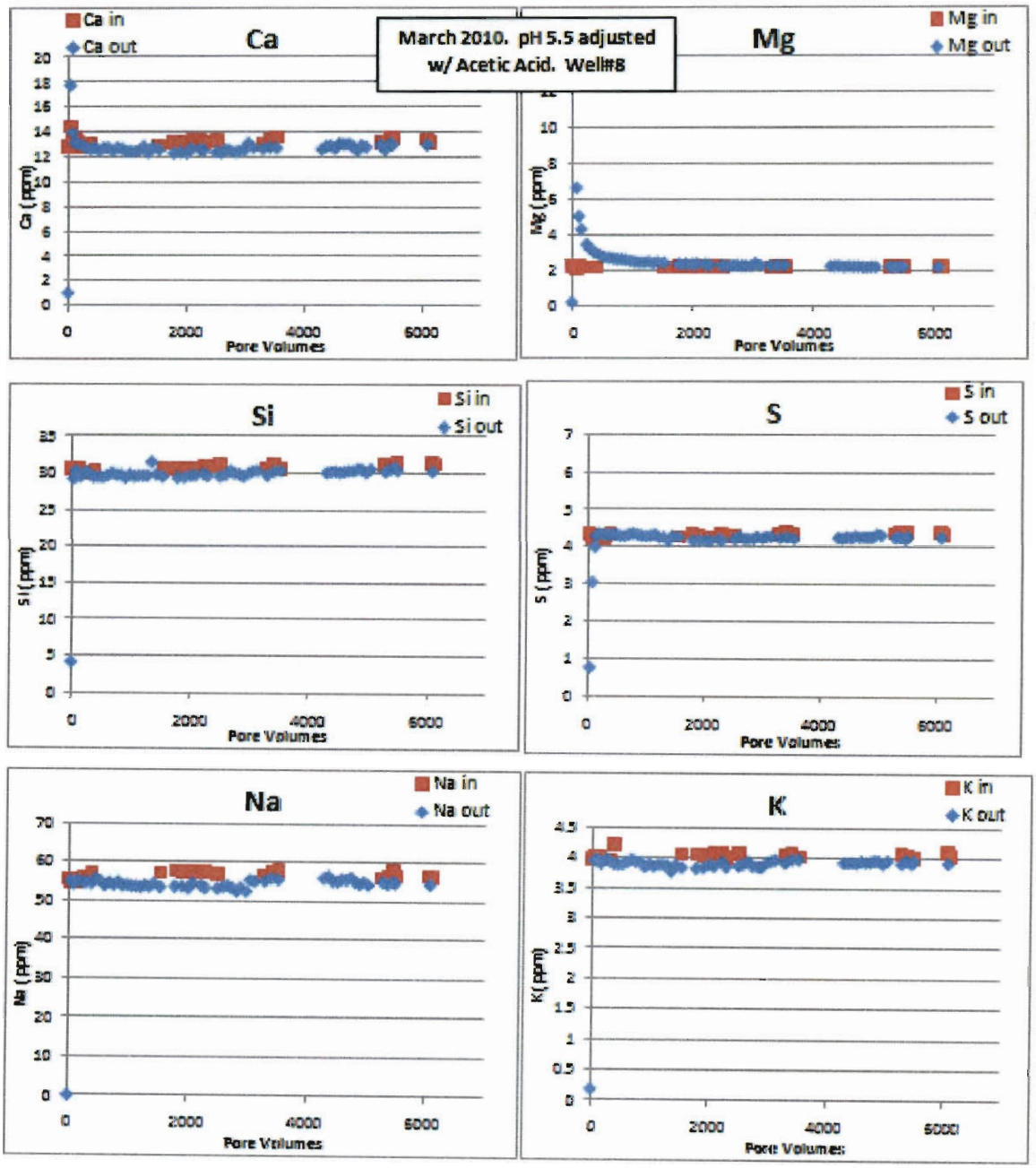
March 2010. pH 5.5 adjusted w/ Acetic Acid. Well#8
Ca
Ca in
Ca out
Ca (ppm)
Pore Volumes
Mg
Mg in
Mg out
Mg (ppm)
Pore Volumes
Si
Si in
Si out
Si (ppm)
Pore Volumes
S
S in
S out
S (ppm)
Pore Volumes
Na
Na in
Na out
Na (ppm)
Pore Volumes
K
K in
K out
K (ppm)
Pore Volumes